Biomass-assisted Catalytic Reduction of Carbon Dioxide to Value-added Products Under Hydrothermal Conditions

Mariia Konstantinova
Supervisor: Dr James McGregor

Department of Chemical and Biological Engineering
University of Sheffield

Thesis submitted for the degree of

Doctor of Philosophy

April 2022

ACKNOWLEDGEMENTS

ABSTRACT

A key challenge for the present century is the advancement of sustainable methods of fuel and chemical production. In the UK the chemical sector is the second-largest CO_2 emitting industry. In this work, sub-critical water was investigated as a reaction medium for hydrothermal conversion of CO_2 to value added products with glucose as a reductant. Analytical methods for the analysis of gaseous, aqueous and organic-soluble products were established to gain mechanistic insight into the reaction. The hydrothermal conversion of $NaHCO_3$, a CO_2 precursor, and glucose to formate was investigated between 225–300 °C. In uncatalyzed reactions, a maximum of 0.502 g l^{-1} $HCOO^-$ was obtained at 250 °C and 2 hours, while at higher temperature of 300°C product degradation occurs. At maximum $HCOO^-$ concentration, >95% of formate was formed from glucose degradation, and a mechanism for this process proposed.

Metal powders were investigated as heterogeneous catalysts to enhance bicarbonate conversion, and nickel was found to simultaneously increase formate formed from both $NaHCO_3$ and glucose. Formate concentration was shown to increase to 1.240 g l^{-1}, with concentration from bicarbonate increasing from 0.022 g l^{-1} in uncatalyzed reactions to 0.330 g l^{-1}. Characterisation of Ni powder showed no changes in functionality, oxidation state, or morphology of particles, indicating stability under the investigated conditions. This study demonstrated that catalytic hydrothermal conversion is a promising route for simultaneous conversion of both CO_2 and biomass to value-added products. Supported Ni catalysts were subsequently investigated, and it was concluded that metal particle size, oxidation state, and nature of the support strongly influence catalyst stability and degradation of formate to CO_2 and H_2.

Bicarbonates, carbonates and gaseous CO_2 were compared as precursors. Formate concentration in carbonate reactions was found to be enhanced by the addition of CO_2 gas, proposedly due to lowering of the reaction pH. Sodium carbonate with CO_2 perform comparatively to sodium bicarbonate, demonstrating that two different CO_2 sources can be used in conjunction to produce value-added organic acids. CO_2 in NaOH solution glucose system was further examined with heterogeneous catalysts. Copper-containing catalysts increased the yield of formate nearly two-fold, although characterization showed that sintering and leaching of active phase results in unstable catalysts. Design and development of stable catalysts for CO_2 and biomass valorisation are promising routes for further research in this area.

Contents

Contents

Contents

Contents

Contents

LIST OF EQUATIONS

List of Equations

LIST OF FIGURES

List of Figures

List of Figures

List of Figures

List of Figures

List of Figures

List of Figures

LIST OF TABLES

List of Tables

List of Tables

1 CHAPTER 1: INTRODUCTION

One of the key technological challenges of the 21st century is the advancement of alternative methods of fuel and chemical production using sustainable technologies. Industrialisation and continued fossil fuel use have resulted in increasing greenhouse gas (GHG) emissions worldwide. The overuse of fossil fuels is also resulting in anthropogenic climate change caused by rising levels of carbon dioxide (CO_2) in the atmosphere (EPA, 2019). Worldwide CO_2 emissions have been increasing 2.7% annually over the last decade (Le Quéré *et al.*, 2014). In the UK, CO_2 is the dominant GHG and accounted for over 80% of total emissions as of 2018, with the chemical sector the second-largest CO_2 emitting industry (Griffin, Hammond and Norman, 2018; DBEIS, 2020). Nevertheless, recent figures demonstrate that most processes still utilize unsustainable hydrocarbons as raw materials, with 95% of organic-based chemicals produced from non-renewable sources (Olajire, 2013). Therefore, novel routes to chemical and fuel production are necessary.

In the natural carbon cycle, carbon dioxide is abiotically converted to hydrocarbons in the earth's crust, while their subsequent combustion releases CO_2 (Wu *et al.*, 2009). A change in land-use due to urbanization and agriculture has reduced the number of natural sinks able to sequester GHGs, resulting in 16 Gt y^{-1} of excess CO_2 after reabsorption (Kalnay and Cai, 2003; Patel, Byun and Yavuz, 2017). Furthermore, an imbalance in fossil fuel production and usage has emerged and fossil fuel use outweighs the amount produced in the earth. Therefore, the direct use of carbon dioxide or carbon-capture products as starting materials in the production of value-added products is highly desirable. As a readily available, non-toxic and economical substance, CO_2 is an attractive feedstock which can be obtained as a by-product of existing industries or carbon capture (Arakawa *et al.*, 2001). By recent estimates, CO_2 produced as a consequence of human activity (approximately 35 Gt y^{-1}) is far greater than the amount used industrially (around 200 Mt y^{-1}) (Bonaventura *et al.*, 2017). Improved energy efficiency and uptake of renewable energy have been proposed to combat emissions, but a complete transition from fossil fuels to renewable energy is not feasible in the short-term. Therefore, carbon capture from industrial plants, *e.g.* as sodium bicarbonate ($NaHCO_3$) or calcium carbonate ($CaCO_3$), is projected to increase (IEA, 2011; Sanz-Pérez *et al.*, 2016).

Chapter 1: Introduction

One option of mitigating emissions is increased carbon capture and storage (CCS), which involves geological CO_2 storage by injecting it deep underground. However, the widespread application of this technology is limited by its cost as it is unprofitable and requires large capital investment (Styring *et al.*, 2011). Furthermore, CO_2 leakage rates are unclear, and injection may only be possible offshore in some countries, thus adding transportation costs (Cuéllar-Franca and Azapagic, 2015). Alternatively, carbon capture and utilization (CCU) is an attractive method of combating emissions because it offers a route to value-added products from CO_2. Instead of viewing CO_2 as a pollutant, it can be regarded as a C1 building block for generating chemicals and fuels. In comparison to CCS, utilization of CO_2 may be profitable as value-added products can be sold. Furthermore, CO_2 is potentially a renewable feedstock if obtained as an emission of existing industry (Yu *et al.*, 2008).

Due to its high thermodynamic stability, CO_2 conversion is a challenge that requires significant energy to overcome. Additional energy in the form of irradiation, electrons, heat or high energy co-reagents is often required. Activation of CO_2 on a catalyst surface can increase reaction rate, promote the production of selective products, and significantly improve yields (Álvarez, Borges, *et al.*, 2017). However, present methods of CO_2 conversion generally require the use of H_2 gas, which is currently produced primarily from methane steam reforming and results in the emission of 8.9 kg of CO_2 per kilogram of hydrogen (Centi, Quadrelli and Perathoner, 2013). By current estimates, hydrogen production is responsible for approximately 830 million tonnes of CO_2 emissions annually, which is equivalent to yearly emissions of UK and Indonesia combined (IEA, 2019b). Hydrogen-free processes commonly require complex catalysts or noble metals for high conversion efficiency, which lowers the overall sustainability of the process and compounds costs. Therefore, other methods must be explored.

A different, nature-inspired method of carbon dioxide conversion mimics conditions occurring around hydrothermal vents. Hydrothermal vents are found throughout the oceans and are hypothesised to have played a crucial role in the origin of life. At deep-sea vents, high temperature and pressure conditions cause water to exist in a sub-critical state where it exhibits properties different from those at ambient conditions. The potential to use sub-critical water as a both a solvent and hydrogen source in CO_2 conversion is attractive as it can overcome the high stability of CO_2 while removing the need for H_2 gas or noble metal catalysts.

Chapter 1: Introduction

In this system, a variety of feedstocks can be explored, such as CO_2 gas and solid CO_2 precursors. The potential advantages of using solid CO_2 pre-cursors are lower transportation costs and eliminated safety concerns associated with pressurised gases. Carbon dioxide can also be paired with earth abundant and low-cost co-reagents and catalysts to improve yields. Recently, biomass and its derivatives have been investigated as reductants for hydrothermal CO_2 conversion. This work focuses on the biomass-assisted, catalytic conversion of carbon dioxide and its precursors to value-added products.

1.1 AIM & OBJECTIVES

The aim of this work is to investigate catalytic hydrothermal conversion of carbon dioxide substrates to value-added products using biomass as a reductant. The following objectives will be met to achieve this:

1. Development of a model system with a sodium bicarbonate as a carbon dioxide precursor and glucose as biomass derivative to determine analytical methods, products, mechanism of conversion and conditions at which the desired product is maximised.
2. Investigation into non-noble metals as heterogeneous catalysts to enhance the conversion of CO_2 to value-added products.
3. Comparison of CO_2 precursors to determine the transferability of findings to systems with differing reagents.

A review of relevant literature on hydrothermal conversion of carbon dioxide and biomass, as well as metal catalysts was undertaken and summarised in Chapter 2. The fundamentals of analytical techniques are discussed in Chapter 3, followed by undertaken analytical method development in Chapter 4. The results of experimental work are found in Chapters 5-8. Final conclusions and recommendations for further work are presented in Chapter 9.

2 CHAPTER 2: LITERATURE REVIEW

In this section, the physical applications of CO_2 will be discussed, followed by current carbon capture technologies. Methods of chemically converting CO_2 to other products will then be examined. Hydrothermal conversion and the unique properties of sub-critical water will be covered and literature on CO_2 reduction with different metals and polymers discussed. Finally, hydrothermal liquefaction of biomass with CO_2 as a green acid, and reduction of CO_2 with biomass and derivatives will be reviewed.

2.1 PHYSICAL APPLICATIONS OF CARBON DIOXIDE

Carbon dioxide naturally occurs as a colourless, odourless gas at ambient conditions, and was first discovered in the 18th century by Joseph Black in the reaction of calcium carbonate with acid (Chetty *et al.*, 2019). In modern times, CO_2 is used in a variety of industries both for its physical properties and as a chemical reagent in new and established processes.

Carbon dioxide is a terrestrially occurring gas and can be obtained directly from natural wells. Currently, approximately 85% is commercially acquired as a by-product of processes such as ammonia production, fermentation, and petrochemical manufacturing, *e.g.* steam reforming (Vansant, 2003). After purification, CO_2 can be used in a variety of applications.

2.1.1 Enhanced Oil Recovery

Carbon dioxide finds major use in oil production as an agent in enhanced oil recovery (EOR). In primary oil production, oil escapes from an underground reservoir as pressure releases and dissolved gases expand. However, this method only extracts 5-20% of available oil and further removal requires injection of another fluid, *e.g.* CO_2 or water (Blunt, Fayers and Orr, 1993). In secondary production, pressurised CO_2 is injected into the reservoir to increase pressure to 10–30 MPa, resulting in oil dissolution and displacement. As the temperature of reservoirs is normally up to 110 ˚C (Blunt, Fayers and Orr, 1993), increased pressure makes oil miscible in CO_2, which increases crude oil density and reduces viscosity, thereby increasing mobility to the surface (Atia and Mohammedi, 2018). In this way, 10-20 % additional oil is obtained (Metz *et al.*, 2005). Globally, CO_2 for EOR application is the second largest

consumer of CO_2 after urea manufacture, and constituted 34 % of all demand for CO_2 in 2015 (IEA, 2019a).

2.1.2   Food & Beverage Industry

In 2015, the food and beverage industry each accounted for 3% of global demand for carbon dioxide (IEA, 2019a). In food processing, CO_2 is used in several applications, and one of the most widespread is as a refrigerant. Flash freezing of food products such as meat and baked goods using liquid CO_2 is carried out to prevent bacterial growth, maintain nutritional quality and prevent deterioration (George, 1993). Liquid CO_2 is also used to refrigerate food during prolonged transport, where deposition of CO_2 as snow on the surface of food provides additional chilling (Hunt *et al.*, 2010).

Supercritical food extraction (SFE) technology is a relatively recent application, where undesirable substances are removed by treating feed with supercritical CO_2 (scCO_2). The non-toxic nature of CO_2 when compared to other solvents, as well its lower density and viscosity when compared to water, make it a good solvent for applications such as decaffeination of tea and coffee (Chang *et al.*, 2000). This technology can be applied in essential oil extraction, production of hop extracts, recovery of flavours from spices, and others (Leeke, Gaspar and Santos, 2002; Ehlers *et al.*, 2006; Zeković, Pfaf-Šovljanski and Grujić, 2007).

A further use of CO_2 in the food industry is in modified atmosphere packaging (MAP). MAP involves introducing CO_2 and other inert gases to food packaging to decrease oxidative damage to food flavour and reduce microbial growth, resulting in longer shelf-life (Taniwaki *et al.*, 2009). Perishables, such as fruit and vegetables, are thus protected by slower ripening during prolonged transport (Yahia, 2009). This curbs the need for preservatives, reduces food waste and extends the range of products that can be made available worldwide (Vansant, 2003).

In the beverage industry the bacteria-inhibiting effects of CO_2 are exploited by dissolving the gas into solution. Dissolved CO_2 has antimicrobial action and acidifies drinks (Ravindra *et al.*, 2014). In this way the shelf life of milk, yoghurt and other dairy products is prolonged (Karagül-Yüceer *et al.*, 1999; Hotchkiss, Werner and Lee, 2006). However, the dominant use of CO_2 in the beverage industry is in soft drink carbonation, which gives a sparkling appearance and sharpens the flavour (Kregiel, 2015). The importance of CO_2 in the beverage industry is substantial, with the global business worth upwards of US $300 billion (Hunt *et al.*, 2010).

2.1.3   Supercritical CO_2

In addition to application in extraction, supercritical CO_2 is used as an industrial solvent in the pharmaceutical and fine chemical industries. Supercritical CO_2 is obtained beyond its critical point of 31°C and 73.8 bar, at which point viscosity and density increase and different properties are observed (Figure 2-1) (Hunt *et al.*, 2010).
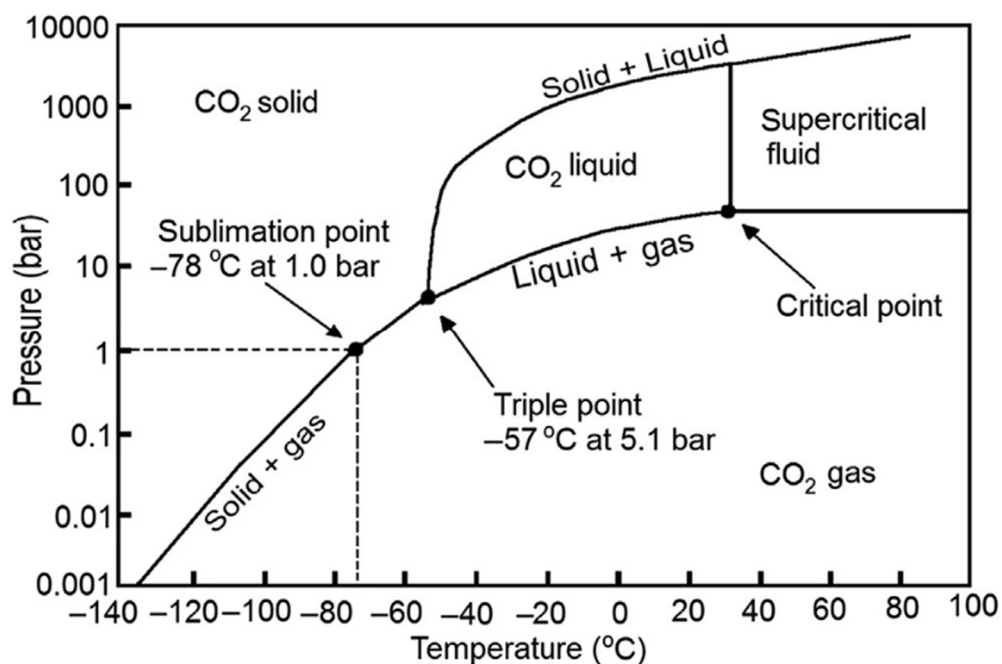
Figure 2-1 Phase diagram of CO_2 (North, 2015)

Conventional solvents are often the main source of waste in a process, and require costly and hazardous disposal by incineration (Jiménez-González, Constable and Ponder, 2012; North, 2015). Supercritical CO_2 does not leave residues and can be vented to the atmosphere after use. Vaporisation of non-volatile substances for contamination removal from process streams can also be carried out with supercritical CO_2 (Vansant, 2003). Polarity can be altered by varying density, which makes $scCO_2$ a good solvent for a wide range of organic chemicals as well as gases like H_2 and O_2 (North, 2015). Finally, supercritical CO_2 can act as a modifier when combined with other solvents, producing a gas-expanded liquid which can have different properties than the original solvent (Jessop and Subramaniam, 2007). For example, in a $scCO_2$-H_2O solvent mixture the formation of carbonic acid reduces pH below 3, enhancing organic reactions (Toews *et al.*, 1995).

The physical properties of carbon dioxide are exploited in numerous other industries, such as agriculture, metalworking, plastic and rubber processing and fire suppression. However, further in-depth description of these applications is beyond the scope of this work. Furthermore, the future scale of CO_2 gas use is uncertain and is expected to remain small in the short term (IEA, 2019a). In order to meet GHG emission reductions, short-term strategies of CO_2 mitigation are being considered, chief among them widespread implementation of carbon capture.

2.2 CARBON CAPTURE TECHNOLOGIES

Carbon capture is an invaluable method of preventing CO_2 expulsion to the atmosphere and can potentially reduce 85–90 % of emissions from large point sources (Leung, Caramanna and Maroto-Valer, 2014). There are three main technologies of carbon capture: pre-combustion, post-combustion, and oxyfuel combustion. Pre-combustion capture is typically used when the feedstock is syngas, CO and H_2, or natural gas. The advantage of pre-combustion capture is higher concentrations of CO_2 (>20 vol%) and easier separation from H_2 in comparison to other gas mixtures (Rackley, 2017). However, pre-combustion capture is limited in application to integrated gasification combined cycle (IGCC) plants, and not conventional coal- or natural-gas fired energy plants (Samanta *et al.*, 2012). On the other hand, oxyfuel combustion can be applied to coal- and natural gas-fired plants. In this method, fuel is burned in an O_2 atmosphere, producing a flue gas composed of CO_2 and H_2O. Water vapour can easily be removed by condensation, resulting in pure CO_2 (Theo *et al.*, 2016). Although this technology is robust and simple to retrofit, it is hindered by high capital costs associated with separating oxygen from air (Sanz-Pérez *et al.*, 2016).

Finally, post-combustion CO_2 is captured from flue gas. A key advantage of post-combustion is that it can be retro-fitted to existing infrastructure and is applicable to a wide variety of industries (Bonaventura *et al.*, 2017). However, there is generally a lower CO_2 concentration of 5–15 vol % after combustion which makes separation more challenging (Sanz-Pérez *et al.*, 2016). In comparison to pre-combustion capture, CO_2 and N_2 are more difficult to separate (Rackley, 2017). Therefore, a variety of separation technologies have been developed.

Chapter 2: Literature Review

2.2.1   Post-combustion CO_2 Separation Methods

2.2.1.1   Chemical Solvents

Solvents such as ionic liquids, alkaline solutions, and amines have been extensively investigated as separation agents. Current large-scale post-combustion capture technology mainly involves the use of regenerable solutions containing amines, such as monoethanolamine (MEA) or diglycol-amine (DGA), to separate CO_2 from other gases (Samanta *et al.*, 2012). In this method, exhaust gases pass through an absorber column where solution flows downwards, allowing CO_2 to react with the amine. The CO_2-rich amine solvent can then be heated to reverse the reaction and free pure CO_2 and recycle the solution (Zhang *et al.*, 2014). Although this technology has already been fitted to existing plants, widespread commercialisation is limited by corrosion and toxicity issues, as well as high solvent costs (>1000 €/tonne) (Gjernes, Helgesen and Maree, 2013; Bonaventura *et al.*, 2017).

Alkaline solvents, such as aqueous sodium hydroxide (NaOH), capture CO_2 non-reversibly, forming sodium carbonate (Na_2CO_3) in the Solvay process (Equation 2-1).

Equation 2-1 Carbon capture of carbon dioxide with sodium hydroxide

$$CO_2 + 2NaOH \rightarrow Na_2CO_3 + H_2O$$
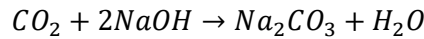
Addition of further CO_2 results in further transformation to $NaHCO_3$. Sodium hydroxide has a higher theoretical adsorption capacity (0.9 t/tCO_2) in comparison to MEA (1.39 t/tCO_2) (Yoo, Han and Wee, 2013). Calcium hydroxide, $Ca(OH)_2$, in aqueous solution is also an effective capture solvent which forms calcium carbonate ($CaCO_3$) upon reaction (Equation 2-2).

Equation 2-2 Carbon capture of carbon dioxide by calcium hydroxide

$$Ca(OH)_2 + CO_2 \rightarrow CaCO_3 + H_2O$$
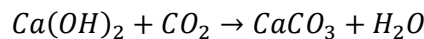
Calcium carbonate can potentially be reclaimed or disposed of more economically than CO_2 gas due to the costs of liquefaction and transportation (Han *et al.*, 2011). Furthermore, both NaOH and calcium are currently more earth-abundant and economical than amines, though corrosion and regeneration issues are presently significant hindrances to widespread application (Yoo, Han and Wee, 2013).

2.2.1.2 Solid Sorbents

Capture sorbents are materials capable of performing both adsorption and desorption and can be physical (physisorbents) or chemical (chemisorbents) in nature (Patel, Byun and Yavuz, 2017). On physisorbents, CO_2 adsorbs on the surface selectively by Van der Waals attractions, pole-ion and pole-pole interactions (Samanta *et al.*, 2012). Many materials, including metal-oxide frameworks (MOFs), zeolites, mesoporous silica, and carbonaceous materials exhibit the qualities of physisorbents. However, at low CO_2 partial pressures that may be encountered post-combustion, most physisorbents are hindered by low adsorption capacities due to competitive binding with H_2O and low selectivity (Patel, Byun and Yavuz, 2017).

Chemisorbents rely on the interaction between the electrophilic carbon of CO_2 with nucleophilic functional groups present on the sorbent surface (Goeppert *et al.*, 2014). For example, amine-functionalised solid sorbents exhibit the characteristics of organic amines, and can be applied to a range of supporting materials. Carbonaceous, zeolite-based, polymer-based, and silica-supported amine capture agents are well documented (Samanta *et al.*, 2012). Of particular note are amine-functionalised silica-supported capture agents, which meet the desired working capture capacity of 3-4 mmol CO_2 g^{-1} sorbent (Hicks *et al.*, 2008). However, stability issues in the presence of moisture, as well as long-term stability and reusability must still be addressed.

An alternative approach employs alkali-metal carbonates. Alkali-metal carbonates adsorb CO_2 in a carbonation process occurring at 60-110 ℃, and can then be heated to 200 ℃ to regenerate the carbonate and release pure CO_2 (Samanta *et al.*, 2012). For example, in the Dry Carbonate Process Na_2CO_3 reacts with CO_2 to form sodium bicarbonate ($NaHCO_3$) at mild temperatures up to 100 ℃ (Equation 2-3) (Nelson *et al.*, 2009). Increasing temperature to 120-140 ℃ regenerates Na_2CO_3 and releases CO_2.

Equation 2-3 Formation of sodium bicarbonate from reaction of sodium carbonate with carbon dioxide

$$Na_2CO_3 + CO_2 + H_2O \leftrightarrow 2NaHCO_3$$
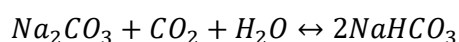
Other alkali metal carbonates such as potassium (K_2CO_3) or lithium carbonate (Li_2CO_3) have been shown to be effective as well (Hayashi *et al.*, 1998). This technology has several notable advantages, such as high CO_2 capture capacity of

approximately 9.43 mmol CO_2 g^{-1} Na_2CO_3, favourable reaction temperatures and relatively low costs (Feng, An and Tan, 2007; Samanta *et al.*, 2012). However, corrosiveness poses a serious operational and safety concern.

Conversion of CO_2 to carbonates can be achieved with mineral carbonates such as calcium oxide, CaO, or magnesium oxide, MgO. Interestingly, alkaline-earth oxides naturally occur in the earth's crust in quantities that exceed the amount required to fix all the CO_2 that would be produced by the combustion of all available fossil fuels (Metz *et al.*, 2005). The process known as carbonation occurs at temperatures over 600 ℃ and requires >900 ℃ for CaO regeneration (Equation 2-4).

Equation 2-4 Capture of carbon dioxide by calcium oxide to form calcium carbonate

$$CaO + CO_2 \leftrightarrow CaCO_3$$
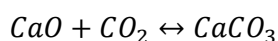
High adsorption capacity, low raw material costs, fast kinetics and established industrial applications are key advantages of mineral oxide capture (Theo *et al.*, 2016). Additionally, the high stability of $CaCO_3$ allows it to be stored for long periods of time or utilised in construction. However, mining and milling of mineral ores may have detrimental environmental effects similar to those of conventional mining (Metz *et al.*, 2005). Fast deactivation and requirement of CaO replacement are another significant disadvantage hindering widespread application (Theo *et al.*, 2016).

While carbon capture is an important and essential technology for mitigating CO_2 emissions, improvement of existing processes and development of novel ones is crucial to create a circular economy with markets for CO_2-derived products (IEA, 2019a). The conversion of CO_2 to value-added products is therefore attracting significant interest worldwide.

2.3 CHEMICAL APPLICATIONS OF CARBON DIOXIDE

Theoretical screening has shown that the production of chemical intermediates and, especially, fuels from CO_2 has the largest potential of scale-up and climate benefits in future (IEA, 2019a). Currently, Carbon dioxide is used in urea and methanol synthesis, but development of new conversion processes is required to attain other value-added chemicals. However, due to the low free energy of CO_2, its use as a feedstock faces several major obstacles.

Generally, reactions with CO_2 encounter two problems: the high stability of the starting material and an activation energy barrier. Molecularly, CO_2 is a triatomic linear molecule composed of a central carbon atom covalently bonded through a σ- and π-bond to two oxygen atoms with a bond length of 116.3 pm (North, 2015). Due to the more electronegative oxygen atoms carrying a partially negative charge, the reactivity of CO_2 is dominated by the reaction of nucleophiles, such as amines, with the partially positive central carbon atom.

Carbon dioxide is thermodynamically stable, with a low Gibbs free energy ΔG^0 = -394 kJ mol^{-1} (Chetty *et al.*, 2019). Although it is commonly stated that CO_2 is unreactive, in fact reactions where a co-reagent can supply sufficient energy, such as a hydroxide, amine or alkene, can occur even at standard conditions (Alper and Orhan, 2017). Furthermore, some products of CO_2 reactions, such as mineral carbonates, have a considerably lower free energy, *e.g.* ΔG^0_{CaCO3} = −1130 kJ mol^{-1} (Song, 2006). Therefore, consideration of the reactivity of CO_2 is important in process development.

Most industries utilising carbon dioxide as a reagent are well established, with both urea synthesis and salicylic acid production developed by the end of the 19th century (Vansant, 2003). Thus, groundwork in newer techniques, such as photochemical and electrochemical conversion, must be set now for competitive introduction in the future.

2.3.1   Existing Industrial Routes

Markets for carbon dioxide as a reagent in several major manufacturing processes currently exist worldwide. By far the greatest industrial usage of CO_2 is in urea production, where it reacts with synthetic ammonia at approximately 190 ℃ and 200 MPa (Alper and Orhan, 2017). In methanol synthesis, CO_2 is fed as an additive to react with extra H_2 present in the stream (Deutschmann *et al.*, 2011). Sodium salicylate is produced by the Kolbe-Schmitt reaction between CO_2 and sodium phenolate in the first step of aspirin synthesis (Lindsey and Jeskey, 1957). In the synthesis of carbonates, CO_2 reacts exothermically with epoxides to produce either cyclic or straight chain carbonates depending on the type of catalyst used (North, 2015). When analysing the production versus use of CO_2 in its major chemical applications, it is immediately apparent that production greatly outweighs use (Table 2-1). Thus, improving carbon economy in current processes and further application of CO_2 as a feedstock are essential to improve sustainability.

Chapter 2: Literature Review

Table 2-1 Annual production of chemicals from CO_2 in 2010 (Adapted from North, 2015, and Alper and Orhan, 2017)

Chemical	Annual Production (tonne)	Annual CO_2 use as feedstock (tonne)
Urea	157,000,000	112,000,000
Methanol	100,000,000	2,000,000
Salicylic acid	90,000	30,000
Cyclic carbonates	80,000	40,000

Converting CO_2 to other C_1 molecules is a challenging but appealing route. For example, reduction to formic acid (HCOOH) has attracted a great deal of investigation as an atom economic reaction which yields a versatile platform chemical (Kabra *et al.*, 2016). Due to the higher energy of other C_1 molecules, with the exception of carbonates, in comparison to CO_2, conversion is not straight-forward (Table 2-2). Strong carbon-oxygen bonds make the CO_2 molecule very stable, while weaker carbon-hydrogen bonds of other C_1 molecules increase their relative energy. Therefore, for a reaction to occur, external energy in the form of high free-energy co-reactants, heat, electrons or irradiation is required (Alper and Orhan, 2017).

Table 2-2 Free energy of C1 molecules relative to carbon dioxide (Adapted from Alper and Orhan, 2017)

C_1 molecule	Gibbs free energy ($kJ\ mol^{-1}$)
Carbon dioxide	-394
Formic acid	-361
Methanol	-166
Carbon monoxide	-137
Formaldehyde	-102
Methane	-51

Catalysis may be key to obtaining workable yields of selective products. The basis of metal-catalysed reactions of CO_2 is the coordination of carbon dioxide to metals, which can have a significant impact on the electron distribution and molecular geometry, thus radically changing its reactivity (North, 2015). Thus, although

homogeneous catalysis can be used, heterogeneous catalysts are generally favoured due to convenient handling, easier separation, and established reactor design principles (Alper and Orhan, 2017).

With the addition of external energy and catalysis, highly valuable platform chemicals can thus be obtained from CO_2. Formic acid is used in agriculture, pharmaceuticals, textiles, leather tanning, and, recently, as a hydrogen carrier in fuel cells (Hietala et al., 2016; Pérez-Fortes et al., 2016). It is also a viable hydrogen storage compound due to its decomposition to CO_2 and H_2 which has the advantage of being liquid and easier to transport than gaseous compounds (Álvarez, Bansode, *et al.*, 2017). Methanol (CH_3OH) is a raw material used in the production of formaldehyde, methyl *tert*-butyl ether (MTBE), acetic acid, and other substances. Methane (CH_4) can be used in energy generation and as a precursor to H_2 gas (Skorek and Włodarczyk, 2018).

Unfortunately, current industrial methods of producing the abovementioned C_1 molecules are heavily reliant on fossil fuels and unsustainable long-term. The main industrial method of formic acid synthesis is fossil fuel-based and involves reacting methanol with CO to form methyl formate, which is then hydrolysed to the product (Chen, Liu and Wu, 2020). Methanol is primarily synthesised from syngas, currently overwhelmingly synthesised by steam reforming of methane (Lange, 2001). Methane is a principal component of natural gas, a non-renewable fossil fuel (Pegov, 2008). Therefore, alternative routes to C_1 molecules, including hydrogenation, photochemical and electrochemical conversion, are drawing increased attention.

2.3.2   Hydrogenation

Hydrogenation involves the use of hydrogen gas to reduce a given species to products such as methanol or hydrocarbons. Methanol is synthesised by reacting syngas over a $Cu/ZnO/Al_2O_3$ catalyst, first by water-gas shift (WGS) to form CO_2, followed by hydrogenation (Equations 2-5, 2-6) (Deutschmann *et al.*, 2011). It should be noted that generally reactions with CO_2 involve initial dissociation to CO and O, followed by further conversion of CO. In the case of methanol synthesis, CO_2 is the species undergoing hydrogenation.

Equation 2-5 Water-gas shift reaction

$$CO + H_2O \rightarrow H_2 + CO_2$$
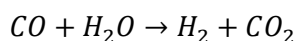
Chapter 2: Literature Review

Equation 2-6 Hydrogenation of carbon dioxide to methanol

$$CO_2 + 3H_2 \rightarrow CH_3OH$$
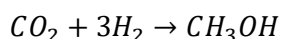
The majority of syngas is obtained from methane, which produces three moles of H_2 per mole of CO, so CO_2 is added to react with excess H_2. As CO_2 is the species undergoing hydrogenation, there is clear advantage in using it directly as a feedstock in methanol production. However, a significant challenge is the competitive reverse water-gas shift reaction (RWGS), which consumes H_2 and lowers methanol yield (Equation 2-7) (Alper and Orhan, 2017). To overcome this, a highly selective catalyst is required.

Equation 2-7 Reverse water-gas shift reaction

$$CO_2 + H_2 \rightarrow CO + H_2O$$
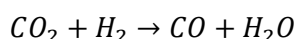
Hydrogenation of CO_2 to hydrocarbons may potentially provide a direct route to fuel and aromatic compounds. Direct conversion of CO_2 to hydrocarbons is difficult due to the high C-C bond coupling barrier and CO_2 stability. Methanation of CO_2 can supply clean energy by providing a route of CO_2 recycling, but requires noble metal catalysts for acceptable selectivity and yield (Qin *et al.*, 2017). Recently a promising method of direct CO_2 hydrogenation to gasoline-range hydrocarbons was reported (Wei *et al.*, 2017). Indirect conversion is another option, which involves CO_2 transformation to methanol or CO, followed by separate transformation to hydrocarbons. For example, RWGS to CO can be followed by a modified Fischer-Tropsch synthesis (Yang *et al.*, 2017).

Farlow and Adkins first reported hydrogenation of CO_2 to formic acid using H_2 and Raney Ni catalyst (Farlow and Adkins, 1935). A large number of homogeneous iridium and ruthenium complexes, as well as Pd and Au heterogeneous catalysts have been investigated in this reaction (Álvarez, Bansode, *et al.*, 2017). However, due to the high thermodynamic stability of CO_2, gas-phase hydrogenation to liquid formic acid, HCOOH, is difficult and entropically unfavourable ($\Delta G^0 = +33$ kJ mol^{-1}) (Moret, Dyson and Laurenczy, 2014). Reactive, high free energy substances, such as H_2, are required (Shen, Zhang and Jin, 2012). The requirement for H_2 is a major limitation of hydrogenation. Currently, most hydrogen gas is produced from fossil fuel sources and results in the release of large quantities of CO_2 by-product. Approximately 8.9 kg of CO_2 are produced per kg H_2 from methane reforming (Centi, Quadrelli and

Perathoner, 2013). Thus, techniques that do not require the use of H_2 gas are preferable.

2.3.3 Photochemical Conversion

Photochemical conversion is an emerging technique that shows great potential. The method is inspired by plant photosynthesis, where CO_2 fixation is the first step in organic chemical production. In photosynthesis, CO_2 reduction occurs simultaneously to H_2O oxidation as a charge-balancing reaction. In this method light is used to excite semiconductor photocatalysts, producing electron-hole pairs that reduce CO_2 to organic chemicals (Lingampalli, Ayyub and Rao, 2017). When the energy of incident light is equal to or greater than the band gap of the photocatalyst, electrons are excited from the valence to the conduction band, generating free electrons that have strong reducing abilities (Inoue *et al.*, 1979). This method is favourable because sunlight is an abundant resource, no additional auxiliary energy is required, and mild conditions can be used (Su *et al.*, 2016).

Carbon dioxide does not absorb light between 200 and 900 nm, and therefore a suitable photocatalyst is required. Semiconductors such as metal oxides (TiO_2, ZnO, CdO) or sulphides (CdS, ZnS) are ideal materials for photocatalysis due to the proximity of the conduction and valence band in their structure (Lazar, Varghese and Nair, 2012).
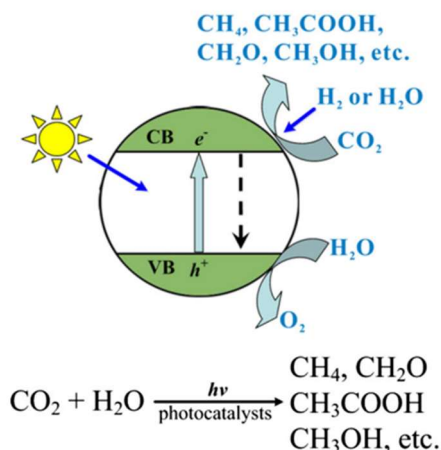
Figure 2-2 Photocatalytic reduction of CO_2 from (Su et al., 2016)

A schematic representation of the photocatalytic reduction of CO_2 on semiconductors is shown in Figure 2-2. This occurs through the following stages (Lingampalli, Ayyub and Rao, 2017):

1. Adsorption of CO_2 on the semiconductor surface
2. Absorption of light by the semiconductor
3. Formation of electron-hole pair
4. Migration of electron-hole pair to the semiconductor surface
5. Redox reaction at surface involving CO_2 reduction coupled with oxidation of second substance, *e.g.* H_2O
6. Desorption of products

However, several major disadvantages prohibit the technology from being implemented. Low efficiency, recombination of electrons and holes, and large band gaps in most commonly used photocatalysts require further catalyst development (Nahar *et al.*, 2017). Furthermore, metal doping, particularly by noble Pt and Au, is required for higher product yields (Su, Yang, Yang, *et al.*, 2015).

2.3.4 Electrochemical Conversion

Electrochemical reduction is another potential route for CO_2 reduction. In it, reaction occurs in an electrolyser typically composed of two chambers, each housing an electrode and separated by an ion-conducting membrane. A current is passed through the cell, resulting in water oxidation to O_2 at the anode and CO_2 reduction at the cathode (Lu and Jiao, 2016). Bulk metals have been widely investigated as electrocatalysts, particularly Au, Ag, Pt and Ni.

There are several advantages to this technique. Reactions can be conducted at ambient conditions and rate controlled by altering the external bias. The products of the reaction are inherently separated by formation at separate electrodes, which eliminates the need for post-reaction separation (Lu and Jiao, 2016). A range of different reduced species can be produced depending on the electrocatalyst used, *e.g.* Au and Ag favour CO production, while Sn, In, and Pb favours formate (Olajire, 2013). Recently investigations have shown that other materials such as nanostructured metallic, ion-modified metallic, and non-metallic materials are also promising materials (Lu and Jiao, 2016).

A major drawback of these systems is the requirement for noble metal electrodes, slow electron transfer kinetics, and low energy efficiency (Sun *et al.*, 2017). Similar redox potentials for numerous reduction products also often result in selectivity issues. In aqueous solution the hydrogen evolution reaction at the cathode not only competes with CO_2 reduction but also poses serious safety issues (Lu and Jiao, 2016).

2.4 HYDROTHERMAL CONVERSION

Recently, a new route of carbon dioxide reduction inspired by deep-sea hydrothermal vents has arisen. First confirmed in the late 1970s by oceanographers, hydrothermal vents are found along mid-ocean ridges, rift arcs and at underwater volcanoes (Crane and Normark, 1977; Tivey, 2007). The mineral and metal composition of vents varies depending on location. Extreme conditions – up to 450 °C and 60 MPa, low oxygen concentration, high acidity and high concentrations of reduced species – make this environment seemingly unfriendly to life; nevertheless an ecosystem thrives (Galkin and Demina, 2016; Li *et al.*, 2018). A widely proposed hypothesis is that primordial life may have originated around hydrothermal vents. Abiotic methane and organic species formed from dissolved CO_2 at vent interfaces may have been sources of energy for bacteria and contributed to fossil fuel accumulation (McCollom and Seewald, 2001).

On the laboratory scale, the conditions around hydrothermal vents are mimicked to attain sub-critical water that can be used as a medium for chemical conversions (Matsuno, 2016). In comparison to other CO_2 reduction methods, water is employed both as an environmentally benign solvent and as a source of hydrogen in hydrothermal conversion, thus avoiding the need for H_2 gas (Yang *et al.*, 2019). The unique properties of sub-critical water are the key to achieving high conversion efficiency in hydrothermal CO_2 conversion (Toor, Rosendahl and Rudolf, 2011).

2.4.1 Properties of sub-critical water

For the purpose of this work sub-critical water is defined as water above its boiling point at ambient pressure (>100 °C and 1 bar) and below its critical point of 374 °C and 221 bar (Möller *et al.*, 2011). The term high temperature water (HTW) applies to water over 200 °C. The properties of sub-critical water differ greatly from that of ambient water (Table 2-3).

Table 2-3 Properties of sub-critical water in comparison to water at ambient conditions (Adapted from Möller *et al.*, 2011; Toor, Rosendahl and Rudolf, 2011)

Property	Ambient Water (25 °C, 0.1 MPa)	Subcritical Water (250-350 °C, 5-25 MPa)
Dielectric constant ($F\ m^{-1}$)	78.5	27.1-14.07
Ionic product pK_w	14.0	11.2-12.0
Density ($g\ cm^{-3}$)	1	0.80-0.60
Viscosity (mPa s)	0.89	0.11-0.064

A decrease in dielectric constant increases the solubility of hydrophobic substances like free fatty acids and gases (Toor, Rosendahl and Rudolf, 2011). An increase in the water ionic product means high levels of H^+ and OH^- are present and acid- and base-catalysed reactions are accelerated. Density decreases, so ionic reactions like carbohydrate dehydration and alcohol splitting dominate (Toor, Rosendahl and Rudolf, 2011). A large decrease in viscosity accelerates diffusion, increasing the rate of mass-transfer limited reactions (Kruse and Dinjus, 2007). Organic reactions, such as pinacol rearrangements, hydrolysis, and hydrogen exchange reactions have been reported to proceed near quantitatively in HTW without the need for heterogeneous catalysts (Kuhlmann, Arnett and Siskin, 1994). Therefore, combined properties of sub-critical water make it a clean, favourable medium for rapid CO_2 conversion.

2.4.2   Solubility of CO_2 in Water

The dissolution of CO_2 in ambient water is dependent on its partial pressure and the interaction of dissolved CO_2 with other species in solution (Butler, 1991). The solvent choice is critical, with certain species, such as hydroxyls, inhibiting absorption and others, such as ethers, promoting it (Gui, Tang and Fei, 2011). The solubility of CO_2 in several solvents is shown in Table 2-4. Although methanol contains the CO_2-phobic hydroxyl group, at standard conditions it is a better solvent than water due to its decreased polarity (Miller *et al.*, 2011). Furthermore, the addition of base KOH greatly increases the solubility of CO_2.

Table 2-4 Solubility of CO₂ in Solvents at Standard Conditions (Chetty et al., 2019)

Solvent	Solubility ($mol\ l^{-1}$)
Water	0.033
Methanol	0.194
KOH/Methanol	0.677

Carbon dioxide dissolution is highly pH dependent, with certain species dominating in solution depending on conditions. At pH < 5, CO_2 concentration can be expressed in terms of Henry's Law, where K_H is Henry's law constant (Equation 2-8).

Equation 2-8 Henry's Law for carbon dioxide concentration in solution

$$[CO_2] = K_H P_{CO_2}$$

In low pH water, a small portion of CO_2 is hydrated to carbonic acid, H_2CO_3, and CO_2 is the dominant species (Figure 2-3). At mildly alkaline conditions, bicarbonate (HCO_3^-) is the most prevalent free species in solution while increasingly more alkaline pH favours the formation of carbonate, CO_3^{2-} (Butler, 1991). In this way, the nature of dissolved CO_2 can be manipulated by changing the pH of the water medium. It has been reported that hydrogenation of bicarbonates to formates is more facile than that of carbonates (Álvarez, Bansode, *et al.*, 2017). For example, Su and co-workers found that in reactions in aqueous phase under CO_2 pressure, HCO_3^- appeared to be the substrate converted to formic acid (Su, Yang, Lu, *et al.*, 2015).
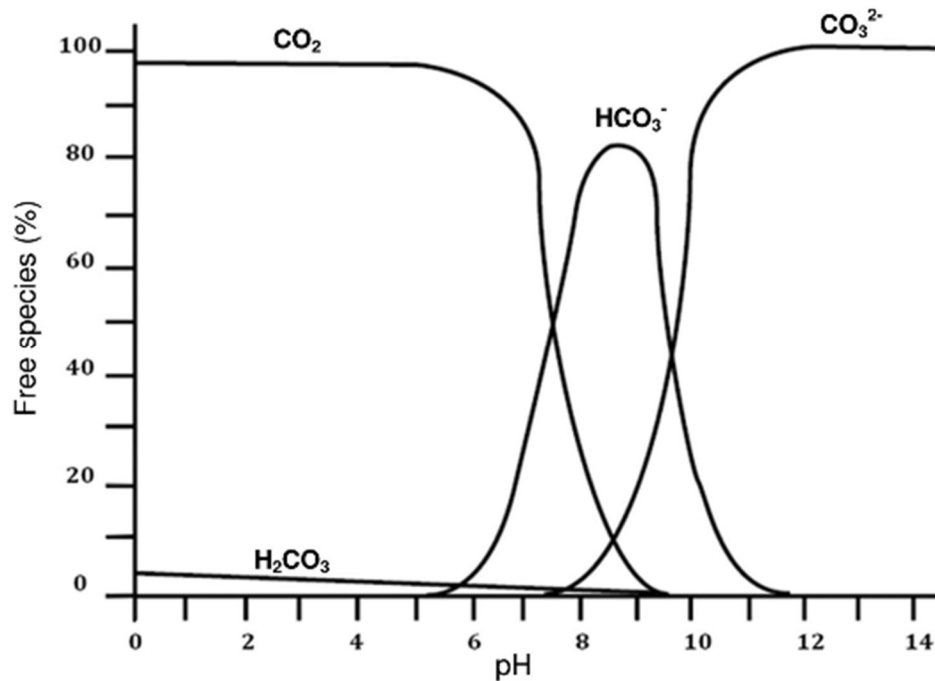
Figure 2-3 Fraction of dissolved carbon dioxide, carbonic acid, bicarbonate and carbonate in water as a function of pH (Chaix, Guillaume and Guillard, 2014)

It is well-known that the solubility of gases in water generally greatly reduces with increasing temperature (Takenouchi and Kennedy, 1964). However, for each gas a minimum solubility can be reached after which solubility increases, *e.g.* for CO_2 solubility begins to increase around 150 ℃ (Figure 2-4) (Hunter and Savage, 2008). For this reason, CO_2 reactions in water are more favourable at higher temperatures, as increased solubility can be attained.
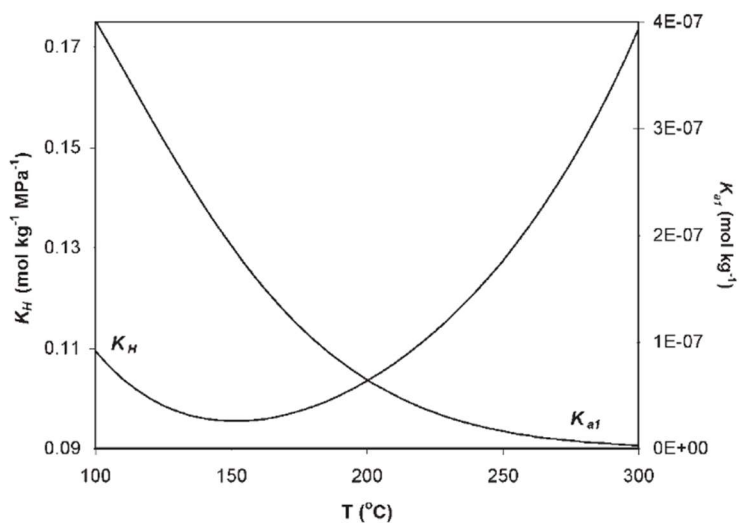
Figure 2-4 Solubility of CO₂ in water, K_H, and first ionization constant of carbonic acid, K_{a1} (Hunter and Savage, 2008)

In addition to sub-critical water being a favourable medium in which to overcome the high stability of CO_2, reduction to HCOOH significantly more favourable in aqueous phase than in the gas phase (ΔG^0= -4 kJ mol^{-1}) (Moret, Dyson and Laurenczy, 2014). Carbon dioxide conversion to formic acid is an equilibrium reaction (Equation 2-9).

Equation 2-9 Aqueous hydrogenation of carbon dioxide to formic acid

$$CO_{2(aq)} + H_{2(aq)} \leftrightarrow HCOOH_{(aq)}$$
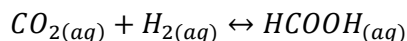
To disturb the equilibrium and make the transformation feasible, a secondary interaction is necessary. For example, esterification of HCOOH with methanol to form methyl formate, reactions with amines to produce formamide, or neutralization with week bases or alkali/alkaline earth bicarbonates prevent the decomposition of HCOOH (Álvarez, Bansode, *et al.*, 2017).

Therefore, hydrothermal conversion offers distinct advantages over alternative CO_2 conversion methods. Furthermore, by employing weakly alkaline conditions, formic acid degradation to CO_2 may potentially be prevented.

2.5 EVOLUTION OF LIFE ON EARTH STUDIES

Early studies on hydrothermal vents focused on their role in the origin of life. Hydrothermal chimneys are composed primarily of sulphides and iron, nickel and cobalt minerals (Roldan *et al.*, 2015; He *et al.*, 2019). Iron-bearing minerals are

abundant on the ocean floor and were proposed to act as reductants for CO_2 to hydrocarbons and other organic species (McCollom and Seewald, 2001). As such, a large number of studies have focused on the role of iron-bearing minerals on the conversion of carbon dioxide to organic species.

A number of origin of life studies on hydrocarbon generation from carbon dioxide have been carried out. The reduction of CO_2 to short hydrocarbons during the serpentisation of olivine at 300 °C and 500 bar was carried out by Berndt and co-workers (Berndt, Allen and Seyfried, 1996). The reduction of carbon dioxide to C_1-C_4 in brine at ambient conditions hydrocarbons by zerovalent Fe was then reported (Hardy and Gillham, 2002). Chen and Bahnemann demonstrated that in the presence of magnetite, Fe_3O_4, CO_2 can be reduced to organic molecules including acetaldehyde, ethanol and acetic acid (Chen and Bahnemann, 2000) or even phenol (Chen and Qian, 2001).

Origin of life studies have also been carried out with iron combined with metals found around hydrothermal vents. In a study on abiogenic methane formation from bicarbonate and H_2 gas, Horita and Berndt found that Ni-Fe catalysts catalyse the formation of CH_4 under hydrothermal conditions (Horita and Berndt, 1999). The activity of cobalt-bearing magnetite was explored by Ji and co-workers. Hydrocarbons of ranges C_1-C_5 were obtained at 300 °C and 300 bar, indicating that the addition of other transition metals in reactions with Fe_3O_4 could enhance yields of organic species (Ji, Zhou and Yang, 2008).

Recently, He *et al.* reported CO_2 reduction with metal sulphide catalysts using hydrogen sulphide, H_2S, which is present in large concentrations in deep-sea vents. It was found that Ni_3S_2 significantly increased yields of formate, $HCOO^-$, obtained in the reaction and yields up to 67.3 % from initial $NaHCO_3$ were obtained (He *et al.*, 2019). As H_2S fumes are produced as a by-product from numerous industrial processes, the use of a waste substance significantly increases the applicability of the process. The results of evolution of life studies have led to increased research into the individual activities of transition metals on CO_2 hydrothermal reduction.

2.6 Hydrothermal Carbon Dioxide Reduction with Metals

2.6.1 Iron

Origin of life studies demonstrated that iron is active in CO_2 conversion to a range of products. Iron catalysts are an attractive option as they are economical and abundant on the ocean floor. Coupled with CO_2, Fe behaves as a sacrificial metal catalyst.

Iron nanoparticles (NP) were tested by He and colleagues in hydrothermal CO_2 gas reduction to formic acid at 200 ℃ (He *et al.*, 2010). After 72 hours, a maximum yield of 8.5 mmol L^{-1} HCOOH was obtained. It was proposed that Fe reacts with H_2O to produce H_2, which then reacts with adsorbed CO_2 to produce a formate intermediate. However, it should be noted that a Fe-H intermediate was not detected, and the main metallic product was $FeCO_3$. In a follow-up study, a single product CH_4 yield of 1.96 mol% from CO_2 gas was obtained after 72 hours (Liu *et al.*, 2013). Smaller nanoparticles formed solely CH_4 as a product rather than a range of organic substances. In the absence of Fe, no CH_4 was obtained. The formation of CH_4 from $NaHCO_3$ with Fe was proposed by Jin and co-workers (Equation 2-10) (Zhong, Yao, *et al.*, 2019).

Equation 2-10 Iron-catalysed hydrothermal reduction of bicarbonate to methane

$$NaHCO_3 + 3Fe + 2H_2O \rightarrow CH_4 + Fe_3O_4 + NaOH$$
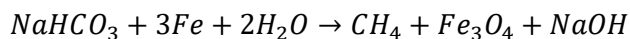
Reduction of CO_2 to HCOOH is more favourable in aqueous solution than gas. Furthermore, it has been shown that hydrogenation is favourable in basic media where the main reactant is bicarbonate, HCO_3^-, or carbonate, CO_3^{2-} (Laurenczy, Joo and Nadasdi, 2000). The use of a basic reaction medium is therefore advantageous. Carbon capture agents containing bicarbonate or carbonate generate alkaline solutions while also acting as a CO_2 source, making them highly beneficial.

In a two-step conversion of $KHCO_3$ to formate over zerovalent iron, Michiels *et al.* generated H_2 using Fe in the first step, followed by CO_2 reduction to HCOOH in the second step. The degree of water filling was found to have a direct effect on the quantity of initial H_2, generated, which subsequently increases carbon conversion. As such, a 50% fill shown to be optimal. It was found that high solubility of H_2 is essential to achieving high carbon conversion rates, and indeed a high conversion of 77.9 wt % carbon was achieved.

Recently, the conversion of CO_2 gas cyclic ketones, aromatics and linear oxygenates in the absence of H_2 was reported (Gomez *et al.*, 2020). Notably, iron particles on different support materials showed remarkably different activities, with longer chained products observed with Fe/Al_2O_3 in comparison to bulk iron. This indicates that the presence and nature of the support material plays a crucial role in the product formed from CO_2 reduction.

In hydrothermal carbon dioxide conversion, iron is observed to behave as a sacrificial metal, as a change in its oxidation state from zerovalent Fe to FeO/Fe_3O_4 is commonly observed (Zhong *et al.*, 2010). As such, it has frequently been utilised as a reductant in conjunction with other catalytic metals, such as Ni or Cu, that do not undergo a change in oxidation.

2.6.2   Nickel

Industrially, nickel is a well-known and highly active methanation catalyst. Methanation, or the catalytic reduction of carbon oxides to CH_4 with H_2, has been studied for over a century and is known as the Sabatier reaction (Equation 2-11). Nickel is the second most active methanation catalyst, second only to ruthenium, and is the most selective to CH_4 production (Rönsch *et al.*, 2016). Nickel can also activate H species through chemisorption (Van Der Laan and Beenackers, 1999). Furthermore, hydrogenation of bicarbonate to formate over Ni catalysts was reported as early as the 1940s (Lundsted, 1949). Due to its presence in minerals on the sea floor and around hydrothermal chimneys, Ni-bearing materials have been the focus of numerous studies on hydrothermal CO_2 conversion.

Equation 2-11 Sabatier reaction

$$CO_2 + 4H_2 \rightleftharpoons CH_4 + 2H_2O$$
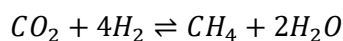
As discussed in Section 2.5, the generation of CH_4 over Ni-Fe catalysts was first investigated in origin of life studies. At more industrially applicable timescales, Yamasaki and co-workers reduced CO_2 gas to CH_4 and HCOOH over Ni catalyst with Fe reductant at temperatures between 200-350 °C and a reaction time of 2 hours. It should be noted that Fe was converted to $FeCO_3$ and Fe_3O_4 after reaction, while Ni did not oxidize. Results showed that at lower temperatures HCOOH is the dominant product (~9 mmol), while at higher temperatures and with increased Ni loading CH_4 is the product of greatest yield (~9.5 mmol) (Takahashi *et al.*, 2006). Takahashi *et al.*

proposed that after initial CO_2 reduction, the intermediate HCOOH is further reduced to CH_4 at higher temperatures.

In a similar study on CO_2 reduction to HCOOH over Ni/Fe at 300 °C, Wu and co-workers found only trace CH_4, and obtained a 15.6 % yield of formic acid with high selectivity (Wu *et al.*, 2009). It should be noted that batch reactor size, volume of filling, and ratio of catalyst used was significantly different between these two studies, indicating the importance of reaction optimisation for a given system. Furthermore, these results indicate that the reaction is tuneable to either HCOOH or CH_4 generation based on the operating conditions and loading of the reagents.

In a recent study on CH_4 generation from CO_2 over in-situ generated Ni particles with Zn/Fe reductant, a 98 % yield of methane from carbon in $NaHCO_3$ was obtained (Zhong, Yao, *et al.*, 2019). Notably, it was found that Ni particle size plays a critical role in CH_4 yield and may explain conflicting results in previous studies. Smaller *in-situ* synthesised Ni particles result in significantly higher CH_4 yields of 98% after 4 hours reaction time, whereas commercial Ni powder of a larger particle size yielded only 43% (Zhong, Yao, *et al.*, 2019). Additionally, the study found that the same yield of CH_4 is obtained when CO_2 gas is used, with an 84 % yield achieved within 0.5 hours. Zhong and co-workers also proposed that methane formation occurs through intermediate HCOOH (Figure 2-5).
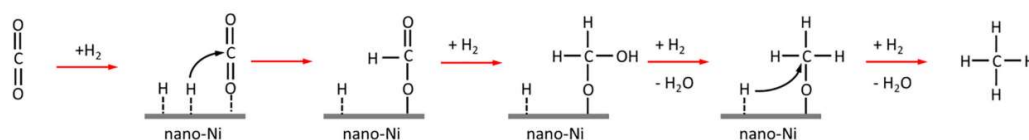
Figure 2-5 Proposed formation of CH_4 from CO_2 through a $HCOO^-$ intermediate (Zhong *et al.*, 2019)

It was further suggested that CH_4 formation occurs from the hydrogenation of CO_2, and not HCO_3^-, and that decomposition of HCO_3^- to CO_2 when using $NaHCO_3$ results in lower yields at reaction time shorter than 1 hour. However, as literature on the kinetics of CO_2/HCO_3^- hydrothermal reduction is not in general agreement, further research in this area is necessary. A summary of reported methane yields with Ni and Fe catalysts is found in Table 2-5.

Table 2-5 Summary of reported methane yields from hydrothermal CO_2 conversion with nickel and iron catalysts (NP – nanoparticles)

Substrate	Catalyst	Reductant	Reaction Time (hours)	Temperature (°C)	Methane yield	Source
CO_2	Fe NP	Fe NP	72	200	1.96%	(Liu *et al.*, 2013)
$NaHCO_3$	Ni	Fe	2	300	15.6%	(Wu *et al.*, 2009)
CO_2	Ni	Fe	6	300	~9.5 mmol	(Takahashi *et al.*, 2006)
$NaHCO_3$	Ni	Fe	4	300	98%	(Zhong, Yao, *et al.*, 2019)
CO_2	Ni	Fe	0.5	300	84%	(Zhong, Yao, *et al.*, 2019)

Further work by Zhong and co-workers on the reduction of bicarbonate to formate with Ni and in-situ formed Zn/ZnO demonstrated that synergism between the two metals can increase yields at lower temperatures (Zhong, Wang, *et al.*, 2019). When both metals were used, a decrease in the formate yield was observed at temperatures up to 300°C, proposed to be caused by reduction for formate to methane. Therefore, with Ni reduced operating conditions of 225 °C and 2 hours were found to be sufficient to give yields up to 80 %. Similarly to previous reports, no change in Ni oxidation state was found post-reaction. Interestingly, in the presence of Ni increased dislocations between Zn and ZnO were observed. The resulting interface between Zn, ZnO and Ni was proposed to be a highly active site for bicarbonate reduction (Figure 2-6). The synergism between other metal species must therefore be further investigated.
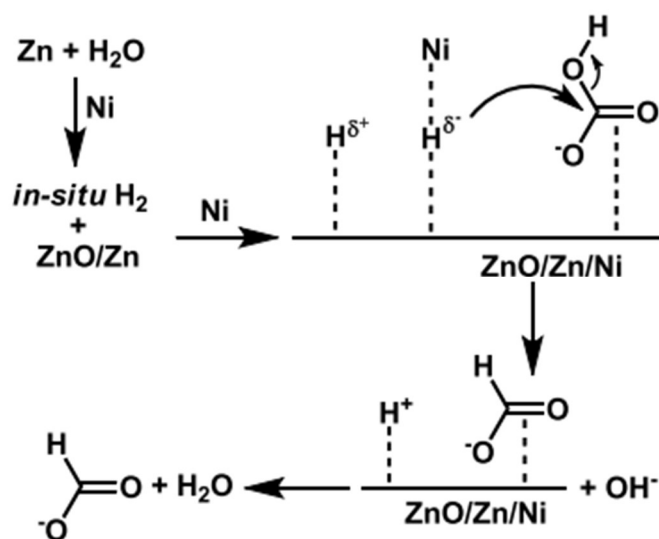
Figure 2-6 Mechanism of HCO$_3^-$ reduction to formate with Ni and Zn (Zhong, Wang, *et al.*, 2019)

Recently Raney Ni (R-Ni) was studied as a catalyst in hydrothermal conversion of CO_2 to acetate with Fe reductant. A 4.1 % yield was reported, with trace HCOOH and propionate also detected (Wang *et al.*, 2019). Wang and co-workers proposed that a bi-functional in-situ catalyst composed of R-Ni and Fe_3O_4 is responsible for acetate production. Other Ni species – Ni/γ-Al_2O_3, NiS_2 and Ni_3S_2 – were also tested as catalysts for C_{2+} production but yielded only trace amounts of product. This work further demonstrates the advantages of using a multi-functional catalyst for hydrothermally forming longer chain products from CO_2. However, thorough screening and optimisation is necessary to determine constituents and conditions.

2.6.3 Copper

Copper activity in hydrothermal reactions has attracted significant attention from the scientific community. High concentrations of Cu can be found at deep-sea vents, and, as a highly active water-gas shift and methanol synthesis catalyst, its effects are interesting (Fisher and Bell, 1997; Murphy and Meyer, 1998). A thorough investigation into the hydrothermal synthesis of methanol from CO_2 over Cu with Zn found that, in addition to HCOOH and CH_4, it is possible to obtain up to 11.4 % CH_3OH at lower pH (Huo *et al.*, 2012). The yield of methanol increases with additional Cu, and the addition of 2.0 M HCl was necessary to obtain higher methanol yields. The proposed mechanism for methanol synthesis involves H_2 generation from zinc, followed by adsorption of CO_2 onto the ZnO surface and H_2 onto the Cu surface. Spill

over of H atoms from Cu onto adsorbed CO_2 then occurs, and CH_3OH is produced. It should be noted that the presence of intermediate $Zn(OCH_3)$ groups was not confirmed, and thus the mechanism cannot be validated.

Methanol production from CO_2 gas using Cu and Al powders was also investigated by Lyu and group. Initially low yields of 1.5 % CH_3OH were obtained, with by-product HCOOH detected (Lyu *et al.*, 2015). Weakly acidic conditions were previously reported to inhibit HCOOH production (Lyu *et al.*, 2014), thus HCl was added and CH_3OH yield increased to 5.4 %. At low pH CO_2 is the dominant species in water, which indicates that methanol is formed from CO_2 (Chaix, Guillaume and Guillard, 2014). Temperatures over 300 ˚C were found to favour methanol production. A maximum yield of 22 % was reported with CO_2 gas after 2 hours at 350 ˚C, higher than 18.5 % obtained with $NaHCO_3$ after 7 hours. This further supports the hypothesis that methanol is formed from the CO_2 species. This study demonstrates how the equilibrium of CO_2 in solution can be altered to yield specific products by altering pH. A summary of methanol yields reported using Cu catalyst is found in Table 2-6.

Table 2-6 Reported methanol yields from hydrothermal CO_2 reduction with copper at 350 ˚C

Substrate	Catalyst	Reductant	Reaction Time (hours)	Methanol yield	Source
$NaHCO_3$	Cu	Zn	3	11.4%	(Huo *et al.*, 2012)
$NaHCO_3$	Cu	Al	7	18%	(Lyu *et al.*, 2015)
CO_2	Cu	Al	2	22%	(Lyu *et al.*, 2015)

In the presence of Cu with Fe reductant and at a temperature of 300°C and 2 hours reaction time, formic acid yields up to 46 % from CO_2 were reported (Zhong *et al.*, 2010). A reagent ratio of 1:6:6 $NaHCO_3$:Fe:Cu was used. In conjunction with previously reported results, it was found that a temperature of 300 °C was optimal for HCOOH formation, as formic acid decomposes readily at higher temperatures under hydrothermal conditions (Yu and Savage, 1998). In a follow-up work by the same group, an increased yield of 71.3 % HCOOH was reported at the same conditions

with an altered reagent ratio of $NaHCO_3$:Fe:Cu at 21:6:6 (Zhong *et al.*, 2015). This signifies the importance of optimising the reagent/catalyst ratio and the profound effect it has on yield. The proposed mechanism of reduction involves H_2 generation with $NaHCO_3$ *via* $FeCO_3$ intermediate as previously proposed by Yamasaki *et al*. It was proposed that formic acid was produced from bicarbonate, and not from CO_2 (Figure 2-7).
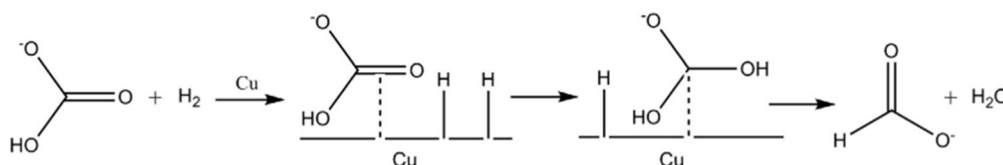
Figure 2-7 Proposed mechanism of bicarbonate reduction over Cu powder and Fe reductant (Zhong *et al.*, 2015)

A formic acid yield of 61 % was achieved at a reduced temperature of 250 °C with Cu and Zn reductant (L. Y. Wang *et al.*, 2014). Wang and co-workers, along with other research groups, have proposed synergism between Cu and Zn/ZnO when present in reaction, which may account for the reported higher yields (Huo *et al.*, 2012; L. Y. Wang *et al.*, 2014; Huang *et al.*, 2015). The addition of other catalysts may therefore allow reactions to be conducted at lower operating temperatures and milder conditions.

The complex synergistic relationship of Cu, ZnO and ZrO_2 in CO_2 hydrogenation was investigated by Huang and co-workers. In contrast with alumina, zirconium is more hydrophobic, preserves both acidic and basic sites and exhibits high thermal stability (Sato *et al.*, 2013). When investigating the catalyst components separately, no methanol was obtained from solely ZnO or ZrO_2, and low yields were obtained with Cu (Huang *et al.*, 2015). The selectivity of solely Cu was reported as 28.8 %, while ZnO and ZrO_2 showed 100 % selectivity to CO formation. This indicates that Cu acts as the active hydrogenation site, while CO_2 dissociation occurs on the other phases. In a catalyst containing all constituents, the selectivity to methanol remained around 30 % while conversion increased from 6.3 % to 28.3 %. As the constituents of the catalyst are highly stable, there is potential to investigate the use of multifunctional catalysts in CO_2 conversion under hydrothermal conditions.

2.6.4 Zinc

Similarly to iron, zinc has been reported to act as a sacrificial metal under hydrothermal conditions in the presence of carbon dioxide. Previous studies indicate that Zn is more effective at reducing CO_2 than other metals, including Fe (Jin *et al.*, 2014), and is very effective in generating H_2 under hydrothermal conditions (Jin *et al.*, 2011). Furthermore, zinc exhibits synergism with both Ni and Cu (L. Y. Wang *et al.*, 2014; Zhong *et al.*, 2015). This activity was reported in the presence of Ni, where Zn first reacts with sub-critical water to form H_2 gas, after which reduction of CO_2 to CH_4 occurs (Equation 2-11) (Zhong, Yao, *et al.*, 2019). The reaction is thermodynamically favourable and exothermic (ΔH^0 = −75.4 kJ mol^{-1}).

Equation 2-12 Nickel-catalysed reduction of bicarbonate to methane with zinc reductant

$$NaHCO_3 + 4Zn + 2H_2O \rightarrow CH_4 + 4ZnO + NaOH$$
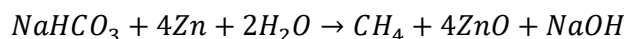
Yao and co-workers proposed that the formation of HCOOH over Zn proceeds *via* an S_N2-type mechanism involving first the formation of hydrogen on the Zn surface from H_2O splitting, followed by reduction of HCO_3^- with H atoms (Figure 2-8) (Yao *et al.*, 2017). However, this mechanism does not propose bicarbonate adsorption on the Zn surface, which would hinder its reduction by introducing a significant mass transfer barrier. As highlighted through the previous sections, there is a great deal of uncertainty surrounding mechanisms in hydrothermal reactions, with previous research theorising that CO_2 dissociation on Zn would occur more readily than H_2 (Huang *et al.*, 2015).
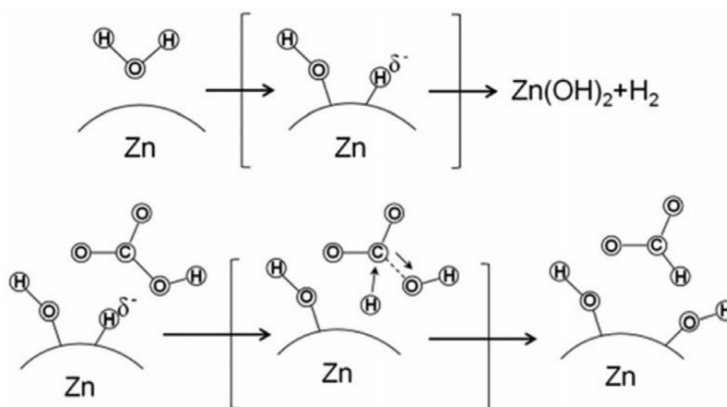
Figure 2-8 Hydrothermal reduction of HCO_3^- over Zn catalyst (Yao *et al.*, 2017)

Jin *et al.* reported HCOOH yields of 70-80 % using $NaHCO_3$ and Zn metal at temperatures between 300-325 °C, and proposed coupling of ZnO reduction to Zn with solar energy increases the energy efficiency and sustainability of the process (Jin *et al.*, 2014). Le and group examined the oxidation of Zn and bind energy of solid samples and proposed that the Zn/ZnO interface is the active site of CO_2 reduction by *in-situ* H_2 (Le *et al.*, 2017). Roman-Gonzalez and co-workers developed a mathematical model to accurately predict both literature results and experimental data with accuracy. In this way, a formic acid yield of 60 % with 100 % selectivity was achieved at 300 °C and 10 μm Zn particles (Roman-Gonzalez *et al.*, 2018). A major drawback in using Zn metal is the relatively low abundance of Zn on Earth (~0.007 % by mass) (Yao *et al.*, 2015). Nevertheless, due to its reported synergism with other metals and impressive formic acid yield and selectivity, further investigation into zinc catalysts is appealing.

2.6.5 Aluminium and Manganese

The activity of aluminium and manganese in H_2 generation and CO_2 reduction has been investigated and compared to that of Zn, Fe and Ni. Interestingly, at 300 °C, no H_2 was generated from Fe or Ni, while the highest yields were obtained in the order Mn > Al > Zn (Jin *et al.*, 2011). In the presence of CO_2, a 62.8 % yield of formic acid from $NaHCO_3$ was obtained with Al, 57.2 % using Zn metal, and 15.8 % over Mn (Jin *et al.*, 2011). This indicates that the hydrogen generating capability of catalysts and the CO_2 reduction activity are not directly related.

A study on $NaHCO_3$ reduction using aluminium and metal mixes at hydrothermal conditions of 300 °C was undertaken by Yao and co-workers. Increasing pH from neutral to 8.6 almost doubled hydrogen yield from 58 mL to 114 ml (Yao *et al.*, 2015). This is a further indication that the use of some carbon capture solutions may be advantageous in hydrothermal reactions, as the presence of bicarbonate creates a weakly basic medium. Bulk Al was fully oxidised to AlO(OH), also known as boehmite.

A mechanism of AlO(OH) formation and $NaHCO_3$ reduction was proposed (Figure 2-9). Initially, reaction of Al with H_2O results in the formation of HAlOH, which contains a hydride that subsequently attacks the carbonyl in $NaHCO_3$, forming formate. Dehydration of $Al(OH)_2$ occurs quickly due to instability, forming AlO(OH).
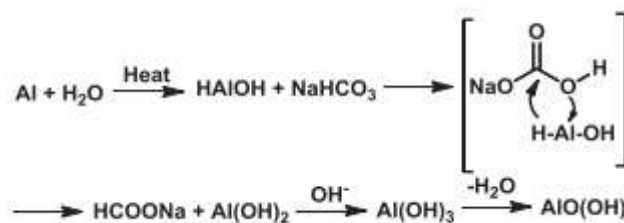
Figure 2-9 Mechanism of Al can oxidation and formic acid production from NaHCO$_3$ hydrothermally (Yao *et al.*, 2015)

An interesting application of this process is in the synthesis of boehmite from aluminium cans coupled with simultaneous HCO$_3^-$ reduction to formate. Boehmite has mesoporous structure with a large surface area and is an industrial precursor in adsorbent, catalyst, and ceramic synthesis (Milanović *et al.*, 2018). Ni and co-workers investigated this application and obtained 65 % formic acid yield with the addition of 0.1M NaOH (Ni *et al.*, 2019). Sodium hydroxide was proposed to promote Al oxidation to produce H$_2$ gas that is available in solution to reduce bicarbonate. In increasingly alkaline conditions, it was suggested that conversion of bicarbonate to carbonate makes conversion to formate less spontaneous based on calculated Gibbs free energies of -614.5 kJ mol^{-1} (CO$_3^{2-}$), -799.1 kJ mol^{-1} (HCO$_3^-$). A kinetic study of NaHCO$_3$ reduction to HCOO$^-$ was carried out to determine activation energy and found to be 50 kJ mol^{-1}. The mechanism of Al oxidation was in-line with the mechanism previously proposed by Yao and group.

Like aluminium and zinc, manganese behaves in a sacrificial matter in hydrothermal reactions. An investigation into the activity of manganese on CO$_2$ reduction was carried out by Lyu *et al*. At 325 ℃, 2 hours reaction time and a NaHCO$_3$:Mn ratio of 1:8 ratio a formic acid yield of 76 % was obtained (Lyu *et al.*, 2014). Jin and group previously reported the exception ability of manganese to generate H$_2$ by water splitting (Jin *et al.*, 2011). Interestingly, the mesh size of Mn had no effect on HCOOH yield, unlike Fe and Ni particle size. The study showed that changing initial reaction pH from ~8.3 in reactions with bicarbonate did not improve yields, signifying that the transformed species is HCO$_3^-$ and not CO$_2$ or CO$_3^{2-}$. When using CO$_2$ gas and NaOH in water, prolonging gas dissolution time decreased pH to weakly alkaline and led to increasing product concentration. This further lends itself to the theory that HCO$_3^-$ is the source of HCOOH.

2.6.6 Zeolites

Zeolites have unique properties, including high surface area, defined micro-porosity and stability, and catalysis on them generally involves acid-catalysed reactions (Abelló and Montané, 2011). Furthermore, zeolites are effective in oligomerization, aromatization and isomerization reactions. It is known that in the presence of water the activity of zeolites irreversibly declines due to framework degradation caused by dealumination (Nielsen *et al.*, 2019), but as acid-catalysed reactions are enhanced in HTW, research into zeolite activity in hydrothermal media has nevertheless been undertaken.

The formation of cyclohexanone and other cyclic ketones from CO_2 was recently found to be promoted by zeolite HY under hydrothermal conditions in the absence of additional metals (Gomez *et al.*, 2020). A stark increase in cyclic species in product mixtures was reported. In comparison to Fe_2O_3, eighteen times more cyclopentanone was obtained with unmodified zeolite HY, with yields over 0.9 mM reported. This encourages further investigation into zeolite catalysts, as the formation of longer-chained products may be enhanced. However, the non-recyclable nature of zeolite-containing catalysts in hydrothermal reaction significantly impedes any potential future industrial implementation.

Recently a multifunctional catalyst containing a zeolite was used by Wei and colleagues in the direct conversion of CO_2 to gasoline. By exploiting the specific activity and abilities of the constituents of Na-Fe_3O_4/HZSM-5, 78 % selectivity to hydrocarbons from CO_2 gas was obtained (Wei *et al.*, 2017). Iron is an excellent reverse water-gas-shift and Fischer-Tropsch catalyst, and forms a high number of olefinic compounds, while alkali metal Na promotes desired activity by increasing the basicity of the surface. The (111) surface of Fe_3O_4 is capable of activating CO_2 (Hakim *et al.*, 2016). Based on structural analysis of the catalyst, it was proposed that conversion occurs in three stages: dissociation of CO_2 to CO followed by CO hydrogenation, then formation of gasoline-range hydrocarbons over the zeolite. Further *in-situ* catalyst analysis to confirm this mechanism would be advantageous. Nevertheless, this valuable study further increases interest in multifunctional catalysts and their potential to enhance CO_2 conversion under hydrothermal conditions.

2.6.7 Summary of hydrothermal CO_2 reduction with metals

A large number of transition metals have been studied as catalysts and reducing species in hydrothermal CO_2 conversion. Metals used in this reaction either undergo oxidation, such as iron, zinc, aluminium and manganese, or alternatively do not change state, like nickel and copper. Zeolites have been shown to favour formation of cyclic species, though dealumination results in irreversible catalyst degradation.

Several products have been reported to arise from CO_2 reduction hydrothermally, including methane, methanol, cyclic ketones, and predominantly formic acid. It has been proposed, and is generally agreed on, that hydrothermally formic acid is formed from the bicarbonate species HCO_3^-, rather than dissolved CO_2 or CO_3^{2-}, and is favoured in mildly alkaline media. A comparison of formic acid reported by different groups is summarised in Table 7. Subsequently, formic acid is theorised to further be converted to methane with appropriate reaction conditions. On the other hand, with Cu or Al catalysts methanol can be obtained as the dominant product by creating an acidic environment. It is proposed that methanol forms from the dissolved CO_2 species which is dominant in equilibrium at low pH.

Table 2-7 Summary of formic acid yields reported in studies on CO_2 reduction with metals

Substrate	Catalyst	Reductant	Reaction Time (hours)	Temperature (°C)	Formic acid yield	Source
CO_2	-	Fe	72	200	8.5 mM	(He *et al.*, 2010)
$KHCO_3$	-	Fe	24	280	77.9%	(Michiels *et al.*, 2015)
$NaHCO_3$	Ni	Fe	2	300	15.6%	(Wu *et al.*, 2009)
CO_2	Ni	Fe	6	300	71%	(Takahashi *et al.*, 2006)
$NaHCO_3$	Ni_3S_2	H_2S	3	300	67.3%	(He *et al.*, 2019)
$NaHCO_3$	Ni	Zn	2	225	80%	(Zhong, Wang, *et al.*, 2019)
$NaHCO_3$	Cu	Fe	2	300	46%	(Zhong *et al.*, 2010)
$NaHCO_3$	Cu	Fe	2	300	71.3%	(Zhong *et al.*, 2015)
$NaHCO_3$	Cu	Zn	3	250	61%	(L. Y. Wang *et al.*, 2014)
$NaHCO_3$	-	Zn	1.5	325	80%	(Jin *et al.*, 2014)
$NaHCO_3$	-	Zn	3	300	60%	(Roman-Gonzalez *et al.*, 2018)
$NaHCO_3$	-	Al	2	300	64%	(Yao *et al.*, 2015)
$NaHCO_3$	-	Al + NaOH	2	300	65%	(Ni *et al.*, 2019)
$NaHCO_3$	-	Mn	2	325	76%	(Lyu *et al.*, 2014)

2.7 BIOMASS LIQUEFACTION

Hydrothermal processing of biomass is attracting interest as a method of converting biomass to valuable products. Biomass is defined as any biologically produced matter, and consists of cellulose, hemicellulose and lignin. Depending on reaction conditions, carbonization, liquefaction and gasification reactions dictate the product make-up achieved. Hydrothermal carbonization normally occurs in a milder region where coal-like fuel is obtained (Table 2-8) (Möller *et al.*, 2011). In contrast, hydrothermal gasification produces primarily methane and hydrogen among burnable gases (Kruse, 2009). Hydrothermal liquefaction (HTL), or the conversion of wet biomass at 200-350 °C and 5-28 MPa, has attracted a great deal of attention as a method of producing bio-crude and organic substances from waste (Behrendt *et al.*, 2008; Möller *et al.*, 2011). An advantage of hydrothermal processing of biomass is the wide array of feedstock that can be used, including slurries and wet biomass, as reactions take place in a water medium.

Table 2-8 Biomass liquefaction regions (Möller *et al.*, 2011)

Hydrothermal Process	Temperature range (˚C)
Carbonization	100-200
Liquefaction	200-350
Gasification	350-750

2.7.1 HTL Products and Mechanisms

The mechanism of biomass liquefaction to value-added products is intrinsically difficult to determine due to the extensive range of products arising from complex starting reagents. As such, many studies have focused on elucidating the products and reaction mechanism using simple model compounds for biomass, such as glucose. The use of glucose in reaction studies is advantageous as it is a monosaccharide commonly obtained from cellulose breakdown, can be used in the production of fuels, and can be converted to platform chemicals such as 5-(hydroxymethyl)furfural (5-HMF) and lactic acid (Corma Canos, Iborra and Velty, 2007; Cantero *et al.*, 2015). It should be noted that lactic acid in particular is an attractive product of glucose conversion due to its use in the production of the biodegradable thermoplastic polylactic acid (PLA) (Lim, Auras and Rubino, 2008).

In highly important work conducted by Poerschmann and co-workers, the full range and yield of products obtained from hydrothermal carbonization of glucose, fructose and xylose at 220°C for 3 hours was reported (Poerschmann *et al.*, 2017). In relation to glucose, levulinic acid was the product obtained at highest yield at 29600 μg per gram of input, followed by formic (27650 μg g^{-1} input), lactic (16210 μg g^{-1}), and glycolic acids (14880 μg g^{-1}). In comparison to all other products, organic acids represent by far the largest quantity of compounds.

Glucose degradation in hydrothermal media up to 400°C was investigated by Cantero and colleagues. A reaction pathway for glucose hydrolysis under hydrothermal conditions was proposed (Figure 2-10), where glucose degradation proceeds via retro-aldol condensation to glycolaldehyde or *via* isomerization to fructose (Cantero *et al.*, 2015). Fructose degradation then proceeds via dehydration to 5-HMF, or by retro-aldol condensation to glyceraldehyde. Glucose isomerization was reported to be favoured in subcritical water and is aided by ions present in the medium (Román-Leshkov *et al.*, 2010). As the water medium shifts from sub- to supercritical water, the ion availability decreases, and isomerization is disfavoured.
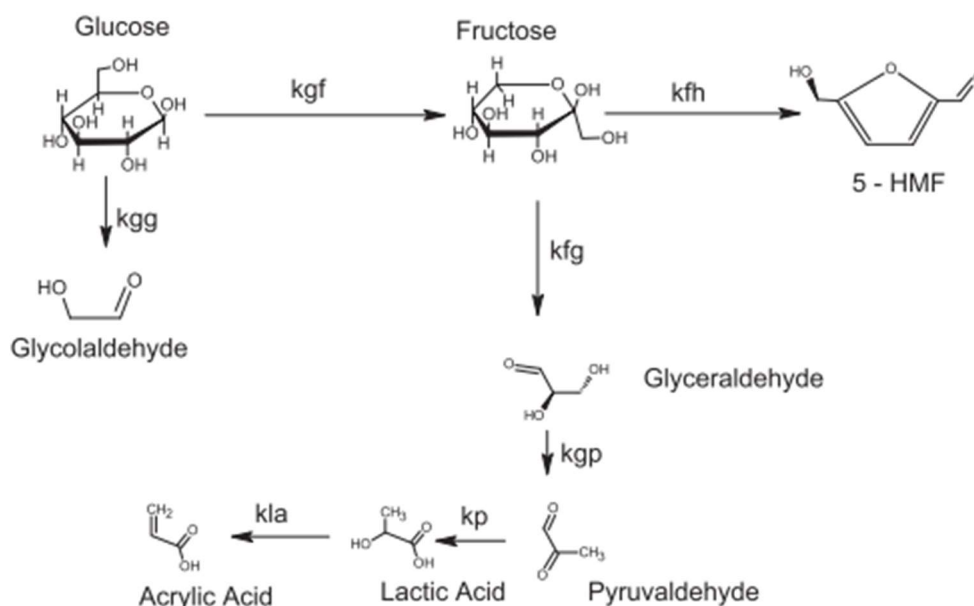
Figure 2-10 Proposed mechanism for glucose degradation in hydrothermal media (Cantero *et al.*, 2015)

Studies on sugar chemistry showed that lactic acid is a product of base-catalysed carbohydrate conversion (Yun Yang and Montgomery, 1996). In the presence of

either NaOH or Ca(OH)$_2$, glucose conversion to lactic acid and other organic acids increases (Yan *et al.*, 2007). It should furthermore be noted that in the presence of bases such as NaOH, interconversion of carbohydrates into isomers occurs *via* the Lobry de Bruyn-Alberda van Ekenstein Transformation (Wang, 2010). In the case of glucose, interconversion to mannose and fructose occurs in alkaline media (Figure 2-11). Therefore, basic conditions have significant impacts on the both product yields and the mechanism of biomass degradation. This is significant, as hydrothermal conversion of CO$_2$ to formic acid is favoured by a mildly alkaline medium.
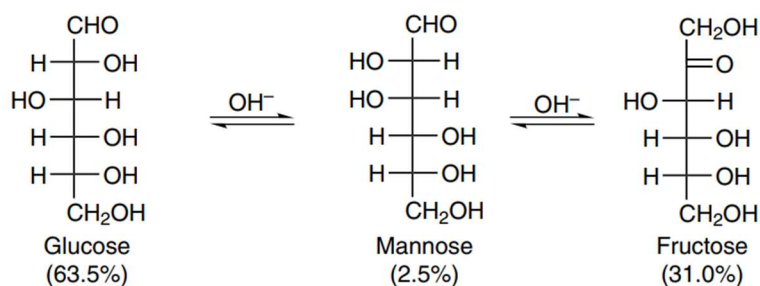
Figure 2-11 General reaction scheme for Lobry de Bruyn-Alberda van Ekenstein transformation of glucose (Wang, 2010)

Co-liquefaction studies can yield valuable mechanistic information when more complex biomass is used. A study on co-liquefaction of the microalgae *Dunaliella teriolecta* with polypropylene was undertaken to study potential synergism between the reagents for improved quality bio-oil. Bio-oils are considered a potential substitute for petroleum, but those obtained from thermochemical conversion of microalgae have disadvantages such as low higher-heating value (HHV) and volatility, delayed ignition time and high oxygen content (Wu *et al.*, 2017). Plastics such as polyethylene or polypropylene (PP) up to 14 % hydrogen, and have been investigated as H-transfer agents in hydrocracking reactions (Bhattacharya *et al.*, 2009). In a work by Wu and co-workers, it was observed that including PP in the hydrothermal conversion of *D. tertiolecta* promoted the formation of ketones and cyclic ketones, indicating that the polymer has a significant role in the decomposition of sugars (Wu *et al.*, 2017). It was proposed that monosaccharides have two main reaction routes: conversion to furfurals and production of cyclopentenone derivatives (Figure 2-12). As PP does not contain -OH groups, it may provide mechanistic insight as a co-reagent in hydrothermal reactions of other species such as carbon dioxide.
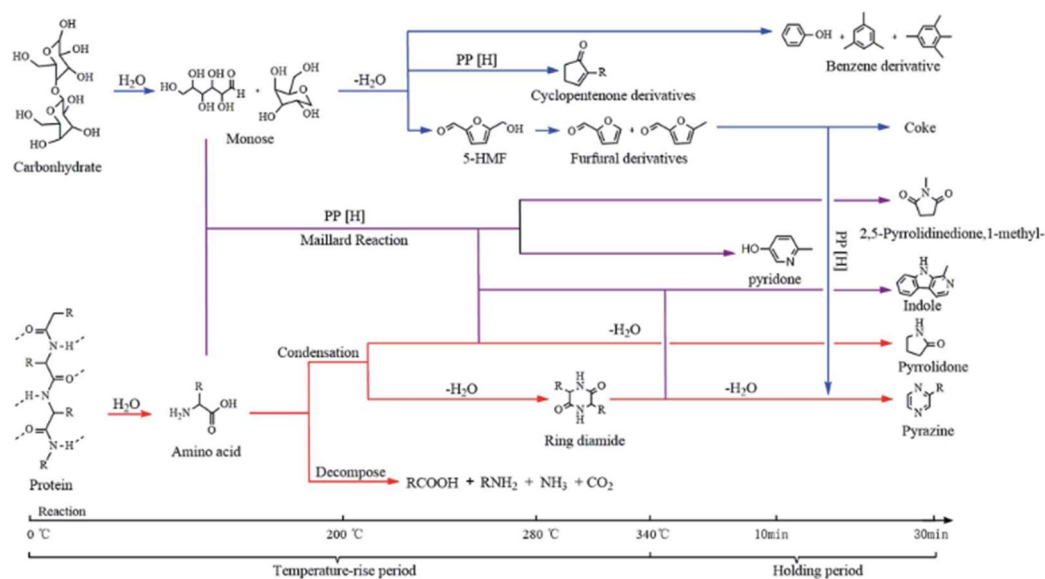
Figure 2-12 Reaction routes for carbohydrate and protein degradation (Wu *et al.*, 2017)

2.8 BIOMASS AND ITS DERIVATIVES AS CO_2 REDUCTANTS

The combination of CO_2 with biomass has been investigated both from the perspective of enhanced biomass conversion, and CO_2 reduction.

2.8.1 Effect of CO_2 on Biomass Liquefaction

The acceleration of acid-catalysed reactions in high-temperature water with the addition of carbon dioxide was first reported by Hunter & Savage. In this work, the dehydration of cyclohexanol to cyclohexene and alkylation of *p*-cresol with tert-butyl alcohol were examined. It was found that CO_2 reacts with H_2O to form carbonic acid, H_2CO_3, which then dissociates and increases the concentration of H_3O^+ in solution (Hunter and Savage, 2003). The yield of products was found to double in the presence of CO_2, and a pH decrease to 5.6 was observed. Subsequent work by Miyazawa and Funazukuri explored the effect of CO_2 on the hydrothermal hydrolysis of polysaccharide, sweet potato starch, to glucose. Carbon dioxide was found to act as a green acid when added, and increased polysaccharide conversion from 3.7 to 53 % after 15 minutes at 200 °C (Miyazawa and Funazukuri, 2005). This increase was again attributed to the formation of carbonic acid and lowering of solution pH.

It is generally accepted that acid hydrolysis of cellulose proceeds through four steps (Figure 2-13). Degradation occurs through cellulose hydrolysis to monosaccharides (1), followed by isomerization to fructose (2), dehydration to 5-HMF (3), and finally

rehydration to levulinic and formic acids (4) (Chen, Liu and Wu, 2020). Thus, acid-hydrolysis of cellulose leads to simultaneous production of several value-added products. As both a Lewis and Brønsted acid, *in-situ* carbonic acid (H_2CO_3) formed from CO_2 dissolution promotes all four steps.
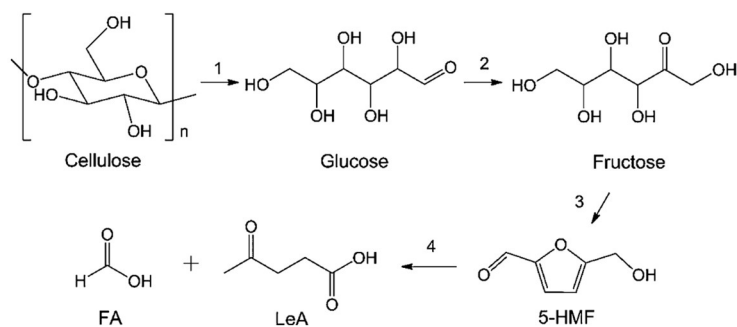
Figure 2-13 Proposed mechanism of cellulose acid hydrolysis (Chen, Liu and Wu, 2020)

Conversion of cellulose to 5-hydroxymethylfurfural (HMF) with CO_2 and metal oxides ZrO_2 and TiO_2 in a THF/H_2O/NaCl system at 200 °C was investigated by Jing and co-workers. Carbon dioxide was again found to promote the conversion of cellulose to oligosaccharides and monosaccharides as the pH drops to 3 (Jing *et al.*, 2018). HMF yields were found to increase with the presence of CO_2 in combination with TiO_2 and ZrO_2. Interestingly, HCOOH was found in reactions with no metal oxides due to CO_2 reduction to HCOOH by biomass in alkaline conditions. This indicates that the oxidation of biomass and the reduction of CO_2 occurs simultaneously.

It should be noted that several studies on the effects of catalysts in biomass liquefaction have been reported. A notable study on the effects of homogeneous catalysts in HTL of waste furniture sawdust at 280 °C was carried out by Jinghal and Jha. Based on bio-oil yield, the activity of the catalysts ranges as follows: K_2CO_3 > KOH > Na_2CO_3 > NaOH (Jindal and Jha, 2016). In terms of heterogeneous catalysts, transition metal effects have also been investigated. The addition of Ni in the conversion of cellulose resulted in increased H_2 yields (Minowa and Inoue, 1999) and increased methane yield in conversion of waste materials (Elliott, Sealock and Baker, 1994, 1994). In another study, CuO was utilised in the conversion of cellulose to organic acids at 325 °C, with yields up to 43 % (F. Wang *et al.*, 2014). It was also demonstrated that, as a hydrogen source, cellulose can be used to reduce metals back to their zerovalent form. Jin *et al.* reported that metals oxidised in hydrothermal reactions can be readily reduced by contact with glycerol in yields up to 100 % for Fe

(Jin *et al.*, 2011). These studies highlight the complexity of hydrothermal reactions containing CO_2 and biomass, as simultaneous conversion of both reagents occurs in high temperature water.

2.8.2 Carbon Dioxide Reduction with Biomass

Interest in the reduction of CO_2 with biomass and biomass-derived substances arose when it was reported that hydrogen can be obtained from simple alcohols without the need for metal catalysts (Shen, Zhang and Jin, 2011). Shen *et al.* first described the reduction of CO_2 by 2-propanol at 300 °C using both dry ice and $NaHCO_3$ as carbon sources. Although formate yields of 70 % were reported, this was calculated from the initial concentration of 2-propanol and casts doubt on the actual quantity of CO_2 reduced. Acetone was simultaneously stoichiometrically formed along with formate in accordance to the scheme presented in Figure 2-14.
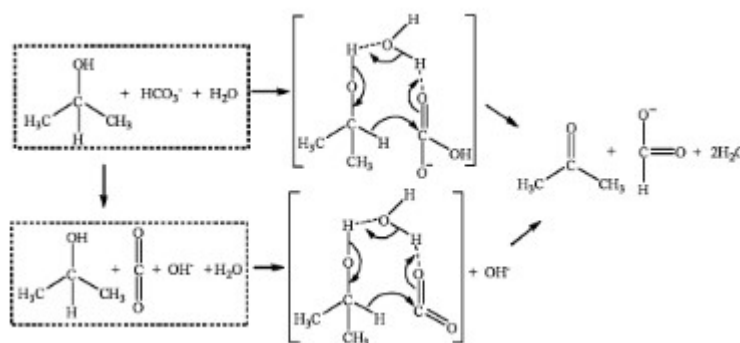
Figure 2-14 Schematic of cyclic transition state in CO_2 reduction with 2-propanol (Shen, Zhang and Jin, 2011)

A follow-up study using glycerol reported up to 90 % formate yields from initial glycerol formed *via* a cyclic transition state (Shen, Zhang and Jin, 2012).

Several studies have examined the effects of elevated temperatures on the reduction of carbonyl compounds to corresponding alcohols, also known as the Meerwein-Ponndorf-Verley disproportionation reaction. Conventionally the reaction is catalysed by trivalent aluminium *via* a cyclic transition state. However, in the presence of secondary alcohols at elevated temperatures of 210-300 °C, the reaction was shown to proceed uncatalyzed through a rate-determining cyclic transition state (Lermontov, Shkavrov and Kuryleva, 2003; Sominsky *et al.*, 2004). This further supports the theory that a cyclic transition state may be the route of CO_2 reduction with biomass constituents.

Wang and co-workers proposed an alternative mechanism of bicarbonate reduction by glycerol. The main products of reaction – lactate, glycolate, and formate – were in turn used as starting materials in the same reaction to investigate the reaction pathway. It was determined that glycerol degrades to lactate, which can further degrade to acetate and formate (Y. Wang *et al.*, 2016). Formate was also found to have the largest decomposition order of the three constituents and would degrade to CO_2 by decarboxylation. Thus, both biomass and carbon dioxide can form formic acid under hydrothermal conditions.

With reference to Figure 2-15, the dominant reaction was found to be the degradation of glycerol (red), while the desired CO_2 reduction reaction is shown in blue. Quantum chemistry calculations conducted by Wang and co-workers to determine transition states disputed the cyclic transition state as the basicity of the bicarbonate molecule is much greater than the water molecule. They proposed that bicarbonate is more likely to deprotonate the –OH on intermediate hydroxyacetone by acid-base reaction, forming $CH_3COCH_2O^-$ and CO_2 (Figure 2-15). It was proposed that a hydrogen on CH_2O^- attacks the carbon of the CO_2 molecule by nucleophilic addition, forming pyruvaldehyde and formate (Y. Wang *et al.*, 2016). This further signifies the difficulty of accurately predicting a mechanism even in a relatively simple reaction.
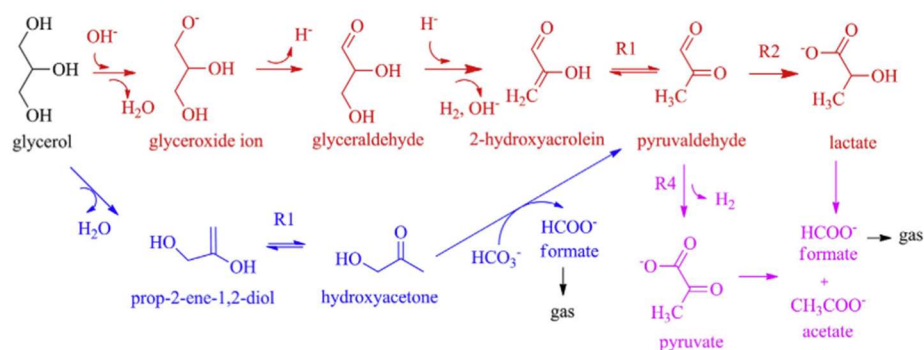
Figure 2-15 Proposed mechanism of hydrothermal glycerol degradation with simultaneous CO_2 reduction (adapted from Wang et al., 2019)

Nevertheless, a mechanistic study on CO_2 gas reduction with glycerol and NaOH was subsequently undertaken by Shen *et al*. A number of valuable mechanistic studies was undertaken using carbon labelled $NaHCO_3$ to evaluate its products, D_2O to determine the mechanistic role of water, as well as the catalytic effects of the SUS316 reactor. Consistent with previous results from this research group, it was concluded that glycerol was the source of lactate, while most of the observed formate was a result of

Chapter 2: Literature Review

CO$_2$ reduction (Shen *et al.*, 2014). In terms of mechanistic results, it was found that in the absence of water, no formate or lactate was detected, signifying that H$_2$O plays an important role. The results of the deuterium study further demonstrate that water is crucial in the conversion of glycerol to lactate. In the absence of NaOH, no formate or lactate was detected, which is proposed to be due to the action of $^-$OH in converting glycerol to acetol, as well as improving gas dissolution in solution. As such, a cyclic transition state was again proposed to be the dominant conversion route.

Yang and colleagues explored the CO$_2$ reduction with hexanehexol as a model compound for carbohydrates. The main products of the reaction were formic, acetic and lactic acids (Yang *et al.*, 2018). To determine the quantity of formate produced from biomass degradation, hexanehexol was hydrothermally reacted with 1M NaOH. The quantity of formate obtained from this control experiment was subtracted from reactions with NaHCO$_3$ to get total NaHCO$_3$-derived formate. However, formate yield was still calculated from the initial hexanehexol concentration, which casts doubt on the quantity of CO$_2$ reduced. Based on this calculation, an 80% yield of formate was achieved after 1 hour at 300 °C.

Simultaneous reduction of carbonate/bicarbonate by glycerol at mild hydrothermal conditions with a palladium on activated carbon catalyst, Pd/AC, was reported by Su *et al.* Based on initial carbon in the CO$_2$ source, K$_2$CO$_3$, conversion to formate up to 40% was achieved at 240 °C and initial pressure of 400 psi after 1 hour (Su, Yang, Yang, *et al.*, 2015). No formate was obtained in the absence of alcohol. Only lactate was observed from glycerol dehydrogenation in the absence of NaHCO$_3$. Interestingly, no products were obtained without the catalyst, with the addition of Pd/AC increasing product yields by one order of magnitude. When K$_2$CO$_3$ was substituted with CO$_2$ gas, very low HCOOH yields were obtained due to low solubility of gas and thus no CO$_3^{2-}$ formation. The Pd/AC catalyst did not undergo any changes during the reaction, though further *in-situ* studies to determine if hydrogen transfer from the alcohol to CO$_2$ is direct would be valuable.

A recent study on CO$_2$ reduction using biomass derivatives was conducted by Anderez-Fernandez *et al.* A range of C$_2$ and C$_3$ molecules, saccharides and phenolic derivatives were tested as reductants for NaHCO$_3$ at a range of temperatures (Andérez-Fernández *et al.*, 2017). The yield of formic acid was calculated from the initial carbon quantity in the organic solution, and a maximum value of 65 % was

reported after 180 minutes at 300 °C with glucose reductant. Reduction was proposed to proceed by the cyclic transition state first proposed by Shen and group. As glucose is commonly employed as a model compound for biomass, results indicate the potential of using raw biomass reductants in CO_2 conversion. Recently, Anderez and co-workers reported synergistic conversion of raw biomass with $NaHCO_3$ at 250 °C, with yields to formic acid of 10 % achieved (Anderez *et al.*, 2019). Further investigation into simultaneous conversion of both reagents must be undertaken to determine if increased selectivity and yields can be achieved with catalytic substances.

Synergistic conversion of microalgae with $NaHCO_3$ was also reported by Yang *et al.* *Spirulina* microalgae was converted to organic acids and substituted lactams, while HCO_3^- was simultaneously converted to formate (Yang *et al.*, 2019). Reported yields of major products increased substantially in the presence of $NaHCO_3$, and formate increased from 5.3 to 114.5 mmol l^{-1}. Carbon labelling experiments were carried out to determine the products of $NaHCO_3$ reduction and percentage of HCOOH that results from CO_2 reduction. Of total formate yield, 70.5 % was attributed to bicarbonate. Carbon labelling experiments were also carried out with glucose, with 7.3 mmol l^{-1} reported, of which 47.9 % was from $NaHCO_3$ reduction (Yang *et al.*, 2019). From these results, biomass type plays a major role in HCOOH yield.

Sodium bicarbonate reduction over Pd/C catalyst using 2-pyrrolidone as a model compound for protein-containing biomass waste was recently reported (Zhu *et al.*, 2019). Although yields only up to 30 % were reported, in optimizing the reaction it was found that both higher temperatures of 350 °C and longer reaction times enhance HCOOH production. This indicates that optimal reaction conditions vary when biomass is present, as previous studies with metal reductants found that CH_4 formation is dominant at higher temperatures (Takahashi *et al.*, 2006; Zhong, Yao, *et al.*, 2019).

2.8.3 CO_2 Reduction with Polymers and Derivatives

Polymer and polymer wastes can also be a hydrogen source in hydrothermal CO_2 reduction while simultaneously converting to hydrocarbons. It was previously reported that hydrothermal cracking of materials such as bitumen or polyethylene (PE) generates hydrogen (Kishita *et al.*, 2003, 2005). Zeng and colleagues investigated CO_2 reduction with simultaneous hydrocracking of PE and ethylene propylene diene

monomer (EPDM), a model compound for sulphur-containing rubber. Interestingly, no CO_2 reduction occurred during the hydrocracking of PE, whereas with EPDM a significant reduction of CO_2 was observed (Zeng *et al.*, 2011). The main species attributed to CO_2 was formic acid, whereas organic acids of C_2-C_6 and straight-chain C_{9+} alkanes were attributed to EPDM cracking. At temperatures of 450 °C, methane was detected, and a CO_2 reduction efficiency of 20 % was reported. Mechanistically, it was proposed that EPDM cracking releases H_2S, which reduces water and forms H_2 in solution. Hydrogen then reduces CO_2 to formic acid and methane.

Carbon dioxide reduction with polyvinyl chloride (PVC) was recently investigated (Lu *et al.*, 2020). The treatment of this type of waste is challenging and currently carried out predominantly by thermal cracking, *e.g.* hydrogenation or pyrolysis (Yu *et al.*, 2016). However, at low temperatures large quantities of hazardous HCl are produced, while at higher temperatures there is a substantial risk of producing chlorinated organics *e.g.* toxic dioxins (Ahmed *et al.*, 2017). Lu and co-workers reported complete dechlorination of PVC and simultaneous selective conversion $NaHCO_3$ to formic acid in the presence of NaOH with a 16% yield at 300 °C after 8 hours (Lu *et al.*, 2020). Mechanistically, lots of valuable information was obtained in the study. When substituting the carbonate source from $NaHCO_3$ to Na_2CO_3 the yield decreased in both cases, demonstrating that formate production is more favourable from HCO_3^- than CO_3^{2-}. It was also found that using $KHCO_3$ resulted in somewhat lower yields of formate, suggesting that the nature of the cation may have an impact on the reaction. It was also experimentally shown that the water medium is important for bicarbonate reduction, as no formic acid was detected when either dodecane or isopropanol were used as the medium even with –OH containing reductants.

2.8.4 Summary of CO_2 reduction with biomass and polymers

Hydrothermal liquefaction is an attractive method of producing a wide range of value-added products in which many different feedstocks can be used. Due to the complex starting material, determining the degradation mechanism of biomass is difficult. Therefore, model compounds such as glucose have been investigated, with the dominant products being organic acids. In the presence of bases, conversion of glucose to organic acids increases. In conjunction with CO_2, biomass is a promising reducing agent and feedstock for the formation of platform molecules, organic acids, cyclic ketones and benzene derivatives. When CO_2 is added to the reaction, it behaves as a green acid to accelerates polysaccharide hydrolysis while simultaneously

undergoing reduction to formic acid. A summary of formic acid yields reported in hydrothermal reactions with CO_2 and biomass can be found in Table 2-9.

A large number of products can be obtained from biomass degradation, so applying a catalyst may improve selectivity towards a specific species while increasing overall conversion. To date, supported Pd catalysts have been examined in hydrothermal reactions with CO_2 and biomass. Alternative, non-noble and more economic metals must be investigated to determine their activity.

In hydrothermal conversion of this nature, both reagents are simultaneously converted to formic acid, making it difficult to determine conversion. It is generally believed that CO_2 reduction and biomass conversion occurs via a cyclic transition state involving water and bicarbonate. However, kinetic models based on theoretical calculations proposed by other researchers suggest that CO_2 is the reduced species, rather than bicarbonate. Therefore, the detailed mechanism is still unclear and is the topic of some uncertainty. Polymers such as polypropylene can be used in mechanistic studies as sources of hydrogen, as they don't contain -OH groups and can yield valuable mechanistic data on CO_2 reduction.

Table 2-9 Summary of formic acid yields reported in studies on CO_2 reduction with biomass and polymers

Substrate	Catalyst	Reductant	Reaction Time (hr)	Temperature (°C)	Formic acid yield	Source
CO_2	-	glycerol + NaOH	1	300	79.8%	(Shen, Zhang and Jin, 2011)
$NaHCO_3$	-	glycerol	1	300	78.1%	(Shen, Zhang and Jin, 2011)
Na_2CO_3	-	glycerol	1	300	55.8%	(Shen, Zhang and Jin, 2011)
$NaHCO_3$	-	hexanehexol	1	300	80%	(Yang *et al.*, 2018)
$NaHCO_3$	Pd/AC	Glycerol	12	240	29.4%	(Su, Yang, Yang, *et al.*, 2015)
$KHCO_3$	Pd/AC	Glycerol	12	240	29.9%	(Su, Yang, Yang, *et al.*, 2015)
Na_2CO_3	Pd/AC	Glycerol	12	240	30.3%	(Su, Yang, Yang, *et al.*, 2015)
K_2CO_3	Pd/AC	Glycerol	12	240	39.8%	(Su, Yang, Yang, *et al.*, 2015)
CO_2	Pd/AC	Glycerol	12	240	1.2%	(Su, Yang, Yang, *et al.*, 2015)
$NaHCO_3$	Pd/C	2-pyrrolidone	2	350	30%	(Zhu *et al.*, 2019)
$NaHCO_3$	-	Glucose	3	300	65%	(Andérez-Fernández *et al.*, 2017)
$NaHCO_3$	-	*Spirulina*	2	300	9.5%	(Yang *et al.*, 2019)
CO_2	-	EPDM	2	450	~20%	(Zeng *et al.*, 2011)
$NaHCO_3$	-	PVC + NaOH	8	300	16%	(Lu *et al.*, 2020)

Chapter 2: Literature Review

Literature indicates that yields of hydrothermal CO_2 reduction products vary remarkably depending on a great deal of variables – temperature, reagent concentration, nature of the reductant, CO_2 source and reactor filling rate. Therefore, preliminary optimisation of a given system is necessary to obtain the best conditions for CO_2 reduction. Crucially, the identity and quantity of products of CO_2 reduction, rather than biomass oxidation, must be experimentally determined. As research is conflicting on the reaction scheme, further mechanistic studies are necessary. Other CO_2 sources such as bicarbonates and carbonates, can be used to gather further mechanistic insight and determine feasible CO_2 precursors. Once an optimised system has been developed as a benchmark, the effect of catalyst addition can be better understood. The effect of catalysts on hydrothermal CO_2 conversion with biomass reductants have not yet been documented. The activity of nickel and copper catalysts must be investigated, as these have well-documented enhancing effects on CO_2 reduction. The effects of bulk cobalt in hydrothermal CO_2 reduction has not previously been reported. Like iron, cobalt is a highly active Fischer-Tropsch catalyst, and may have interesting effects in this reaction.

3 CHAPTER 3: FUNDAMENTALS OF ANALYTICAL TECHNIQUES

In this work a range of analytical techniques were used to analyse different product phases and to characterise catalysts. The present chapter introduces the fundamentals of utilised methods. Firstly, methods used for liquid analysis are discussed in Sections 3.1–3.4. The principles of gas chromatography and associated detectors are presented. High performance liquid chromatography with photodiode array and refractory index detectors is then introduced. Nuclear magnetic resonance and inductively coupled plasma were used in liquid analysis and are also discussed in this chapter. Finally, methods used to characterise solid samples are presented in Sections 3.5–3.8.

3.1 GAS CHROMATOGRAPHY

In this work, gas, liquid and ion chromatography were explored for qualitative and quantitative product analysis. In principle, chromatography is a technique used to separate mixtures into their constituents. The sample is dissolved in a liquid or gaseous mobile phase and carried to a column where the components are partitioned. The physical state of the mobile phase dictates the system set-up. Gas chromatography (GC) is a common type of chromatography used for compounds that can be volatilised without decomposition. Complex mixtures can be separated into constituent molecules primarily based on differences in boiling point, vapour pressure and polarity (Blumberg, 2012).

A GC is composed of several key components: an injection port, flow controller, column, oven, and detector (Figure 3-1). First, a sample is introduced into the injection port set at a temperature at which the entire sample volatilises. Injection of liquid samples into the column may be performed by splitless or split injection. Splitless mode is used for mixtures containing trace levels of analytes. More commonly, split injection is used for pure samples or those containing high concentrations of analytes over 100 µg ml^{-1} (Sparkman, Penton and Kitson, 2011). In split mode, only a fraction of the injected sample is directed onto the column, with the remainder vented. A carrier gas, helium in the present work, pushes the sample onto a column located in a temperature-controlled oven. The column may be either a

packed silica column, or, more commonly, a tubular capillary column on which the stationary phase is coated. Separation of components occurs when the constituents interact with the stationary phase of the column. Separated components then enter a detector, which produces a chromatogram (Stauffer, Dolan and Newman, 2008).
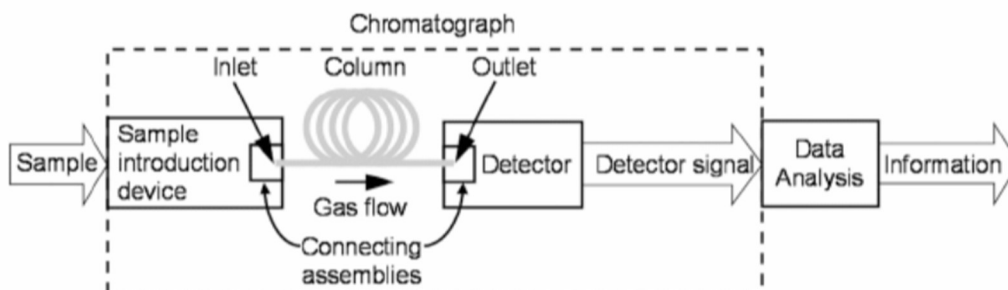
Figure 3-1 General GC Schematic (Blumberg, 2012)

Headspace analysis was another injection method used in the present work. In this technique, a liquid sample is sealed in a vial with significant headspace left over the sample. The vial is then heated to accumulate volatile solutes in the gas phase until equilibrium is reached according to Equation 3-1, where C_L is the concentration of analyte in the liquid at equilibrium, and C_G is its concentration in the gas phase at equilibrium. At this point, the analyte concentrations in the gas and liquid phases are constant. The partition coefficient K varies depending on the matrix and temperature (Sithersingh and Snow, 2012). Once equilibrium is reached, the gas phase is removed using a gas-tight syringe.

Equation 3-1 Partitioning of analyte between liquid and gas phase

$$K = \frac{C_L}{C_G}$$

Analysis of mixtures by GC relies on differences in the components partitioning behaviour. The interaction between the sample constituents and the column stationary phase results in different distribution of the analytes between the stationary phase and the He carrier gas, which is the basis of separation (Blumberg, 2012). Components have different affinities for the stationary phase depending on intermolecular interactions such as dispersion, dipole-dipole and H-bonding (Vitha, 2016). Temperature and mobile phase velocity are other key variables that control the retention time of solutes The gas-phase concentration of solutes increases with increasing temperature, and therefore partitioning is strongly temperature

dependent. Analysis may thus be performed with isocratic or gradient temperature. Carrier gas flow rate also impacts retention time. A flow rate too high may prevent sufficient interaction between the analyte and the stationary phase, while low flow rates lead to prolonged analysis time and resource use (Sparkman, Penton and Kitson, 2011). Therefore, stationary phase selection, analysis temperature and carrier gas flow rate must be carefully controlled for optimal analysis.

Due to the gaseous nature of this technique, GC analysis is limited to volatile and thermally labile analytes. However, non-volatile compounds may be derivatized to their volatile form, significantly expanding the number of analytes. Different detectors, including flame ionization detectors (FID), mass spectrometers (MS), and thermal conductivity detectors (TCD) may be used in conjunction with GC. In this work, MS and TCD were utilised.

3.1.1 Mass Spectrometry

Mass spectrometry (MS) involves the generation and detection of ions produced by bombarding sample constituents with high-energy electrons. A conventional mass spectrometer is operated under high vacuum and consists of an ion source, mass analyser, and detector (Figure 3-2).
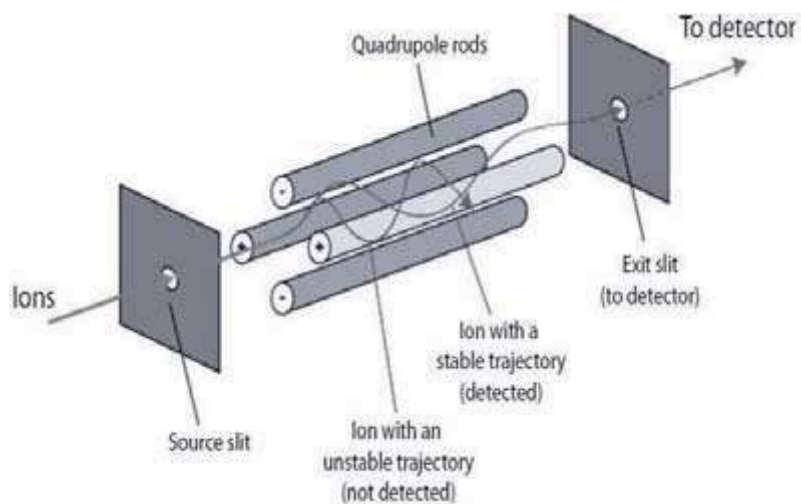
Figure 3-2 Schematic illustration of quadrupole mass analyser (Taouatas et al., 2008)

Ionization is the first step in MS and occurs in the ion chamber. This may be achieved by a number of techniques, of which electron ionization (EI) is most common. In EI, bombardment of analytes with electrons produces ions with a positive charge (Equation 3-2) (Ekman *et al.*, 2009).

Equation 3-2 Electron ionization in mass spectrometer

$$M + e^- \rightarrow M^+ + 2e^-$$
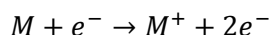
Ions may be separated by different means. In this work, a quadrupole mass analyser was utilised, which consists of four parallel cylindrical rods. The application of a direct current (DC) and radiofrequency signal (RF) results in oppositely charged rods. The generated fields determine the ions which reach the detector. If selected, ions flow down the mass analyser, while non-selected ions decay (McMaster and McMaster, 1998). Ions are thus separated based on their mass-to-charge ratio (m/z) and detected by their m/z and abundance, producing a mass spectrum (Gross, 2017). As opposed to other analytical techniques such as NMR or Raman spectroscopy, MS is a destructive technique in which samples are non-recoverable. However, only small quantities of sample are required and, in conjunction with GC, analytes in complex mixtures can be identified with high accuracy.

3.1.2   Thermal Conductivity Detector

In addition to MS, thermal conductivity detection was also used in this work. The thermal conductivity detector (TCD) is a universal, intrinsically safe, and non-destructive GC detector commonly used for light gas analysis. In this detector a Wheatstone bridge circuit is used to measure resistance change in a heated filament as the analyte passes over it (Figure 3-3) (Klee, 2012). Changes in conductivity are detected by the TCD and converted to a chromatogram. A reference gas, in this work argon, flows over a second filament. A constant voltage is applied through the circuit and the opposite filaments monitored. As TCD detectors are highly sensitive to temperature fluctuation, the main purpose of the reference filament is to minimize baseline drift caused by temperature or flow variation.
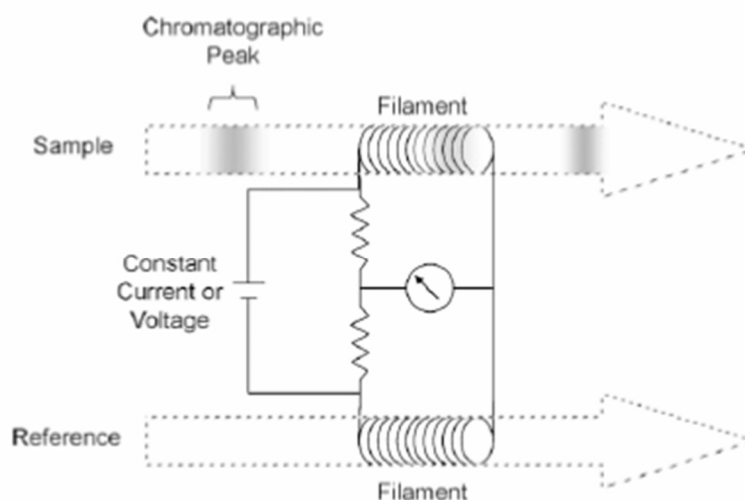
Figure 3-3 Schematic of thermal conductivity detector (Klee, 2012)

3.2 HIGH PERFORMANCE LIQUID CHROMATOGRAPHY

Liquid chromatography (LC) was the main method of aqueous phase analysis in this work. It must be noted that ion chromatography (IC) was briefly explored as an analytical technique in Chapter 4. However, due to equipment limitations this technique was not carried forth beyond preliminary tests. Thus, details of this technique were omitted from this work for conciseness. Briefly, IC involves separation of ions and polar molecules based on their affinity to the oppositely-charged stationary phase (Cummins, Rochfort and O'Connor, 2017). High performance liquid chromatography (HPLC) was found to be a more effective method of liquid phase analysis, and therefore was the main liquid analysis technique used in this work.

The separation principle in HPLC is based on the distribution of an analyte between a mobile phase and the stationary phase of the column. In this technique, any compounds with solubility in a liquid that can be used as a mobile phase, including water or organic solvents, can be analysed (Reuhs, 2017). The intermolecular interaction between analytes and the stationary and mobile phases results in different retention times of the constituents on the column. Many mechanisms impact retention, including the composition and polarity of the mobile phase, column particle size, temperature, and flow rate (Trojer *et al.*, 2010). Therefore, careful selection of the stationary phase and mobile phase composition is vital in achieving adequate molecule separation.

Chapter 3: Fundamentals of Analytical Techniques

Many types of HPLC analysis exist, including reversed-phase, normal phase, ion-pair, ligand exchange, chiral chromatography HPLC, and so forth. In the present work, ion-exclusion chromatography was used for constituent separation and is thus selectively discussed in further detail. In this technique, an ion-exchange resin containing a porous polymer network acts as a stationary phase (Figure 3-4).
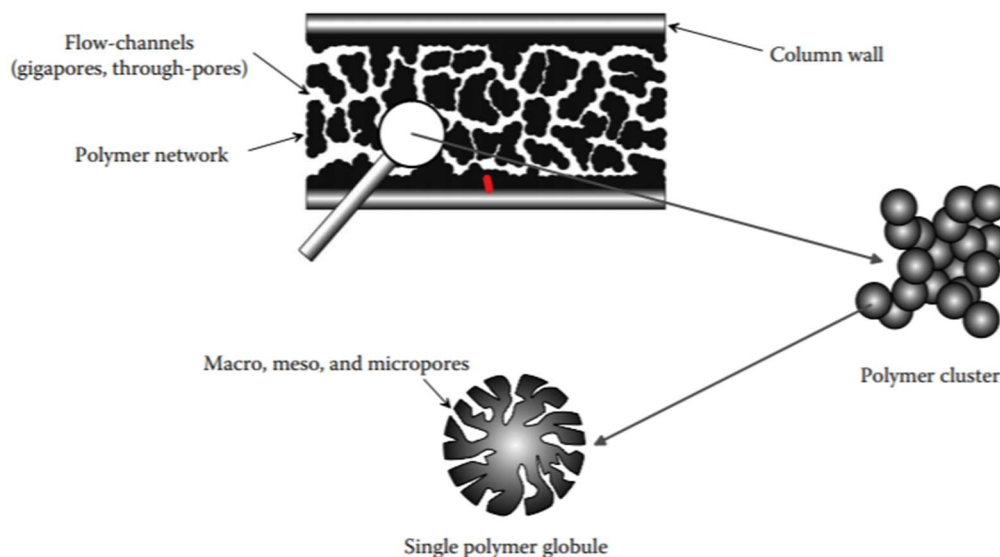
Figure 3-4 Schematic of general structure of typical polymer stationary phase in HPLC column (Trojer et al., 2010)

Ionic compounds from the solution are unretained by the resin through the Donnan effect, which describes the distribution of ions in solution in two compartments separated by a semi-permeable membrane (S. Moldoveanu and David, 2013). Non-ionic and weakly ionic compounds penetrate the resin pores and are selectively retained and partitioned on the polymer bed. Therefore, generally neutral to acidic medium pH is used. In this type of analysis, equilibrium based on size exclusion also plays a dominant role in analyte retention time. Large molecules are unable to enter the pore system and elute faster, while small molecules partition based on passage through long polymer channels.

The column is generally filled with uniform particles (<10 μm) of silica or cross-linked polymer. HPLC Columns are stainless steel tubes with specialised packing material, commonly silica or porous polymer resins that serve as a stationary phase. Requirements for the packing material are chemical stability, mechanical strength to serve as support matrix, and a well-defined particle size with narrow size distribution

(Reuhs, 2017). When the pump delivers the mobile phase to the column, it is therefore met with resistance which has to be pumped through at a high pressure (Lindsay, 1992).

The main components of an HPLC system are a pump, injector, column, detectors, and data analysis system (Figure 3-5). As the system is operated under pressure and polymer columns are highly porous, samples and the mobile phase must be filtered to eliminate particulate matter. In the present work, a syringe was used to manually inject samples into a fixed-volume loop. The loop is attached to a valve injector, which is either in a load or inject position. In the load position, the mobile phase is pumped directly into the column. In the inject position, the loop is rotated to be part of the eluent stream, and the sample carried to the column. Switching the sample loop allows to vary the sample volume from between 10 μl to 10 ml. The pump is commonly a piston-type and delivers the sample in mobile phase through the system with a controlled flow rate. In the present work isocratic elution was used, although gradient elution may be used to vary the mobile phase concentration during the run. To prevent gas bubble formation, an on-line degasser is used to remove dissolved air.
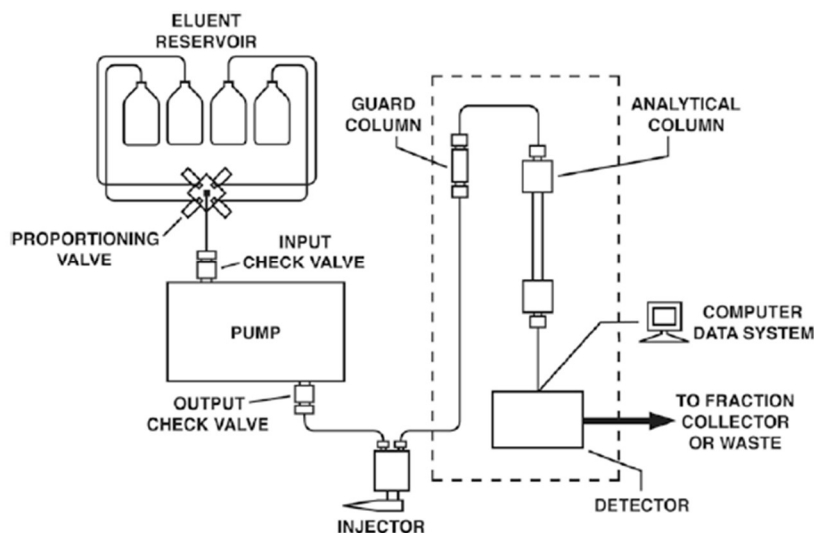
Figure 3-5 Schematic of general HPLC (Reuhs, 2017)

After partitioning on the analytical column, the analytes flow to a detector. Two different detectors were used in this work and are described in the following sections (3.2.1, 3.2.2).

Chapter 3: Fundamentals of Analytical Techniques

3.2.1 Refractory Index Detector

Refractory index (RI) detectors are universal in HPLC. RI detectors measure changes in reflex index, which describes how fast light travels through the material, of a sample relative to the solvent (Equation 3-3). In Equation 3-3, n is the dimensionless reflex index, c is the speed of light in vacuum, and v is phase velocity of light in the medium.

Equation 3-3 Reflex Index used in RI Detection

$$n = \frac{c}{v}$$

RI detectors contains two cells – a sample cell and a reference cell. A light source, commonly a tungsten lamp, emits an incident beam through both cells. When solely the eluent travels through the detector, the contents of both cells are the same and the measured refractive index of both cells is equivalent. However, when analytes are present in the mobile phase, the incident beam bends due to the reflex index between the two liquids. The deflection of the light beam is then detected by a light receiving element, such as a 4-field photodiode, and measured as displacement (Reuhs, 2017).

3.2.2 PDA Detector

Alongside RI detectors, ultraviolet-visible light (UV-Vis) absorbance detectors are the most common detectors in liquid chromatography. In principle, this detection method measures the ability of solutes to absorb light at a specific range of wavelengths. Thus, a key advantage of UV detection is that any compound that absorbs light within the available range can be detected.

There are three general designs of UV-Vis absorbance detectors: fixed wavelength, variable, and photodiode array detectors. Fixed wavelength detectors detect a single wavelength monitored by the system continuously, whereas in variable detectors, any wavelength in a wide spectral range can be selected for monitoring. Photodiode array (PDA) detection operates by simultaneously monitoring the absorbance of solutes at different wavelengths, producing an entire spectrum (Morgan and Smith, 2010). In the present work, a PDA detector was used in conjunction with HPLC. Unlike fixed wavelength detection, PDA detectors have multiple light-receiving arrays which can capture a wide range of wavelengths spanning UV to visible light.

Chapter 3: Fundamentals of Analytical Techniques

Figure 3-6 depicts a schematic of PDA detector. A wavelength range for detection is selected prior to analysis, typically within 200-400 nm. An acquisition wavelength of choice is selected, and bandwidth set to minimise background noise. For example, an acquisition wavelength of 210 with a bandwidth of 20 would record the light falling on the diodes corresponding to 190–230 nm. In a typical unit, the light from two lamps, tungsten (>350 nm) and deuterium discharge (190–380 nm), is merged and shone onto a flow cell through which the sample is passing (Bidlingmeyer, 1992).
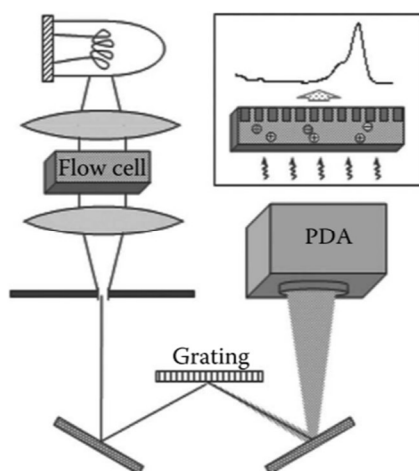
Figure 3-6 Schematic of PDA Detector (Morgan and Smith, 2010)

The amount of incident light, I_0, transmitted through a solution of given concentration c, in a flow cell of length l is described by the Beer-Lambert law (Equation 3-4):

Equation 3-4 Beer-Lambert Law

$$I_{tr} = I_0 \times 10^{\varepsilon lc}$$

where ε is the molar absorption coefficient of the solute and the exponent εlc is equal to the absorbance of the solution. The equation is valid as long as long as absorbers do not shadow each other (Morgan and Smith, 2010) .

The emergent light is then focused onto a slit and dispersed by a diffraction grating onto a photodiode array, which continuously records the full absorption spectrum of the sample. Typically, there are 1024 elements within the photodiode array. The light intensity is then converted to an electrical signal for each wavelength and presented on the software, producing a chromatogram.

3.3 NUCLEAR MAGNETIC RESONANCE

Nuclear magnetic resonance (NMR) was used in this work for analysis of liquids with labelled components. NMR is a phenomenon that occurs due to certain atoms possessing spin. The nuclear spin quantum number I may take integer or half integer values, with generally $I = ½$ of most interest. Nuclei with even atomic and mass numbers possess zero spin and cannot be observed by NMR. In this work, ^{13}C- and ^{1}H- NMR was employed as these are the most observed nuclei, with an abundance of approximately 1.1 % and 99.98 %, respectively (Harwood and Claridge, 1997). Nuclei that possess spin have associated with them a weak magnetic field and possess a magnetic moment. When these nuclei are placed in an external magnetic field, B_0, they experience a torque which forces them into precession about the axis of the external field, also known as Larmor precession, at a frequency proportional to the strength of B_0. Nuclei with spin of ½ can align themselves in only two quantized positions, the lower α and the higher β. Application of electromagnetic radiation at an appropriate frequency excites the lower energy state α to β, inducing nuclear magnetic resonance (Günther, 2013). Likewise, relaxation from the higher energy state may occur. Recording an NMR spectrum is therefore a sampling of the population difference between the energy states, which is relatively small even with the strongest available fields (Harwood and Claridge, 1997). Therefore, NMR is inherently insensitive and requires large sample size.

In a general set-up of liquid NMR, a sample solution held in a glass tube is inserted into the magnet. The tube sits within a coil which is tuned into the nuclear frequency of interest. Radiofrequency pulses from a transmitter are delivered *via* the coil, which also receives emitted frequencies from the stimulated sample in the form of oscillating voltage. The reference frequency of the original pulse is subtracted from the measured frequency, revealing differences between them. The measured difference is converted to digital values and analysed (Cowan, 1997).

3.4 INDUCTIVELY COUPLED PLASMA

Inductively coupled plasma optical emission spectroscopy (ICP-OES) is a technique that was used to determine the elemental composition of samples. In this technique, plasma is generated by argon gas ionised by a plasma torch, with a radio frequency generator generating and maintaining the plasma. The sample is introduced into the plasma as an aerosol. On contact with plasma, the aerosol is gasified and electrons are

excited to higher energy levels. As electrons relax to their ground state, energy is emitted from the atoms as photons, producing an emission spectrum characteristic to each element. The spectrometer, typically a polychromator capable of determining multiple elements in a sample, separates the wavelengths of light and light intensity is measured by a detector (Nölte, 2021).

In this work, both liquid and solid samples were compositionally analysed using ICP-OES. Solid samples were first acid digested, for example in aqua regia, to dissolve the desired species into solution. Sample preparation and analysis was carried out by colleagues Heather Grievson and Shania Laming at the University of Sheffield Department of Chemistry.

3.5 FOURIER-TRANSFORM INFRARED SPECTROSCOPY

Fourier-transform infrared (FTIR) spectroscopy is a technique used to characterise samples by measuring the absorption or emission of IR radiation by functional groups. Infrared radiation is divided into three regions – far (400–10 cm^{-1}), mid (4000–400 cm^{-1}), and near IR (14285–4000 cm^{-1}), and functional groups absorb IR radiation at specific frequencies (Che Man, Syahariza and Rohman, 2010). To be IR active, molecule bonds must have a net change in the dipole moment of the functional group due to vibration such as stretching, which results in a change in bond length, or bending, which changes bond angle (Driggers, Friedman and Nichols, 2012). For example, symmetric C-O stretching of CO_2 is not IR active but bending produces a measurable dipole change.

Analysis is commonly carried out either by absorption or transmission FTIR, in which IR radiation passes through the sample. In this work, FTIR-ATR was used in the characterisation of catalysts to analyse surface functionality, and spectra were gathered in transmission mode. Attenuated Total Reflectance (ATR) is an advantageous technique as the data collected is surface sensitive and minimum sample preparation is required. In this technique, the sample is placed on an internal reflection element (IRE), a crystal with a high reflection index such as germanium or zinc selenide (Figure 3-7). In the present work, a diamond crystal was used owning to its chemical inertness and wide spectral range. The IR beam passes from the source to a series of mirrors that direct it to the crystal. The angle at which the beam passes through the ATR crystal must exceed the critical angle for internal reflectance, resulting in an evanescent wave penetrating the sample (Paraskevaidi, Martin-Hirsch

and Martin, 2018). Rapid degradation of the wave occurs outside the crystal, and only the superficial 0.5–5 μm of the sample is penetrated (Che Man, Syahariza and Rohman, 2010). The distortion of the evanescent wave by the sample is detected, and a Fourier transform if performed by the software to convert the signal to a spectrum.
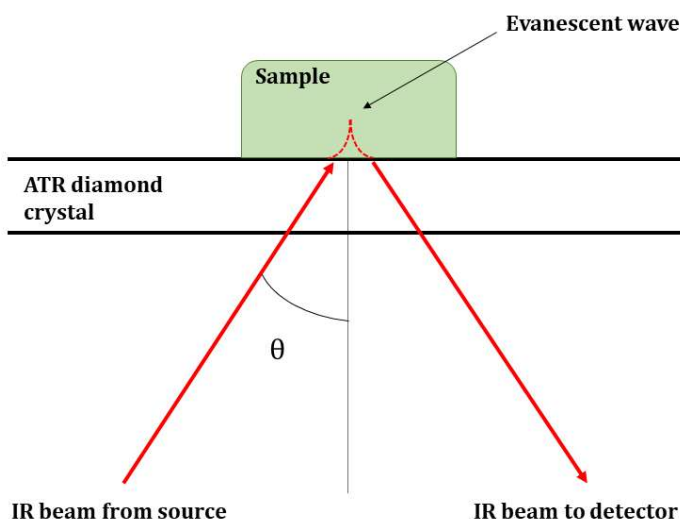
Figure 3-7 Schematic of operating principle of FTIR-ATR Principle. Adapted from Driggers, Friedman and Nichols, 2012

3.6 SCANNING ELECTRON MICROSCOPY

Scanning Electron Microscopy (SEM) was used for high magnification imaging of catalyst surfaces to study their physical appearance and morphology. Using SEM, resolution of 10 nm, can be achieved with high resolution (Raval *et al.*, 2018). In this technique, the sample is probed with a focused high-energy beam of electrons generated by an electron gun with a cathode, commonly made of tungsten. The electron beam is accelerated through a high voltage system between 0.1 and 50 KeV. The electron beam interacts with the sample atoms, producing characteristic and varying emissions of low-energy (<50 eV) secondary electrons (SEs), elastically scattered back-scattered electrons (BSEs), Auger electrons, and characteristic X-rays (Reimer, 1998). Electrons can be detected by various methods and used to produce an image.

The electron beam may cause atomic inner-shell ionization, creating a vacancy into which a higher shell electron may drop, producing an X-ray with energy equal to the difference between the two energy levels. This energy difference is characteristic to different elements and is the basis of energy dispersive X-ray spectrometry (EDX or

EDS) (Schatten, 2010). This technique is commonly used in conjunction with SEM to determine the elemental composition of the sample. EDS was used to determine the atomic composition of copper catalyst surfaces in this work.

3.7 X-RAY DIFFRACTION

X-ray diffraction (XRD) was used to analyse powder samples of bulk metal powders, and synthesized supported and commercial catalysts. In principle, diffractometers are composed of three elements: an X-ray tube, sample holder, and detector. X-rays are generated in a cathode ray tube by heating a filament to produce electrons, accelerating them towards a towards a target by applying voltage, and bombarding the target material, commonly copper, molybdenum or iron. In this work, a PANalytical Aeris (Malvern Panalytical Ltd, UK) diffractometer was used with a Cu target. When electrons have sufficient energy to dislodge inner-shell electrons, electrons in higher shells cascade down to fill the empty space left by the dislodged electron, producing X-rays in the process (Jenkins and Snyder, 1996). The diffraction pattern produced is characteristic to different crystal phases, and were identified using the PDF 4+ software 2021 database (ICDD, USA).

The crystallite size of the active phase of catalysts was determined by the Scherrer equation (Equation 3-5), where τ is the crystallite size, λ is the X-ray bean wavelength (1.5406 Å), β is the full width half maximum of the peak in radians, and θ is the Bragg angle. K is a dimensionless shape factor assigned the value 0.9 for spherical particles (Joni *et al.*, 2018). It must be noted that crystallite size calculated from the Scherrer equation applies to nano-scale crystallites, not larger particles over 0.1 μm.

Equation 3-5 Scherrer equation for crystallite size calculation

$$\tau = \frac{K\lambda}{\beta cos\theta}$$

3.8 NITROGEN ADSORPTION ISOTHERMS

Gas adsorption isotherms were used for the determination of material surface area. The substrate, in this work catalysts, was placed in a sample tube of known volume, and adsorption was carried out in liquid nitrogen at 77 K. Inert gas, in this case nitrogen, was injected into the sampling tube, and the pressure dropped until equilibrium is reached. The amount of gas adsorbed by the catalyst is calculated as

the difference between introduced gas and gas required to fill the sampling tube (Sing, 2001). Successive gas injections were used to plot isotherms. The analysis was based on the BET (Brunauer, Emmett, Teller) model, in which multiple layers of gas are proposed to be adsorbed. In this model, an energetically uniform surface with no interactions between neighbouring molecules is assumed, and the probability of site occupation does not depend on the level of occupation of neighbouring sites (Rouquerol, Rouquerol and Sing, 1999). BET measurements were conducted on selected copper catalysts used in Chapter 8, and were carried out by post-doctoral researcher Dr Carlos Brambila of the Department of Chemical and Biological Engineering at the University of Sheffield

4 CHAPTER 4: ANALYTICAL METHOD DEVELOPMENT

Hydrothermal conversion of carbon dioxide with biomass has been attracting increasing interest in recent years. As discussed in the literature review (Chapter 2), the focus of hydrothermal CO_2 reduction has predominantly been on the formic acid product. As such, identifying and quantifying formic acid derived from this reaction is crucial. However, other compounds formed in this reaction have not been discussed at length in literature. While only a limited number of products, mostly C_1 molecules, have been reported from hydrothermal CO_2 conversion, biomass and its derivatives can degrade to vast numbers of compounds (Li *et al.*, 2016). Identifying products of the reaction beyond C_1 molecules may be valuable for obtaining mechanistic insight and potentially reaction intermediates. If the system were to be applied industrially, detailed information on organic products present for subsequent water treatment is vital and currently lacking (Poerschmann *et al.*, 2017). Identifying the most suitable analytical techniques is crucial for obtaining a full picture of the complex reaction products. Due to the highly dilute product solution, highly sensitive chromatographic techniques were utilised. An advantage of GC is faster analysis of complex mixtures, but is limited to neutral, volatile compounds or gases. On the other hand, HPLC and IC may be used for analysis of charge-carrying molecules but is not ideal for gas samples (S. C. Moldoveanu and David, 2013). Thus, various analytical methods were explored for a thorough investigation into reaction products.

To avoid mass transfer kinetic limitations, sodium bicarbonate was chosen as a CO_2 source. An additional benefit of using $NaHCO_3$ is that it creates a mildly alkaline environment in which reduction of CO_2 to formate is more facile (Álvarez, Bansode, *et al.*, 2017). Glucose was selected as a model compound for biomass, as raw biomass varies widely in its composition and homogeneity. Glucose is a constituent of biomass which has a simpler molecular structure, and can be produced from polysaccharide hydrolysis or hydrothermally through cellulose breakdown (Miyazawa and Funazukuri, 2005; Bhaumik and Dhepe, 2016). Therefore, a $NaHCO_3$ and glucose reaction was investigated at temperatures up to 300 °C.

Identification of molecules in a complex reaction mixture poses a challenge, however, particularly as glucose undergoes numerous conversions at the extreme conditions in sub-critical water. Furthermore, the reaction pH is > 8 in the presence of $NaHCO_3$, at which point organic acids exist mainly in their ionized form, with formic acid adopting

the formate form, HCOO$^-$ (Puchajda *et al.*, 2006; Morrison *et al.*, 2019). This further complicates analysis due to the non-volatile nature of ions. In this chapter, the best available methods for qualitative and quantitative analysis of sample components were developed. No significant solid products were obtained during the reactions, so solid products were not characterised in this work. Aqueous phase, organic phase containing bio-oil constituents, and gas products were identified using gas and liquid chromatography.

4.1 METHODOLOGY

The fundamentals of chromatographic techniques used in this chapter were discussed in Sections 3.1 – 3.2.

4.1.1 Materials

In addition to deionised water obtained from a Suez L300130 (>1 MΩ cm), numerous reagents were used in this work. A summary of reagents is available in Table 4-1.

Table 4-1 Materials used in analytical method development

Entry	Chemical name	Formula	Grade	Supplier
1	Sodium bicarbonate	$NaHCO_3$	99+ %	Sigma-Aldrich
2	D-(+)-Glucose	$C_6H_{12}O_6$	≥99.5 %	Sigma-Aldrich
3	2-propanol	C_3H_8O	≥99.7 %	Sigma-Aldrich
4	Sodium carbonate	Na_2CO_3	≥99.0 %	Sigma-Aldrich
5	Sulfuric acid	H_2SO_4	95-98 %	Sigma-Aldrich
6	Dichloromethane	CH_2Cl_2	≥99.8 %	Sigma-Aldrich
7	Magnesium sulfate anhydrous	$MgSO_4$	≥99.5 %	Sigma-Aldrich
8	Sodium hydroxide	$NaOH$	98 %	Alfa Aesar
9	Ammonia solution	NH_3	25 %	Fisher Scientific
Standards				
10	Acetaldehyde	C_2H_4O	≥99.5 %	Sigma-Aldrich
11	Acetic acid	CH_3COOH	≥99 %	Fisher Scientific
12	Acetone	C_3H_6O	>95 %	Fisher Scientific
13	Acrylic acid	$C_3H_4O_2$	99 %	Sigma-Aldrich
14	Citric acid	$C_6H_8O_7$	≥99 %	Alfa Aesar

15	Dihydroxyacetone	$C_3H_6O_3$	≥98 %	Sigma-Aldrich
16	Ethanol	C_2H_5OH	≥99.5 %	Sigma-Aldrich
17	Ethylene glycol	$C_2H_6O_2$	99 %	Fisher Scientific
18	Formaldehyde	CH_2O	37-41%	Fisher Scientific
19	Formic acid	CH_2O_2	98-100 %	Sigma-Aldrich
20	D-(-)-Fructose	$C_6H_{12}O_6$	≥99 %	Sigma-Aldrich
21	Furfural	$C_5H_4O_2$	99 %	Sigma-Aldrich
22	DL-Glyceraldehyde	$C_3H_6O_3$	≥90 %	Sigma-Aldrich
23	Glycolaldehyde dimer	$C_4H_8O_4$	99 %	Sigma-Aldrich
24	Glycolic acid	$C_2H_4O_3$	99 %	Sigma-Aldrich
25	Glyoxylic acid	$C_2H_2O_3$	98 %	Sigma-Aldrich
26	5-(Hydroxymethyl)furfural	$C_6H_6O_3$	≥99 %	Sigma-Aldrich
27	Isovaleric acid	$C_5H_{10}O_2$	99 %	Sigma-Aldrich
28	L-(+)-Lactic acid	$C_3H_6O_3$	≥85 %	Sigma-Aldrich
29	Levulinic acid	$C_5H_8O_3$	99 %	Sigma-Aldrich
30	Maleic acid	$C_4H_4O_4$	≥99.0 %	Sigma-Aldrich
31	Methanol	CH_3OH	≥99.8 %	Fisher Scientific
32	Oxalic acid	$C_2H_2O_4$	98 %	Fisher Scientific
33	Propanoic acid	$C_3H_6O_2$	≥99.5 %	Sigma-Aldrich
34	1,2-Propanediol	$C_3H_8O_2$	≥99.5 %	Sigma-Aldrich
35	Pyruvaldehyde	$C_3H_4O_2$	40 %	Sigma-Aldrich
36	Pyruvic acid	$C_3H_4O_3$	98 %	Sigma-Aldrich
37	Sodium formate	$NaCOOH$	≥99.0 %	Sigma-Aldrich
Gases				
38	Helium	He	≥99 %	BOC Gases Ltd.
39	Argon	Ar	≥99.99 %	BOC Gases Ltd.
40	Gas Standard	40 % H_2, 35 % CO_2, 23 % CO, 1 % CH_4		Air Products

4.1.2 Reactor Set-up

The reactor set-up used for conducting hydrothermal experiments is shown in Figure 4-1. Reactions were carried out in a stirred 100 mL EZE-Seal pressure vessel made of Hastelloy C (Parker Autoclave Engineers®). A carbon dioxide or a helium gas cylinder were attached to the vessel. The autoclave is equipped with a rupture disk

(1) set to rupture at 300 bar. A heating jacket placed around the vessel was controlled using a Solo Temperature Controller model 4824 (2), which also monitored internal temperature and mixing speed. The reactor was stirred using a Series MAG075 in-line MagneDrive® II (3) connected to an impeller. The magnetic drive was cooled throughout operation by an external cooling bath set to 10 °C to prevent overheating. Reaction mixtures may be injected using the sample injection valve (4) and collected through valve (7), but in this work reagents were loaded into the vessel before it was secured into the rig and samples collected after deconstruction. Pressure was monitored using an analogue pressure gauge (5). Gaseous samples were collected into a gas bag by opening the venting valve (6) after cooling the reactor to room temperature. After reaction the vessel and internal parts were manually cleaned to prevent contamination.
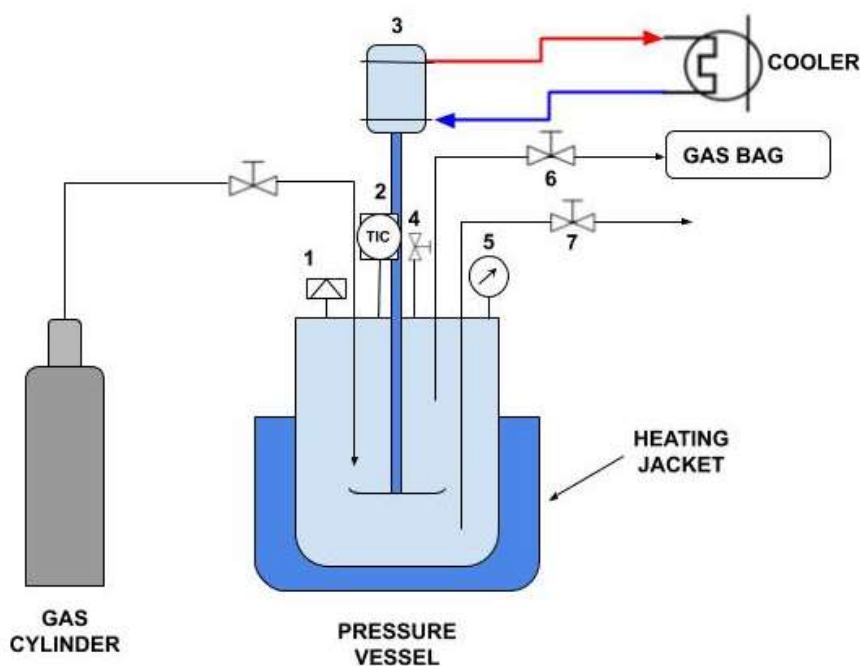
Figure 4-1 Reactor set-up used in hydrothermal reactions. 1 – rupture disk; 2 – T controller; 3 – magnetic stirrer; 4 – reagent loading valve; 5- pressure gauge; 6 – gas venting valve; 7 – sample collection valve

4.1.3   General Experimental Procedure

For a general experiment, a glucose solution of specified concentration was volumetrically measured and placed in the reactor. Then, a specific quantity of

$NaHCO_3$, if used, was added to solution and manually stirred to dissolve. The reactor was subsequently sealed. A leak test was performed by pressurising the reactor with 30 barg He for 10 minutes. If no drop of pressure was detected, the autoclave was deemed fully sealed. The vessel was then purged three times with 30 barg He to eliminate ambient air. The heating jacket and mixer, set to 500 rotations per minute, were then turned on. The start of the reaction was determined to be when the reactor reached the pre-set temperature, with an approximate 40 minutes to reach temperature. Reactions were carried out in duplicate as a minimum to assess error. Error was assessed by averaging product concentrations from multiple reactions and assessing the standard deviation from the mean. Error bars on graphs thus represent the standard deviation of products over multiple experiments.

After a set reaction time, the pressure vessel was quickly quenched in ice until room temperature. Once temperature was below 30 °C, gas was vented into a gas bag and analysed by GC/TCD. The reactor was subsequently broken down and the liquid phase products were filtered three times through a 0.22 μm syringe filter to remove solids. Filtered liquid was then stored either at 4 °C or in 2 ml aliquots at -20 °C. The measurement of solution pH was performed using a pH meter (pHenomenal™ 1000L, VWR, USA) that was calibrated before each use using supplier-provided pH 7.000 and pH 14.000 calibration standards.

4.1.4 Gas Chromatography

Liquid products and bio-oil were analysed using a Shimadzu 2010 GC equipped with a QP2010 SE Mass selective detector with electron impact ionisation and AOC 2Oi autosampler (Shimadzu Corp., Japan). Inlet temperature was maintained at 250 °C to vaporise all substances. Helium gas was used as a mobile phase and split ratio was set to 30. The MS interface temperature was set to 5 °C higher than the maximum temperature reached in the oven programme to prevent condensation in the detector.

Two different GC columns were used for analysis – DB-1MS (60 m x 0.25 mm I.C.; 0.25 μm) dimethylsiloxane column and an HP-INNOWax (30 m x 0.25 mm I.C.; 0.2 μm) polyethylene glycol phase capillary column (both Agilent Technologies, USA). The oven programme used for analysis over each column is described in Table 4-2 and 4-3, respectively. Split ratio was maintained at 30 with both columns, and m/z set to 33-500.

Table 4-2 Oven program for GC/MS analysis of liquid samples with DB-1ms column (LV = 30 cm s^{-1})

Step no.	T rate (°C min^{-1})	Final T (°C)	Hold time (min)
0	-	35	1.00
1	7	120	1.00
2	5	150	2.00
3	10	160	1.00

Table 4-3 Oven program for GC/MS analysis of liquid samples with HP-INNOWax column (LV = 65 cm s^{-1})

Step no.	T rate (°C min^{-1})	Final T (°C)	Hold time (min)
0	-	35	1.00
1	10	70	1.00
2	15	250	1.00

4.1.4.1 Headspace Analysis

Derivatization of formic acid standards and liquid samples was performed in accordance with a method described in literature (Bursová, Hložek and Čabala, 2015). Briefly, 100 μl of 10 % v/v 2-propanol in H_2O was placed in a 20 ml headspace vial, then 5 μl of concentrated sulphuric acid (98 %) was added as a homogeneous catalyst. Following this, 100 μl of 7 % HCOOH standard were added, and the vial sealed with a PTFE/butyl septa and steel cap. The sample was then manually shaken and heated to 80 °C for 10 minutes on a hot plate. A gas tight syringe needle was meanwhile heated in an oven to approximately 50 °C. The needle was injected into the vial and vapour was pumped three times to ensure homogeneous mixing, after which 500 μl was manually injected into the HP-INNOWax column. The oven was held at 50 °C for 4 minutes, then increased to 180°C at a heating rate of 65°C min^{-1}. Inlet temperature was maintained at 250 °C with linear velocity of 16 cm s^{-1} and an MS interface temperature of 200 °C. Injection were performed in 1:30. split mode

4.1.4.2 Extraction and Analysis of Oil Phase

The total quantity of oil in the sample could not be quantified as some of the sample was removed and stored for HPLC analysis. Individual substances were not

quantified, but species matching the mass spectroscopy library with accuracy over 85 % were noted.

The liquid phase post-reaction was filtered to separate the water-insoluble fraction. Separation of the oil and aqueous phase was carried out according to a published protocol (Wu *et al.*, 2017). After removing liquid product, the reactor walls were washed with 5 ml dichloromethane (DCM), after which this fraction was combined with 15-30 ml of filtered liquid. The liquid was extracted with 25 ml dichloromethane (DCM) thrice. Residual water was removed with magnesium sulfate. The DCM-extracted phase was rotary evaporated at reduced pressure and 40℃ until no more solvent was present. The remaining mass was denoted bio-oil. Subsequently 1 ml of DCM was re-introduced into the flask to solubilise the bio-oil, which was then analysed by GC/MS with DB-5ms column (25 m x 0.25 mm I.C, 0.25 µm) using a method adapted from Wu and co-workers (Table 4-4) (Wu *et al.*, 2017). The He carrier air flow was 1 ml min^{-1}, injection volume was 0.1 µl and split ratio set to 50.

Table 4-4 Oven program for GC/MS analysis of bio-oil

Step no.	T rate (℃ min^{-1})	Final T (℃)	Hold time (min)
Initial	-	60.0	1
1	5	150.0	5
2	10	300.0	5

4.1.4.3   Gas Sample Analysis

Gas samples were analysed using a TRACE 131 GC/TCD (Thermo Scientific, USA) equipped with a HayeSep Q column (2 m x 0.95 mm I.D., 1/16" O.D.) and MS-5A column (2 m x 1.00 mm I.D., 1/16" O.D.) (both Restek Corp., USA). The detector temperature was maintained at 150℃ with an argon reference gas flow rate of 1 ml min^{-1}. Auxiliary heating was set to 80℃. Gas samples were extracted from gas bags using a 50 ml syringe and injected through to the GC injection loop. Analysis was started once the sample loop equilibrated and no more bubbles were exiting the column. The oven programme is shown in Table 4-5.

Table 4-5 Oven program for GC/TCD analysis of gas samples

Step no.	T rate ($^{\circ}$C min^{-1})	Final T ($^{\circ}$C)	Hold time (min)
Initial	-	50.0	2.50
1	30	70.0	8.80
2	80	150.0	0

4.1.5 Ion Chromatography

Liquid product analysis carried out using an Metrohm 883 Basic IC plus ion chromatographer equipped with Metrosep A Supp 4 column (250/4.0 mm) (both Metrohm, UK). An eluent of 1.7 mM $NaHCO_3$ with 1.8 mM Na_2CO_3 was used with a flow rate of 0.5 ml min^{-1} with 100 mM H_2SO_4 as regen. Solutions were prepared by degassing 1 L of deionised H_2O in a sonicator for 20 minutes, followed by addition of $NaHCO_3/Na_2CO_3$ or H_2SO_4. The column was left to equilibrate for a minimum of one hour before analysis. Standards of 100 ppm formic, acetic, lactic, glycolic, and propionic acids were prepared from commercially purchased chemicals.

4.1.6 High Performance Liquid Chromatography

HPLC was carried out using an ECO2080 HPLC (ECOM, Czech Republic) equipped with an ECP 2010 HPLC pump, ECDA2800 UV-Vis PDA detector and RI2000 Refractive Index Detector. An organic acid specialised Agilent Metacarb 87H column (300 x 7.8 mm) with a MetaCarb 87H (50 x 4.6 mm) guard column (both Agilent Technologies, USA) was used. Clarity software (DataApex, Czech Republic) was used for analysis. An analysis protocol was developed by manipulating conditions, including flow rate, column oven temperature, and the concentration of sulfuric acid in the mobile phase. For conciseness, the details of HPLC method development were omitted in this report. Ultimately, a flow rate of 0.6 ml min^{-1} 5 mM H_2SO_4 was selected, with oven temperature set to 60 °C. The RI and PDA detectors were set at 30 °C and the PDAD wavelength set to 210 nm. The mobile phase was prepared using 98 % H_2SO_4 and Type I deionised water. Prior to analysis, 0.500 µl of liquid sample was acidified with 5 µl 98 % H_2SO_4 and filtered through a 0.22 µm filter. Acidification of samples was necessary due to the column requiring pH $\leq$ 7 while collected samples had a pH between 8–10.

Sample matrix clean-up was carried out by solid phase extraction (SPE) with Bond Elut Plexa PAX strong anion-exchange sorbent cartridges (Agilent Technologies, USA). A standard of 1 g l^{-1} HCOOH was used in the SPE method development. Air was used to push the liquid through the cartridge by use of a 50 ml syringe and attached tubing. Methanol was used as a conditioning and washing solvent.

4.2 RESULTS AND DISCUSSION

Preliminary experiments were carried out based on optimal conditions reported in various literature. A concentration of 0.5 M NaHCO$_3$ was chosen for primary experiments in accordance with previous literature (Andérez-Fernández *et al.*, 2017). A 1:5 ratio of glucose to sodium bicarbonate was selected to ensure sufficient reductant was present with an excess of CO$_2$ carrier. Previous research into optimal filling volume found that 50 vol % was optimal for maximum HCOOH yield (Michiels *et al.*, 2015). Temperature was set at 300 °C in accordance with optimal temperature reported in literature (Shen, Zhang and Jin, 2011; Yang *et al.*, 2019). Reactions were carried out for 1 hour on the basis that biomass degrades quickly at this temperature, and hydrogen will therefore be available for CO$_2$ reduction (Miyazawa and Funazukuri, 2005). It should be noted that mixing speed has not been commonly reported in literature due to the large variety of reactors used. Therefore, a mixing speed of 500 RPM was chosen for homogeneous mixing.

4.2.1 Gas Chromatography

Gas chromatography was used in the first place to analyse products formed in the reaction. The stationary phase of the GC column was found to have a significant effect on product identification. Using a non-polar DB-1ms column, the dominant products were cyclic ketones, while only a few small molecules were observed using the polar HP-INNOWax column. The chromatograph obtained over a non-polar GC column is found in Figure 4-2, with species identified in Table 4-6.
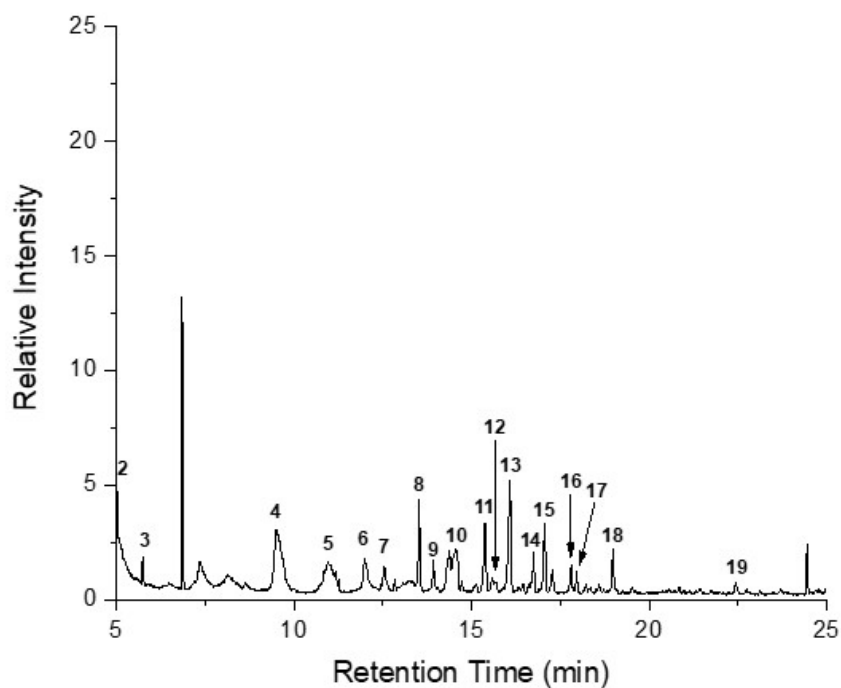
Figure 4-2 GC/MS Chromatogram of liquid products of hydrothermal reaction of NaHCO₃ with glucose over DB-1ms column (reaction conditions: 1h, 300°C, 0.05M glucose, 0.5M NaHCO₃, 50 ml water filling); species are assigned in Table 4-6

Table 4-6 Liquid species identified by GC/MS analysis via DB-1MS column

Peak no.	Retention Time	Chemical Formula	Compound
1	4.24	CH_2O_3	Carbonic acid
2	5.00	C_3H_6O	Acetone
3	5.75	$C_2H_4O_2$	Acetic acid
4	9.50	$C_6H_{10}O$	2-methyl-cyclopentanone
5	10.95	C_6H_8O	2-methyl-2-cyclopenten-1-one
6	12.00	C_8H_{14}	2,3-dimethyl-2,4-hexadiene
7	12.55	$C_6H_{14}O_5$	Diglycerol
8	13.53	$C_8H_{16}O$	2-Octanone
9	13.93	$C_8H_{18}O$	5-methyl-2-heptanol
10	14.55	$C_7H_{10}O$	2,3-dimethyl-2-cyclopenten-1-one
11	15.39	$C_8H_{12}O$	3,4,4-trimethyl-2-cyclopenten-1-one,
12	15.69	C_7H_8O	m-Cresol
13	16.08	$C_8H_{12}O$	1-acetyl-1-cyclohexene
14	16.75	$C_9H_{14}O$	2,3,4,5-tetramethyl-2-cyclopenten-1-one,
15	17.06	$C_9H_{14}O$	Isophorone
16	17.81	$C_9H_{16}O$	1-methyl-2-methylene-cycloheptanol
17	17.96	$C_{10}H_{18}$	1-methyl-1-(2-methyl-2-propenyl) cyclopentane
18	18.98	$C_6H_6O_2$	Catechol
19	22.44	$C_{10}H_{10}O$	2-methyl-1-indanone

Several interesting species were detected, including the industrially applied solvents acetone and isophorone, and commodity chemicals like acetic acid and catechol. Many cyclic ketones were also observed.

No formic acid could be identified using this GC/MS analysis of pure samples, and no products could be attributed specifically to bicarbonate reduction. Furthermore, the relative intensity of species in aqueous samples was low. Due to the alkaline pH of the aqueous matrix, organic acids in samples were present predominantly in ionized form rather than as free acids (Álvarez, Bansode, *et al.*, 2017). As gas chromatography requires volatilization, these species cannot be identified from pure samples, and

decreasing matrix pH is required to form volatilizable free acids. However, acidification with mineral acids is generally not compatible with GC columns due to rapid stationary phase degradation, and the use of organic acids was discouraged due to unknown species in the reaction. Furthermore, the sensitivity of the instrument to HCOOH was found to be low. Injection of a 7 % (v/v) 95 % HCOOH standard showed that the impurity in the standard, acetic acid, resolved more clearly than the main constituent (Figure 4-3). As concentrations of formic acid were expected to be significantly lower in hydrothermal samples, direct analysis of HCOOH by GC/MS was deemed unsuitable in this work.
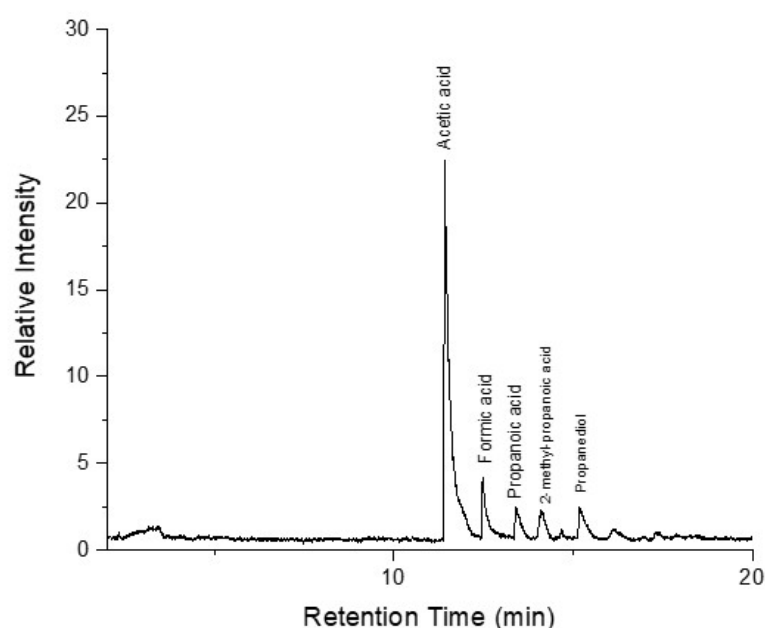
Figure 4-3 GC/MS Chromatogram of liquid injection of 7 % (v/v) commercial HCOOH over HP-INNOWax column

4.2.1.1 Headspace Analysis

An alternative method of quantifying formic acid is through headspace analysis, which involves derivatizing HCOOH with an alcohol and quantifying the derivatized product by injecting the vapour phase. A sample of 10 % (v/v) HCOOH in H_2O was derivatized with 2-propanol (Bursová, Hložek and Čabala, 2015). Derivatization of commercial formic acid yields 1-methylethyl ester formic acid (Figure 4-4). Interestingly, in stark contrast with liquid injection, vapour phase injection of the derivatized sample also showed a large peak for pure HCOOH (Figure 4-5). This is

further indication that quantification of liquid phase HCOOH is not optimally done by GC/MS.
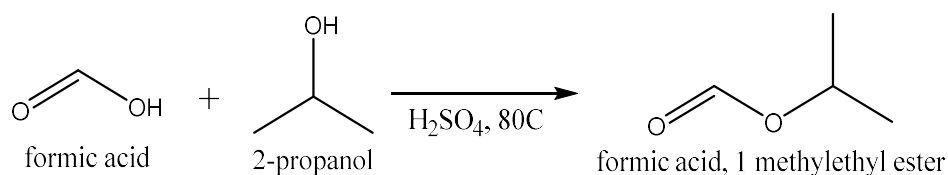
Figure 4-4 Derivatization of formic acid with 2-propanol
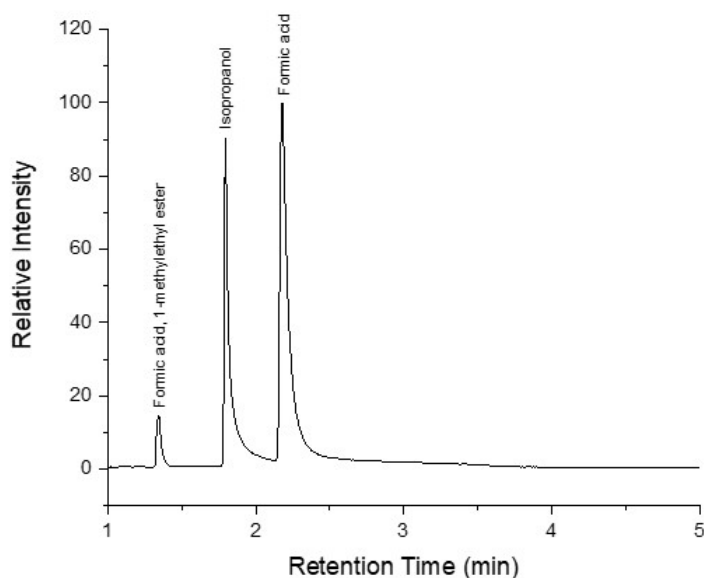
Figure 4-5 GC/MS Chromatogram of headspace injection of 1-propanol derivatized 10 % (v/v) HCOOH standard over HP-INNOWax column

It was found that headspace analysis of HCOOH is valuable for qualitative analysis to test for the presence of the acid. Derivitization of only a fraction of the 10 % (v/v) HCOOH occurred, as evidenced by the strong free formic acid peak (Figure 4-5). Furthermore, this technique requires manual sample injection which may result in additional errors. When applying this technique to hydrothermal samples, unfortunately no formic acid ester or pure product could be determined. This is believed to be due to relatively low concentration of HCOOH in the product. Therefore, this technique was not deemed to be insufficiently sensitive to quantify the low concentrations of formic acid in hydrothermal samples. As a result, liquid chromatography was investigated for quantitative analysis.

4.2.2 Ion Chromatography

Further method development was carried out by ion chromatography (IC), which is used to detect cations or anions in solution and is commonly used for organic acid analysis. The focus of IC method development was identifying the formate ion. An analysis of NaCOOH solution verified that the technique is highly sensitive to this species, and a linear response was generated to produce a calibration curve (Appendix A). However, it was found that anions which can reportedly form in the reaction may overlap disruptively with formate due to the column not being specialised for organic anions (Figure 4-6).
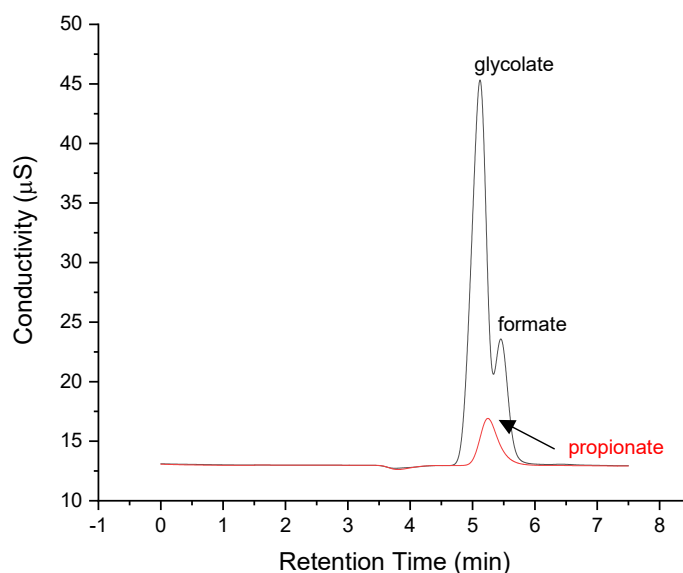
Figure 4-6 IC Chromatogram of 1 g l^{-1} mixed glycolate and formate solution, and 1 g l^{-1} propionate standard

Liquefaction literature reports that a wide variety of organic acids may form from glucose, including formic, acetic, glycolic, lactic and maleic acids (Yun Yang and Montgomery, 1996; Calvo and Vallejo, 2002). Therefore, sufficient separation of organic anions could not be achieved with the available set-up. Existing equipment was limited by the lack of a more specialized column and a column oven, which is required for satisfactory organic acid separation. Thus, further method development was carried out by HPLC using a specialized column.

4.2.3   High Performance Liquid Chromatography

High performance liquid chromatography with a specialised organic acids column was utilised to further analyse the liquid phase reaction products. Standards of organic acids were well-resolved and separated, however real samples showed a large tailing peak at approximately 6 minutes retention time caused baseline drift (Figure 4-7).
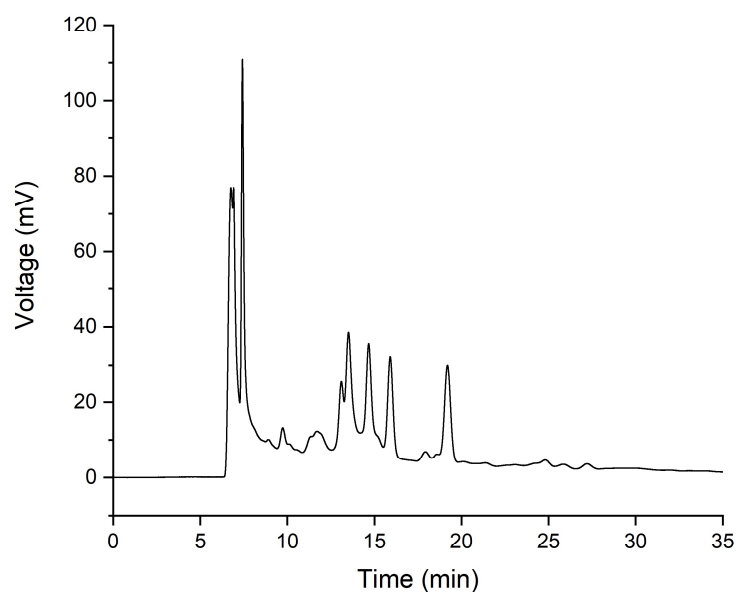
Figure 4-7 Representative HPLC chromatogram of hydrothermal reaction of NaHCO₃ with glucose

Liquid-liquid extraction with DCM to remove ketones and other bio-oil constituents was carried out in an attempt to remove the tailing species. This did not result in any improvement to the chromatogram, which signifies that the species is preferentially water-soluble and is likely a sugar derivative. To determine if matrix clean-up would be effective in removing the tailing peak with minimum analyte losses, solid phase extraction was explored.

4.2.3.1 SPE Method Development

Solid phase extraction (SPE) is used to clean up sample matrices and may be used for both polar and non-polar anions. One of the main advantages of SPE is that only a small sample volume is required for separation. A single standard of 1 g l⁻¹ HCOOH

was used in the development of an SPE method to compare results and determine retention on the sorbent bed.

Several different procedures were attempted for successful SPE extraction and sample clean-up. Generally, SPE extraction involves five steps – sample preparation, cartridge conditioning, sample loading, washing, and elution. The methods attempted in this work are summarised in Table 4-7.

Table 4-7 SPE Methods used for organic acid extraction

Step	Method 1	Method 2	Method 3
Sample Preparation	pH adjusted to 13.5 with NaOH	diluted 1:3 with 2 % NH_4OH	1:3 dilution with 2 % NH_4OH
Condition	0.5 ml MeOH 0.5 ml H_2O	2 x 1.5 ml MeOH 2 x 1.5 ml H_2O	1 ml MeOH 1 ml H_2O
Load	100 µl	2 x 1 ml	500 µl loaded
Wash	0.5 ml MeOH 0.5 ml H_2O	2 x 1.5 ml MeOH 2 x 1.5 ml H_2O	1 ml MeOH 1 ml H_2O
Elute	2 x 250 µl 1M H_2SO_4	3 x 250 µl 5 % acetic acid OR 3 x 250 µl 1M H_2SO_4	2 x 250 µL 15 % acetic acid

Method 1 was carried out according to instructions by the cartridge manufacturer. However, only trace formic acid was eluted with this method. Increasing the volume of the elution step from 250 to 750 µl sulfuric acid did not result in increased elution. It is proposed that this is caused by strong interaction between the anions and the strong ion exchanger bed. However, when attempting Method 1 on a sample of a hydrothermal reaction, sample clean-up was successful with complete elimination of the large tailing peaks eluting at the front of the chromatogram. To improve anion elution, Method 2 using ammonia was recommended by the manufacturer.

Using Method 2 initially with H_2SO_4 eluent, some HCOOH was observed to elute off the cartridge. However, this was below the quantifiable range of the HPLC software, and organic acids were still detected in the third collected aliquot of elute signifying sulfuric acid is not ideal for eluting anions off the sorbent bed. In comparison, it was found that HCOOH elutes in the first 2 aliquots when 5 % acetic acid was used instead. The baseline was also observed to be more stable with acetic acid as the elute, as the early eluting H_2SO_4 peak causes additional tailing which impacts the baseline stability. Subsequent method development was thus performed with acetic acid as the elution solution.

To facilitate cartridge loading, the volumes of all steps was reduced and protocol adjustment made (Table 4-7, Method 3). To optimise and test the quantitative possibility of SPE, a standard of 1 g l^{-1} HCOOH was used. The elution step was optimised by varying acetic acid concentration to determine the optimal concentration for highest recovery of organic acid. Solutions of 5 %, 10 %, 15 % and 20 % (v/v) acetic acid were used. It must be noted that a theoretical maximum of 0.25 g l^{-1} was expected if full retention of formic acid on the sorbent bed and complete elution in the final step were achieved. The two aliquots of 250 μl eluent were combined for HPLC analysis and calculation of recovery. It was found that HCOOH recovery was maximised at 15 % acetic acid based on results obtained in Table 4-8.

Table 4-8 Recovery of formic acid with increasing acetic acid concentration in eluent in SPE elution of 1 g l^{-1} HCOOH standard

Acetic acid (v/v %)	Detected HCOOH Conc.	Recovery (%)
5	0.008	3.2
10	0.195	78.0
15	0.214	85.6
20	0.188	75.2

In the present work, a maximum of 85.6 % recovery of formic acid from SPE was achieved. This was deemed to be insufficient for quantification of HCOOH due to low concentrations in hydrothermal samples. However, SPE was found to be valuable for determining retention times of different organic anions present in the solutions. Organic acids were selectively adsorbed on the sorbent bed, and their retention times noted as species of interest for identification.

Quantification was instead carried out on pure samples with valley-to-valley baseline extrapolation. Calibration was carried out by analysing formic acid samples from 0.01 to 5 g l^{-1}. To ensure this simple method was sufficiently accurate, a hydrothermal sample was quantified, then spiked with a 2 g l^{-1} formic acid. The resulting quantification showed a rise in HCOOH detected concentration corresponding to the original concentration plus the spiking. Thus, although SPE proved useful in determining the retention times of organic acids, further quantification was carried out using valley-to-valley peak integration.

4.3 PRODUCT IDENTIFICATION

Aqueous species were identified by exhaustive literature search of similar reactions, followed by analysing standards of potential analytes. The full list of thirty-two standards and their retention times is available in Appendix B. A representative chromatogram demonstrating identified organic acids can be viewed in Figure 4-8.
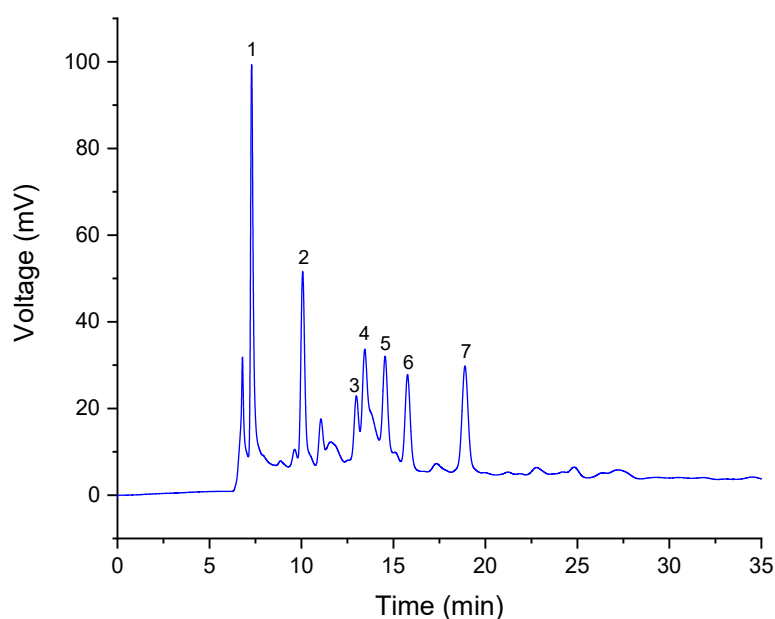
Figure 4-8 HPLC PDA Chromatogram of liquid product of hydrothermal conversion of NaHCO$_3$ with glucose (reaction conditions: 1h, 250°C, 0.05M glucose, 0.5M NaHCO$_3$, 50 ml water filling). Peaks denoted – 1: oxalate, 2: pyruvate, 3: glycolate, 4: lactate, 5: formate, 6: acetate, 7: acrylate
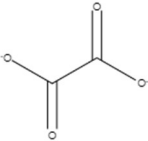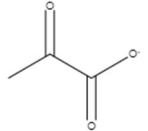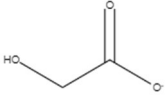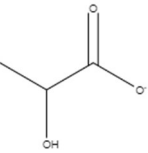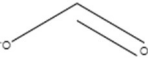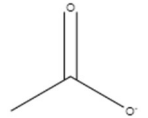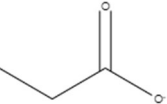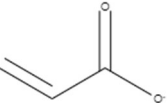
A disadvantage of analysing samples in this manner was that some species could not be quantified due to strong overlap with neighbouring peaks. For example, lactate

overlaps strongly with glycolate as well as a second species forming a shoulder on the right. Quantification of these species was carried out by manually deconvoluting peaks in OriginPro software using the peak fitting function. However, most species of interest could be effectively analysed in the HPLC software. Organic acids identified in hydrothermal samples can be seen in Table 4-9. Propionate was observed to have a retention time closely associated with acrylate, but distinguishable by the formation of a small shoulder in some samples. 5-HMF was also identified in some samples.

Chapter 4: Analytical Method Development

Table 4-9 Organic acids identified in samples of hydrothermal reaction of $NaHCO_3$ with glucose

Retention Time	Species	Formula	Structure
7.3	Oxalate	C_2O_4	
10.2	Pyruvate	$C_3H_3O_3$	
13.1	Glycolate	$C_2H_4O_3$	
13.5	Lactate	$C_3H_5O_3$	
14.8	Formate	CHO_2	
15.9	Acetate	$C_2H_3O_2$	
18.4	Propionate	$C_3H_5O_2$	
18.5	Acrylate	$C_3H_3O_2$	

Chapter 4: Analytical Method Development

Of the species described in Table 4-9, oxalate, pyruvate, formate and acetate have been reported from CO_2 reduction by various methods (Takahashi *et al.*, 2006; Shen, Zhang and Jin, 2012; Wang *et al.*, 2019). Other products have been widely reported from biomass liquefaction. However, identification of these species is valuable as the relationship between products is invaluable in gaining mechanistic insight. For example, pyruvate has been reported to form from CO_2 reduction with lactate (Shen, Zhang and Jin, 2012). Although the latter is not a product of CO_2, it is key for CO_2 reduction by this reaction.

HPLC results were coupled with GC/MS analysis of extracted bio-oil to obtain a full picture of reaction products. Both aqueous and organic-soluble species were thus identified, which assists in quantitative analysis and mechanistic insight into the reaction. Furthermore, initial analysis of pure aqueous samples showed numerous molecules, but solutions were dilute and the relative intensity of compounds low. Extraction of organic-soluble molecules concentrated samples, thus increasing the peak intensity and allowing species to be identified. Dichloromethane was chosen as an organic solvent for extraction. Previous reports have indicated that the polarity of the extraction solvent has a significant impact on the yield of composition of the extracted bio-oil. Yan and co-workers assessed ten solvents in the extraction of bio-oil derived from hydrothermal liquefaction of duckweed and found that DCM was the most effective due to its polarity and immiscibility in water, which resulted in the highest material recovery rate (Yan *et al.*, 2016). In the present work the concentration of different bio-oil constituents was not quantified but was used for compositional analysis of the oil phase. Some products originally detected by GC/MS were not found in the bio-oil DCM extract due to being more water-soluble, for example acetone.

Identified products in the organic phase are shown in Table 4-10. Analysis found that cyclic ketones are the dominant class of products, as well as aromatics and some long-chain compounds. Numerous substituted cyclopentanone species were found, which have previously been reported from monosaccharide dehydration in HTW (Wu *et al.*, 2017). Within this work, it was also suggested that the formation of cyclopentenone prevents the conversion of sugars to 5-HMF and furfural derivatives, and subsequently coke, thereby inhibiting char formation. Aromatics such as substituted phenols were also detected in samples and have previously been reported as products of cellulose liquefaction (Russell, Miller and Molton, 1983). Benzenediols have

previously been reported as a product of sugar alkaline treatment. For example, 2,5-dimethyl-1,4-benzenediol, has been reported to form from alkaline treatment of biacetyl, a fragmentation product of sugar alkaline treatment (Russell, Miller and Molton, 1983). It should be noted that long chain esterified organic acid hexadecenoic acid methyl ester has previously been reported as a biomass liquefaction product (Gangwal *et al.*, 2016). Catechol and acetic acid previously reported in biomass liquefaction of other biomass sources (Isahak *et al.*, 2012). Literature supports the formation of these species directly from glucose, and it is highly challenging to assign any species to CO_2 reduction.

Chapter 4: Analytical Method Development

Table 4-10 Bio-oil composition of extracted sample of hydrothermal reaction of NaHCO₃ with glucose (reaction conditions: 2 h, 250 °C, 0.05 M glucose, 0.5 M NaHCO₃, 50 ml H₂O)

Retention Time	Name	MS Library Match
3.10	2,5-dimethyl-cyclopentanone	90
3.25	2,4-dimethyl-cyclopentanone	92
3.28	Cyclohexanone	89
3.30	2,3-dimethyl-cyclopentanone	95
3.40	2-methyl-2-cyclopenten-1-one	98
3.55	trans-3,4-dimethylcyclopentanone	91
3.95	2,3-dimethyl-2,4-hexadiene	88
4.00	2-ethyl-cyclopentanone	91
4.09	(1-methylethylidene)-cyclopentane	88
4.40	3-Ethylcyclopentanone	90
4.43	3-methyl-2-cyclopenten-1-one	92
5.63	4,4-dimethyl-2-cyclopenten-1-one	92
5.97	2,3-dimethyl-2-cyclopenten-1-one	96
6.39	3-methyl-phenol	93
6.91	p-Cresol	92
7.23	1-(1-cyclohexen-1-yl)-ethanone	88
7.67	2,3,4,5-tetramethyl-2-cyclopenten-1-one	95
8.79	2,3-dimethyl-phenol	94
11.65	4-methyl-1,2-benzenediol	94
12.27	2,3-dihydro-1H-inden-1-one	90
12.46	4-methyl-1,2-benzenediol	94
14.13	2,6-dimethyl-1,4-benzenediol	86
14.89	4-ethylcatechol	88
21.05	Tetradecanal	95
29.24	Hexadecanoic acid, methyl ester	94
33.67	12-hydroxy-9-octadecenoic acid	91

Gas products formed from the reaction were found to be solely H_2 and CO_2. Calibration was also carried out for CH_4 although this species was not detected in any reactions between NaHCO₃ and glucose under any conditions used in this work.

4.4 CONCLUSION

In this chapter, analytical techniques for the identification and quantification of formate and other key organic acids and species formed in the reaction of $NaHCO_3$ with glucose were developed. Initial analysis with GC proved ineffective due to the low concentration of products and mildly alkaline environment forming non-volatile species. GC/MS analysis of pure samples showed predominantly cyclic species in solution. Ion chromatography was found to be a good method for ionised acid analysis but was limited by the equipment limitations. HPLC proved to be the most effective method of organic acid analysis, although baseline broadening occurs due to the sample matrix. Liquid-liquid extraction was ineffective at improving the baseline. Solid phase extraction of samples was effective at removing the species causing the broadening, but some loss of formate was observed. Due to concentrations of this species being relatively low, SPE loses were determined to be too substantial in the current work and this method was deemed insufficient for accurate product concentration analysis. However, it was valuable in showing the retention times of anions.

HPLC of pure samples was carried forward with valley-to-valley extrapolation of peaks and manual deconvolution of closely overlapping species carried out in OriginPro software. Although the reaction is deceptively simple with two reagents, a very large number of species is formed, as evidenced by GC/MS analysis of extracted bio-oil which showed a large range of cyclic ketones and aromatics formed alongside organic acids. Furthermore, H_2 and CO_2 were found in the gas phase as additional products of the reaction.

This chapter forms the analytical foundation for the remaining work and demonstrates the complexity of analysing a solution containing many molecules and ions. Knowledge of species formed in the reaction is valuable for gaining mechanistic insight into the reaction. Based on reported literature of similar reactions, the bio-oil products were determined to be a results of glucose conversion in the present work. However, other products, including formate, oxalate, acetate and pyruvate may form from either reagent. The formation of these species from CO_2 and glucose is further explored in Chapter 5.

5 CHAPTER 5: HYDROTHERMAL CONVERSION OF BICARBONATE AND GLUCOSE TO FORMATE

Hydrothermal conversion of $NaHCO_3$ with glucose has been established as a complex series of reactions yielding a range of products. As detailed in Chapter 4, analytical methods were established to analyse the expected products resulting from CO_2 reduction, including formate ($HCOO^-$). As the most reported product of hydrothermal CO_2 conversion, establishing conditions at which formate concentration is maximised is crucial. In this chapter, reaction variables were manipulated to identify conditions at which NaCOOH concentration was maximised and the fate of this species at elevated conditions was studied.

As discussed in Section 2.8.2, studies investigating the impact of reaction variables on CO_2 conversion have been carried out with various biomass sources. These works established reaction temperature, time, filling volume, and feedstock concentration as variables that have a significant impact on product formation and yield (Shen, Zhang and Jin, 2011; Michiels *et al.*, 2015). Therefore, these variables were investigated in the present work. The stability of sodium formate at the extreme end of reaction conditions was also investigated, and the relationship between liquid and gaseous products observed. It was established in Chapter 4 that glucose liquefaction gives rise to a large range of molecules, of which organic acids are a significant portion. Therefore, a quantitative ^{13}C-NMR study was undertaken to establish the percentage of formate which can be attributed to glucose and bicarbonate, respectively. The mechanism of glucose degradation in mildly alkaline media was subsequently investigated.

This chapter seeks to provide an insight into the reactions occurring under the investigated conditions and sets the foundation for future investigation into heterogeneous catalysts and alternative CO_2 precursors.

5.1 METHODOLOGY

The source and purity of materials used in this work can be found in Section 4.1.1. The batch reactor set-up and general procedure employed for hydrothermal reactions is described in Section 4.1.2. Analysis of liquid products by HPLC and gases by GC/TCD was carried out by methods established in Sections 4.2.1 and 4.2.3, respectively.

Chapter 5: Hydrothermal Conversion of Bicarbonate and Glucose to Formate

Organic acids were quantified by producing calibration curves of peak area versus known concentration of standard (Appendix C). Error bars on graphs represent the standard deviation of products over multiple experiments. Two gas mixtures supplied by Air Products (USA) containing different proportions of CO_2, H_2, and CH_4 were used as standards (Table 5-1). A sample of 100 % CO_2 extracted from a compressed gas cylinder was used as a third calibration point in CO_2 quantification (BOC, UK), while for H_2 a pure sample was obtained from a H2PEM-100 H_2 generator (Parker Hannifin, USA). A pure standard was used to for methane calibration (Air Liquide, France).

Table 5-1 Composition of gas calibration standards

Standard	% H_2	% CO_2	% N_2	% O_2	% CO	% CH_4
1	2	30	2	1	-	65
2	40	35	1	-	23	1
3	-	100	-	-	-	-
4	100	-	-	-	-	-
5	-	-	-	-	-	100

A series of control reactions was carried out, as detailed in Table 5-2. All control reactions were carried out at the same reaction conditions of 300 °C and 3 hours. A blank reaction of solely water was carried out to establish if water splitting was occurring on the surface of the vessel walls in the absence of other reagents (Table 5-2, Entry 1). Reactions with solely $NaHCO_3$ and glucose in H_2O were also carried out to establish any products of conversion in sub-critical water (Table 5-2, Entry 2, 3). Finally, two reactions of solely glucose in pH adjusted water were carried out. Firstly, pH was adjusted to the starting pH of reactions with $NaHCO_3$, 8.2 (Table 5-2, Entry 4). In the second control experiment, the solution pH was adjusted to the final pH in reactions with $NaHCO_3$, 9.4 (Table 5-2, Entry 5). The pH of glucose controls was adjusted with 1M NaOH solution and measured by a pH meter (ETI 8100 Plus, SLS). Due to the structure of the internal reactor structures as well as operating conditions, controls in an inert reactor could not be carried out to fully negate the catalytic effects of the reactor material.

Chapter 5: Hydrothermal Conversion of Bicarbonate and Glucose to Formate

Table 5-2 Reaction parameters for control reactions (300 °C, 3 h, 50 ml H$_2$O filling)

Entry	NaHCO$_3$ (mol l^{-1})	Glucose (mol l^{-1})	Initial pH
1	-	-	7
2	0.5	-	8.2
3	-	0.05	7
4	-	0.05	8.2
5	-	0.05	9.4

Studies of filling volume and sodium bicarbonate concentration were carried out at 250 °C for 2 hours. In assessing filling volume impact, volumes of 30, 50 and 70 ml H$_2$O were considered and reagent concentrations were fixed at 0.50M NaHCO$_3$ and 0.05M glucose (Andérez-Fernández *et al.*, 2017). Subsequently, to determine if the concentration of bicarbonate in the study was sufficient, a series of experiments with increasing NaHCO$_3$ concentration were carried out. Sodium bicarbonate concentrations of 0.5, 1.2, 1.5 and 2.0 M were used in reactions carried out at 250 °C and 2 hours reaction time with a 50 ml filling volume. It should be noted that initially the concentration of glucose was doubled to 0.10 M to observe the effects on product yields. However, this was accompanied by significantly more char formation which impacted reactor cleaning time. To provide enough hydrogen for CO$_2$ reduction but prevent overwhelming influence of biomass liquefaction, the quantity of glucose was maintained at 0.05 M for the purpose of this study (Andérez-Fernández *et al.*, 2017). With increasing glucose concentration, more products of glucose liquefaction form which makes analysis more challenging, and an increase in char formation results in increased reactor cleaning and downtime. The effect of stirring was also investigated by carrying out a reaction with no stirring and comparing the outcome with a stirred reaction at identical conditions.

Temperatures of 225, 250 and 300 °C and reaction times of 1, 2 and 3 hours were investigated. The lower value of 1 hour was chosen due to the heat up time limitations of the reactor. The temperature ramp from room temperature to the set-point takes approximately 40 minutes, so a reaction time of less than 1 hour was deemed too short in the current study. A maximum time of 3 hours was chosen based on the results of published literature, as detailed in Section 2.8.2. When varying time and temperature, other variables were fixed according to the results of previous

experiments. Stirring was maintained at 500 RPM, and reagent concentrations maintained at 0.5 M NaHCO$_3$ and 0.05 M glucose in 50 ml H$_2$O. In investigating the degree of formate formation in the temperature ramp time, the reactor was heated over the course of 40 minutes to the set point. Once the set point was reached, stirring was stopped and the reactor promptly quenched in an ice bath.

To investigate and compare the decomposition of free formic acid and formate salts produced in the reaction, stability studies of both species were undertaken. A 50 ml volume of either 3.00 g l^{-1} sodium formate or 500 μl free formic acid (12.20 g l^{-1}) was reacted in 50 ml H$_2$O at 300°C for 3 hours. The extent of decomposition was calculated by Equation 5-1. Subsequently, spiking of a NaHCO$_3$/glucose reaction with 0.240 g NaCOOH was carried out to establish the products of HCOO$^-$ conversion under real reaction conditions. In mechanistic investigations, 1 ml of 40 % pyruvaldehyde solution was injected into a NaHCO$_3$/glucose reaction to determine if this species is an intermediate in organic acid formation. In reactions with fructose, 2.5 mmol of fructose were employed in place of glucose.

Equation 5-1 Percentage of sodium formate/formic acid decomposition

$$1 - \frac{Final\ [HCOONa](g\ L^{-1})}{Initial\ [HCOONa](g\ L^{-1})} \times 100 = \%\ Decomposition$$

Finally, quantitative 13C-NMR spectroscopy with inverse gated ^{1}H-decoupling using pulse program zgig with a 90° pulse was used to determine the proportion of HCOOH derived from bicarbonate reduction. NMR analysis was carried out by Khalid Doudin of the Department of Chemistry at the University of Sheffield. NaH^{13}CO$_3$ (CP 99 %) was purchased from Sigma-Aldrich. Samples were placed in a 5 mm i.d. NMR tube. Samples were also analysed by ^{1}H-NMR with water suppression. QNMR was then performed on a Bruker AVIIIHD 500 MHz Spectrometer (Bruker, USA). Unlabelled and labelled samples were compared to determine the percentage of H^{13}COOH from NaH^{13}CO$_3$ in samples.

5.2 RESULTS & DISCUSSION

5.2.1 Controls

To establish the products of solely $NaHCO_3$ and glucose in hydrothermal media, a series of control reactions were undertaken. No significant or quantifiable water splitting was found to occur in blank reactions of solely water. Similarly, no products were detected from solely $NaHCO_3$ in H_2O, signifying that bicarbonate conversion does not occur on the surface of the reactor walls or in the absence of additional species. This indicates that $NaHCO_3$ requires an additional reagent to undergo conversion. With solely glucose in water, trace formic acid was detected in concentrations below detectable range, and the solution contained significant char. In contrast, samples containing both glucose and $NaHCO_3$ were clear. This indicates that $NaHCO_3$ retards glucose conversion to char, as expected from reports on alkalis preventing char formation in biomass liquefaction (Koven *et al.*, 2017). In reactions of glucose in pH-adjusted water, trace formate was detected in concentrations below the quantifiable range. As in reaction of glucose in neutral water, lactate, glycolate, acetate and 5-HMF were detected, signifying that glucose is a satisfactory reagent for obtaining these products without the need for alkali.

Stirring was not found to impact NaCOOH formation. With stirring, the average yield was found to be 0.244 g l^{-1} formate, while without the yield was 0.240 g l^{-1}. This indicates that at sub-critical conditions with relatively low concentrations of glucose, agitation is not necessary to ensure sufficient mixing. However, the parameters developed in this work were expected to be used future investigations of heterogeneous catalytic reactions, in which stirring was expected to be more crucial for suspension of solids in solution. Therefore, although not vital, stirring was maintained at 500 RPM throughout this work.

5.2.2 Impact of Reaction Variables

5.2.2.1 Filling Volume

Subsequently, the impact of filling volume on formate was explored by varying H_2O volume from 30–70 ml. Results showed that among the three volumes investigated, 50 ml filling resulted in maximum $HCOO^-$ concentration (Figure 5-1).
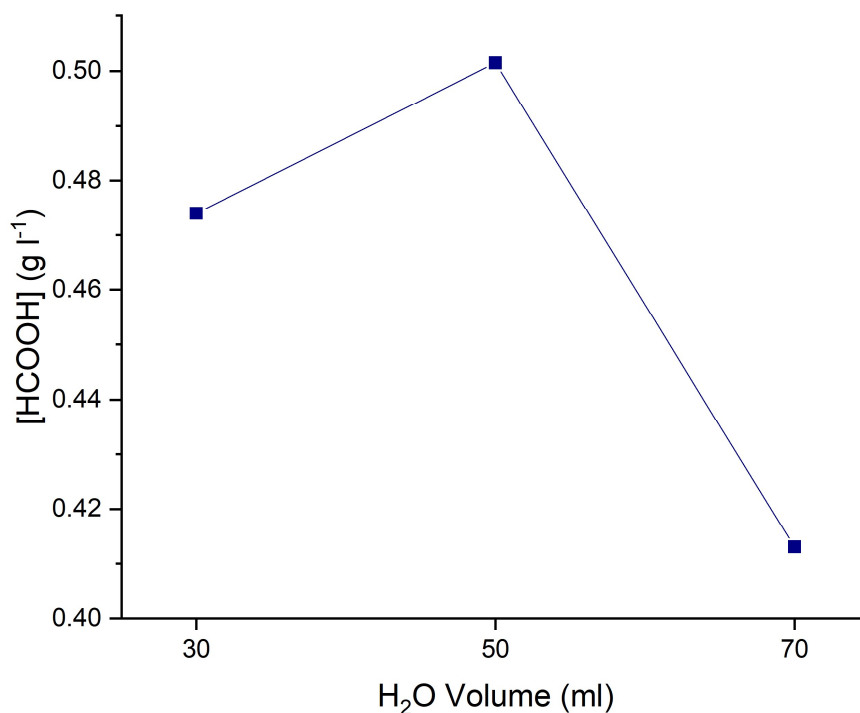
Figure 5-1 Impact of water filling volume on formate concentration. Reaction conditions: 0.50 M NaHCO₃, 0.05 M glucose, 30-50 ml H₂O, 250 °C, 2 h

Differences between lower and higher filling volume are likely a result of autogeneously generated pressure, which is higher with increasing volume. Increasing the filling vol % results in a maximum, after which the concentration decreases marginally. A similar maximum of 50 vol % was observed by Michiels and co-workers, and 60 % was observed as a maximum for Jin and co-workers (Jin *et al.*, 2008; Michiels *et al.*, 2015). Under the investigated conditions, little variation was observed between 30 and 50 ml water filling, while a decrease occurred at 70 ml. As described in Section 2.6.1, Michiels and co-workers found that filling volume directly impacted the quantity of initial H_2 generated due to its impact on reaction pressure. Higher filling volume contributes to higher pressure generation in the vessel, which is proposedly not beneficial to the present reaction. Therefore, subsequent reactions were carried out with a water volume of 50 ml.

5.2.2.2 *Sodium Bicarbonate Concentration*

Experiments were subsequently carried out examining the impact of increasing $NaHCO_3$ concentration. As the CO_2 precursor, it is important to establish if sufficient concentrations are available to undergo reduction. Formate concentrations continuously increased up to the maximum investigated $NaHCO_3$ concentration of

2.0 M (Figure 5-2). However, the increase of the product was not found to be proportional to that of the reagent, with a four-fold increase in $NaHCO_3$ resulting in a modest 0.06 g l^{-1} increase in formate. A similar trend of increasing HCOOH with increasing $NaHCO_3$ were observed by Yang and co-workers, who attributed this to increased decomposition of hexanehexol with more alkali leading to more H_2 availability for HCO_3^- reduction (Yang *et al.*, 2018). In the present study, this effect was only marginally observed, and it is therefore likely that the concentration of $NaHCO_3$ is not the main limiting factor for higher concentrations of HCOOH.
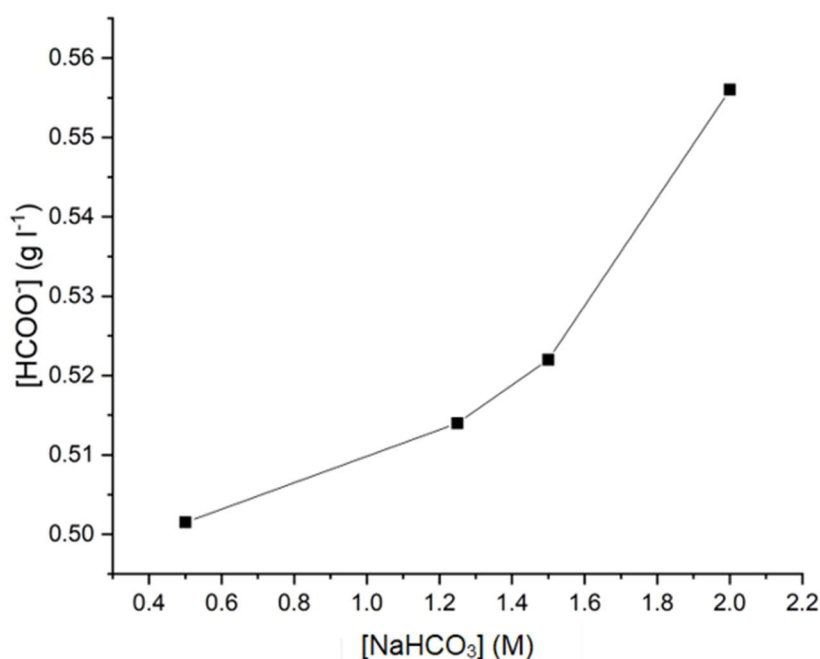
Figure 5-2 Formate concentration as a function of starting $NaHCO_3$ concentration. Reaction conditions: 0.05 M glucose, 50 ml H_2O, 250 °C, 2 h

Increasing $NaHCO_3$ concentration above 0.50 M did not result in a significant increase in formate formation, and thus the concentration was maintained at 0.50 M in subsequent experiments. The effect of starting $NaHCO_3$ concentration on gaseous and aqueous products was also investigated. No impact of higher concentrations on bio-oil composition was observed, while increase resulted in higher CO_2 concentration in the gas phase.

5.2.2.3 Temperature and Time Variation

The impact of temperature and reaction time on formate production was next investigated to determine conditions at which concentration was maximised. Prior to carrying out the reaction condition optimization and in the context of literature discussed in Section 2.8.2, highest HCOOH concentration was predicted at higher temperatures and longer reaction time. The results of the study are demonstrated in Figure 5-3. It was found that at 225 °C formate production generally plateaued at approximately 0.45 g l^{-1}. Increasing temperature to 250 °C demonstrated a maximum of 0.502 g l^{-1} after 2 hours. Differences between these temperatures may be due to additional bicarbonate reduction occurring at the higher temperature. Notably, at the highest temperature of 300 °C, a decrease in concentration was observed with increasing reaction time, with 0.244 g l^{-1} HCOO$^-$ remaining after 3 hours.
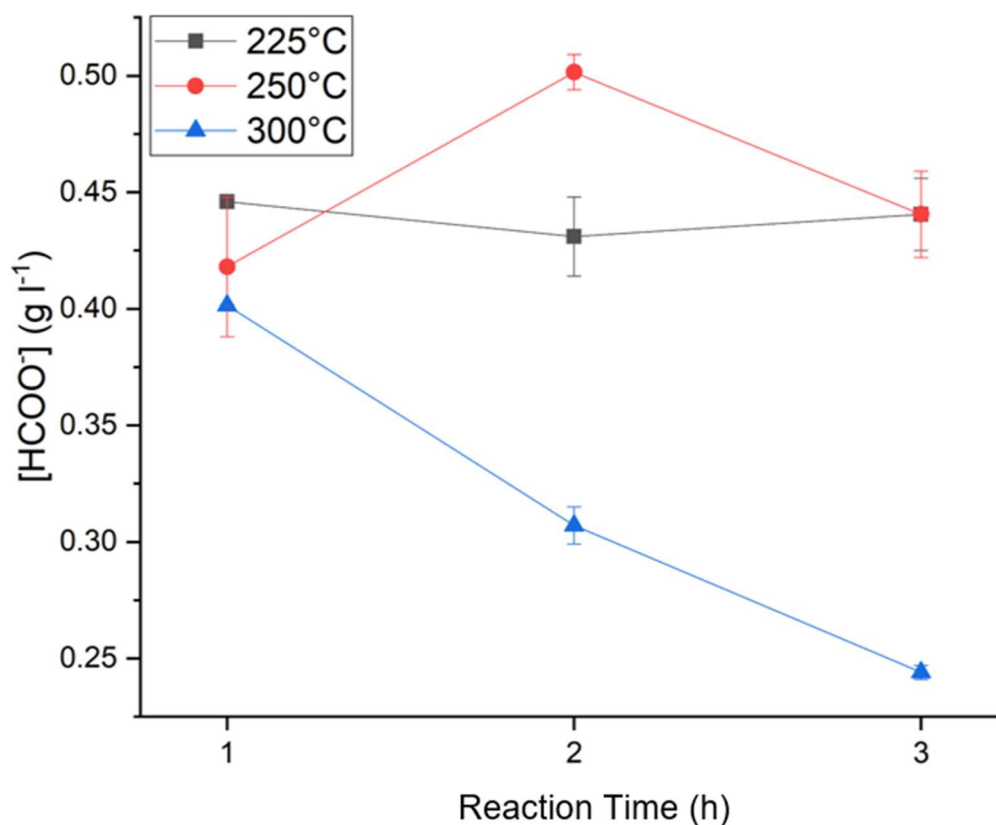
Figure 5-3 Formate concentration with varying reaction time (0–3 h) and temperature (black ■ – 225 °C, red ● – 250 °C, blue ▲ – 300 °C). Reaction conditions: 0.50 M NaHCO$_3$, 0.05 M glucose, 50 ml H$_2$O

Chapter 5: Hydrothermal Conversion of Bicarbonate and Glucose to Formate

Results indicate a significant portion of formate is formed during the temperature ramping time for all temperatures (Table 5-3). At the lowest temperature studied, the maximum formate formation occurred within the ramping time, after which no further changes occurred (Table 5-3, Entry 1). Similar concentration was detected at 250 °C, though concentration eventually peaked after 2 hours (Table 5-3, Entry 2). Surprisingly, the maximum detected concentration of HCOO⁻ at 300 °C was at t_0, after which a decrease occurred over time (Table 5-3, Entry 3). As the concentration at 300 °C decreases with increasing reaction time, the majority of the reaction is completed, and a maximum is reached before time zero. Overall, the temperature ramp studies showed that the formation of formate occurs rapidly at all investigated temperatures, indicating that shorter reaction times may be employed with satisfactory product yields.

Table 5-3 Formate concentration detected at time zero versus maximum detected at a given temperature. Reaction conditions: 0.50 M NaHCO₃, 0.05 M glucose, 50 ml H₂O

Entry	Temperature (°C)	[HCOO-] at t_0 (g l⁻¹)	Max [HCOO-] at set T
1	225	0.436	0.446
2	250	0.412	0.502
3	300	0.424	0.402

Analysis of bio-oil composition with increasing temperature indicated that an increase in substituted cyclopentanones was detected at the highest temperature. As discussed in Section 4.1.3, solely the composition, and not the concentration of species in the bio-oil was analysed in the present work, and substituted cyclopentene-1-ones were identified as the main products in this phase. While the relative intensity of peaks associated with cyclopentene-1-ones was higher at 250 °C than 300 °C, the intensity of saturated cyclopentanones was found to increase at 300 °C compared to 250 °C (Figure 5-4). At 250 °C, peaks associated with saturated cyclopentanones (peaks 1-4, 6, 8, 10, Figure 5-4) are relatively low. However, at 300 °C the peaks associated with saturated species increase in relative intensity compared to cyclopentene-1-ones (peaks 5, 11, Figure 5-4). Comparing the ratio of 3-ethylcyclopentanone (peak 10) and 3-methyl-2-cyclopenten-1-one (peak 11), an increase in the peak ratio from 0.15 to 0.51 indicates that there is an increase in saturated cyclic species at 300 °C. This indicated the possibility that increased

concentrations of H_2 may be present at higher temperatures which saturate double bonds. Hydrogen production and the results of gas analysis are further discussed in Section 5.2.3.
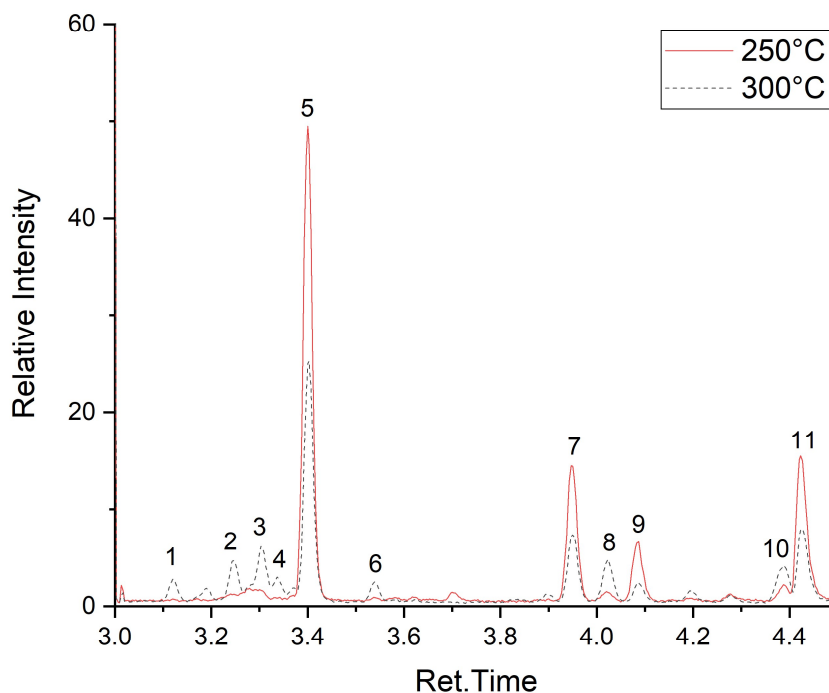
Figure 5-4 GC/MS of extracted bio-oil from reactions at 250 °C (solid red) and 300 °C (dashed black). Designations – 1: 2,5-dimethyl-cyclopentanone, 2: 2,4-dimethyl-cyclopentanone, 3: cyclohexanone, 4: 2,3-dimethyl-cyclopentanone, 5: 2-methyl-2-cyclopenten-1-one, 6: trans-3,4-dimethylcyclopentanone, 7: 2,3-dimethyl-2,4-hexadiene, 8: 2-ethyl-cyclopentanone, 9: (1-methylethylidene)-cyclopentane, 10: 3-Ethylcyclopentanone, 11: 3-methyl-2-cyclopenten-1-one. Reaction conditions: 0.50 M NaHCO$_3$, 0.05 M glucose, 50 ml H$_2$O

To assess any species which formate may be converting to at higher temperatures, quantitative analysis of organic acids was undertaken. At 225 °C, organic acids showed a similar trend to formate – concentrations remained generally stable between 1 and 3 hours and no oxalate was formed (Figure 5-5A). With increasing temperature to 250 °C, an increase in lactate and acetate was observed with increasing reaction time (Figure 5-5B). Due to the strong overlap between lactate and glycolate, significant error was recorded when quantifying these species.
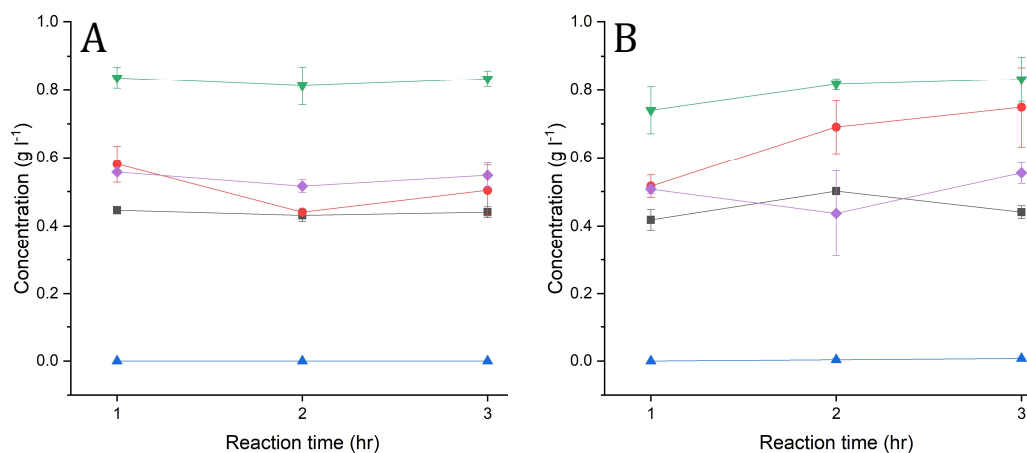
Figure 5-5 Concentrations of organic acids at 225 °C (A) and 250 °C (B) with increasing reaction time. Line designations: green ▼ – acetate, red ● – lactate, purple ◊ – glycolate, black ■ – formate, blue ▲ – oxalate. Reaction conditions: 0.50 M NaHCO₃, 0.05 M glucose, 50 ml H₂O

At 300 °C, most species were observed to gradually decline over time, with the exception oxalate and acetate (Figure 5-6). This illustrated the possibility that formate may be further converted to acetate or oxalate. It has been reported that in the presence of Raney-Ni, formate is an intermediate in acetate formation (Wang *et al.*, 2019). High concentrations of Ni in the reactor material present this as a possible reaction pathway. Likewise, oxalate can be formed from formate by pyrolysis (Riemenschneider and Tanifuji, 2012). Trace to no O_2 was detected in the gas phase at the investigated reaction conditions, indicating that the oxygen-free environment may enhance this conversion.
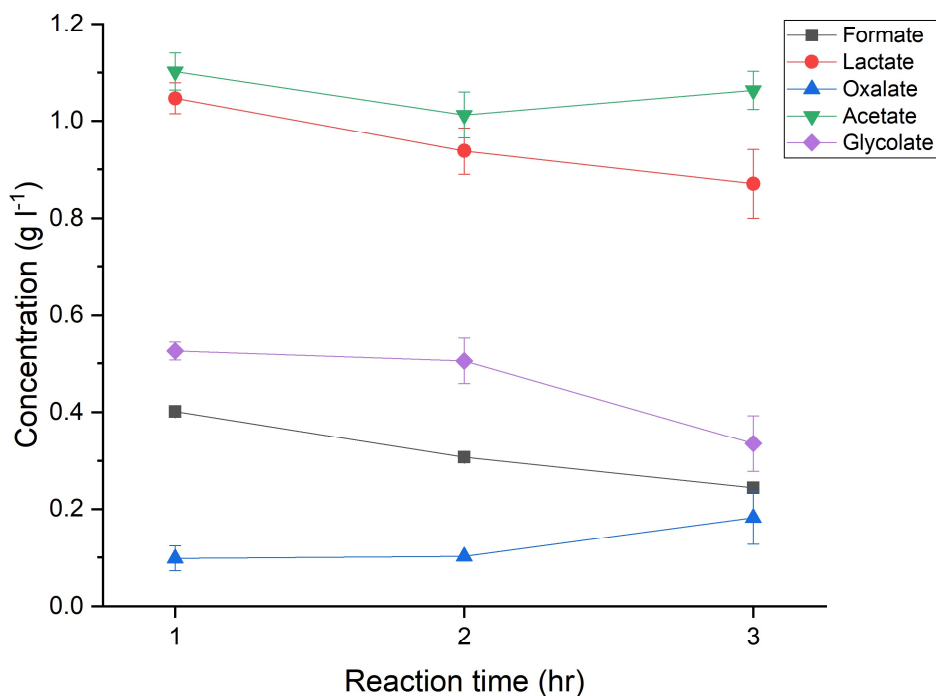
Figure 5-6 Concentration of organic acids at 300 °C with increasing reaction time. Line designations: green ▼ – acetate, red ● – lactate, purple ◊ – glycolate, black ■ – formate, blue ▲ – oxalate. Reaction conditions: 0.50 M NaHCO₃, 0.05 M glucose, 50 ml H₂O

The results of temperature and reaction time studies identified 250 °C and 2 hours as the conditions at which maximum formate concentration was detected. In combination with the results of filling volume and bicarbonate concentration studies, a set of conditions was found at which formate concentration was maximised without excess reagents. Conditions of 50 ml 0.50 M NaHCO₃ solution, 250 °C and 2 hours reaction time were identified experimentally as optimal for maximised HCOO⁻ concentrations. However, to understand the trend observed at 300 °C and the increase in saturated cyclic species, analysis of gas phase products was carried out to determine if decomposition to H_2 and CO_2 was occurring.

5.2.3 Hydrogen Production during NaHCO₃ Conversion

When formate concentrations were compared with the results of gas analysis, a strong correlation between HCOO⁻ and H_2 was observed (Figure 5-7). At 225 °C, virtually no hydrogen was detected in the gas phase. At 250 °C, H_2 constituted up to 2 % of the gas phase with an increasing proportion at increasing reaction time.

However, at 300 °C up to 11 % H_2 was detected, equating to 1.3 mmol H_2. In comparison, at 250 °C, the maximum obtained was 0.13 mmol – ten times less. Furthermore, as discussed in Section 5.2.2.3, increasing temperature from 250 to 300 °C resulted in a marked increase in the relative peak intensity of saturated cyclopentanones in relation to cyclopenten-1-ones. This may indicate that higher availability of hydrogen saturates double bonds.
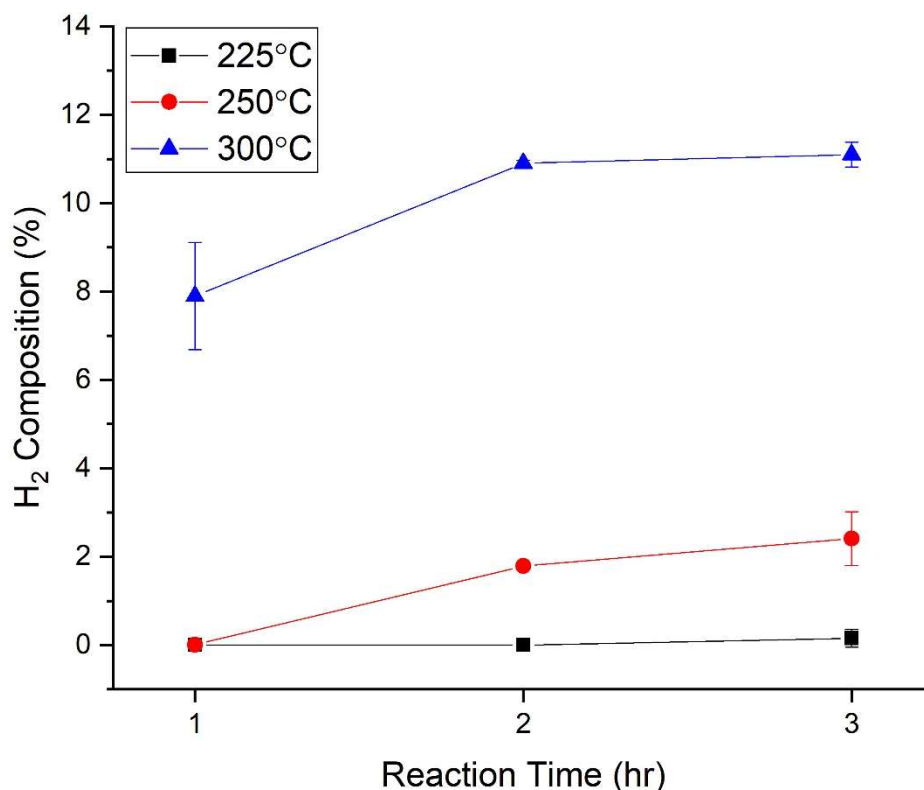
Figure 5-7 Hydrogen composition in the gas phase as a function of reaction time (1-3 h) with varying reaction temperature (black ■ – 225°C, red ● – 250°C, blue ▲ – 300°C). Reaction conditions: 0.50M NaHCO₃, 0.05M glucose, 50 ml H₂O

A higher fraction of H_2 in the gas phase indicated that formate decomposition may be occurring at elevated temperatures. To determine the stability of NaCOOH under the present reaction conditions, controls of both NaCOOH and free HCOOH in water were undertaken at 300 °C. After 3 hours, it was found that both molecules degrade to form solely CO_2 and H_2, however the degree of degradation varies (Table 5-4). Formate stabilised with Na showed approximately 70 % degradation, while free formic acid showed over 90 % degradation. This signifies that the presence of a cation is advantageous for stabilising the product and supports the use of bicarbonate

solutions in place of CO_2 gas, which would generate acidic conditions. In both cases, solely CO_2 and H_2 were identified as decomposition products.

Table 5-4 Formate species degradation. Reaction conditions: 0.25 g NaCOOH or 0.61 g HCOOH, 300°C, 3h, 50 ml H_2O

Species	Decomposition (%)
HCOOH	91.7 ± 1.5
NaCOOH	71.2 ± 5.1

In order to establish whether the observed formate decrease at 300 °C was solely due to degradation, a reaction of $NaHCO_3$ and glucose spiked with NaCOOH was carried out. No changes in the concentration of acetate or oxalate were detected, while a significant increase in H_2 composition from 13.2 to 20.7 ± 0.9 % H_2 was detected. Therefore, it was concluded that in reactions of $NaHCO_3$ with glucose, formate decomposition is the cause of decreased concentrations at 300 °C, establishing $HCOO^-$ as an intermediate in H_2 production.

Previous literature reported formate concentration was maximised at 300 °C and longer reaction times. Interestingly, in the current work a maximum was reached at 250 °C, 2 hours reaction time, while degradation to CO_2 and H_2 occurred at 300 °C with increasing reaction time. The reason for this discrepancy is proposed to be caused by the reactor material, which contains 58 wt % Ni, as well as internal structures made of the same material. In contrast to other studies on $NaHCO_3$ conversion with biomass derivatives, which generally employ SS316 batch reactors, the reactor used in the present work is composed of Hastelloy-C which contains significantly more Ni (58 %) than SS316 (10-14 %). Furthermore, this alloy contains significantly more molybdenum (15-17 %) than SS316 (2-3 %) and additional metals such as tungsten. It has been widely reported that Ni may catalyse the reduction of $NaHCO_3$ to formic acid, and indeed Wang *et al.* observed a similar maxima at 250 °C in $NaHCO_3$ reduction with Raney-Ni (Wang *et al.*, 2019). Bicarbonate controls in water indicated that the reactor material was not effective in converting bicarbonate to formate in the absence of a catalyst or H-source. However, Ni in the reactor may catalyse only the decomposition of formate to CO_2 and H_2, rather than its formation. This result highlights the importance of careful selection of reactor materials.

5.2.4 Mechanistic Investigations

To establish the percentage of formate derived from $NaHCO_3$ reduction as opposed to glucose degradation, ^{13}C-QNMR analysis of $NaH^{13}CO_3$ reactions was carried out. Results showed that at the maximum concentration of formate, only 4.3 % was derived from bicarbonate reduction. Bicarbonate-derived formate was expected to form through a cyclic transition state with glucose hydroxyl groups, as proposed in literature (Shen, Zhang and Jin, 2011). As the main precursor to formate in uncatalyzed reactions, investigation into the mechanism of glucose degradation to organic acids was undertaken. Due to the number of homogeneous reactions that glucose undergoes in sub-critical water, there are many potential routes to HCOOH formation. It has been proposed that glyceraldehyde is a key intermediate in this pathway, but this species was not detected in the present system most likely due to fast degradation under hydrothermal conditions (Srokol *et al.*, 2004). However, pyruvaldehyde was detected and can be formed from glyceraldehyde dehydration (Katryniok, Paul and Dumeignil, 2013). It should be noted that although this species was identified, the HPLC set-up used in the present work could not be used to quantify pyruvaldehyde due to strong overlap with a neighbouring lactate peak.

To establish if pyruvaldehyde is an intermediate in the formation of organic acids, a reaction was spiked with pyruvaldehyde solution. Compared with an unspiked reaction (Table 5-5, Entry 1), analysis established significant increase in formate, acetate, lactate and pyruvate (Table 5-5, Entry 2), thus confirming pyruvaldehyde as a key intermediate in organic acid formation in the present system. Further mechanistic studies were undertaken by swapping glucose for fructose, as glyceraldehyde can only form from a 2-ketose such as fructose (Srokol *et al.*, 2004). Carrying out the reaction with fructose instead of glucose showed comparable yields of most acids, and an increase in both lactic and pyruvic acids (Table 5-5, Entry 3). This indicates that in the present system Lobry de Bruyn-Alberda van Ekenstein transformation (LBET) of glucose to fructose in alkaline sub-critical water likely occurs quickly.

Chapter 5: Hydrothermal Conversion of Bicarbonate and Glucose to Formate

Table 5-5 Average concentration of organic acids in mechanistic probing reactions. Reaction conditions: 0.50 M NaHCO$_3$, 0.05 M monosaccharide, 1 ml 40 % pyruvaldehyde solution (where used), 250 °C, 1 h, 50 ml H$_2$O

Entry	Reaction	Average concentration (g l^{-1})			
		Formate	Lactate	Acetate	Pyruvate
1	Glucose	0.418	0.516	0.740	0
2	Pyruvaldehyde Spike	0.986	1.201	1.998	0.420
3	Fructose	0.460	1.061	0.696	0.250

Lactate decomposition to acetate in alkaline hydrothermal media through an ethanol intermediate has previously been proposed in literature (Shen *et al.*, 2014). However, in controls of glucose in 1M NaOH, where high concentrations of lactate were present (4.93 g l^{-1}), low concentrations of acetate were detected (0.04 g l^{-1}). Furthermore, spiking of lactic acid to NaHCO$_3$/glucose reactions resulted in only an increase in pyruvate, and therefore is not expected to be a significant route of acetate formation in the present work.

Based on the results of mechanistic studies and existing literature, a reaction mechanism for glucose degradation to organic acids in sub-critical water with NaHCO$_3$ was proposed (Figure 5-10). It should be noted that these transformations occur independently of the formation of bio-oil constituents, for which discerning a mechanism is challenging. Due to the mildly alkaline reaction medium formed from NaHCO$_3$, it is proposed that glucose initially converts to fructose by the LBET. D-glucose may decompose to form D-erythrose and glycolaldehyde, which were not detected in this study likely due to fast decomposition to further products. On the other hand, different species originate from fructose depending on conditions. 5-HMF forms by dehydration of fructose and may theoretically be further converted to levulinic and formic acids. However, in the present work, 5-HMF was not deemed to be the intermediate in formic acid formation due to the absence of levulinic acid in samples.

Retro-aldol reaction of fructose yields glyceraldehyde, which interconverts with dihydroxyacetone. Neither of these species were detected proposedly due to decomposition. Dehydration of glyceraldehyde yields pyruvaldehyde, whose conversion to organic acids is promoted in a basic medium. In the presence of a base,

simultaneous formation of acetic acid and formaldehyde occurs, after which further conversion of formaldehyde to formic acid by the Cannizzaro reaction may occur (Figure 5-8). Formaldehyde is gaseous at standard conditions and could not be detected by the analytical methods available.
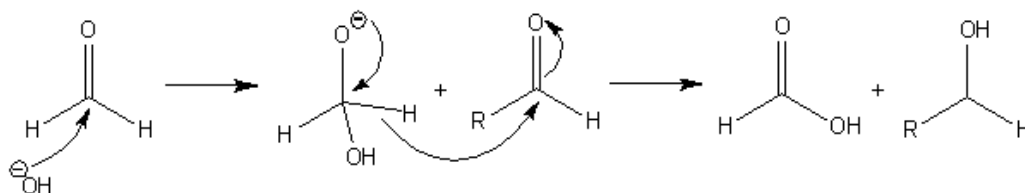
Figure 5-8 Cannizzaro reaction of formaldehyde with aldehydes to form formic acid and alcohol

Alternatively, pyruvaldehyde conversion to formic acid and acetaldehyde may occur. The present analytical set-up had low sensitivity to acetaldehyde. However, through 3D analysis of PDAD spectral data, a peak corresponding to acetaldehyde at 290 nm absorption was observed in $NaHCO_3$/glucose reactions at 250 °C. The third potential pathway of pyruvaldehyde conversion in basic media is by 1,2-rearrangement (benzylic acid rearrangement) to lactic acid (Figure 5-9).
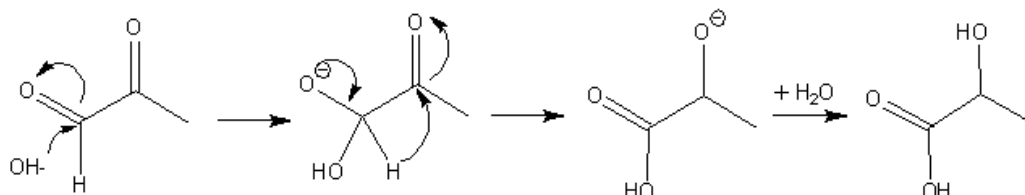
Figure 5-9 Benzylic acid rearrangement of pyruvaldehyde to lactic acid

Lactic acid, in the presence of CO_2, can be converted to pyruvic acid with simultaneous reduction of CO_2 to HCOOH. Alternatively, pyruvaldehyde can be converted to pyruvic acid in the presence of a base, generating H_2 in the process. Investigations with NaCOOH suggest that this is not a major route of H_2 formation in this case, and that first formation of formate, followed by decomposition is the main route. Lactic acid can be converted to acrylic acid in an acid-catalysed dehydrogenation reaction, which may further be hydrogenated to propionic acid. Acrylic acid was detected only in trace concentrations in the present system, which was suppressed under basic conditions as this reaction is acid-catalysed. Trace propionic acid was also detected in glucose samples.

Chapter 5: Hydrothermal Conversion of Bicarbonate and Glucose to Formate

Replacing glucose with fructose as a starting reagent showed remarkable similarity in reaction products (Table 5-5, Entry 3). Acetate yield remained comparable at approximately 0.7 g l^{-1} between the two sugars, however lactate and pyruvate yield were found to strongly increase. This may signify that conversion to pyruvaldehyde occurs faster with fructose, after which its rearrangement to lactic acid or conversion to pyruvic acid are the dominant pathways under the investigated conditions. CO_2 reduction of lactate may be the cause of marginally increased formate concentration from fructose. As expected, an increase in 5-HMF was also observed with fructose compared to glucose.
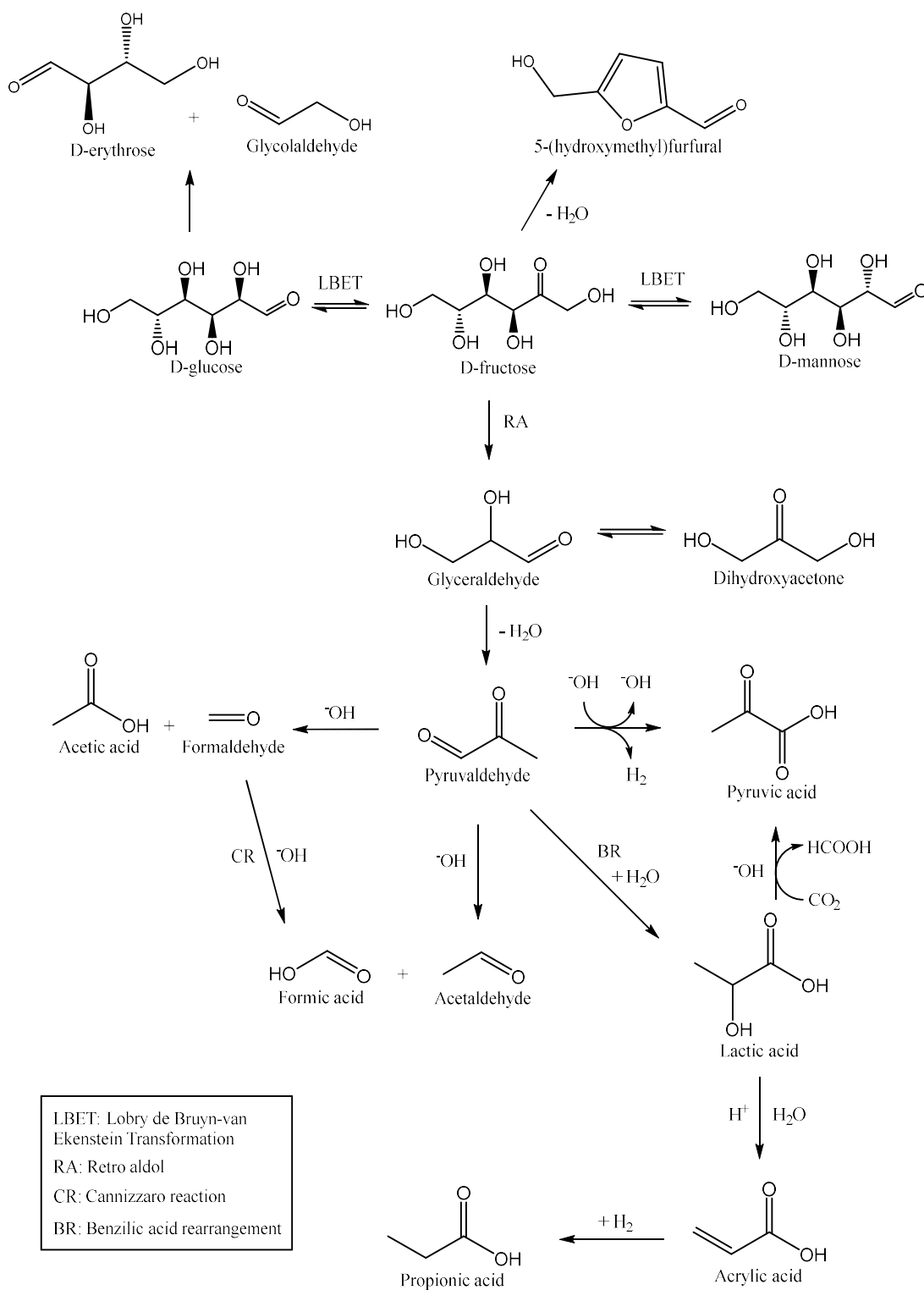
Figure 5-10 Mechanistic scheme of glucose degradation to organic acids in sub-critical media

In the present work, the mechanism of glycolate formation could not be ascertained. The concentration of glycolate remained relatively unchanged between fructose and glucose. As no oxygen was detected in the gas phase, and CO_2 is only a soft oxidant, it is unlikely that glycolate formation occurs from glycolaldehyde oxidation. It has been proposed that glycolate forms through an enediol of the LBE transformation between monosaccharides, after which conversion to glycolate is catalysed by basic reactions (Srokol *et al.*, 2004). Interconversion between monosaccharides may yield comparable concentrations of glycolate from both glucose and fructose in this case. Alternatively, glycolic acid may be generated through a Cannizzaro reaction of glycolaldehyde with small aldehydes (Omran *et al.*, 2020). It is possible that glycolate may form from a combination of mechanisms. Further investigations of reactions spiked with glycolaldehyde may be carried out in future to discern a mechanism.

Mechanistic investigations showed that pyruvaldehyde is a key intermediate in the formation of organic acids from glucose, and both the formation and further conversion of this species is enhanced by basic conditions. In conjunction with the ^{13}C-QNMR study, these results form the foundation of further investigations with heterogeneous catalysts and alternative CO_2 precursors.

5.3 CONCLUSION

The impact of reaction variables was investigated to determine conditions at which formate concentration is maximised. Water filling volume, $NaHCO_3$ concentration, temperature and time were varied, and trends observed. Temperature variation was found to have a significant impact on products. At 250 °C, a maximum of 0.502 g l^{-1} HCOO$^-$ was achieved, while at 300 °C a gradual decrease in concentration occurs. The opposite trend was observed in H_2 production, which peaked at 11 % at the maximum investigated temperature. Bio-oil analysis demonstrated an increase in saturated cyclopentanone species at higher temperatures, proposedly due to an increased quantity of H_2 saturating the double bonds of cyclopentene-1-ones which predominate at lower temperatures. Subsequently, potential routes of formate conversion at 300 °C were investigated, with acetate, oxalate and hydrogen as potential products. Sodium formate studies showed that decomposition of formate to CO_2 and H_2 was occurring at elevated temperatures, and no further conversion to other species occurs. The extent of decomposition was found to vary between 91.7 % for free acid to 71.2 % for NaCOOH, indicating that the cation may have a stabilising

effect in preventing degradation of the species. Based on similar trends observed in literature, it was proposed that the higher nickel composition of the reactor may have catalytic effects on the reaction studied. The impact of reactor materials on the formation of products may thus have significant impacts on future scale-up studies.

Quantitative ^{13}C-NMR determined that at the maximum concentration of formate, only 4.3 % is derived from $NaHCO_3$ reduction, with the rest yielded from glucose. As such, mechanistic investigation into the mechanism of organic acid formation from glucose was undertaken. Pyruvaldehyde was identified as a key intermediate in the formation of almost all organic acids formed in the reaction, and alkaline conditions enhance this conversion. Based on mechanistic data from literature and probing reactions, a mechanistic scheme of glucose conversion was proposed.

This chapter forms the foundation for studies on heterogeneous catalysts and their impact on the conversion of each reagent. As previously stated, at the maximum concentration of formate, over 95 % originates from glucose degradation rather than bicarbonate reduction. In the following chapter, metals were investigated as heterogeneous catalysts to enhance the reduction of bicarbonate. Furthermore, the results were used as a benchmark when comparing other CO_2 precursors in Chapter 8.

6 CHAPTER 6: BULK METALS AS HETEROGENEOUS CATALYSTS

6.1 INTRODUCTION

In uncatalyzed hydrothermal reactions of bicarbonate with glucose at 250 °C, over 95 % of formate was found to be derived from glucose degradation rather than HCO_3^- reduction, as established in Section 5.2.4. The use of heterogeneous catalysts is hypothesised to enhance conversion. As summarised in Section 2.6, both sacrificial metals, which undergo oxidation during hydrothermal reaction, and non-oxidising metals have been explored as catalysts for hydrothermal CO_2 reduction. However, non-oxidising metals have been utilised in the presence of additional metal reductants. In this work, the catalytic activity of metal catalysts was investigated alongside glucose reductant to determine if bicarbonate reduction can be enhanced in the presence of biomass as a hydrogen source. Conversion of both reagents to formic acid is an opportunity to tune the products of biomass degradation while simultaneously reducing CO_2.

In this chapter, the activity of nickel, cobalt and copper powders in hydrothermal conversion of $NaHCO_3$ was explored. Copper is active in methanol formation and biomass liquefaction and has been shown to be active in hydrothermal CO_2 reduction with sacrificial metals (Section 2.6.3). Nickel is a methanation catalyst and has been shown to be effective in CO_2 reduction (Section 2.6.2). Cobalt has not previously been reported in CO_2 hydrothermal reduction and, as a Fischer-Tropsch catalyst, may promote hydrocarbon formation. Subsequently, the bulk metals were characterised to determine if any morphological or oxidative changes occur during the reaction. This work forms the basis of future investigation into supported catalysts for hydrothermal CO_2 reduction with biomass reductants.

6.2 METHODOLOGY

Starting reagents $NaHCO_3$ (99+ %), D -(+)- glucose (≥99.5 %), copper (99.5 %, <425 μm particle size) and cobalt powders (99.8 %, 2 μm) were purchased from Sigma-Aldrich. Nickel powder (99.9 %, 3-7 μm) was purchased from Alfa Aesar.

Chapter 6: Bulk Metals as Heterogeneous Catalysts

The general protocol of hydrothermal reactions is described in Section 3.2. Error bars on graphs represent the standard deviation of products over multiple experiments. To assess the impact of heterogeneous catalysts, 25 mmol of metal powder was weighed alongside 25 mmol $NaHCO_3$ and 2.5 mmol glucose and placed in the pressure vessel. Post-reaction, metal powders were removed from liquid products by vacuum filtration through Grade 542 filter paper (Whatman, UK), then dried in an oven at 105 °C for 18 hours. Quantitative ^{13}C-NMR of the post-reaction liquid in Ni-catalysed reactions was carried out by Khalid Doudin of the Department of Chemistry at the University of Sheffield as described in Section 5.2.

The morphological characteristics of the catalysts were investigated by SEM using a Jeol JSM-6010 LA Analytical Scanning Electron Microscopy. The accelerating voltage (V) employed ranged from 15 kV to 20 kV and a working distance of 11 mm was used throughout. Metal powders were placed on conductive carbon tape adhered to an aluminium sample holder. In addition to SEM, the physical structure of the bulk metal catalysts was investigated by X-ray diffraction to determine if any oxidative changes occur. XRD patterns were recorded using a diffractometer (PANalytical Aeris) operated in transmission mode at a voltage of 40 kV and a tube current of 15 mA. Data were collected at room temperature in the 2θ range from 10 ° to 100 ° using nickel-filtered Cu Kα radiation (Kα$_1$ λ = 1.540598 Å, Kα$_2$ λ = 1.544426 Å). Measurement was conducted in continuous rotating, reduced fluorescence mode with a step size of 0.0217 °.

ICP-OES was carried out by colleagues Shania Laming and Heather Grievson in the Department of Chemistry at the University of Sheffield to determine the extent of metal leaching into solution. Analysis was carried out on a Spectrogreen ICP-OES (Spectro) with dual side-on interface. The sample was introduced at a rate of 1 ml min^{-1}. Plasma power of 1150 W was used with a coolent flow of 13 L min^{-1} and auxiliary flow of 0.8 L min^{-1}. Finally, FTIR-ATR was carried out to determine if any changes in surface functionality occur. An IRAffinity-1S (Shimadzu) was used and spectra gathered in transmission mode at a resolution of 8 cm^{-1} with 32 scans over the range 400-4000 cm^{-1}.

6.3 RESULTS AND DISCUSSION

6.3.1 Hydrothermal Reactions

The experimental parameters used for catalytic studies were established in Chapter 5, and conditions at which formate concentration was maximised – 250°C and 2 hours – were used. Results of organic acid analysis of reactions with bulk metal powders are shown in Figure 6-1.
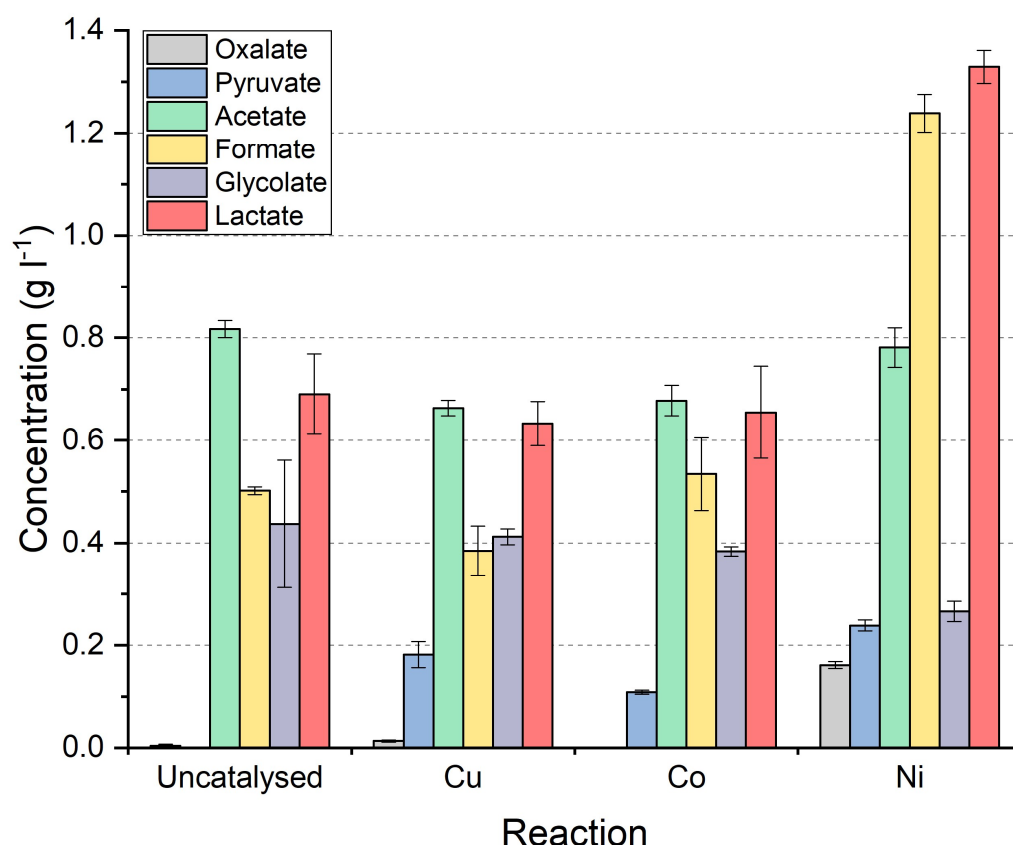
Figure 6-1 Concentration of organic acids in the absence and presence of heterogeneous catalysts Cu, Co and Ni. Reaction conditions: 0.50 M NaHCO₃, 0.05 M glucose, 250 °C, 2 h, 50 ml H₂O

Copper and cobalt were not found to be active in the production of NaCOOH and little variation in reaction products was observed. While no change in formate concentration was observed with cobalt, marginal inhibition occurs in the presence of copper. However, with both metals pyruvate concentration increased. As no corresponding increase in lactate was detected, this indicates that Co and Cu may facilitate pyruvaldehyde conversion to pyruvate.

Interestingly, acetate concentration was observed to be either mildly inhibited, or unchanged in the presence of catalysts. It is proposed that the metals investigated in this work do not significantly influence the path from pyruvaldehyde to acetate formation. No 5-HMF was detected in Co or Cu reactions, indicating that they do not promote an alternative route in glucose degradation. Furthermore, no changes in bio-oil composition were found in comparison to uncatalyzed reactions, indicating these substances are not active in either glucose degradation or bicarbonate conversion at the conditions investigated. In the gas phase, H_2 composition remained low and no methane was formed with either Co or Cu. This indicates that hydrocarbons are unlikely to be formed at the investigated conditions even with FTS-active Co. Similarly, no methanol was detected with copper. It was therefore concluded that at the conditions studied, bulk cobalt and copper powders are not active in either the degradation of glucose or hydrothermal reduction of bicarbonate.

In contrast, nickel was found to be highly active in formate production, with an increase over two-fold from 0.502 to 1.240 g l^{-1}. An increase in pyruvate and oxalate to 0.162 and 0.239 g l^{-1}, respectively, was also detected. Lactate followed similar trends to formate, with concentration nearly doubling from 0.70 to 1.33 g l^{-1}. Nickel was also discovered to be very active in H_2 production at lower temperatures of 250 °C, with H_2 composition increasing from 1.8 % to 23.6 ± 1.6 % in the presence of Ni.

To assess whether any correlation between lactate and formate exists mechanistically, a reaction spiked with lactic acid was carried out. Only pyruvate concentration increased from 0 to 0.100 g l^{-1}, while all other organic acids remained consistent. These results were consistent with the reaction mechanism proposed in Section 5.2.4, and Ni may therefore enhance the conversion of intermediate pyruvaldehyde to formate and lactate. Further investigation into the role of Ni in bicarbonate conversion was carried out by quantitative NMR.

6.3.2 NMR

The effects of nickel on formate production from bicarbonate were determined by carrying out experiments with labelled NaH^{13}CO$_3$ and glucose in the presence of Ni catalyst. The results were quantified by ^{13}C-NMR. The NMR spectrum showed a peak at 161.2 ppm for unreacted NaH^{13}CO$_3$, and a second peak at 171.1 ppm for H^{13}COOH (Figure 6-2). ^{1}H-NMR with water suppression showed a ^{12}C-H shift for formate at

8.36 ppm, as well as two formate ^{13}C-H shifts at 8.55 and 8.16 ppm, confirming reduction of bicarbonate occurs with Ni catalyst (Figure 6-3).
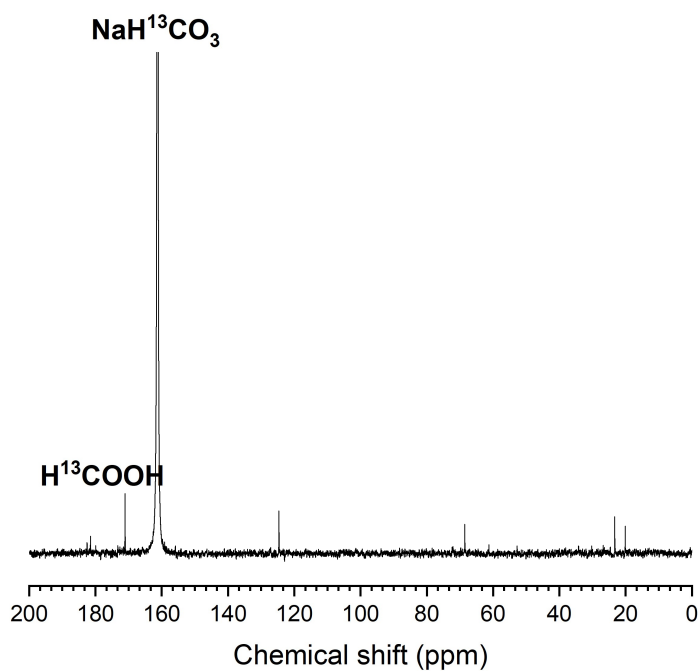
Figure 6-2 ^{13}C-NMR Spectrum of liquid products arising from the hydrothermal reaction of NaH^{13}CO$_3$ with glucose and Ni catalyst. Reaction conditions: 0.50 M NaHCO$_3$, 0.05 M glucose, 250 °C, 2 h, 50 ml H$_2$O
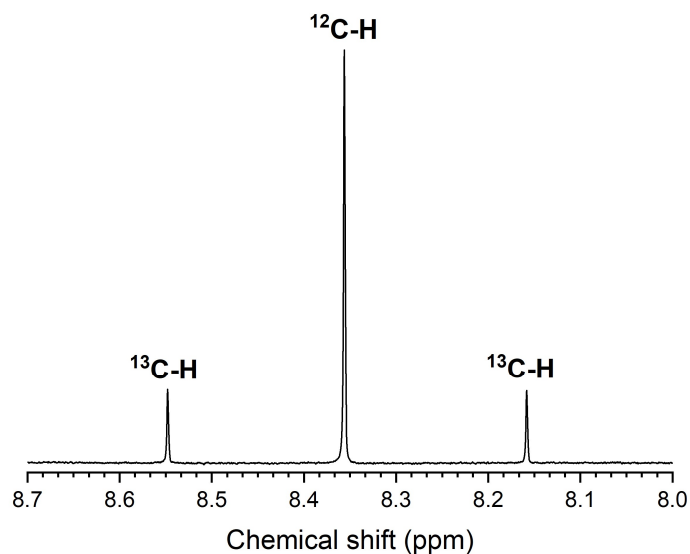
Figure 6-3 ^{1}H-NMR Spectrum of formate in hydrothermal reaction of NaH^{13}CO$_3$ with glucose and Ni catalyst. Reaction conditions: 0.50 M NaHCO$_3$, 0.05 M glucose, 250 °C, 2 h, 50 ml H$_2$O

In the presence of Ni, a fifteen-fold increase in the concentration of formate derived from bicarbonate occurs (Table 6-1). Remarkably, the concentration of formate from glucose simultaneously nearly doubles. It is possible that Ni may enhance lactate production from glucose as well as formate, although this could not be experimentally validated in the absence of ^{13}C-labelled glucose.

Table 6-1 ^{13}C-QNMR Results depicting formate percentage and concentration from NaH[13]CO$_3$ and glucose in uncatalyzed and Ni-catalysed hydrothermal reactions

Entry	Reaction	% HCOO$^-$ from HCO$_3^-$	*HCOO- Concentration (g l^{-1})*	
			From HCO$_3^-$	From glucose
1	Uncatalysed	4.3	0.022	0.480
2	Ni-catalysed	26.6	0.330	0.910

Thus, the results of labelling studies determined that Ni enhances the conversion of both of NaHCO$_3$ and glucose to formate. It must be noted that although Ni enhanced the conversion of glucose to formate, a range of other products is still present in solution, including organic acids shown in Figure 6-1 and bio-oil constituents summarised in Section 4.3. Nevertheless, this study demonstrates the potential of simultaneous conversion of CO$_2$ and biomass to a single product by heterogeneous catalysis. Further insight into the stability and morphology of the metals was gained through catalyst characterisation.

6.3.3 FTIR Spectroscopy

FTIR spectroscopy was carried out on fresh and post-reaction metal powders to determine if changes in surface functionality occur during the reaction. This analysis is also valuable in determining if significant amounts of char form in the reaction, as C-C bonds have a unique wavenumber range. Characterisation of Ni powder before and after reaction showed that no changes in functionality occurred during the reaction (Figure 6-4). This indicates no strong organic bonding to the Ni surface. Similarly, no changes were observed in cobalt and copper spectra (Appendix D). The absence of C-C or C-H bonds indicates there is little char formation in the reaction, and that organic molecules are not bound to the bulk metal surfaces post-reaction.
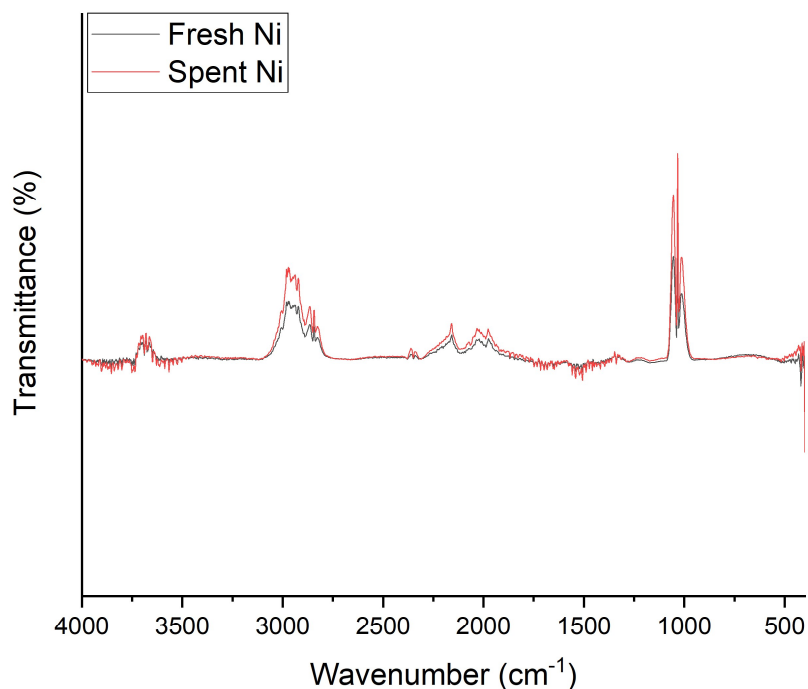
Figure 6-4 FTIR of fresh (black) and spent (red) Ni powder after hydrothermal reaction (reaction conditions: 0.50 M NaHCO₃, 0.05 M glucose, 250 °C, 2 h, 50 ml H₂O). Spectra acquired in transmission mode at a resolution of 8 cm⁻¹ with 32 scans over the range 400-4000 cm⁻¹

6.3.4 XRD

X-ray diffraction was used to determine if changes in oxidation state or phases occur during hydrothermal reaction. Nickel XRD showed a face centred cubic (fcc) lattice structure, and all characteristic diffraction peaks were assigned (Figure 6-5) (Jović *et al.*, 2006; Jung and Choi, 2014). The nickel particles did not undergo a change in oxidation state, as evidenced by the absence of diffraction peaks associated with nickel oxides (Neiva *et al.*, 2016).

The Ni(111) surface identified by the peak at 2θ = 44.4 ° has been reported to be favourable for dissociative H₂ adsorption, where this reaction is exothermic (-91 kJ mol⁻¹) and results in the formation of a strong Ni-H bond (Wellendorff *et al.*, 2015). Dissociation of H₂ on the Ni(111) surface has been described as comparable to that of Pd, with the main difference between the metals attributed to surface electrons (Kresse, 2000). Adsorption of hydrogen carbonate on the Ni(111) surface is also favoured over other CO₂ adsorption species such as CO₃²⁻, CO or methoxy (Cai *et al.*, 2019).
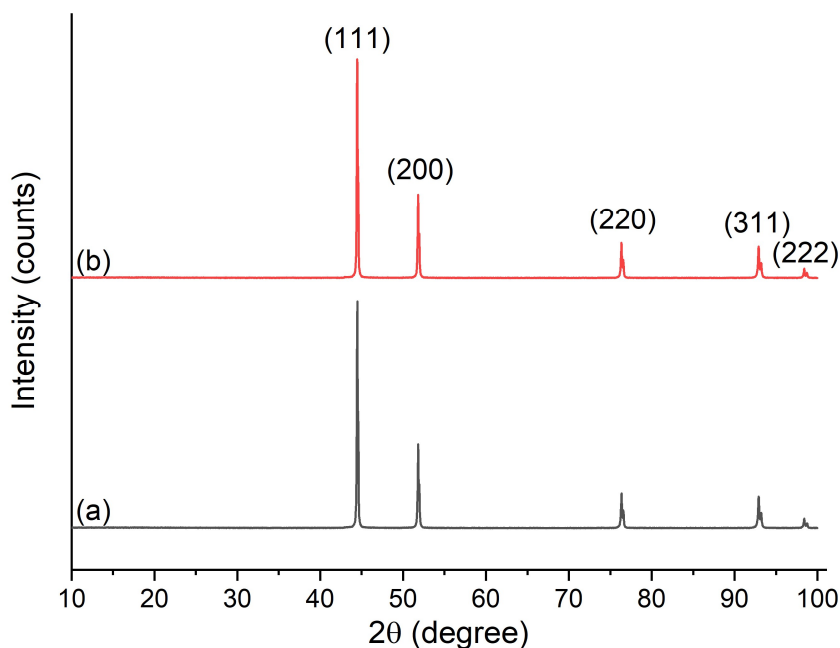
Figure 6-5 XRD Patterns depicting phases of (a) fresh and (b) spent Ni powder after hydrothermal reaction. Reaction conditions: 0.50 M NaHCO$_3$, 0.05 M glucose, 25 mmol Ni powder, 250 °C, 2 h, 50 ml H$_2$O

Similarly to nickel, copper XRD diffraction peaks were consistent with fcc Cu planes (Figure 6-6) (Shenoy and Shetty, 2014). The lack of activity by copper in this study may be caused by reportedly poor H$_2$ dissociation on the available Cu (111) surface (Álvarez-Falcón *et al.*, 2016). The material remained reduced post-reaction, as evidenced by the lack of distinctive cuprous/cupric oxide peaks between 30-40 °. This indicates that the material does not undergo oxidation under the conditions investigated.
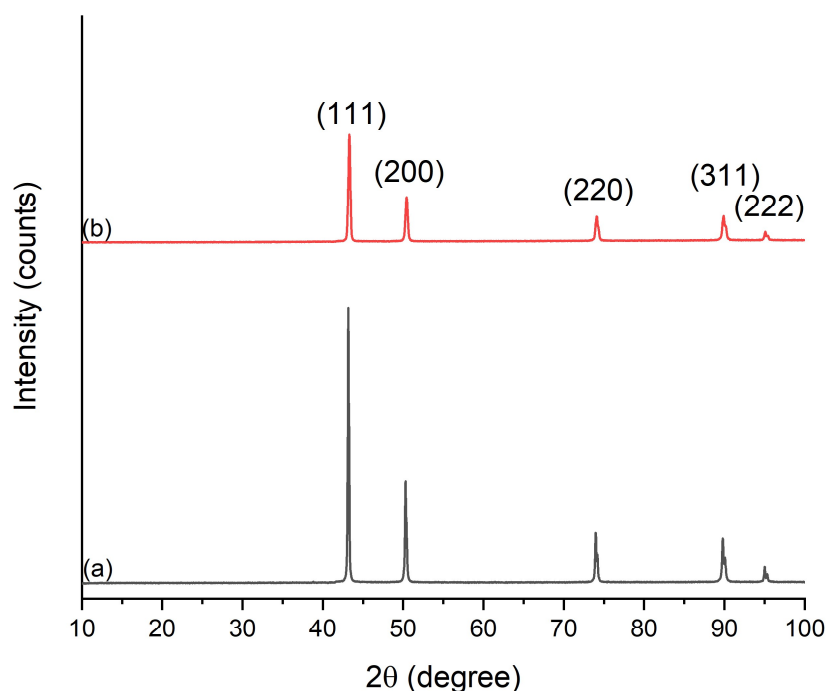
Figure 6-6 XRD Patterns depicting phases of (a) fresh and (b) spent Cu powder after hydrothermal reaction. Reaction conditions: 0.50 M NaHCO₃, 0.05 M glucose, 25 mmol Cu powder, 250 °C, 2 h, 50 ml H₂O

The crystallography results of cobalt reveal a mixture of hexagonal close-packed (hcp) and face centered cubic lattice phases (Jović *et al.*, 2006). The diffraction peak at $2\theta = 51.5$ ° corresponds to the (200) plane of the fcc Co, while the peaks at 41.5 ° and 47.4 ° correspond to (10-10) and (10-12) planes of the hcp phase (Liu *et al.*, 2015) (Figure 6-7). The diffraction peak at 44.4 ° may correspond to either fcc (200) surface or hcp (0002) plane and is likely a mixture of both. Similarly, the diffraction peak at 76 ° corresponds to the fcc (200) and hcp (1100) surfaces. Cobalt was not found to undergo oxidative changes to Co(II) or Co(III) when used as a bulk substance in hydrothermal media. This is determined by an absence of characteristic cobalt oxide peaks between 30 – 40 ° in the XRD pattern.

Hcp-Co has been reported to exhibit higher activity compared to fcc-Co in Fischer-Tropsch synthesis of hydrocarbons (Lyu *et al.*, 2018). However, this requires the presence of both H₂ and CO, which was not detected in gas products. Therefore, Co is not active in bicarbonate reduction to HCOOH, and does not promote hydrocarbon formation likely due to the absence of CO.
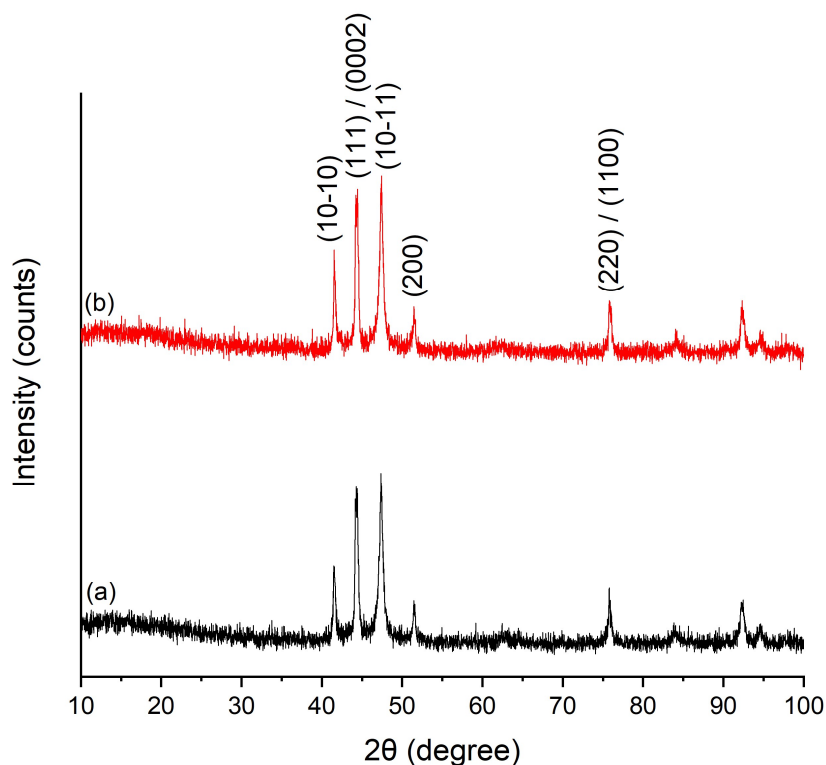
Figure 6-7 XRD Patterns depicting fcc and hcp phases of (a) fresh and (b) spent Co powder after hydrothermal reaction. Reaction conditions: 0.50 M NaHCO₃, 0.05 M glucose, 25 mmol Co powder, 250 °C, 2 h, 50 ml H₂O

It was therefore found that all bulk metals used in this study exhibit stability in their oxidative state at the reaction conditions investigated. In the case of Ni, diffraction patterns are valuable in assessing the reaction mechanism.

6.3.5 ICP-OES

The extent of metal leaching into solution was determined by ICP-OES analysis of liquid products (Table 6-2). Cobalt was found to leach most into solution, losing 0.17 % of starting mass in comparison to the other metals. On the contrary, Ni was the most stable catalyst and exhibited the lowest mass loss of 0.011 %. Overall, all metals showed relatively low leaching into solution in mildly alkaline hydrothermal media after a single reaction, indicating stability under the investigated conditions.

Table 6-2 ICP-OES of liquid solutions after reactions of NaHCO$_3$ with glucose and metal powders. Reaction conditions: 0.50 M NaHCO$_3$, 0.05 M glucose, 25 mmol metal powder, 250 °C, 2 h, 50 ml H$_2$O.

Metal	Leaching to solution (mg l^{-1})	Mass loss (%)
Nickel	0.329	0.0011
Copper	0.481	0.0015
Cobalt	50.600	0.17

6.3.6   SEM

SEM imaging was carried out to assess powder morphology and changes that may occur during reaction. Imaging found Ni particles of approximately 5 μm size in both fresh and spent powder (Figure 6-8). Closer magnification of the Ni particles showed a complex structure containing many different surfaces. Nickel was not found to undergo noticeable changes in particle size or morphology.
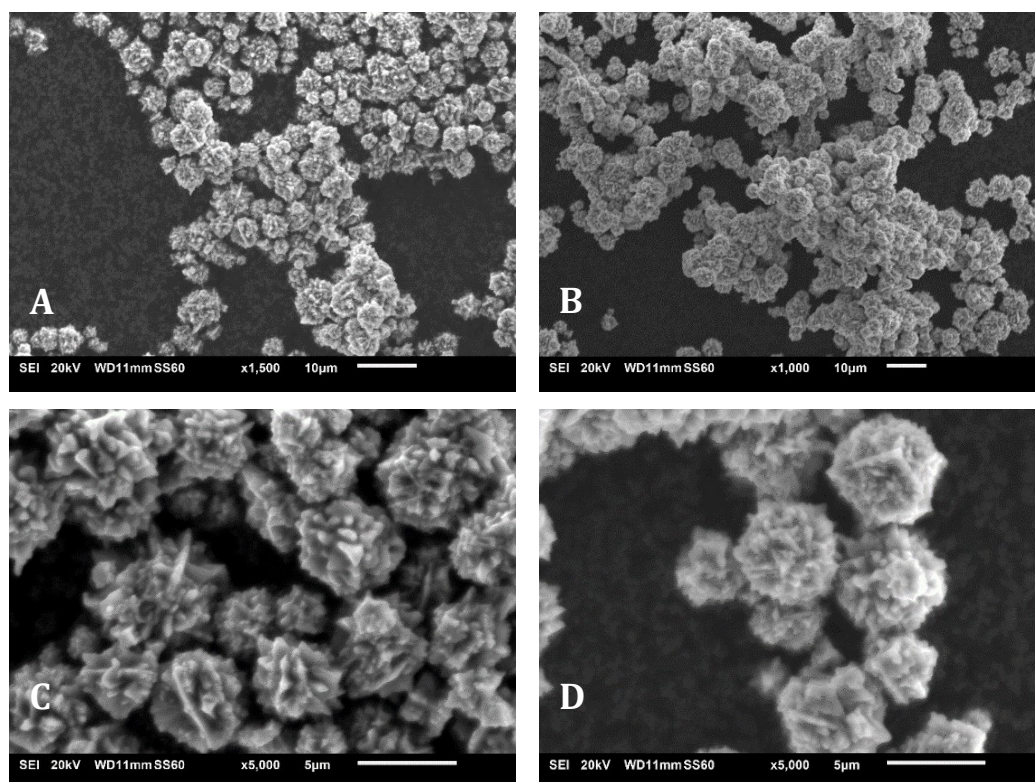
Figure 6-8 SEM of Ni powder. A) Fresh Ni powder x1500 magnification, B) Spent Ni powder x1000 magnification, C) Fresh Ni powder x5000 magnification, D) Spent Ni powder x5000 magnification

In comparison, cobalt was observed to have less defined particles of smaller size below 2 μm (Figure 6-9). Similarly, no observable changes in morphology post-reaction were observed.
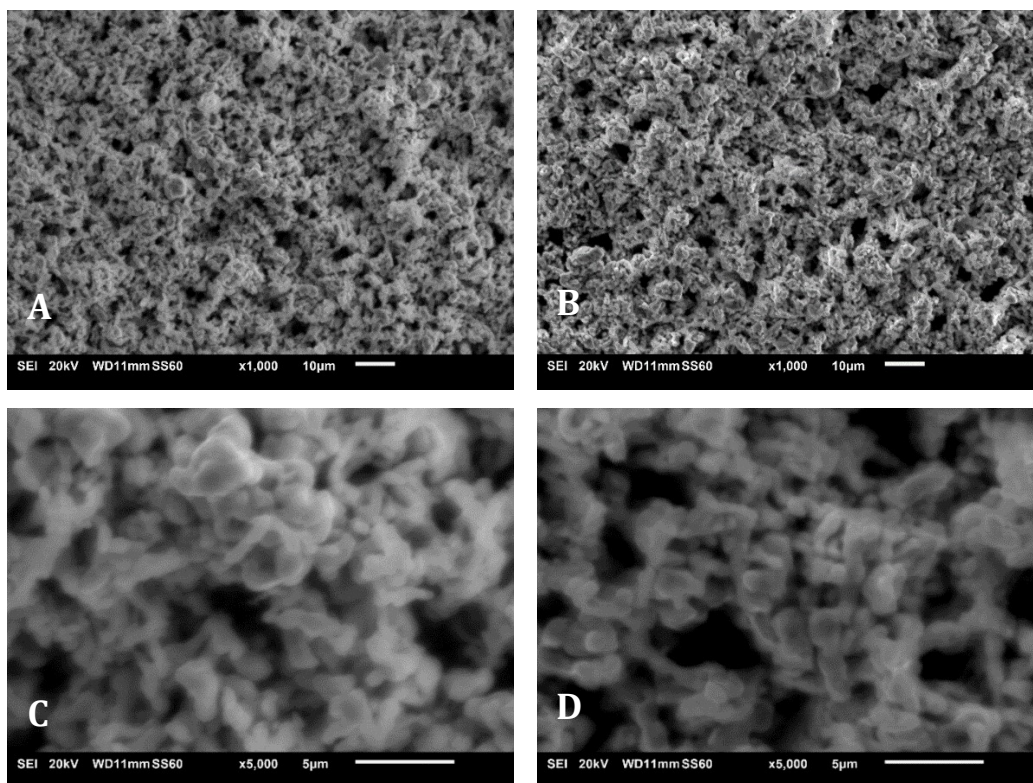
Figure 6-9 SEM of Cobalt powder A) Fresh Co powder x1000 magnification, B) Spent Co powder x1000 magnification, C) Fresh Co powder x5000 magnification, D) Spent Co powder x5000 magnification

Copper particles were of a significantly larger size – up to 425 μm (Figure 6-10). SEM imaging of the particle surfaces was carried out, and an increase in the pore sizes on the Cu particle surface was observed post-reaction (Figure 6-8, C and D). The increase in pore size may signify decreasing specific surface area due to collapse of pore structures within the copper particles at hydrothermal conditions. However, due to bulk metal powders exhibiting very low surface area below the sensitivity range of the available porosity and surface area analyser, this could not be experimentally validated.
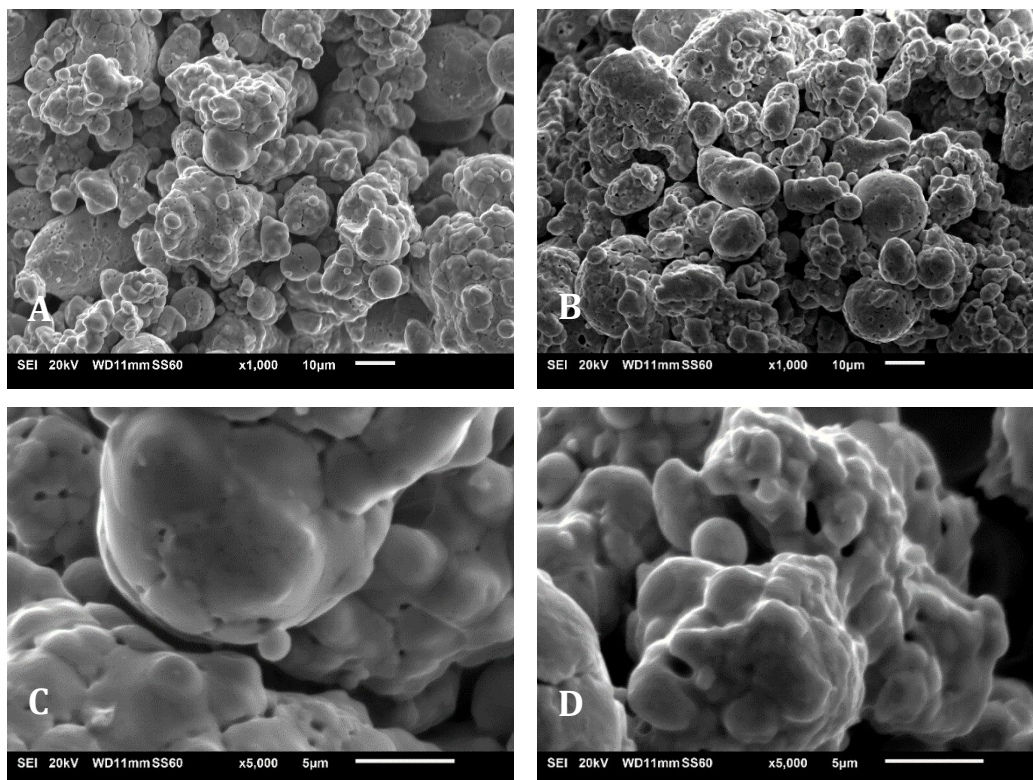
Figure 6-10 SEM of Copper Powder A) Fresh Cu powder x1000 magnification, B) Spent Cu powder x1000 magnification, C) Fresh Cu powder x5000 magnification, D) Spent Cu powder x5000 magnification

The combination of FTIR, XRD, ICP and SEM characterisation of catalysts demonstrated the relative stability of the metals under hydrothermal conditions. It was discovered that in addition to its remarkable activity in enhancing the yield of NaCOOH from both bicarbonate and glucose, nickel exhibits high stability and resistance to leaching under the investigated conditions. Therefore, this work established Ni as a suitable active phase for investigations into supported catalysts, in which higher physical stability, distribution of the active phase, and increased surface area can be achieved.

6.3.7 Mechanism of Ni Activity

NMR analysis ascertained that Ni simultaneously increases the conversion of both $NaHCO_3$ and glucose to NaCOOH. In terms of glucose conversion, the role of Ni is difficult to ascertain. The Ni surface may provide an energetically favourable site for pyruvaldehyde and hydroxide adsorption, followed by its conversion to lactate and formate. Base-catalysed conversion of pyruvaldehyde to pyruvate may also be responsible for a large increase in H_2.

High concentrations of H_2 in the gas phase suggest that the first step of bicarbonate reduction over Ni is likely H_2 dissociation on the Ni surface and adsorption of bicarbonate (Figure 6-11). Small concentrations of 2 % H_2 were detected even in uncatalyzed reactions. Hydride attack on the bicarbonate carbon results in the formation of surface formate. This may also clarify the contrast between Co and Ni activity, as nickel has been described as preferential for hydrogenation of the carbonyl group (Merabti *et al.*, 2010). Formate formation is accompanied by the removal of the bicarbonate hydroxyl group, which can react with adsorbed H to form H_2O. It is proposed that some ⁻OH does not get neutralised by surface H, as evidenced by the reaction pH altering from 8.2 at the beginning of the reaction, to 9.4 post-reaction.
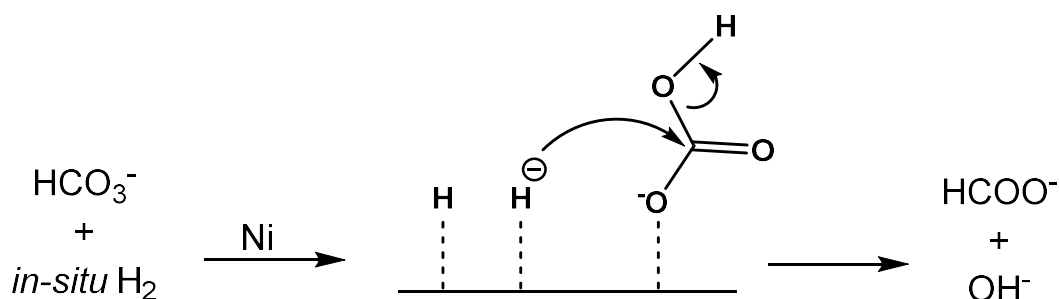
Figure 6-11 Ni-catalysed reduction of bicarbonate to formate

Due to the increase in gaseous H_2 in reaction with nickel, it is proposed that Ni also catalyses the decomposition of formate to CO_2 and H_2. The rate of the decomposition reaction is suggested to be lower than that of HCOO⁻ formation, as evidenced by high concentrations of NaCOOH in reactions with Ni. Coupled with HCOO⁻ formed from glucose, this results in more formate formation than decomposition. Thus, in Ni-catalysed reactions the gas phase was composed of over 20 % H_2, compared to 2 % in uncatalyzed reactions.

6.4 CONCLUSION

Bulk metal powders nickel, cobalt and copper were investigated as heterogeneous catalysts for enhancing bicarbonate reduction to NaCOOH. In uncatalyzed reactions, NMR studies found that over 95 % of HCOOH was derived from glucose degradation, rather than bicarbonate reduction. While cobalt and copper were not found to be active in the reaction, nickel increased NaCOOH concentration over two-fold from 0.502 to 1.240 g l⁻¹, while also enhancing lactate yield. In the presence of Ni, formate

derived from bicarbonate increased from 0.022 to 0.330 g l^{-1}, while simultaneously formate from glucose improved from 0.480 to 0.910 g l^{-1}. Characterisation of Ni powder showed no changes in functionality, oxidation state, or morphology of particles, as well as low metal loss into solution, indicating catalyst stability under the investigated conditions. A mechanism for Ni-catalysed bicarbonate reduction was proposed, involving firstly dissociative H_2 adsorption, followed by hydride reduction of adsorbed HCO_3^- to $HCOO^-$. The increase of gaseous H_2 composition in reactions with Ni from 2 to 23.6 % suggests that Ni also catalyses the degradation of formate to CO_2 and H_2, although it is proposed that the rate of degradation is slower than $HCOO^-$ formation. The results demonstrated in this chapter show that Ni is remarkably active and stable under investigated conditions and form the foundation of further studies of supported Ni catalysts. Further work on supported Ni catalysts is discussed in Chapter 7.

7 CHAPTER 7: INVESTIGATION INTO SUPPORTED NICKEL CATALYSTS

7.1 INTRODUCTION

Catalyst supports play a crucial role in overall catalyst performance. Although the active phase is primarily responsible for the conversion efficiency, the support increases its surface area, and provides physical stability for the catalyst. Desirable attributes of a catalyst support are high surface area, chemical stability, and capability for dispersing active phase over the surface. Furthermore, synergistic or dual function effects may arise from the interaction of the active metal with the support. For example, hydrogen spillover involves migration of dissociated hydrogen atoms from the active metal catalyst particle onto the catalyst support (Conner and Falconer, 1995). Therefore, screening and careful selection of the support may be vital for an active catalyst.

In this chapter, metal and metalloid oxides were investigated as nickel supports. Metal oxides are an important class support materials utilised on an industrial scale. Silica (SiO_2) occurs in numerous crystalline forms and is utilised as a catalyst support in catalytic reforming due to its high tolerance to poisoning. Alumina also occurs in several distinct crystalline forms and has higher thermal stability compared to silica (Karatzas *et al.*, 2011). Higher thermal conductivity allows heat to escape more readily, reducing the likelihood of thermal deactivation of the catalyst. Likewise, zirconia exhibits high thermal stability, high strength, and chemical compatibility (Nielsen and Wilfing, 2010). The acid-base behaviours of these materials differ. Zirconium oxide has been characterised as the only metal oxide possessing acidic, basic, oxidising and reducing properties on its surface on which CO_2 can adsorb (Tanabe, 1985; Viinikainen *et al.*, 2009). Alumina is similarly amphoteric while silica contains acidic sites (Damodaran, Nagarajan and Rao, 1990; Da Silva *et al.*, 2019).

The use of biomass residues as supports is an attractive alternative as it utilises a waste resource and forgoes typical mining methods to obtain minerals. Rice is the second most cultivated crop in the world, and production yields approximately 78 wt % rice and 20 wt % rice husks (Pereira *et al.*, 2016). Rice husk is thus an abundant agricultural by-product, and its use could result in potential economic and

social benefits in agro-economic countries which produce large amount of rice. Due to its high calorific value of 3410 kcal kg^{-1}, rice husk can be used as a renewable energy source, *e.g.* by burning in a boiler, which results in the formation of low-value ash (Riza and Rahman, 2015). Up to 95 % of rice husk ash (RHA) is composed of silica, a widely-utilised catalyst support (Natarajan, Nordin and Rao, 1998). Consequently, rice husk ash is an attractive material to consider as a catalytic support material

As established in Chapter 6, bulk nickel powder enhanced the formation of formate. In this chapter, a range of supported Ni catalysts were synthesised, tested and characterised for hydrothermal bicarbonate reduction with glucose. Nickel supported on SiO_2, Al_2O_3, ZrO_2 and commercial Ni on mixed SiO_2/Al_2O_3 were investigated as catalysts. Furthermore, Ni on rice husk-derived silica (RH-SiO_2) was also synthesised and investigated. To contrast with mineral supports, activated carbon (AC) was also investigated as a support. AC possesses high surface area with bulk porosity and is stable in both acidic and basic media (Merabti *et al.*, 2010). Finally, as an industrial catalyst, Raney-Ni was investigated alongside the supported Ni catalysts to evaluate the activity of established Ni catalysts in this reaction and gain insight into the effects of catalyst properties.

7.2 METHODOLOGY

7.2.1 Materials

A summary of reagents used in the synthesis and testing of supported nickel catalysts may be found in Table 7-1.

Table 7-1 Materials used in Ni catalyst synthesis and testing

Entry	Chemical name (Acronym)	Formula	Grade	Supplier
1	Rice husk (RH)	-	-	Briess Malt & Ingredients Co., USA
2	Aluminium oxide	Al_2O_3	99.9 %	Sigma-Aldrich

3	Silicon dioxide	SiO_2	≥99.995 %	Sigma-Aldrich
4	Commercial nickel on silica-alumina (Ni/SiAl)	$Ni/SiO_2/Al_2O_3$	65 % Ni/NiO	Sigma-Aldrich
5	Nickel nitrate hexahydrate	$Ni(NO_3)_2.6H_2O$	99.999 %	Meck Millipore
6	Zirconyl chloride octahydrate	$ZrOCl_2.8H_2O$	98 %	Sigma-Aldrich
7	Cetyltrimethylammonium Bromide (CTAB)	$C_{19}H_{42}BrN$	≥98 %	Merck Millipore
8	Norit GSX Activated carbon powder (AC)	-	100 %	Alfa Aesar
9	Raney® -Nickel 2800 slurry (Raney-Ni)	AlNi	≥89 % Ni	Sigma-Aldrich
10	Ethanol	C_2H_6O	≥99.5 %	Sigma-Aldrich
11	Nitric acid	HNO_3	64-66 %	Sigma-Aldrich
12	Sodium hydroxide	NaOH	≥97.0+ %	Sigma-Aldrich
13	Acetone	C_3H_6O	>95 %	Fisher Scientific
14	Nitrogen	N_2	100 %	BOC Gases Ltd.
15	Compressed air	-	79 % N_2 21 % O_2	BOC Gases Ltd.

7.2.2 Experimental Procedure of Catalytic Hydrothermal Reactions

Reactions with supported Ni catalysts and Raney-Ni were carried out using the same conditions as with bulk metal catalysts. Experiments were carried out at 250 °C for 2 hours with a water filling volume of 50 ml. In addition to 25 mmol $NaHCO_3$ and 2.5 mmol glucose, a nominal 1 g of supported catalysts or bare supports was added

into the pressure vessel. Post-reaction, solids were filtered out by vacuum filtration and dried for 18 hours at 105 °C to remove moisture, followed by characterisation.

In reactions with Raney-Ni, 1.5 g of Raney-Ni slurry was weighed ensuring the solids remain wetted with H_2O, then added to the pressure vessel. Post-reaction Raney-Ni was deactivated in 25 % HCl solution. As a pyrophoric substance, ignition in analytical equipment may pose a safety hazard and cause irreversible equipment damage. As the extent of deactivation during the reaction was unknown, spent Raney-Ni was thus not characterised in this work.

7.2.3   Rice Husk Proximate and Compositional Analysis

For the synthesis of rice husk-derived SiO_2 supported catalyst, proximate analysis of the risk husks was first carried out to determine the percentage of ash in the feedstock. Following this, compositional analysis of the RHA was carried out to determine the percentage of silica. Silica content is important was determining the ratio of reagents during sol-gel synthesis of Ni/RH-SiO₂, as described in Section 7.2.4.1. Steam-sterilized rice husks were obtained from home brewing distributor Briess Malt & Ingredients Co and was previously steam sterilized at temperatures up to 130 °C for up to 30 minutes to prevent bacterial growth. Proximate analysis of rice husk was carried out in triplicate to ensure reproducibility and minimize error.

7.2.3.1   *Total Solids and Moisture Content*

The method of calculating the total solids of biomass was carried out according to the NREL convection oven procedure (Sluiter *et al.*, 2008). Three glass petri dishes were dried for 24 hours at 105 °C and left to cool in a desiccator. The weight was then recorded to the nearest 0.01 g until no more fluctuation was observed. A nominal amount of as-received biomass was placed on the glass dishes to cover it in one level layer, then placed into a Memmert convection oven (Schwabach, Germany) at 105 °C. After 4 hours, the plates with samples were cooled in a desiccator and their mass noted, after which the samples were left for a further 20 hours. The percentage of total solids was calculated by Equation 7-1, and moisture content by Equation 7-2, where W_P is mass of plate, W_{P+S} is mass of plate and sample, and W_{SAR} is the mass of sample as received.

Equation 7-1 Total Solids Calculation

$$\% \, total \, solids \; = \frac{(W_{P+S} - W_P)}{W_{SAR}} \times 100 \, \%$$

Equation 7-2 Moisture Content Calculation

$$\% \, moisture = 100 - \left(\frac{(W_{P+S} - W_P)}{W_{SAR}} \right) \times 100 \, \%$$

7.2.3.2 Volatile Matter

For the quantification of volatile matter present in biomass samples, conventional proximate analysis method ASTM E872-82 was used (ASTM, 2011). The sample was dried as per Section 7.2.3.1, ground and sieved through a 35 mesh to give a maximum particle size of 0.500 mm. The biomass was then dried at 105 °C for 24 hours to remove moisture. A crucible and lid were pre-fired at 950 °C for 30 minutes, after which they were cooled to room temperature in a desiccator and weighed. The crucible was then loaded with 1 g of dry biomass, covered and its mass noted. The sample was then placed in a pre-heated Carbolite CSF1100 muffle furnace with Eurotherm controller set to 950 °C for 7 minutes, after which it was quickly removed and cooled to room temperature in a desiccator. Once cooled, the final mass of the covered biomass sample was noted. The percentage of volatile matter is determined by Equation 7-3.

Equation 7-3 Volatile Matter Calculation

$$\% \, volatile \, matter \; = \frac{W_i - W_f}{W_i - W_c} \times 100$$

Where W_i is the initial weight of the pre-fired crucible, lid and rice husks, W_f is the weight of the fired crucible, lid and sample after firing at 950 °C, and W_c is the weight of the pre-fired crucible and lid.

7.2.3.3 Ash

The percentage of ash in the samples was determined by using a method adapted from ASTM D1102-84 (ASTM, 2001). Prior to combustion, a crucible was heated at 600 °C to remove adsorbed moisture. The crucible was cooled in a desiccator and weighed to constant mass. Ground, 35-meshed RH was pre-dried in a Memmert universal oven at 105 °C overnight to remove moisture. Approximately 2 g of dried RH was placed in the pre-fired crucible and heated in a muffle furnace from room

temperature to 580 °C to avoid flaming. The sample was held at this temperature for 30 minutes, then removed, cooled in a desiccator and weighed. Subsequently the crucible was reintroduced into the muffle furnace, cooled and weighed until a constant weight to within 0.2 mg was recorded. The percentage of ash was determined using Equation 7-4:

Equation 7-4 Ash Calculation

$$\% \ ash = \frac{W_f - W_c}{W_i - W_c} \times 100 \ \%$$

where W_i is the initial weight of the pre-fired crucible and rice husk, W_c is the weight of the crucible and W_f is the weight of the fired crucible and RH. In volatile matter and ash procedures the rice husks were dried prior to carrying out the protocol. Therefore, the final percentage was adjusted to account for moisture present in as-received rice husks.

Ash was analysed by ICP-OES for elemental composition by colleague Heather Grievson of the Department of Chemistry at the University of Sheffield. Samples were digested in HF/Aqua-regia and analysis carried out in duplicate as described in Section 6.2.

7.2.4 Catalyst Synthesis Protocols

7.2.4.1 Ni/RH-SiO₂

The procedure for preparing nickel on rice husk silica was adapted from Thabet and co-workers (Thabet *et al.*, 2015). Rice husk (RH) was dried for a minimum of 8 hours at 100–110 °C to remove adsorbed moisture, then mixed with 1 M HNO_3 in a ratio of 1 g RH:25 ml 1 M HNO_3. The mixture was stirred at room temperature for 24 hours to remove carbon, then washed with copious amounts of distilled water to neutral pH and dried at 120 °C for 24 hours. The RH was then placed in a muffle furnace at 600 °C for 6 hours to obtain RHA. RHA was then added to 1 M NaOH and stirred for 24 hours to obtain sodium silicate solution. The ratio of RHA:NaOH was maintained at 3 g RHA:350 mL 1 M NaOH. CTAB was added to the sodium silicate solution in the molar ratio 1:1.2 Si:CTAB and dissolved completely. The amount of silica present in RHA was determined by ICP-OES as described in Section 7.2.3.

Prior to titration, the nickel precursor $Ni(NO_3)_2.6H_2O$ was dissolved in 50 mL of 3 M HNO_3. The sodium silicate solution was then titrated with 3 M HNO_3 containing metal

precursors at a rate of approximately 1 ml min^{-1} under constant stirring until approximately pH 3 was read on a pH meter (ETA 8100 Plus, SLS). The resulting gel was aged for 12 days until no further gelation occurred. The gel was then filtered and thoroughly washed with distilled water until neutral pH, then also washed with acetone to remove CTAB. The gel was dried at 120 °C for 24 hours, ground to a fine powder and calcined in a tube furnace (Three Zone Horizontal, Elite, UK) at 500 °C for 12 hours under 1 ml min^{-1} Ni flow.

7.2.4.2 Ni/ZrO$_2$

Nickel supported on silica, alumina and zirconia was synthesised by the sol-gel method. Silica and alumina-supported nickel catalysts were prepared by PhD candidate Gareth Davies, with detailed protocol available in print, while 20 % Ni/ZrO$_2$ was prepared by MEng student Chimmakwa Gaius-Assor (Davies *et al.*, 2021). The protocol for Ni/ZrO$_2$ synthesis was adapted from literature (Martínez *et al.*, 2019). Two solutions were mixed to prepare a gel. In the synthesis of the 20 wt % catalyst, solution A contained 34.6 ZrOCl$_2$.8H$_2$O, 90 ml ethanol and 0.6 ml nitric acid. The solution was left to homogenise for approximately 1 hour with agitation. Solution B was formed by diluting 6.2 ml of distilled water with 36 ml ethanol. The nickel precursor Ni(NO$_3$)$_2$.6H$_2$O was then added to form theoretical yield of 20 wt % Ni. Solution B was agitated for 10 minutes to homogenise, then added dropwise to Solution A under continuous stirring. The mixed solution was heated at 75 °C for 2 hours under reflux. The resulting gel was washed with ethanol to neutral pH, then dried at 60 °C for 19 hours. Dried samples were ground and calcined for 2 hours in a tube furnace (Three Zone Horizontal, Elite, UK) at 900 °C with 10°C min^{-1} heating under 1 ml min^{-1} air flow.

In the synthesis of higher loaded 60 wt % Ni/ZrO$_2$ catalyst, the method was modified to reduce observed losses. The formed gel was left to age overnight for 18 hours. It was observed that the gel has low retention on the filter paper. Instead, the catalyst gel was left to sit on a hot plate set to 35 °C for approximately 2 hours to gently evaporate excess ethanol. The gel was then dried overnight for 18 hours at 110 °C to remove ethanol and residual water. Calcination was carried out in static air in a Carbolite CSF1100 muffle furnace at 900 °C for 2 hours, ramped at 10 °C min^{-1}. The final yield of catalyst was 97.2 % (4.86 g), with a theoretical yield of 5.00 g.

7.2.4.3 Ni/AC

Nickel on activated carbon was prepared by modifying existing protocols for impregnation (Fidalgo *et al.*, 2010; Merabti *et al.*, 2010). Commercial activated carbon powder was oxidised with 3 M HNO_3 in a volume ratio of 1:5 carbon:solution for 22 h at 90 °C under reflux. This step was included as studies have shown that surface oxygen is key to obtaining high metal dispersion on AC. To improve the interaction between metal and surface carbon, acidic oxygen groups on the AC surface have been shown to be highly advantageous (Fidalgo *et al.*, 2010). Therefore, pre-treatment with an oxidant nitric acid was carried out to achieve higher catalytic activity. Approximately 6 grams of carbon equating to about 20 ml was refluxed in 100 ml 3 M HNO_3. After reaction, the flask was cooled and carbon suction filtered, then washed with DI water until neutral pH. The carbon was then dried overnight for 18 hours at 110 °C. Impregnation of the AC support was carried out by adding aqueous solution of 20 wt % Ni equivalent $Ni(NO_3)_2.6H_2O$ precursor of concentration in a ratio of 1 g AC to 5 ml solution. The mixture was sonicated for 7 hours, suction filtered and dried for 48 hours at 105 °C with extraction. The resulting catalyst was ground to a fine powder and calcined in static air at 350 °C for 3 hours.

7.2.5 Catalyst Characterisation

Several techniques were used in catalyst characterisation. FTIR-ATR was carried out to determine if any changes in surface functionality occur. An IRAffinity-1S (Shimadzu) was used and spectra acquired in transmission mode at a resolution of 8 cm^{-1} with 32 scans over the range 400-4000 cm^{-1}. X-ray diffraction was carried out by the same procedure as described in Section 6.2. Analysis of data was carried out by a combination of existing literature and the PDF-4+ 2021 database (ICDD, USA). The morphological characteristics of the catalysts were investigated by SEM using a Jeol JSM-6010 LA Analytical Scanning Electron Microscopy. The accelerating voltage (V) employed ranged from 3 kV to 10 kV with working distance of 11-13 mm. Samples were placed on conductive carbon tape adhered to an aluminium sample stub and pre-coated with gold for 10 s in an Agar Sputter Coater to improve conductivity. A current of 40 mA and pressure of 0.04 mbar was used.

7.3 RESULTS AND DISCUSSION

7.3.1 Characterisation of Rice Husk Ash

Proximate analysis showed that as-received rice husks contained 92.4 % total solids. Detailed results of proximate analysis are shown in Table 7-2.

Table 7-2 Proximate Analysis of Rice Husk

Component	Weight Percent (%)
Moisture	7.6 ± 0.2
Volatile matter	63.8 ± 0.7
Ash	4.3 ± 0.1
Fixed carbon	24.3

It was found that ash constitutes approximately 4 wt % of rice husks used in this study. ICP analysis found that approximately 94.5 % of RHA is SiO_2 (Table 7-3). With the exception of potassium and calcium, the concentration of other inorganics is on average less than 1 %. Therefore, the total silica content of rice husks constitutes 3.8 %. It must be noted that the variety of rice strongly impacts the ash and silica content of rice husks. Ash content up to 28.6 % of dry basis has been reported, and of this up to 96 wt % silica can be obtained (Ogwang *et al.*, 2021). Therefore, careful selection of rice husk variety is key in obtaining higher quantities of silica.

Table 7-3 Elemental Composition of Rice Husk Ash

Element	% of RHA as oxide
Si	94.5
Al	<0.1
K	2.6
Ca	1.1
Fe	0.5
Mg	0.4
Na	<0.1
P	0.5

The results of proximate and compositional analysis of rice husks were used when determining the ratio of reagents in the synthesis of Ni/RH-SiO$_2$. A similar protocol can be used for other biomass residues. Thermogravimetric analysis (TGA) can used in place of proximate analysis to hasten analysis and reduce experimental time.

7.3.2 Aqueous products with supported Ni catalysts

Higher dispersion and smaller particle size of Ni on supports was predicted to yield higher concentrations of HCOO$^-$ due to an increase in catalyst-reactant contact area with increased Ni surface area. In the presence of all supported Ni catalysts there was visibly reduced char formation on the reactor and impeller, indicating retarding of char formation. This aligns with literature, where it has been reported that acidic sites on the supports prevent the formation of tar by promoting hydrocracking reactions, while basic sites give higher resistance to coke formation (Viinikainen et al., 2009). However, analysis of aqueous products showed that formate concentrations decreased in reactions with supported Ni (Figure 7-1).
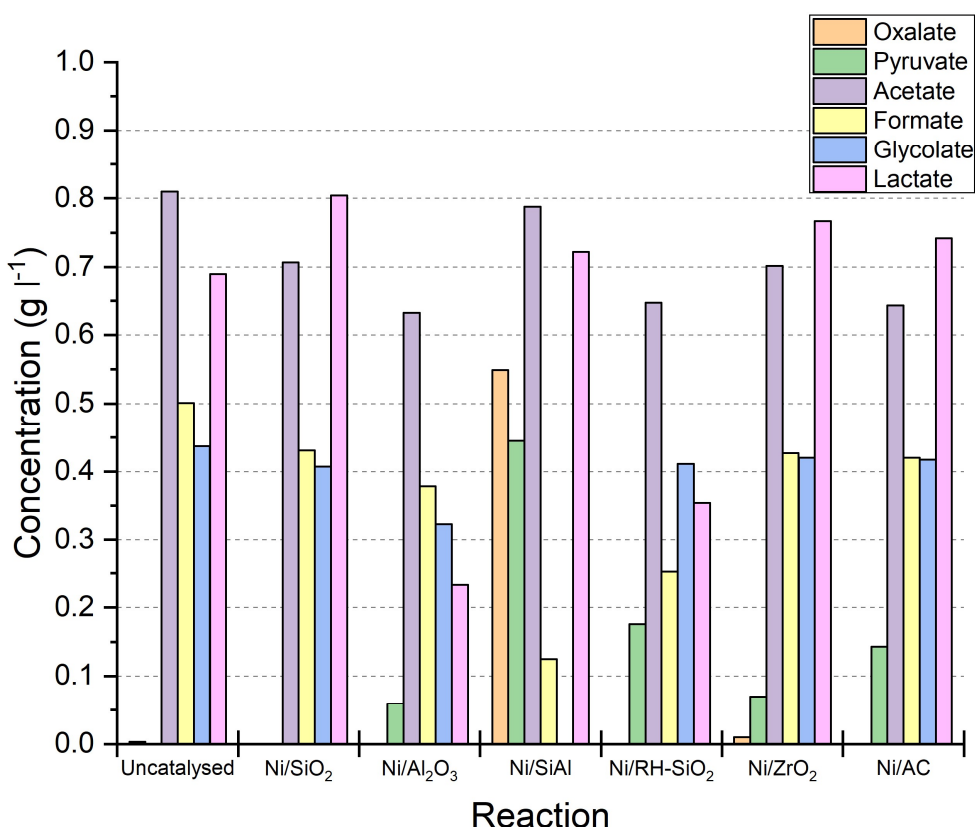
Figure 7-1 Organic acid production in hydrothermal conversion of NaHCO$_3$ and glucose with supported Ni catalysts. Reaction conditions: 0.50 M NaHCO$_3$, 0.05 M glucose, 1 g 20 wt % Ni catalyst (where used), 50 ml H$_2$O

The organic acid profile with Ni/SiO_2, Ni/ZrO_2 and Ni/AC was found to be broadly similar. Formate concentration dropped from 0.501 g l^{-1} to 0.431, 0.427 and 0.420 g l^{-1} with Ni/SiO_2, Ni/ZrO_2 and Ni/AC, respectively, compared to uncatalyzed reactions, while lactate increased. Acetate also showed a decrease from 0.810 g l^{-1} in uncatalyzed reactions to 0.703, 0.702, and 0.645 g l^{-1}, respectively, with these species. With Ni/ZrO_2, a marginal increase was recorded in oxalate and pyruvate concentrations, though these remained <0.100 g l^{-1}. Similarly, Ni/AC promoted the formation of pyruvate, which increased to 0.145 g l^{-1} Based on the changes in the concentration of products, it is proposed that Ni/SiO_2, Ni/ZrO_2 and Ni/AC may influence the conversion of intermediate pyruvaldehyde to lactate and, to a lesser extent, pyruvate, as opposed to acetate or formate in accordance with the mechanism proposed in Section 5.2.4.

Conversely, with Ni/Al_2O_3 and Ni/RH-SiO_2 a decrease in all organic acids except pyruvate was recorded. In the presence of Ni/RH-SiO_2, formate concentration decreased two-fold from 0.501 to 0.252 g l^{-1}, while pyruvate increased to 0.176 g l^{-1}. Similarly, formate dropped with Ni/Al_2O_3 to 0.378 g l^{-1}. The most dramatic change in aqueous products occurred with commercial nickel on silica-alumina (Ni/SiAl). With the addition of Ni/SiAl, formate concentration dropped to 0.125 g l^{-1}, while simultaneously oxalate and pyruvate increased to 0.550 and 0.445 g l^{-1}, respectively. Notably, acetate and lactate concentrations remained comparable to uncatalyzed reactions, indicating that this catalyst may provide a site for the conversion of pyruvaldehyde to pyruvate alongside the more favoured lactate and acetate pathways. The increase in oxalate also indicates that Ni/SiAl may promote the coupling of formate to form oxalate.

To determine if the decreased yields with supported catalysts were due to low Ni loading, a 60 wt % Ni/ZrO_2 was prepared for comparison to lower loading. However, higher loading of Ni on ZrO_2 did not result in increased $HCOO^-$ (Table 7-4).

Table 7-4 Concentration of organic acids with 20 and 60 wt % Ni/ZrO_2 catalysts. Reaction conditions: 0.50 M $NaHCO_3$, 0.05 M glucose, 1 g catalyst, 250 °C, 2 h, 50 ml H_2O

Catalyst	Concentration (g l^{-1})				
	Pyruvate	**Acetate**	**Formate**	**Glycolate**	**Lactate**
20% Ni/ZrO_2	0.07	0.702	0.427	0.42	0.767
60% Ni/ZrO_2	0.113	0.67	0.394	0.412	0.465

As previously discussed, Ni supported on non-mineral AC also showed a lack of activity towards HCOOH formation. This indicates that the drop in HCOOH concentration can likely be attributed to the Ni phase more so than the activity of the supports. However, to test their effects independently, reactions with bare SiO_2 and Al_2O_3 were carried out. Results showed that both silica and alumina presence in the reaction leads to a decrease of all organic acids except pyruvate (Figure 7-2). Therefore, solely SiO_2 or Al_2O_3 are not active in the production of organic acids from $NaHCO_3$ and glucose and marginally inhibit the yield of organic acids. As no significant changes in products were observed, decreased concentrations may be due to adsorption of reagents or products into the support structure. Alumina generally contains a surface area between 200 – 500 $m^2 g^{-1}$, and some product may be adsorbed within the catalyst structure (Patel, Sarma and De, 2015). The same phenomena may occur with SiO_2 as silica surface area is in a similar range of 300 – 500 $m^2 g^{-1}$ depending on synthesis method (Vansant, Vrancken and Van Der Voort, 1995). Due to reactor damage, neither reactions with bare ZrO_2 nor AC could be carried out. Furthermore, the mechanisms occurring with supported Ni catalysts could not be experimentally validated due to equipment downtime.
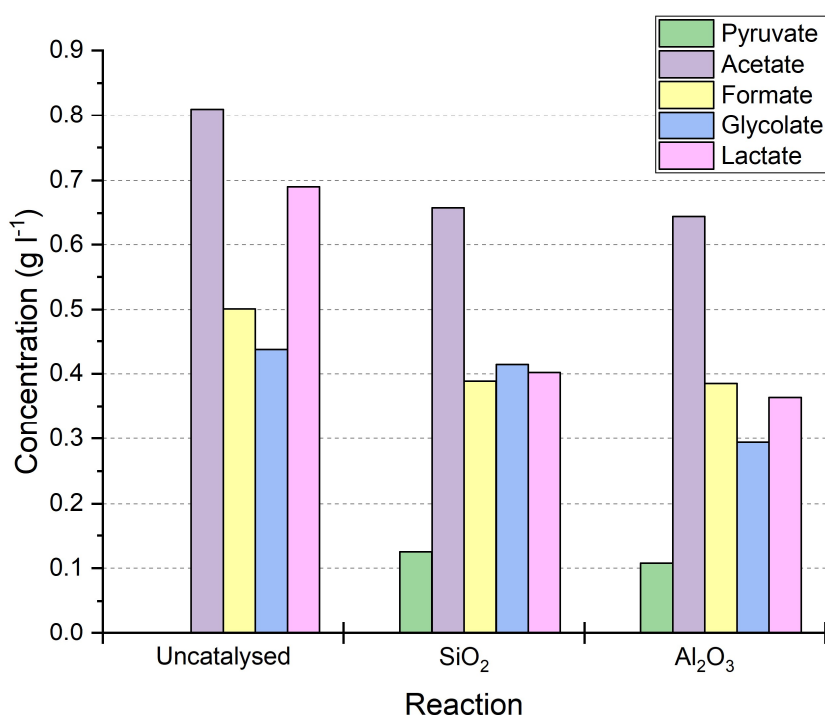
Figure 7-2 Organic acid production in hydrothermal conversion of NaHCO₃ and glucose with bare SiO₂ and Al₂O₃. Reaction conditions: 0.50 M NaHCO₃, 0.05 M glucose, 1 g support (where used), 250 °C, 2 h, 50 ml H₂O

The effects of supported Ni catalysts and bare supports on gas products was examined. Results demonstrate a strong correlation between formate yield and H_2 (Table 5). In reactions with Ni/SiO_2, Ni/Al_2O_3, Ni/ZrO_2, Ni/AC and bare supports, H_2 composition remained comparable to uncatalyzed reactions (Table 7-5, Entries 1-5, 8-10). In contrast, commercial Ni/SiAl and $Ni/RH-SiO_2$ resulted in an H_2 increase to 34.8 % and 11.5 %, and the lowest formate concentrations of 0.125 g l^{-1} and 0.252 g l^{-1}, respectively (Table 7-5, Entries 6, 7). Liu and co-workers previously proposed that formic acid is an intermediate in hydrothermal CO_2 reduction to CH_4, but as there was only trace CH_4 present it is unlikely that this is occurring in the present system (Liu *et al.*, 2013). Thus, it was hypothesised that these catalysts promote the $HCOO^-$ decomposition to CO_2 and H_2. As both Ni/SiAl and $Ni/RH-SiO_2$ are composed of a similar support to the inactive catalysts, this further indicated that low activity stems from the Ni active phase. Characterisation of the catalysts to investigate this hypothesis is discussed in Section 7.3.4.

Table 7-5 Formate concentration and H_2 composition in gas products in reactions with supported Ni catalysts and bare supports. Reaction conditions: 0.50 M $NaHCO_3$, 0.05 M glucose, 1 g catalyst/support (where used), 250 °C, 2 h, 50 ml H_2O

Entry	Ni (wt %)	Catalyst	[Formate] (g l^{-1})	H_2 (%)	CH_4 (%)
1	-	None/uncatalysed	0.501	1.8	0
2	20	Ni/SiO_2	0.431	0.5	<1
3	-	SiO_2	0.389	1.0	<1
4	20	Ni/Al_2O_3	0.378	1.0	<1
5	-	Al_2O_3	0.285	3.3	<1
6	65	$Ni/SiO_2-Al_2O_3$	0.125	34.8	<1
7	20	$Ni/RH-SiO_2$	0.252	11.5	<1
8	20	Ni/ZrO_2	0.427	2.9	<1
9	60	Ni/ZrO_2	0.394	4.2	<1
10	20	Ni/AC	0.420	0.4	<1

7.3.3 Comparison of Raney-Ni and Bulk Ni

As a well-understood commercial hydrogenation catalyst, Raney-Ni was investigated as a catalyst in the reaction. With the addition of Raney-Ni, the post-reaction solution

was transparent with white suspended solids, and only acetic acid was present in aqueous phase in comparable concentrations, 0.730 g l^{-1}, to uncatalyzed reactions (0.810 g l^{-1}). In comparison to bulk Ni, no HCOO$^-$ was formed with Raney-Ni, and a substantial increase of H_2 in gas products was observed (Table 7-6). Furthermore, with Raney-Ni, methane constituted 4 % of gas products while the rest is attributed to CO_2.

Table 7-6 Formate and gas products formed from reactions with Raney-Ni and bulk Ni. Reaction conditions: 0.50 M NaHCO$_3$, 0.05 M glucose, 1.5 g Raney-Ni slurry (where used), 25 mmol Ni powder (where used), 250 °C, 2 h, 50 ml H$_2$O

Ni (wt %)	Catalyst	[Formate] (g l^{-1})	H$_2$ (%)	CH$_4$ (%)
≥89%	Raney-Ni	0	60.5%	4
99.9	Bulk Ni	1.213	23.6%	0

Compared to bulk Ni, Raney-Ni has a higher surface area of 50-100 m^2 g^{-1}, high volume of contained H_2, and contains Al impurity (Rodella *et al.*, 2008). In contrast, bulk Ni powder used in this study had a surface area below the analytical range of available porosimetry equipment, <4 m^2 g^{-1}, and high purity of 99.9 %. In addition to H_2 present in Raney-Ni pores, the Al impurity in Raney-Ni may additionally facilitate the production of *in-situ* H_2 by reacting with water (Equations 7-5, 7-6) (Godart *et al.*, 2019). In the present study, approximately 1.5 g of Raney-Ni slurry was used, constituting about 0.09-0.14 g Al impurity. The formation of insoluble white suspended solids indicated the conversion of Al to one or both hydroxides.

Equation 7-5 Reaction of aluminium with water to form aluminium hydroxide and hydrogen

$$2Al + 6H_2O \rightarrow 3H_2 + 2Al(OH)_3$$
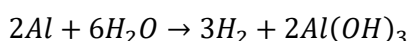
Equation 7-6 Reaction of aluminium with water to form aluminium hydroxide oxide and hydrogen

$$2Al + 4H_2O \rightarrow 3H_2 + 2AlOOH$$
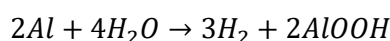
Thus, the key differences that distinguish Raney-Ni and bulk Ni catalysts are surface area and the ability to generate H_2, which led to vastly different products. As described in Chapter 6, bulk Ni enhanced formate and H_2 formation while other organic acids remained in solution. With Raney-Ni, H_2 is the main product, methane is formed, and

solely acetate is present in aqueous products. In line with previous work on hydrothermal gasification of glucose with Raney-Ni, it is proposed that in the present study this catalyst promotes gasification of the glucose to CO_2, H_2 and CH_4 (Azadi *et al.*, 2009). Notably, Raney-Ni does not appear to impact the formation of acetic acid. To validate its effects on glucose, further reactions with Raney-Ni with varying concentrations of glucose must be carried out and the composition of gas and liquid products monitored.

In terms of the impact on bicarbonate reduction, the lack of $HCOO^-$ in solution and high concentrations of H_2 indicate that Raney-Ni promotes formate degradation. High surface area of Raney-Ni is proposed to provide more contact sites for H_2 and HCO_3^- adsorption, and high concentrations of H_2 provided by the catalyst and Al reactions create more reductant than can be achieved from solely glucose. The combination of these two factors is hypothesised to enhance bicarbonate reduction to formate. Furthermore, bulk Ni was established as being active in HCOOH degradation to CO_2 and H_2 in Section 6.3. It is proposed that Raney-Ni contains more sites for the degradation reaction to proceed in comparison to bulk Ni, therefore resulting in no intermediate $HCOO^-$ and high H_2 concentrations.

In contrast to supported Ni catalysts, Raney-Ni was not characterised in this study, although the mechanism of its activity appears to be different. With the exception of Ni/SiAl and Ni/RH-SiO$_2$, supported Ni catalysts exhibited low concentrations of both H_2 and $HCOO^-$. The study on Raney-Ni demonstrated that surface area of metallic Ni in the reaction must be carefully controlled, and the H_2 generation capability considered to prevent degradation of intermediate formate. To confirm that these factors are critical in influencing reaction outcome, experiments with added H_2 or metallic Al to generate *in-situ* H_2 may be carried out with bulk Ni to test the influence of starting H_2 concentration on products. Synthesis and testing of Ni catalysts with different surface areas and metallic Ni sites may be valuable in determining the impact of increased surface area on formate formation and degradation.

7.3.4 Characterisation of Catalyst Supports

As minerals, silica and alumina may undergo changes to structure and oxidation in sub-critical water. Characterisation of bare supports was carried out to assess the stability of these materials under hydrothermal conditions. Due to equipment

breakdown, zirconia and activated carbon were not tested as catalysts and consequently not characterised.

7.3.4.1 Silica Characterisation
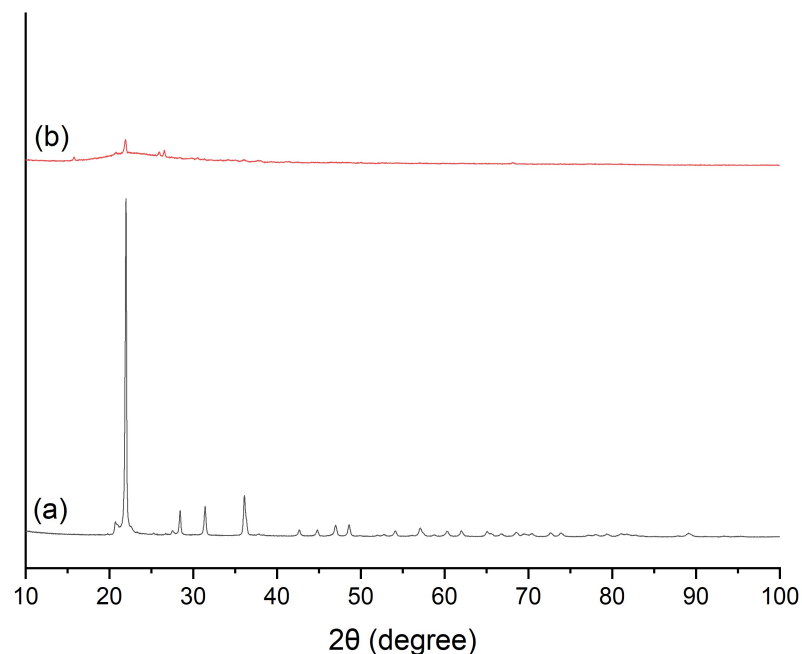
Figure 7-3 XRD of (a) fresh and (b) spent SiO$_2$. Reaction conditions: 0.50 M NaHCO$_3$, 0.05 M glucose, 1 g SiO$_2$, 250 °C, 2 h, 50 ml H$_2$O

The XRD of fresh and post-reaction SiO$_2$ is shown in Figure 7-3. Fresh silicon dioxide demonstrates crystalline nature corresponding to cristobalite low type SiO$_2$ (PDF4+ Card 01-071-0785, Joni *et al.*, 2018). Post-reaction, silica is converted to primarily an amorphous form with a wide peak around 21.8 ° with some remaining diffraction peaks corresponding to cristobalite SiO$_2$. These results indicate that silica undergoes a phase change from crystalline to amorphous under hydrothermal conditions.

Imaging of silica showed that the fresh silica particles undergo significant morphological changes during reaction. Fresh silica exhibits large particles with a smooth surface and large pores (Figure 7-4, A, C). In spent SiO$_2$, the surface topography is varied and the smooth surface is destroyed (Figure 7-4, B, D).
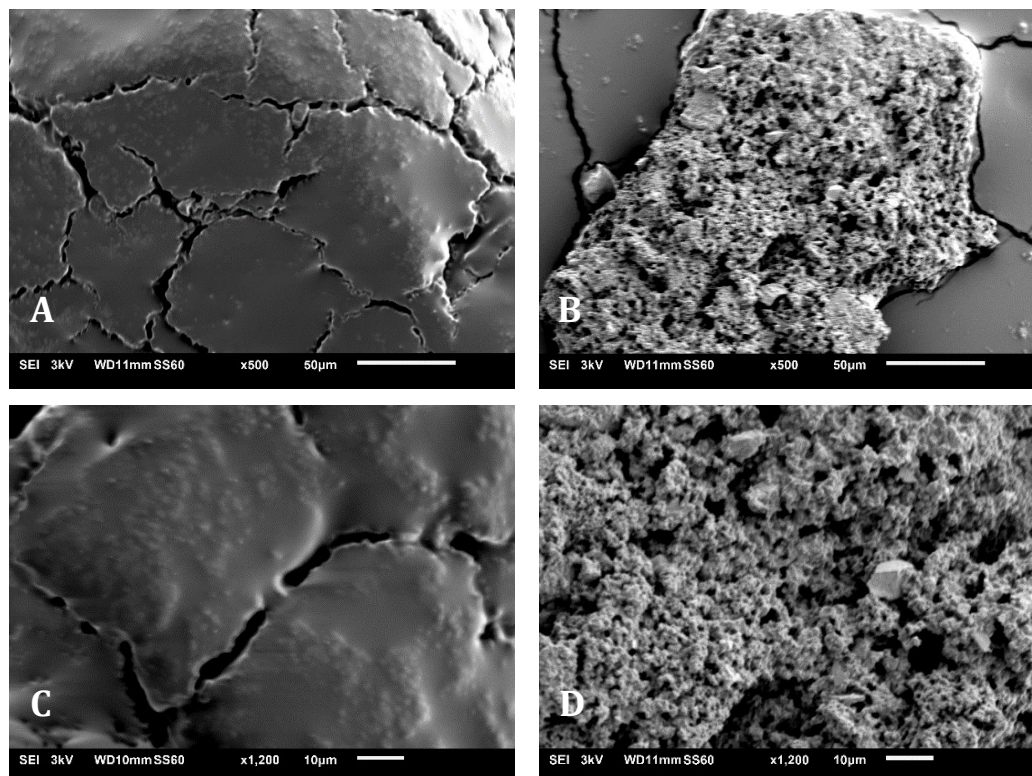
Figure 7-4 SEM of SiO₂. A) Fresh SiO₂ x500 magnification, B) Spent SiO₂ x500 magnification C) Fresh SiO₂ x1200 magnification, D) Spent SiO₂ x1200 magnification

7.3.4.2 Alumina Characterisation

In XRD patterns of fresh alumina pellets, a typical amorphous pattern of Al_2O_3 was observed (Figure 7-5) (Z. Wang *et al.*, 2016). Post-reaction, the support contains diffraction peaks at 2 θ = 14.4 °, 28.2 °, 38.2 °, 48.8 °, 65.0 ° and 71.9 ° corresponding to phases of AlO(OH) (PDF4+ Card 00-021-1307, Dar, Sofi and Shah, 2015). Therefore, alumina undergoes significant phase changes and does not exhibit stability under the investigated conditions.
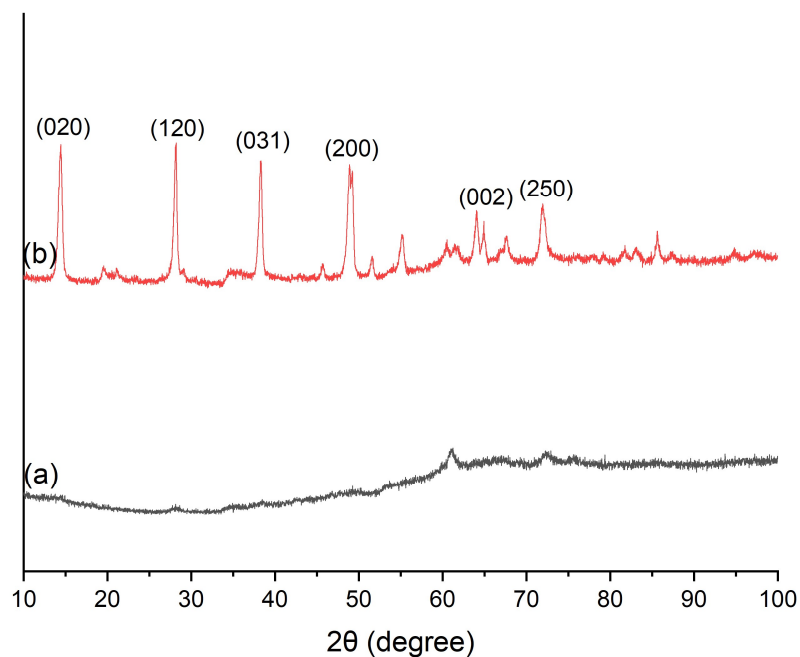
Figure 7-5 XRD of (a) and (b) fresh Al$_2$O$_3$ depicting phases of AlO(OH). Reaction conditions: 0.50 M NaHCO$_3$, 0.05 M glucose, 1 g Al$_2$O$_3$, 250 °C, 2 h, 50 ml H$_2$O

Due to the spherical shape of commercial Al$_2$O$_3$ pellets, gold coating the surface was challenging and resulted in pellet sides remaining uncoated. Therefore, SEM images were not well resolved due to surface charging. Fresh alumina has spherical particles with complex surface morphology (Figure 7-6, A, C). During reaction, spherical particles undergo a macroscopic change to less uniform particles (Figure 7-6, B). Furthermore, surface features are lost on the spent catalyst, and the surface appears smoother (Figure 7-6, C-D).
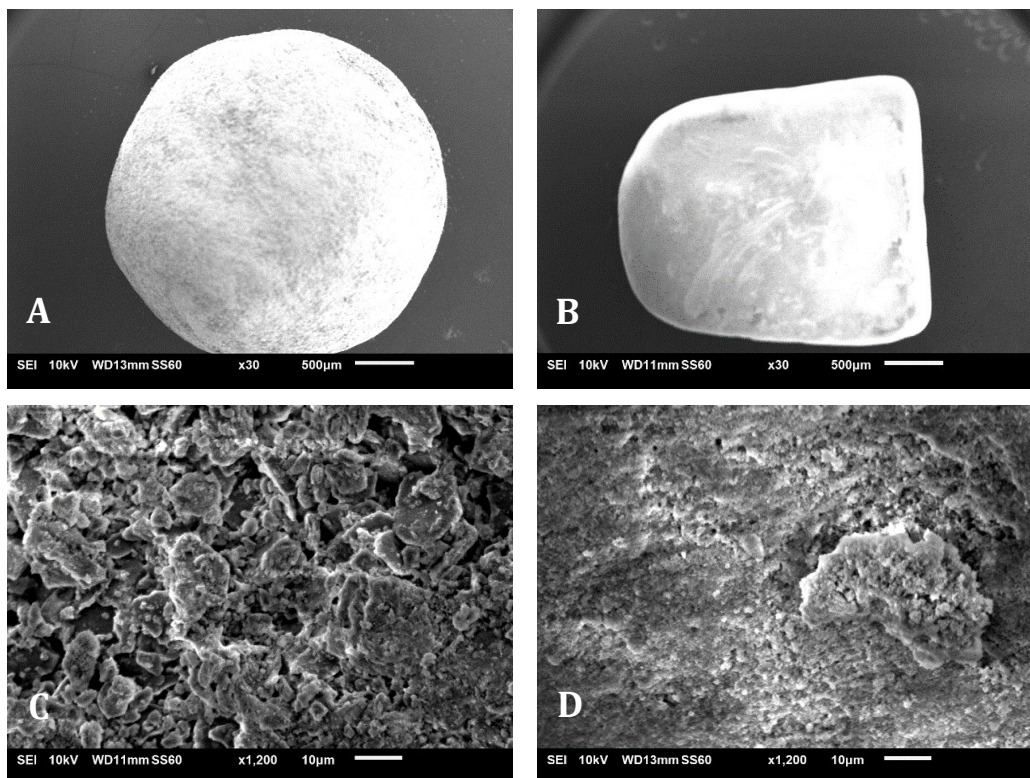
Figure 7-6 SEM of Al₂O₃. A) Fresh Al₂O₃ x30 magnification, B) Spent Al₂O₃ x30 magnification C) Fresh Al₂O₃ x1200 magnification, D) Spent Al₂O₃ x1200 magnification

The results of XRD and SEM characterisation of alumina indicate that this material is not well-suited for use in hydrothermal media. The reaction of alumina with sub-critical water to form aluminium oxide hydroxide is well reported and proceeds at temperatures as low as 200 °C (Equation 7-7) (Mironenko *et al.*, 2014). Alumina undergoes morphological changes, resulting in a loss of both its macroscopic spherical shape and surface features.

Equation 7-7 Reaction of alumina with water to form aluminium oxide hydroxide

$$Al_2O_3 + H_2O \rightarrow 2AlO(OH)$$
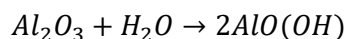
In contrast, silica exhibited mainly a loss of crystallinity during hydrothermal reaction. As catalysts may be supported on amorphous silica, there is indication that this material may be more suitable as a support under the investigated conditions. Further work investigating the stability of amorphous silica is required to validate this hypothesis. Although zirconia and activated carbon were not investigated due to equipment breakdown, some observations of the behaviour of these materials were made during characterisation of supported Ni catalysts in the following section (7.3.5).

7.3.5 Characterisation of Supported Nickel Catalyst

7.3.5.1 Ni/SiO$_2$ Characterisation

FTIR analysis of fresh and spent catalysts was carried out to determine if changes to the surface functionality of catalysts occur during reaction (Figure 7-7). The peaks at 799 cm^{-1} and 1080 cm^{-1} correspond to Si-O bending vibration band and asymmetric stretching vibration of Si-O-Si bonds. Broadening around 470 cm^{-1} corresponds to bending vibration modes of O-Si-O (Joni *et al.*, 2018). The broad peak at 3600-3055 cm^{-1} and 1655 cm^{-1} in the spent catalyst can be attributed to –OH groups of SiO$_2$ caused by physically adsorbed H$_2$O (Ramalla, Gupta and Bansal, 2015). The peak appearing at 680 cm^{-1} that appears in the spent catalyst does not correspond to any SiO$_2$ bonds but may be C=C bending caused by residual char in the solid sample.
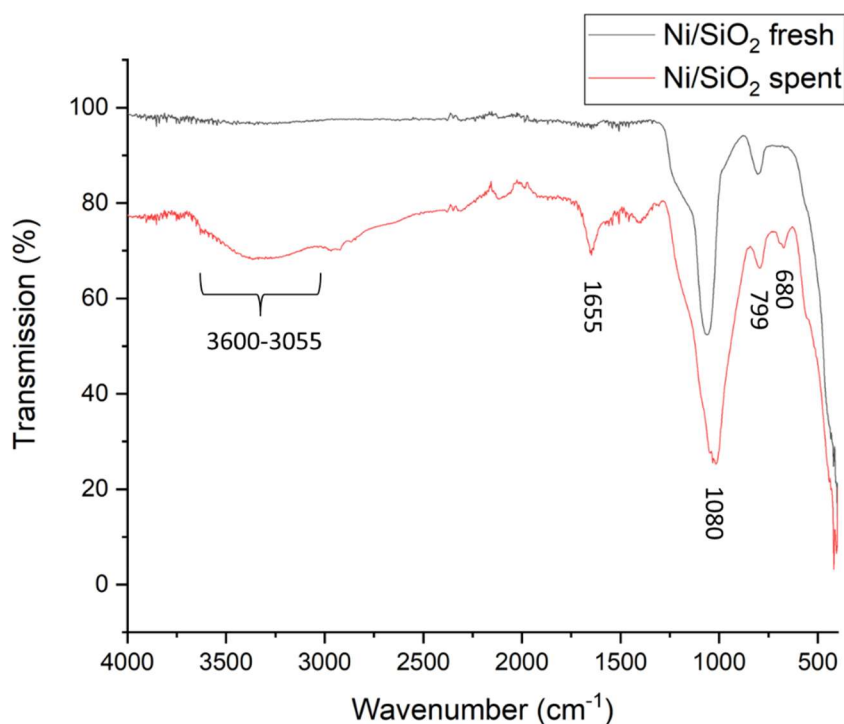
Figure 7-7 FTIR spectra of fresh (black) and spent (red) Ni/SiO$_2$. Reaction conditions: 0.50 M NaHCO$_3$, 0.05 M glucose, 1 g Ni/SiO$_2$, 250 °C, 2 h, 50 ml H$_2$O. Spectra acquired in transmission mode at a resolution of 8 cm^{-1} with 32 scans over the range 400-4000 cm^{-1}

XRD of fresh and spent Ni/SiO$_2$ showed a characteristic broad peak at 21.8 ° corresponding to amorphous SiO$_2$ (Figure 7-8). The peaks at 37.10 °, 43.30 °, 62.90 °,

76.55 °, and 79.20 ° correspond to crystal planes of NiO, indicating a fcc NiO phase (PDF4+ Card 04-004-6330, El-Kemary, Nagy and El-Mehasseb, 2013). Silica maintains an amorphous state, with a broad diffraction peak around 21.8 °. No peaks for metallic nickel appeared post-reaction, indicating that the bulk of the nickel remains in the oxidized form post-reaction.
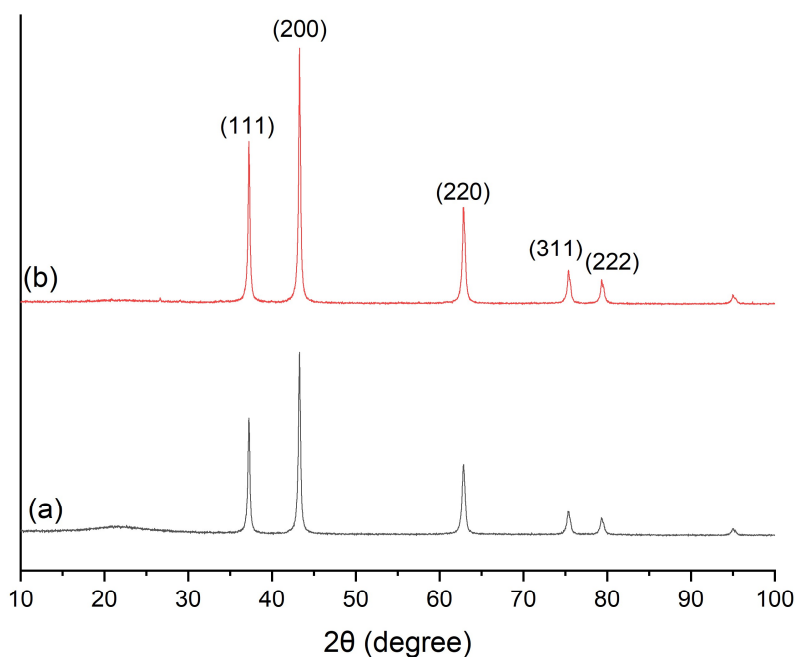
Figure 7-8 XRD of (a) fresh and (b) spent NiO/SiO₂ catalyst depicting phases of NiO. Reaction conditions: 0.50 M NaHCO₃, 0.05 M glucose, 1 g Ni/SiO₂, 250 °C, 2 h, 50 ml H₂O

Reduction of bulk NiO to Ni with H_2 has been reported at temperatures as low as 220 °C (Li and Chen, 1995). However, it has also been documented that dispersing NiO on SiO_2 increases the required reduction temperature to 295 °C for 20 wt % Ni/SiO₂ catalyst (Zhang, Lin and Chen, 1992). This indicates that the poor activity observed in the supported catalysts may be due to the oxidation state of NiO and difficulty reducing NiO to metallic Ni *in-situ*. Carbon dioxide and carbonate adsorb to both NiO and Ni through coordination of O on the Ni surface (Matsumoto *et al.*, 1999). Therefore, the lack of activity observed in Ni/SiO₂ is likely not due to poor adsorption of CO_2 on the active phase. This further indicates that H_2 dissociation is probably the rate-limiting step of the process.

Seminal work by Benton and Emmett showed that NiO reduction occurs at the interface of NiO and metallic Ni, and that added water reduces the reduction rate and

increases the induction time during which H_2 dissociates (Benton and Emmett, 1924). Furthermore, reduction is slow until 275 °C, which is higher than the operating conditions used in this study (Richardson, Scates and Twigg, 2003). Richardson and co-workers also found that in the presence of H_2O even at higher temperatures NiO reduction is strongly hindered. Furthermore, these results indicate that glucose is not reducing the NiO sites either, which is supported by reports that reduction of NiO to Ni with glucose starts at 420 °C (Cheng, Dupont and Twigg, 2016). Therefore, it is proposed that NiO is not active in bicarbonate reduction, and, as evidenced by XRD, at the investigated conditions *in-situ* reduction of NiO to Ni does not proceed.

Furthermore, SEM imaging of fresh Ni/SiO$_2$ catalyst showed NiO particles of defined octahedron form on the SiO$_2$ surface (Figure 7-9, C), while after reaction the surface appears more homogeneously globular (Figure 7-9, D). This indicates that sintering of the active phase may be occurring during reaction, and that changes in morphology are occurring.
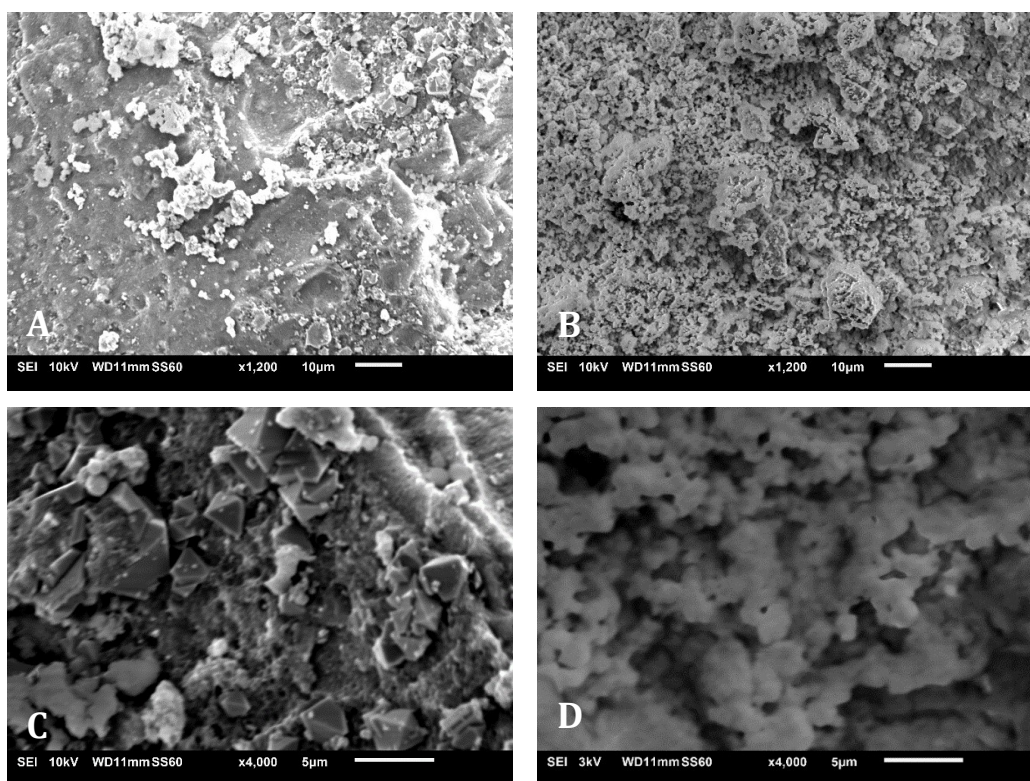
Figure 7-9 SEM of Ni/SiO₂. A) Fresh Ni/SiO₂ x1200 magnification, B) Spent Ni/SiO₂ x1200 magnification C) Fresh Ni/SiO₂ x4000 magnification, D) Spent Ni/SiO₂ x4000 magnification

7.3.5.2 Ni/Al₂O₃ Characterisation

FTIR spectra of Ni/Al_2O_3 showed several additional peaks in spent Ni/Al_2O_3 (Figure 7-10). The band at 1070 cm^{-1} in spent catalyst has been attributed to Al-O-H (Liu *et al.*, 2012). Bands at 3300, 1645, 1525 and 1390 cm^{-1} have also been attributed to AlO(OH) (Chen, Sue Huh and Lee, 2007). This indicates that a transition from Al_2O_3 to AlO(OH) occurs in the reaction.
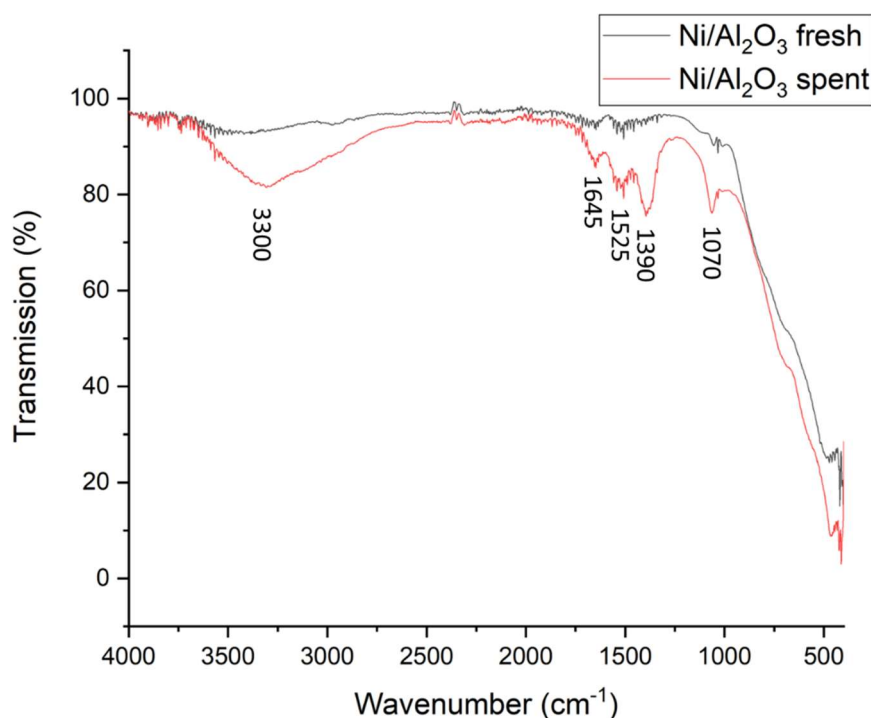
Figure 7-10 FTIR spectra of fresh (black, top) and spent (red, bottom) Ni/Al₂O₃. Reaction conditions: 0.50 M NaHCO₃, 0.05 M glucose, 1 g Ni/Al₂O₃, 250 °C, 2 h, 50 ml H₂O. Spectra acquired in transmission mode at a resolution of 8 cm^{-1} with 32 scans over the range 400-4000 cm^{-1}

XRD results were in agreement with FTIR data. Fresh and spent Ni/Al_2O_3 demonstrates characteristic low intensity NiO bands at 37.2 °, 45.6 °, and 66.0 ° (Figure 7-11). Fresh alumina does not have high intensity characteristic peaks, as shown in section 7.3.4.2. Post-reaction, the catalyst exhibits new diffraction peaks at 14.4 °, 28.2 °, and 48.8 ° corresponding to AlO(OH) (Zhang *et al.*, 2015). This indicates that, similar to bare alumina, hydrothermal treatment of alumina-containing catalysts leads to dealumination of the framework and loss of functionality (Feliczak-Guzik, 2018). Similarly to Ni/SiO₂, no diffraction peaks corresponding to metallic Ni were

detected in fresh or spent catalyst. Furthermore, compared to bulk NiO, Al_2O_3-supported NiO has been reported to require higher reduction temperatures of up to 420-500 °C (Li and Chen, 1995). Li and Chen attributed these changes to interaction of NiO with different alumina sites, with tertrahedrally-coordinated Ni displaying the highest reduction temperature. Pre-reduction of supported catalysts or calcination in an oxygen-free environment may be required to form metallic Ni.
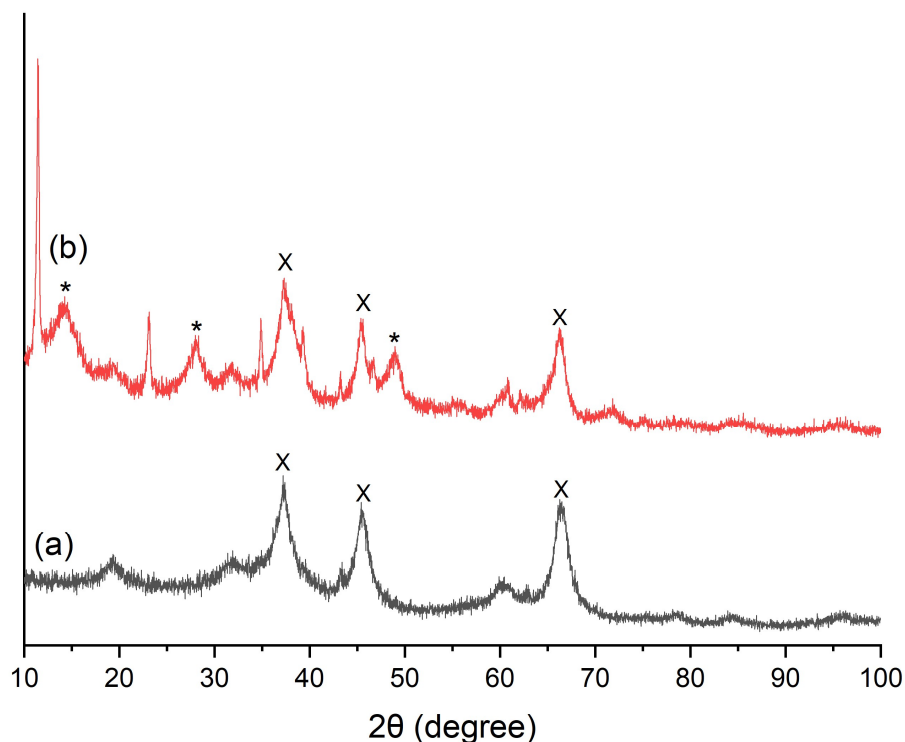
Figure 7-11 XRD of (a) fresh and (b) spent NiO/Al$_2$O$_3$, x – NiO, * - AlOOH. Reaction conditions: 0.50 M NaHCO$_3$, 0.05 M glucose, 1 g Ni/Al$_2$O$_3$, 250 °C, 2 h, 50 ml H$_2$O

SEM of fresh Ni/Al$_2$O$_3$ showed the structure contains a porous structure which disappears post-reaction (Figure 7-11). This indicates that hydrothermal processing is further destructive to the catalyst by forming an amorphous structure.
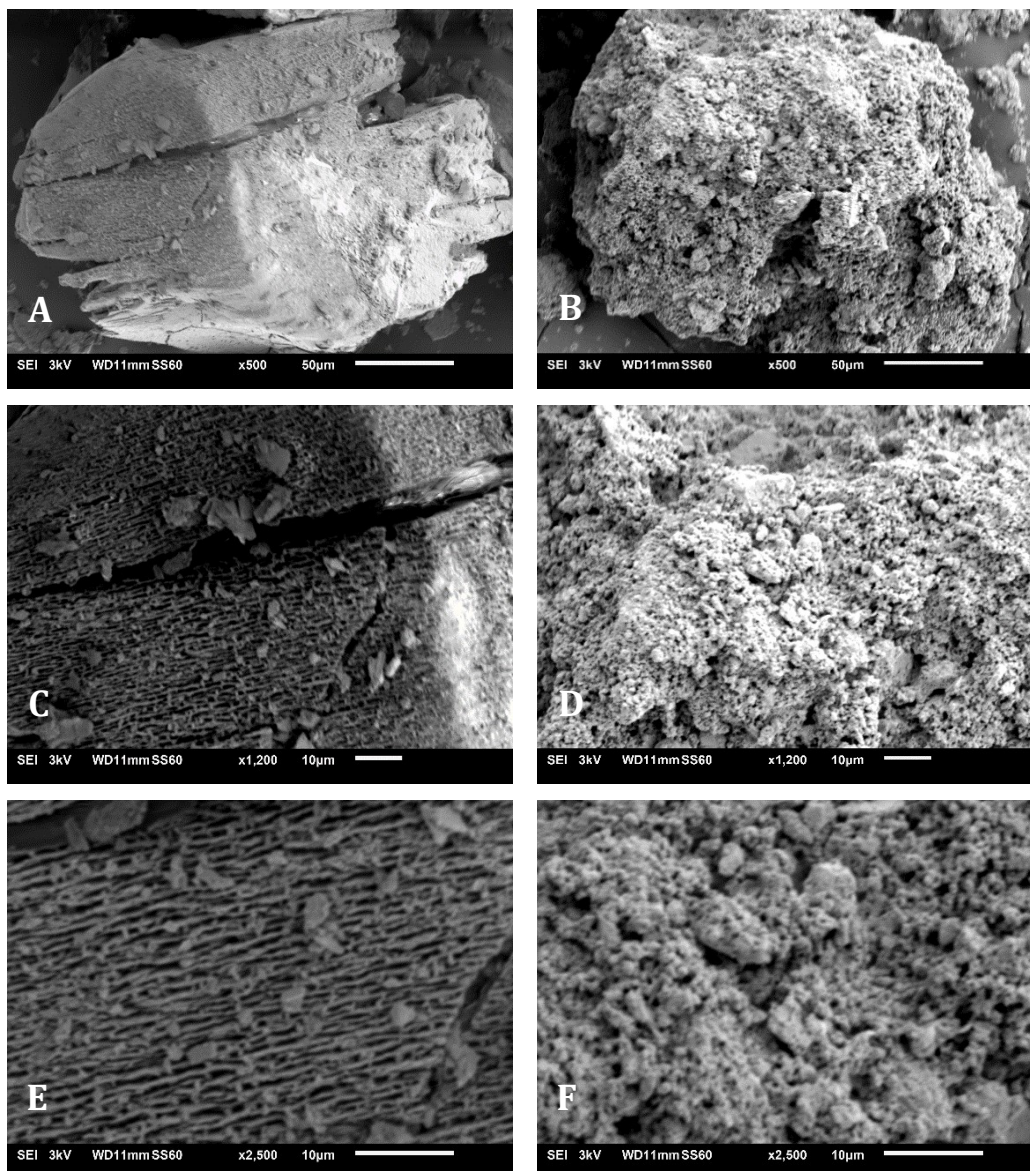
Figure 7-12 SEM of Ni/Al$_2$O$_3$. A) Fresh Ni/Al$_2$O$_3$ x500 magnification, B) Spent Ni/Al$_2$O$_3$ x500 magnification C) Fresh Ni/Al$_2$O$_3$ x1200 magnification, D) Spent Ni/Al$_2$O$_3$ x1200 magnification E) Fresh Ni/Al$_2$O$_3$ x2500 magnification, F) Spent Ni/Al$_2$O$_3$ x2500 magnification

7.3.5.3 Ni/SiO$_2$-Al$_2$O$_3$ Characterisation

Similarly to the Ni/Al$_2$O$_3$ catalyst, commercial nickel on silica-alumina displayed peaks corresponding to AlOOH post-reaction (Figure 7-13). The characteristic silica peaks of Si-O and -OH groups are also present, as described in Section 7.3.5.1. In spent Ni/SiAl, the new peak at 620 cm^{-1} may be caused by C-H bending of residual char in the sample.
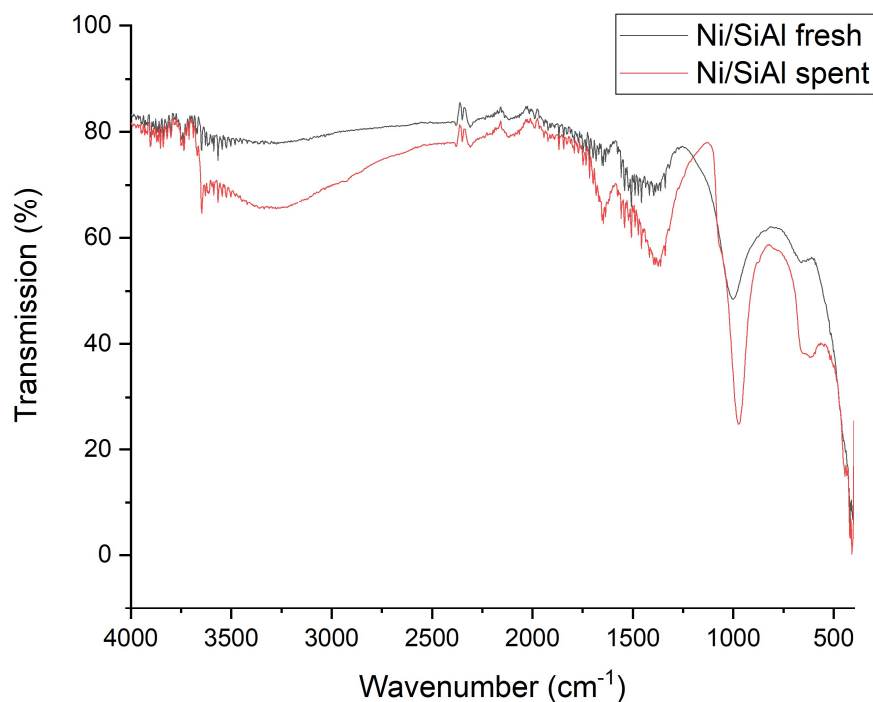
Figure 7-13 FTIR spectra of fresh (black, top) and spent (red, bottom) Ni/SiAl. Reaction conditions: 0.50 M NaHCO₃, 0.05 M glucose, 1 g Ni/SiAl, 250 °C, 2 h, 50 ml H₂O. Spectra acquired in transmission mode at a resolution of 8 cm⁻¹ with 32 scans over the range 400-4000 cm⁻¹

X-ray diffraction data indicated the presence of both NiO and metallic Ni on the mixed-support catalyst (Figure 7-14). Characteristic AlO(OH) peaks were difficult to distinguish from the Ni and NiO peaks on the highly amorphous catalyst. The new peaks forming at 12 ° and 25 ° are attributed to boehmite. Notably, the intensity of the Ni peaks at 44.4 ° and 51.7 ° post-reaction decreases, which may point to a decrease in the reduced Ni sites. Furthermore, the NiO sites persist post-reaction, indicating that even in the presence of H_2 gas, which was recorded at 34.8 % of the gas products with this catalyst, reduction of NiO does not proceed. It is proposed that this is an effect of NiO particle size resulting in higher temperature requirements for reduction, as described in previous sections. However, the metallic Ni sites may be responsible for degrading of formate to H_2, which indicates that particle size is an important consideration for designing Ni catalysts which enhance HCOO⁻ yield.
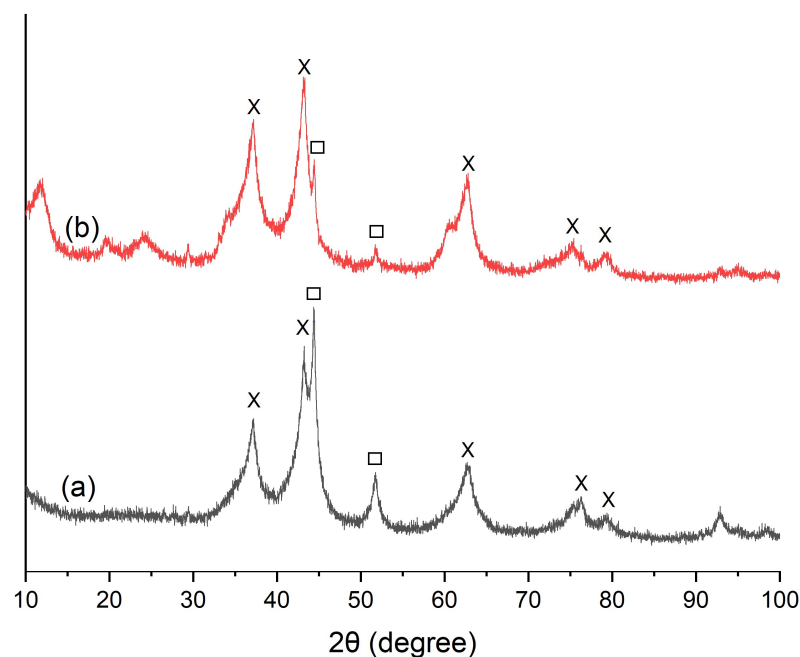
Figure 7-14 XRD of (a) fresh and (b) spent Ni/SiAl x - NiO, □ – Ni. Reaction conditions: 0.50 M NaHCO₃, 0.05 M glucose, 1 g Ni/SiAl, 250 °C, 2 h, 50 ml H₂O

Consistent with the results of XRD, SEM imaging of Ni/SiAl did not show discernable changes in particle morphology (Figure 7-15). Particles exist as clusters of different sizes in both fresh and post-reaction samples. It has been reported that mixed silica-alumina exhibits higher stability in hydrothermal media (Hahn *et al.,* 2013). This may account for less dramatic changes observed in the Ni/SiAl morphology compared those of silica- and alumina-supported Ni catalysts.
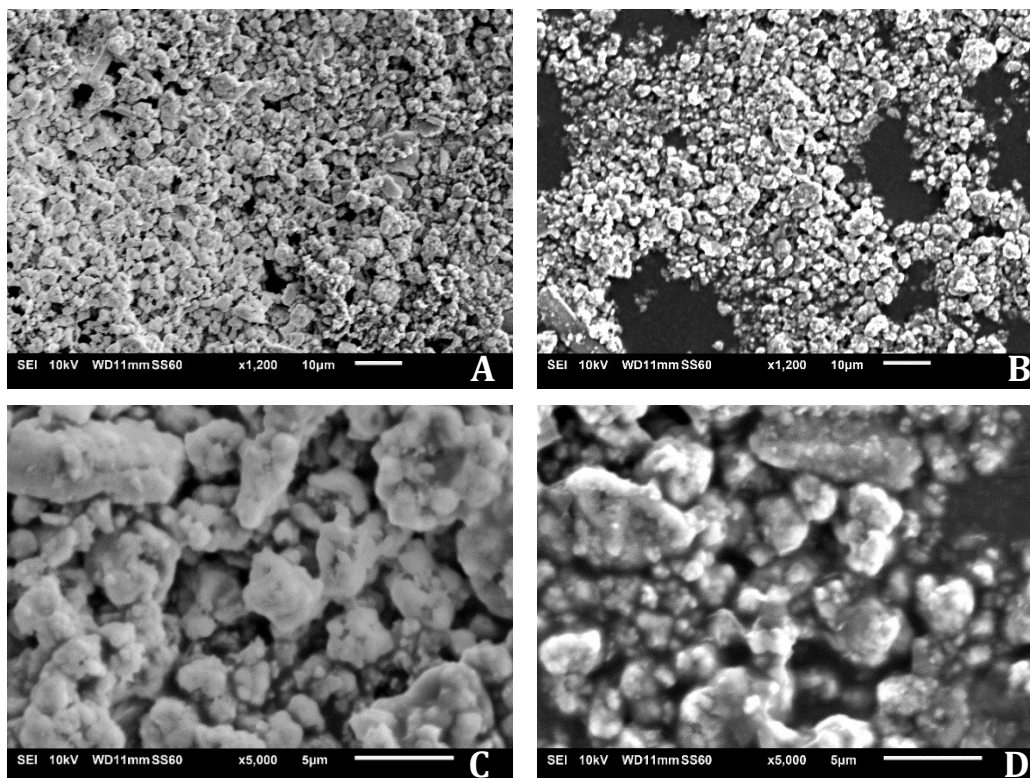
Figure 7-15 SEM of Ni/SiAl. A) Fresh Ni/SiAl x1200 magnification, B) Spent Ni/SiAl x1200 magnification C) Fresh Ni/SiAl x5000 magnification, D) Spent Ni/SiAl x5000 magnification

7.3.5.4 Ni/RH-SiO₂ Characterisation

As silica constitutes ~95 % of rice husk ash, FTIR of Ni/RH-SiO$_2$ synthesised from RHA shows numerous peaks corresponding to SiO$_2$ (Figure 7-16). As discussed in Section 7.3.4.1, peaks at 470, 800, 1080, 1655 and 3600-3055 cm^{-1} are modes of SiO$_2$. For the spent catalyst, several new bands indicate a change in surface functionality. New peaks around 1430, 880 and 690 cm^{-1} may correspond to C-H bending and C=C bending of various carbon-bearing compounds (Smith, 2018). Although specific species could not be assigned, this corresponds likely to char formation during the reaction.
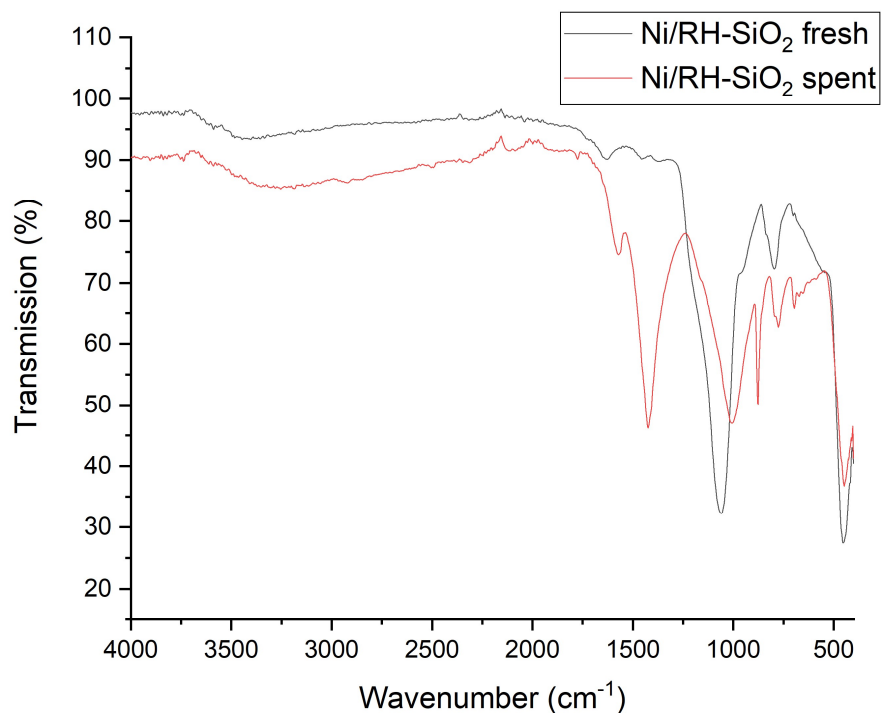
Figure 7-16 FTIR spectra of fresh (black, top) and spent (red, bottom) Ni/RH-SiO$_2$. Reaction conditions: 0.50 M NaHCO$_3$, 0.05 M glucose, 1 g Ni/RH-SiO$_2$, 250 °C, 2 h, 50 ml H$_2$O. Spectra acquired in transmission mode at a resolution of 8 cm^{-1} with 32 scans over the range 400-4000 cm^{-1}

XRD analysis of fresh Ni/RH-SiO$_2$ showed peaks only for amorphous silica and metallic Ni (Figure 7-17). The broad peak in the fresh catalyst around 21 ° corresponds to amorphous silica. Unlike the other Ni catalysts synthesized by the sol-gel method in this work, Ni/RH-SiO$_2$ was calcined in the absence of air under N$_2$ flow, which appeared to form a metallic Ni phase on the catalyst rather than the oxide. The main Ni diffraction peak at 44.4 ° appears in the spent catalyst, similarly to the Ni/SiAl catalyst. Furthermore, H$_2$ accounted for 11.5 % of the gas products in the reactions with Ni/RH-SiO$_2$, indicating that this catalyst also promotes the decomposition of formate to H$_2$ but that it does not in-turn reduce NiO. This further signifies the importance of controlling Ni oxidation state in the active catalyst, and investigating the impact of Ni particle size in formate formation and degradation reactions.

In the spent catalyst, phases could not be accurately assigned due to the presence of numerous diffraction peaks. It is clear there is a morphological transformation change that occurs in this catalyst. Matches above 16 % to PDF cards could not be achieved even with the use of PDF4+ database, although analysis indicates the formation of

complex mineral structures involving impurities in the support, including Ca and Na (Appendices E.4–E.6). Therefore, although these species are present in low concentrations in the rice husk ash, hydrothermal conditions may enhance their conversion to crystalline mineral structures.
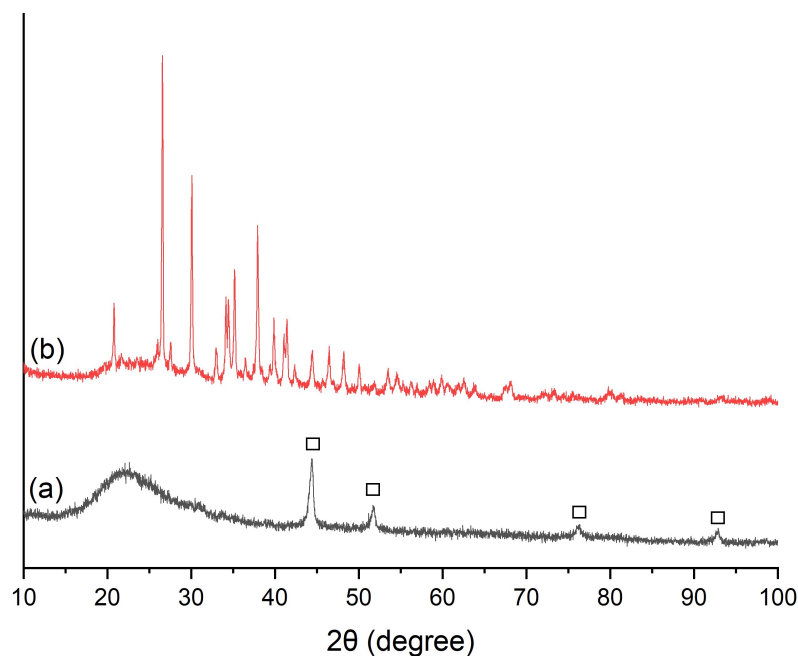
Figure 7-17 XRD of (a) fresh and (b) spent Ni/RH-SiO$_2$. □ – Ni. Reaction conditions: 0.50 M NaHCO$_3$, 0.05 M glucose, 1 g Ni/RH-SiO$_2$, 250 °C, 2 h, 50 ml H$_2$O

Prior to reaction, SEM images of Ni/RH-SiO$_2$ contain elongated features that are likely residual from rice husks (Figure 7-18, A). Post-reaction, these features disappear, and particles appear smoother (Figure 7-18, F). The spent catalyst morphology closely resembles spent Ni/SiO$_2$ (Figure 7-9).
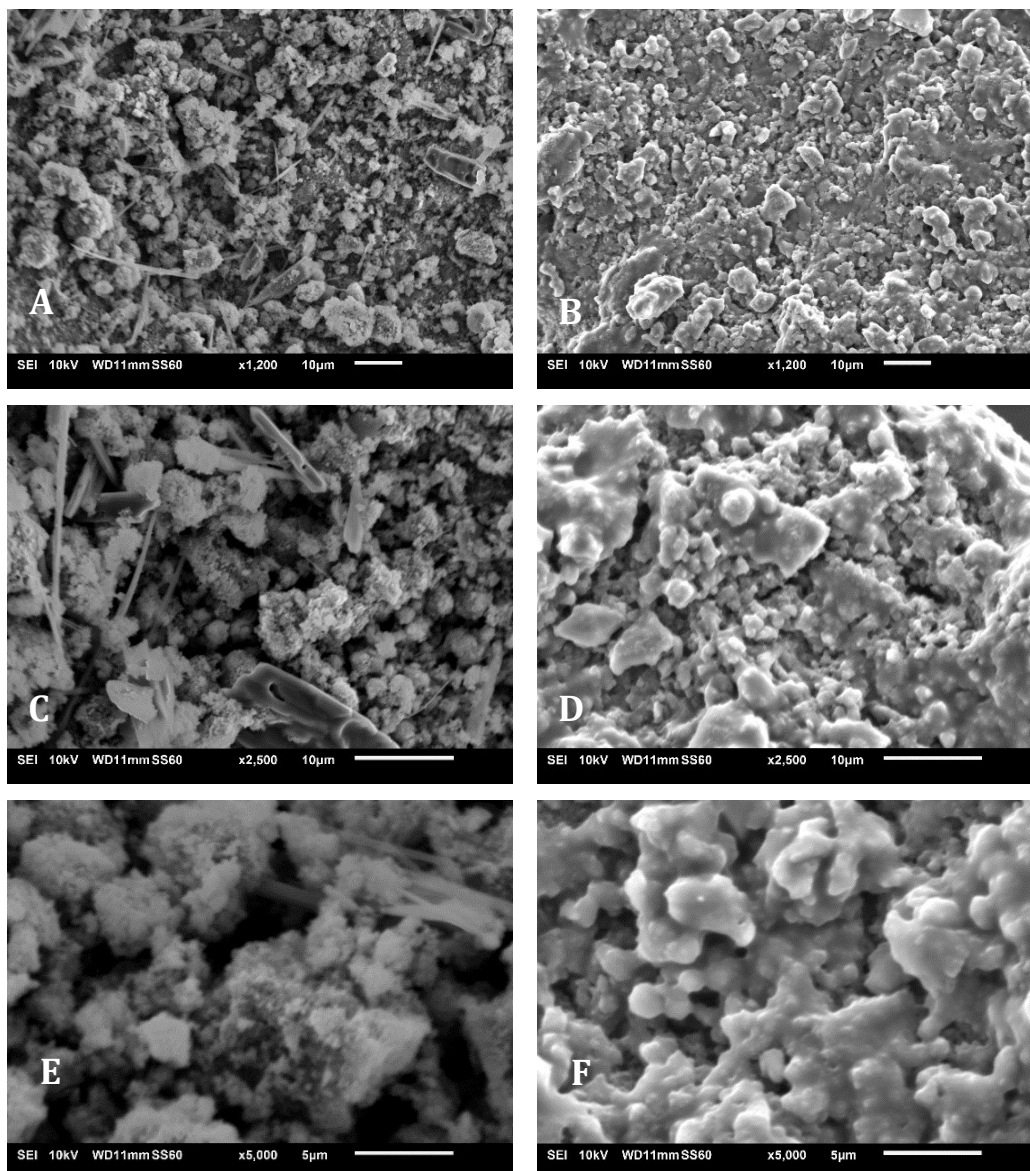
Figure 7-18 SEM of Ni/RH-SiO₂ A) Fresh Ni/RH-SiO₂ x1200 magnification, B) Spent Ni/RH-SiO₂ x1200 magnification, C) Fresh Ni/RH-SiO₂ x2500 magnification, D) Spent Ni/RH-SiO₂ x2500 magnification, E) Fresh Ni/RH-SiO₂ x5000 magnification, F) Spent Ni/RH-SiO₂ x5000 magnification

7.3.5.5 Ni/ZrO₂ Characterisation

FTIR spectra of 60 wt % Ni/ZrO$_2$ contained numerous bands that can be attributed to ZrO$_2$ (Figure 7-19). The absorption bands at 495 cm^{-1} and 575 cm^{-1} is assigned to Zr-O-Zr and Zr-O of tetragonal zirconia, while the peak at 745 cm^{-1} corresponds to Zr-O vibration of monoclinic ZrO$_2$ (Majedi, Davar and Abbasi, 2014). No significant changes in the spectra of Ni/ZrO$_2$ were observed after hydrothermal reaction.
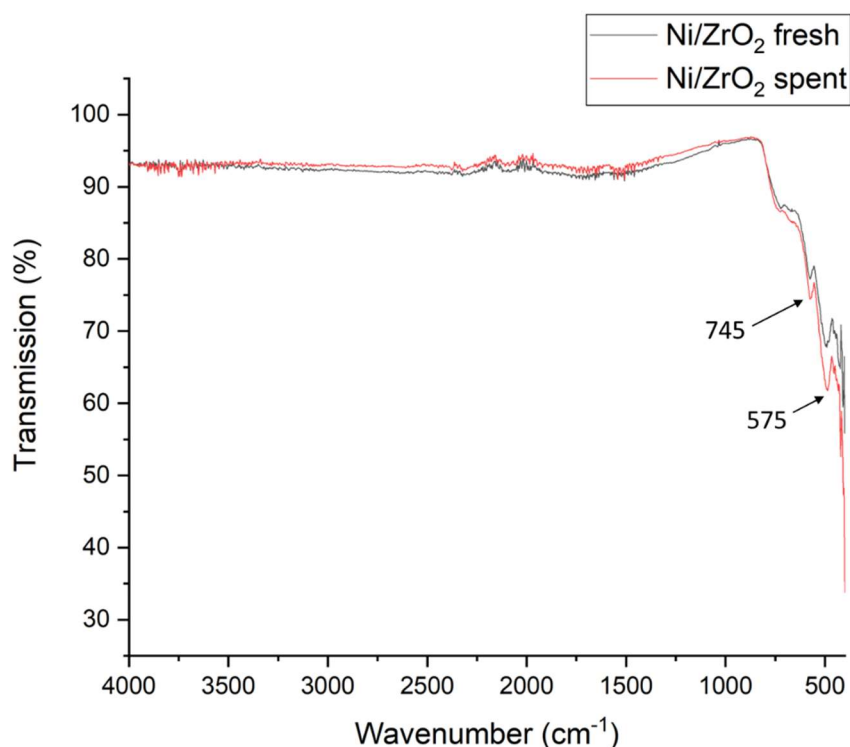
Figure 7-19 FTIR spectra of fresh (black, bottom) and spent (red, top) 60 wt% Ni/ZrO$_2$. Reaction conditions: 0.50 M NaHCO$_3$, 0.05 M glucose, 1 g Ni/ZrO$_2$, 250 °C, 2 h, 50 ml H$_2$O. Spectra acquired in transmission mode at a resolution of 8 cm^{-1} with 32 scans over the range 400-4000 cm^{-1}

Both the lower and higher loaded Ni/ZrO$_2$ catalysts exhibited characteristic ZrO$_2$ peaks at 2 θ = 28.2 °, 30.2 °, 31.4 °, 34.1 °, 50.2 ° (Figure 7-20) (S. Elshazly and A. A. Abdelal, 2013). In the lower loading, NiO peaks were not apparent, likely due to high dispersion and small crystallite size (Appendix F). In the higher loaded catalyst, NiO peaks are visible on the surface signifying increased particle size. Similarly to silica-supported Ni, zirconia-supported catalysts did not undergo any detectable changes in diffraction peaks after reaction.
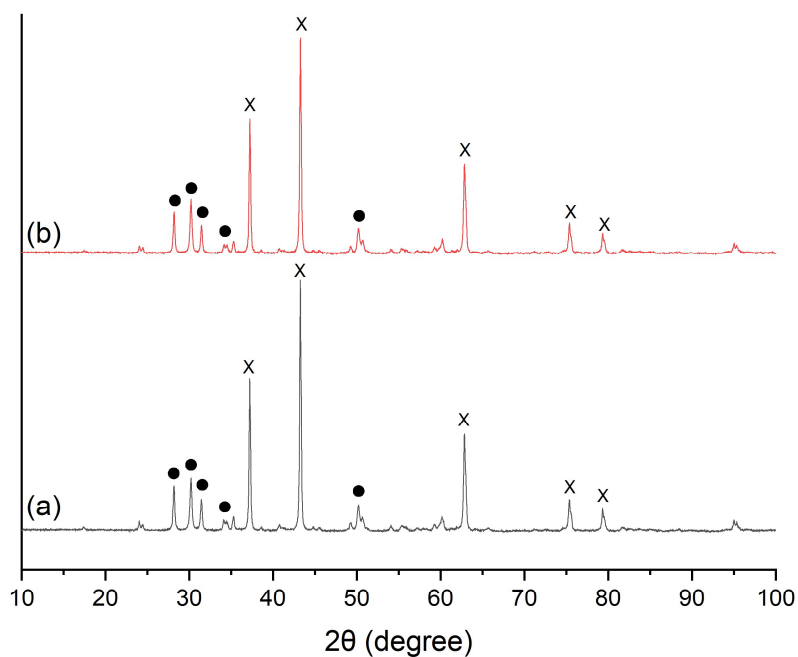
Figure 7-20 XRD of (a) fresh and (b) spent 60 wt% Ni/ZrO$_2$, x – NiO, ●– ZrO$_2$. Reaction conditions: 0.50 M NaHCO$_3$, 0.05 M glucose, 1 g Ni/ZrO$_2$, 250 °C, 2 h, 50 ml H$_2$O

SEM imaging of Ni/ZrO$_2$ showed that particles generally exhibit a smoother surface topography post-reaction, although this may be caused by submergence in water removing small particles from the surface (Figure 7-21). At the highest magnification, the surface of fresh and spent catalyst appears similar.
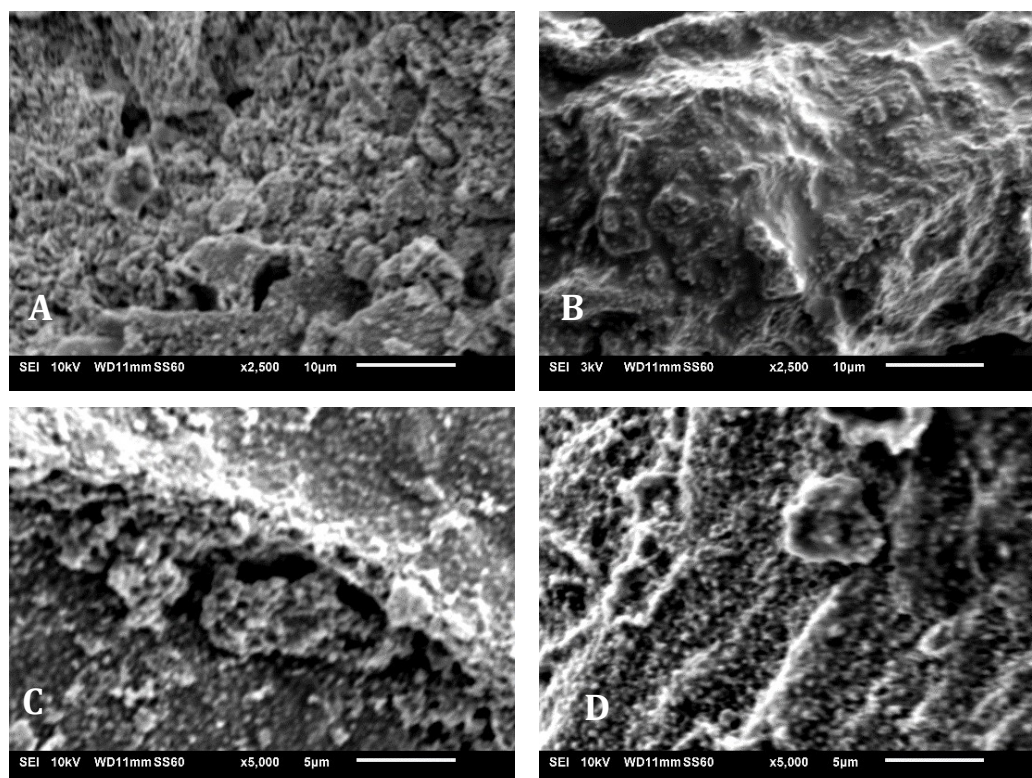
Figure 7-21 SEM of 60 wt% Ni/ZrO$_2$. A) Fresh Ni/ZrO$_2$ x2500 magnification, B) Spent Ni/ZrO$_2$ x2500 magnification, C) Fresh Ni/ZrO$_2$ x5000 magnification, D) Spent Ni/ZrO$_2$ x5000 magnification

The results of Ni/ZrO$_2$ characterization indicates that the catalyst remains stable post-reaction, with no changes detected by utilized analytical methods. Unlike silica, no discernible changes in surface topography were discovered in zirconia-supported catalysts. Therefore, Ni/ZrO$_2$ is a promising starting point for further investigations under hydrothermal conditions.

7.3.5.6 Ni/AC Characterisation

Unfortunately, due to sample loss, fresh Ni/AC could not be characterised. However, XRD analysis of spent Ni/AC was carried out to confirm the presence and oxidation state of Ni post-reaction. Figure 7-22 demonstrates the diffraction pattern of spent Ni/AC, where the broad peak between 20-30 ° corresponds to amorphous carbon, and NiO phases are designated (Lazzarini *et al.*, 2016).
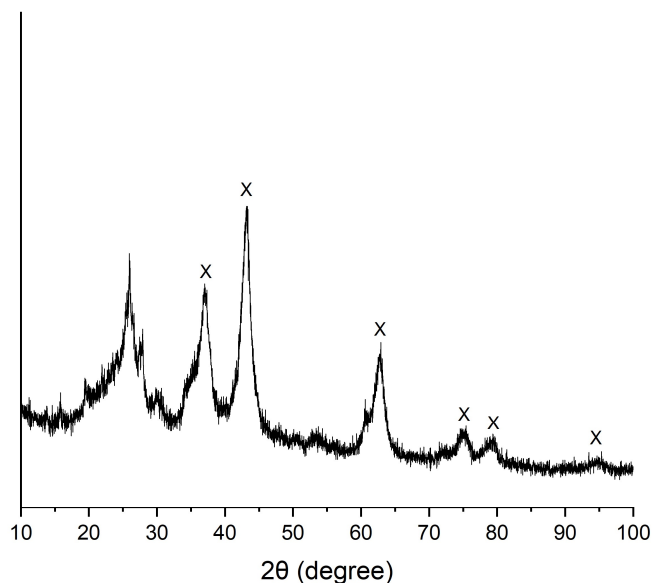
Figure 7-22 XRD of spent Ni/AC, x – NiO. Reaction conditions: 0.50 M NaHCO₃, 0.05 M glucose, 1 g Ni/AC, 250 °C, 2 h, 50 ml H₂O

Preliminary XRD analysis found solely amorphous carbon and NiO particles are present on the catalyst. Further investigation comparing fresh and spent Ni/AC is valuable in assessing the stability of this catalyst. Although reduced activity of supported Ni catalysts is likely ascribed to the active phase more so than the support, choosing a hydrothermally stable support is key. Similarly to Ni/SiO$_2$ and Ni/ZrO$_2$, further investigation on synthesis of metallic Ni particles with controlled size would be useful in assessing AC as a support material.

7.4 CONCLUSION AND FUTURE WORK

Synthesis, testing and characterisation of supported nickel catalysts was carried out to increase the yield of formate arising from bicarbonate reduction. Neither supported Ni catalysts nor bare supports enhanced the yield of formate in solution, which led to further investigation into the causes. The loading of nickel on the catalyst was initially explored, but a higher 60 wt % Ni/ZrO$_2$ did not result in significant changes to the products compared to 20 wt% Ni/ZrO$_2$. Testing of bare silica and alumina in place of loaded catalysts showed that these materials do not significantly influence the products formed in the reaction. Furthermore, Al$_2$O$_3$ was found to be unstable under hydrothermal conditions, forming AlO(OH), while SiO$_2$ remained amorphous and ZrO$_2$ did not undergo significant changes to structure. Analysis of gas-phase hydrogen showed that commercial Ni/SiAl and Ni/RH-SiO$_2$ catalysts strongly

enhanced its concentration in the gas phase. Characterisation of catalysts showed that these two catalysts contained metallic Ni phases, while other Ni catalysts contained NiO as the active phase. Based on evidence reported in literature, it was proposed that NiO cannot be *in-situ* reduced to metallic Ni under investigated conditions.

Experiments with Raney-Ni in place of bulk Ni showed the impact surface area and H_2 generation ability on reaction products. Due to safety concerns over handling Raney-Ni it was not characterised in this work. With Raney-Ni, only acetate was formed in the aqueous phase, and gas products consisted of 60.5 % H_2 and 4 % CH_4. In addition to presence of H_2 in the catalyst pores, additional H_2 is proposed to be generated by Al reaction with water and gasification of glucose. It is proposed that high concentrations of H_2 facilitate bicarbonate reduction to formate, which is then decomposed to CO_2 and H_2 over high surface area Raney-Ni. To assess the importance of H_2 concentration, additional H_2 gas can be added in reactions with bulk Ni powder. Alternatively, Al metal can be added to generate H_2 by reaction with water.

This chapter concludes work carried out on hydrothermal reduction of bicarbonate with Ni catalysts. Although there are numerous avenues of interest to continue exploring in this area, the following section focuses on the use of alternative CO_2 precursors and the use of commercial catalysts for these reactions. Suggestions for future work on supported Ni catalysts is discussed in Section 9.2.2.

8 CHAPTER 8: ALTERNATIVE SOURCES OF CARBON DIOXIDE

8.1 INTRODUCTION

As established in the literature review (Sections 2.6 – 2.8), numerous studies using bicarbonate as a CO_2 precursor have been conducted. Up to this point, $NaHCO_3$ had been utilised as a CO_2 precursor in this work. Although the use of $NaHCO_3$ is beneficial for comparison to literature, exploration of other precursors is valuable for expanding the application of hydrothermal systems to different reagents. In this chapter, several CO_2 precursors were investigated and compared, including CO_2 gas, $NaHCO_3$, $KHCO_3$, $CaCO_3$ and Na_2CO_3.

Prior to use, CO_2 captured as a by-product of ammonia, steam reforming of other industrial processes must first be purified to reduce oxygen and water impurities. This can be achieved by different methods, *e.g.* catalytic oxidation of H_2 to remove O_2, then refrigeration to condense H_2O and produce a purified CO_2 stream (Abbas, Mezher and Abu-Zahra, 2013). Carbon dioxide can also be dissolved in alkaline media where CO_2 solubilises as carbonate or bicarbonate, which can be precipitated out of solution (Chesny, 1932). Solid reagents are generally more favourable as reagents as they are easier to transport and do not require pressurized cannisters, however CO_2 gas may be captured directly from energy producers. The capture of CO_2 by alkali metal hydroxide solution to form carbonate and bicarbonate (Equations 8-1, 8-2), and by calcium hydroxide (Equation 8-3) to form $CaCO_3$ is described in Section 2.2.1.

Equation 8-1 Formation of sodium carbonate by reaction of carbon dioxide with sodium hydroxide

$$CO_2 + 2NaOH \rightarrow Na_2CO_3 + H_2O$$
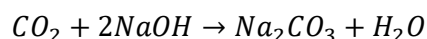
Equation 8-2 Formation of sodium bicarbonate from reaction of sodium carbonate with excess CO_2

$$Na_2CO_3 + CO_2 + H_2O \rightarrow 2NaHCO_3$$
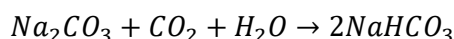
Chapter 8: Alternative Sources of Carbon dioxide

Equation 8-3 Formation of calcium carbonate from reaction of calcium hydroxide with CO_2

$$Ca(OH)_2 + CO_2 \rightarrow CaCO_3 + H_2O$$
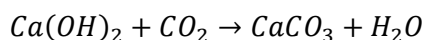
Furthermore, previous reports indicate that the nature of the counterion, K^+ or Na^+, may affect the yield of HCOOH from HCO_3^- reduction. For example, a 0.3 % reduction in yield was reported when $NaHCO_3$ was replaced with $KHCO_3$ (Lu *et al.*, 2020). Therefore, comparison of sodium and potassium bicarbonate may yield valuable insight and determine if the cation has an effect in the reduction of $NaHCO_3$ with glucose.

Furthermore, carbonates have been reported to be poorer CO_2 precursors in hydrothermal CO_2 reduction than bicarbonates. For example, when exchanging $NaHCO_3$ for Na_2CO_3 a drop in formate yield from 5.0 % to 4.2 %, was attributed to more facile conversion from bicarbonate due to stronger electrophilicity of this species (Lu *et al.*, 2020). Numerous reports have indicated that HCO_3^- acts as a reactive intermediate in CO_2 and CO_3^{2-} reduction to $HCOO^-$ (Su, Lu and Lin, 2015; Liu *et al.*, 2017). The addition of CO_2 gas to carbonate-rich media may therefore present an opportunity to utilise two CO_2 sources to create a favourable pH for bicarbonate formation *in situ*. Thus, Na_2CO_3 was investigated with and without additional CO_2 gas.

Finally, $CaCO_3$ was explored as a precursor for CO_2. Calcium carbonate is widely used in a range of industries, including construction, paints, and agriculture (Naydowski, 2001). Unlike sodium carbonate, calcium carbonate is poorly soluble in water (<50 mg l^{-1}) and will not readily liberate neither CO_3^{2-} nor CO_2 at the operating conditions used in this work. However, in the presence of water saturated with carbon dioxide, $CaCO_3$ may form soluble calcium bicarbonate, $Ca(HCO_3)_2$ (Equation 8-4). Calcium bicarbonate exists only in aqueous media where Ca^{2+}, HCO_3^-, CO_3^{2-}, and dissolved CO_2 co-exist.

Equation 8-4 Solubilisation of calcium carbonate to calcium bicarbonate in CO_2-saturated water

$$CaCO_{3(s)} + CO_{2(g)} + H_2O_l \rightarrow Ca(HCO_3)_{2(aq)}$$
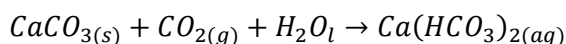
Different CO_2 capture sources are examined in this chapter and compared with $NaHCO_3$. The stability of formate salts was examined. The reaction of CO_2 gas with glucose in NaOH was further examined in terms of products and mechanism. The

impact of increasing NaOH concentration on the organic acids profile was examined. Thereafter, commercial catalysts were investigated in the CO_2/NaOH system to enhance the yield of formic acid from CO_2. Commercial nickel on silica-alumina (Ni/SiAl) and copper-based methanol synthesis catalyst ($CuO/ZnO/Al_2O_3$), denoted henceforth as CZA, was added to enhance conversion. Based on the results of support stability studies undertaken in Chapter 7, a $CuO/ZnO/ZrO_2$ (CZZ) catalyst was also synthesized to improve the stability of the support.

8.2 METHODOLOGY

8.2.1 Materials

In addition to deionised water obtained from a Suez L300130 (>1 MΩ cm), numerous reagents were used in this work. A summary of reagents is available in Table 8-1.

Table 8-1 Materials used in carbon dioxide precursor studies and copper catalyst synthesis

Entry	Chemical name	Formula	Grade	Supplier
1	Sodium bicarbonate	$NaHCO_3$	99+%	Sigma-Aldrich
2	Potassium bicarbonate	$KHCO_3$	99.7%	Sigma-Aldrich
3	Sodium carbonate	Na_2CO_3	≥99.0%	Sigma-Aldrich
4	Calcium carbonate	$CaCO_3$	≥99.0%	Sigma-Aldrich
5	Formic acid	HCOOH	98-100%	Sigma-Aldrich
6	Sodium formate	NaCOOH	≥99.0%	Sigma-Aldrich
7	Potassium formate	KCOOH	99%	Sigma-Aldrich
8	Calcium formate	$Ca(COOH)_2$	98%	Alfa Aesar

9	Sodium hydroxide	NaOH	98%	Alfa Aesar
10	Carbon dioxide	CO_2	99.8%	BOC
11	Nickel on silica-alumina	$Ni/SiO_2/Al_2O_3$	65 wt % Ni/NiO	Alfa Aesar
12	Copper-based methanol synthesis catalyst	$CuO/ZnO/ZrO_2$	65% CuO 25% ZnO 10% ZrO_2 1.5% MgO	Alfa Aesar
13	Copper nitrate trihydrate	$Cu(NO_3)_2 \cdot 3\,H_2O$	≥99%	Sigma Aldrich
14	Zinc nitrate hexahydrate	$Zn(NO_3)_2 \cdot 6H_2O$	98%	Sigma Aldrich
15	Zirconium oxynitrate hydrate	$ZrO(NO_3)_2 \cdot xH_2O$	99%	Sigma Aldrich

8.2.2 Reaction Procedures

The general experimental procedure is detailed in Section 4.1.2. All experiments were carried out minimum in duplicate to reduce error. Error bars on graphs represent the standard deviation of products over multiple experiments. All experiments with CO_2 precursors and catalysts were carried out at 250 °C for 2 hours with a water filling volume of 50 ml. In reaction with solid CO_2 precursors $NaHCO_3$, $KHCO_3$, Na_2CO_3 and $CaCO_3$, 25 mmol of each reagent was used alongside 2.5 mmol glucose. In designated reactions, the reactor vessel was also pressurised with 30 barg CO_2 gas. The stability of formic acid and formate salts was undertaken to investigate the impact of the counterion. Stability studies were carried out with 15 mmol HCOOH or 3 mmol given formate salt in 50 ml deionised water. Ambient air in the vessel was purged by He prior to reacting constituents at 300 °C for 3 hours. The percentage of formic acid or formate salt decomposition was calculated by Equation 8-5, where C_i denotes initial concentration of reagent in grams per litre, and C_f denotes its final concentration.

Equation 8-5 Decomposition of formate salts or free formic acid

$$\left(1 - \frac{C_i}{C_f}\right) \times 100 = \%\,Decomposition$$

The system containing CO_2 gas and glucose in NaOH solution was investigated further. The impact of increasing NaOH concentration from pH 9.5 to 1.5 M was explored. Control reactions were carried out at 250 °C for 2 hours to deconvolute different products. Solely glucose was reacted in 1 M NaOH to assess the products of alkaline liquefaction of this species. 30 barg of CO_2 in 1 M NaOH was also reacted in the absence of an H_2 source to assess if any conversion occurs in the absence of a reductant. To determine if lactic acid was reducing CO_2, a reaction was spiked with 21 μl (5 g l^{-1}) lactic acid and products analysed.

Following control reactions, this system was also investigated in the presence of heterogeneous catalysts – commercial nickel on silica-alumina (Ni/SiAl), copper-based methanol synthesis catalyst (CZA), and lab-synthesised $CuO/ZnO/ZrO_2$ (CZZ). The protocol for CZZ synthesis is described in Section 8.2.3. In catalytic reactions of CO_2 with glucose in NaOH solution, a nominal 1.5 g of catalyst was added to the vessel. After reactions, the solution pH was measured using a pH meter (ETI 8100 Plus, SLS), and solids filtered by vacuum filtration and dried for 18 hours in a Memmert convection oven (Schwabach, Germany) at 105 °C to remove moisture. Characterisation was carried out by methods described in Section 8.2.4.

Contrary to previous experimental sections, the gas phase of reactions with CO_2 gas was not analysed in this chapter. Due to the high starting concentrations of CO_2 gas, the gas phase consisted primarily of CO_2 with other species present in concentrations below 1%. Furthermore, it is well-reported that altering the basic catalyst impacts the products of glucose liquefaction (Ogi, Yokoyama and Koguchi, 1985). Variations in solution pH with different precursors impact the degradation of glucose to cyclic ketones. As such, the bio-oil component, attributed primarily to glucose conversion in Section 4.3, was not analysed in this section. As this work focuses on CO_2 reduction, rather than glucose liquefaction, C_1 molecules were instead the focus.

8.2.3 $CuO/ZnO/ZrO_2$ Synthesis Protocol

The protocol for synthesizing $CuO/ZnO/ZrO_2$ (CZZ) was adapted from Suh and co-workers (Suh, Moon and Rhee, 2000). A volume of 50 ml of mixed solution containing copper, zinc, and zirconium nitrates was prepared with a Cu:Zn:Zr ratio of 13:5:2. The ratio was calculated based on the quantity of these metal oxides in the commercial CZA catalyst. The precursor solution was then added dropwise to 100 ml of 1.1 M $NaHCO_3$ solution at 70 °C over a period of 20 minutes under vigorous stirring,

followed by aging for 90 minutes at the same temperature. The precipitates were filtered and washed 10 times with distilled water to remove residual sodium. The washed precipitates were dried at 120 °C in a convection oven (Memmert, Schwabach, Germany) and calcined in static air in a Carbolite CSF1100 muffle furnace at 350 °C for 9 hours.

8.2.4 Catalyst Characterisation

The morphological characteristics of the catalysts were investigated by SEM using a Jeol JSM-6010 LA Analytical Scanning Electron Microscopy. The accelerating voltage (V) employed ranged from 15 kV to 20 kV with a working distance of 11-13 mm. Surface elemental composition and mapping was carried out by attached energy dispersive spectroscopy (EDS). Samples were placed on conductive carbon tape adhered to an aluminium sample stub and pre-coated with gold for 10 s in an sputter coater (Agar Scientific, UK) to improve conductivity. A current of 40 mA and pressure of 0.04 mbar was used. XRD was carried out by the same procedure as described in Section 6.2. Analysis of data was carried out by a combination of existing literature and the PDF-4+ 2021 database (ICDD, USA).

Copper catalyst surface area was measured by post-doctoral researcher Dr Carlos Bambrilla of the Department of Chemical & Biological Engineering at the University of Sheffield on a Micromeritics Tristar II Plus surface area analyzer. Catalysts were preliminarily dried in an oven at 120 °C 18 hours. Thereafter, catalysts were placed in sampling tubes and degassed under vacuum between 16 and 72 hours. Nitrogen adsorption was thereafter carried out and monitored by MicroActive software. Finally, ICP-OES analysis of catalysts was used to determine the Cu and Zn concentration in CZA and CZZ catalyst post-reaction. Sample acid digestion and analysis was carried out by colleague Shania Laming of the Department of Chemistry at the University of Sheffield.

8.3 RESULTS AND DISCUSSION

Hydrothermal reduction of CO_2 generally involves its conversion to C_1 molecules such as formic acid, methanol, methane or formaldehyde. As discussed in Section 8.2.2, gas phase products were not analysed in the present work due to the gas phase being composed mainly of CO_2 where it was used as a reagent. Therefore, CH_4 and CH_2O

could not be monitored. Thus, aqueous products were the main focus of the present work.

Formate was established as a key product in $NaHCO_3$ reduction in Chapters 4-7. Analysis of aqueous products showed that, under the investigated conditions, no methanol was detected in with any CO_2 precursors. Methanol formation has been reported to be facilitated in acidic conditions (Huo *et al.*, 2012). Huo and co-workers previously investigated CO_2 hydrothermal reduction to methanol using Cu catalysts and found that 2 M HCl was required to obtain yields over 1 %. As bicarbonates and carbonates create an alkaline environment CH_3OH formation may be inhibited and requires further investigation in acidic conditions. Therefore, comparison of different CO_2 precursors was carried out by contrasting the concentration of formate and observing trends in other organic acids.

8.3.1 Potassium and Sodium Bicarbonate

When comparing the aqueous products of $NaHCO_3$ and $KHCO_3$ reduction, several key differences in products were noted (Figure 8-1). Due to strong overlap between lactate and pyruvaldehyde in these samples, lactate quantification could not be carried out and glycolate concentrations carry high error margins. The main difference between reactions with these two species was the decrease in formate and acetate concentration. When exchanging $NaHCO_3$ for $KHCO_3$, $HCOO^-$ decreased from 0.502 to 0.400 g l^{-1}. A decrease from 0.817 to 0.668 g l^{-1} was also observed in acetate. No pyruvic or oxalic acids were detected in reactions with bicarbonates. This indicates that the bicarbonate counter-ion may strongly impact the reaction.
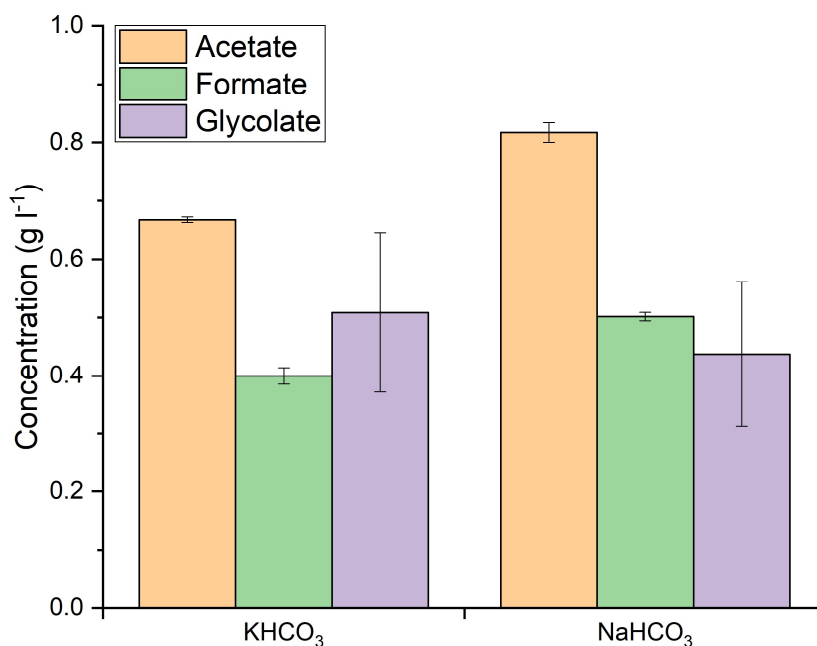
Figure 8-1 Concentration of organic acids in reactions of KHCO$_3$ and NaHCO$_3$ CO$_2$-precursors. Reaction conditions: 0.5 M bicarbonate, 0.05 M glucose, 250 °C, 2 h, 50 ml H$_2$O

Although this effect has been observed in literature, it is difficult to ascertain the cause. It is possible that the potassium blocks some active sites on the reactor surface which facilitate the reaction. Mortensen and co-workers investigated the effects of sulfur, potassium and chlorine on the activity of Ni catalysts, and found that K$^+$ deactivates Ni/ZrO$_2$ by blocking deoxygenation sites (Mortensen *et al.*, 2014). To ascertain whether the change in formate yield may be attributed to interaction with the reactor surface, the reaction may be duplicated in an inert reactor, *e.g.* with a Teflon sleeve, which was not available in the present rig set-up.

Alternatively, different cations may have differing affinity to carboxylates. In this context, water molecules with restricted translational and orientational dynamics are referred to as 'slow water', while some show high diffusivity and are deemed 'fast water'. A study examining the hydration of carboxylate groups with alkali cations Li$^+$, Na$^+$, K$^+$, and Cs$^+$ found that Na$^+$ is a strongly hydrating cation which contains the highest number of slow water molecules which, in the presence of formate, slows down reorientation and may provides stability through the formation of solvent-separated NaCOOH ion pairs (Pastorczak, Van Der Post and Bakker, 2013). To determine whether cations influence the stability of the formate product, a series of

stability studies on formate salts was carried out. The results of this study are described in Section 8.3.2.

It must also be noted that interaction between two ions is stronger in supercritical water compared to ambient. It has been reported that increasing pressure results in lowered distance between molecules and ions in Na_2CO_3 in H_2O (Wu, Wang and Zheng, 2016). In a separate modelling study, the potential mean force interaction between Na^+ and Cl^- in supercritical water and ambient was calculated and compared to measured water dielectric constant. It was proposed that the decreasing H_2O dielectric constant observed in supercritical water reduced the solubility of inorganic salts (Cui and Harris, 1994). Therefore, the dissolution of $NaHCO_3$ and $KHCO_3$ in sub-critical water may be variable and complex, and requires further study outside of the scope of this work. However, this highlights the importance of further investigations into molecular interactions of hydrothermal systems.

8.3.2 Stability of Formate Salts

The decomposition of formate salts with different counter ions was investigated to determine if the stability of salts results in varying concentrations of the product (Table 8-2). Formate salts degraded to a lesser extent than free formic acid, potentially due to a stabilising effect of the cation. It was also observed that in the case of monovalent species, an increase in cation size ($K^+ > Na^+ > H^+$) was found to correlate with higher hydrothermal stability. Free formic acid showed the highest degree of degradation, with over 91% decomposed after 3 hours. Calcium formate had the second highest degree of degradation, with nearly 86 % of starting $Ca(COOH)_2$ degraded. Sodium and potassium formate were comparably stable, although KCOOH showed highest stability overall with 32.4 % remaining after 3 hours at 300 °C. Analysis of gas products from degradation of HCOOH, NaCOOH and KCOOH showed solely CO_2 and H_2 as products, while with $Ca(COOH)_2$ an unidentified peak may be attributed to formaldehyde.

Table 8-2 Average decomposition of formic acid and formate salts. Reaction conditions: 15 mmol HCOOH (where used), 3 mmol formate salt (where used), 300 °C, 3 h, 50 ml H₂O

Species	Average Decomposition %	% Error
HCOOH	91.7	1.5
NaCOOH	71.2	5.0
KCOOH	67.6	4.8
Ca(COOH)$_2$	85.9	4.2

Notably, calcium formate was found to be less stable than NaCOOH or KCOOH. This contrasts with thermal degradation of formate salts in air, where NaCOOH degrades around 330 °C and Ca(COOH)$_2$ at ~470 °C (Meisel *et al.*, 1975). This indicates that decomposition of formate salts in hydrothermal media is starkly different to thermal decomposition in air. Furthermore, the comparable stability between NaCOOH and KCOOH signifies that product stability is likely not the cause of difference in product concentration observed between KHCO$_3$ and NaHCO$_3$. Further studies on the dissolution of these species in hydrothermal media, as well experiments in non-metallic reactors, would be valuable in assessing the difference of activity between these species.

8.3.3 Carbonates

Calcium and sodium carbonate were subsequently investigated in the presence of CO$_2$. Due to unforeseen issues with the reactor vessel, reactions with potassium carbonate could not be carried out. Products of reaction of CaCO$_3$ and CO$_2$ with glucose included lactic, glycolic, and acetic acid, as well as numerous unidentified species. However, no formic acid or methanol was detected in the presence CaCO$_3$ and CO$_2$, indicating that calcium bicarbonate either does not form, or does not undergo reduction under the investigated conditions. However, the presence of numerous high retention time species indicates that CaCO$_3$ may act as a base that promotes glucose conversion to further species. Thus, under the investigated conditions with CO$_2$ gas calcium carbonate is not a suitable precursor for reduction to C$_1$ molecules.

In contrast, reactions with Na$_2$CO$_3$ both with and without CO$_2$ contained HCOOH (Figure 8-2). In the absence of CO$_2$ gas, formate yield remained lower than with

$NaHCO_3$ at 0.408 g l^{-1}, while oxalate and pyruvate were present in trace concentrations. With the addition of 30 barg CO_2 gas, formate and pyruvate increased to 0.509 and 0.201 g l^{-1}, respectively. Acetate and glycolate also increased, while lactate concentration marginally decreased. Changes in the concentrations of products may be caused by CO_2 interaction with intermediates, or by a change in reaction pH with its addition. In the absence of CO_2 gas, the post-reaction pH of reactions of glucose in 0.50 M Na_2CO_3 was strongly alkaline at 10.9, whereas with the addition of CO_2 gas pH of 7.1 was recorded. The presence of CO_2 gas may be facilitating the formation of the more desirable HCO_3^- species from carbonate by decreasing the medium pH, thereby increasing reduction to $HCOO^-$. The impact of CO_2 gas of reaction mechanisms in alkaline media is further discussed in Section 8.3.4.
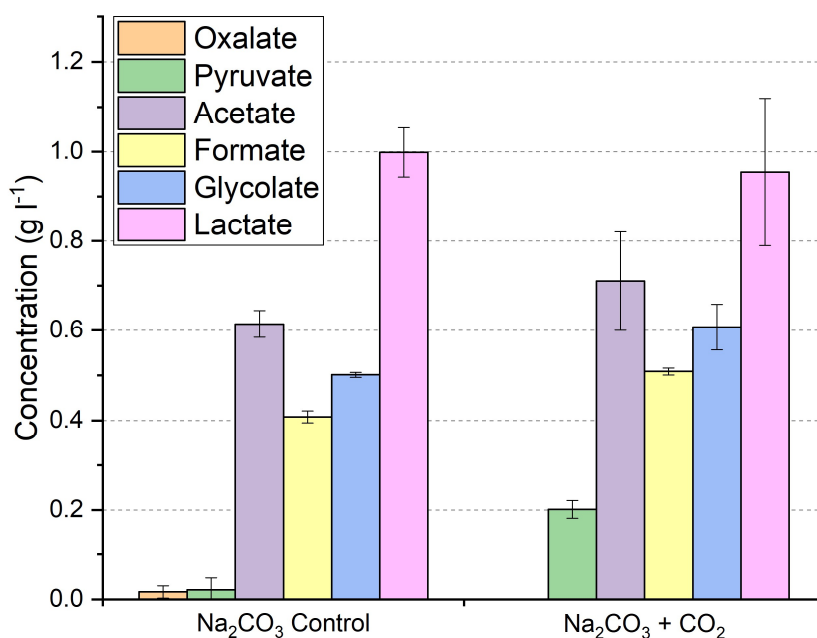
Figure 8-2 Concentration of organic acids in control reaction of glucose in Na₂CO₃ (no CO₂) and glucose in Na₂CO₃ + CO₂. Reaction conditions: 0.5 M Na₂CO₃, 0.05 M glucose, 30 barg CO₂ (where used) 250 °C, 2 h, 50 ml H₂O

The results of studies on the reduction of Na_2CO_3 and CO_2 demonstrated that concentrations of formate, 0.509 g l^{-1} are comparable to those achieved with $NaHCO_3$, 0.502 g l^{-1}. Furthermore, increased formate was detected with the addition of CO_2 gas. Carbon dioxide lowers reaction pH, potentially facilitating the formation of the more desirable HCO_3^- species from carbonate. This study demonstrates the feasibility of using a CO_2 capture product in combination with CO_2 gas to create a more favourable

dissolved species, HCO_3^-, to undergo reduction. To study solely the activity of CO_2 in alkaline media, investigation into CO_2 reduction with in NaOH was undertaken.

8.3.4   Carbon dioxide

Carbon dioxide gas was investigated in the absence of bicarbonates or carbonates. As discussed in literature review Sections 2.4-2.6, alkaline conditions strongly enhance CO_2 hydrothermal reduction. Therefore, preliminary studies on the impact of starting NaOH concentration were carried out to determine the concentration at which formic acid concentration was maximised. The post-reaction pH of the aqueous phase at room temperature was measured to monitor the dissolution of CO_2 into solution.

The profile of organic acids formed in reactions of CO_2 gas and glucose in pH adjusted H_2O is shown in Figure 8-3. At pH 9.5, the concentration of all acids remains relatively low, with HCOOH at 0.031 g l^{-1}. In this reaction the final solution pH was 3.2, where carbonic acid and dissolved CO_2 are the dominant species. This indicates that in the absence of alkaline conditions, neither CO_2 nor glucose undergo significant conversion to formate. With increasing NaOH concentration to 0.5 M, post-reaction pH increased to 7.1, and further to 7.3 at 1 M and 7.8 at 2 M NaOH. Therefore, 30 barg CO_2 effectively dissolved into aqueous solution at all NaOH concentrations and neutralised even the most concentrated 2 M NaOH solution which has a pH >14.

The concentration of all acids increased at 0.5 M and 1 M NaOH, after which acetate and glycolate decreased, lactate increased and pyruvate and formate plateaued. Thus, further investigation into this system was carried out at 1 M NaOH, where a maximum concentration of 0.537 g l^{-1} formate was achieved.
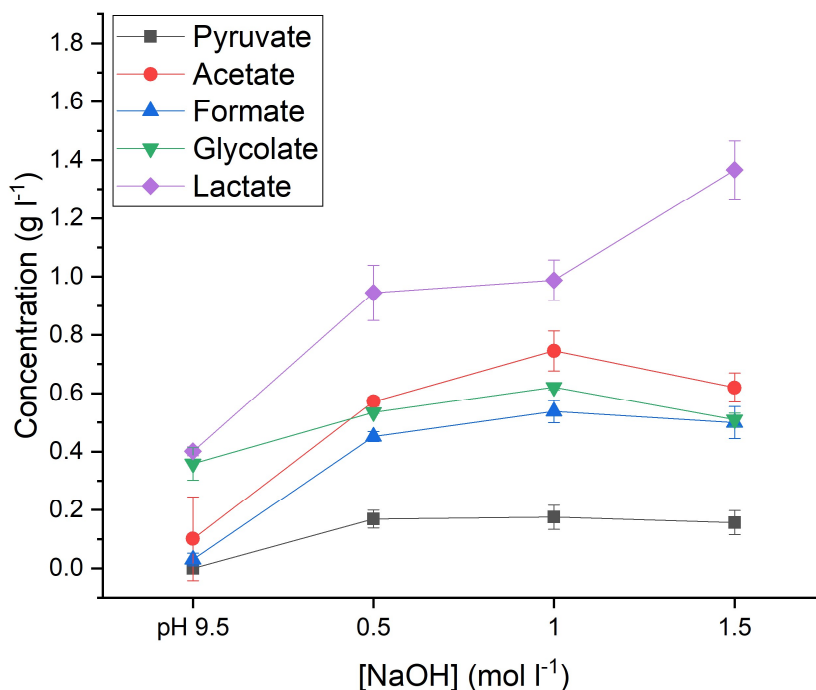
Figure 8-3 Concentration of organic acids as a function of NaOH molar concentration. Line designations: green ▼ – glycolate, red ● – acetate, purple ◊ – lactate, black ■ – pyruvate, blue ▲ – formate. Reaction conditions: 30 barg CO_2, 0.05 M glucose, 250 °C, 2 h, 50 ml NaOH solution volume

Notably, an inverse relationship between acetate and lactate was observed, similar to reactions with Na_2CO_3. Increasing NaOH concentration from 1.0 to 1.5 M resulted in increasing lactate concentration, while acetate and glycolate decreased. Similarly, lactate decreased while acetate and glycolate increased between Na_2CO_3 reactions without and with CO_2 gas. Therefore, increasing alkalinity is observed to facilitate lactate formation while inhibiting acetate and glycolate. This points to a common intermediate, likely pyruvaldehyde, connecting these species, and altering solution pH promoting specific routes of conversion.

Subsequently, control reactions of individually CO_2 and glucose in 1 M NaOH were carried out. With solely CO_2 in NaOH, no products were detected in the aqueous phase. In the absence of CO_2, glucose liquefaction in 1 M NaOH resulted in lactic acid dominating aqueous products at 4.929 g l^{-1}, and no H_2 in the gas phase (Figure 8-4). This is consistent with numerous studies which found that alkaline degradation of cellulose and glucose yields lactic acid as the main decomposition product (Gao *et al.*, 2013). When 30 barg CO_2 was added, lactate decreases to 0.998 g l^{-1}, while acetate,

and glycolate increased from 0.035 and 0.228 g l^{-1} to 0.746 and 0.621 g l^{-1}, respectively. A concentration of 0.175 g l^{-1} pyruvate was also formed.
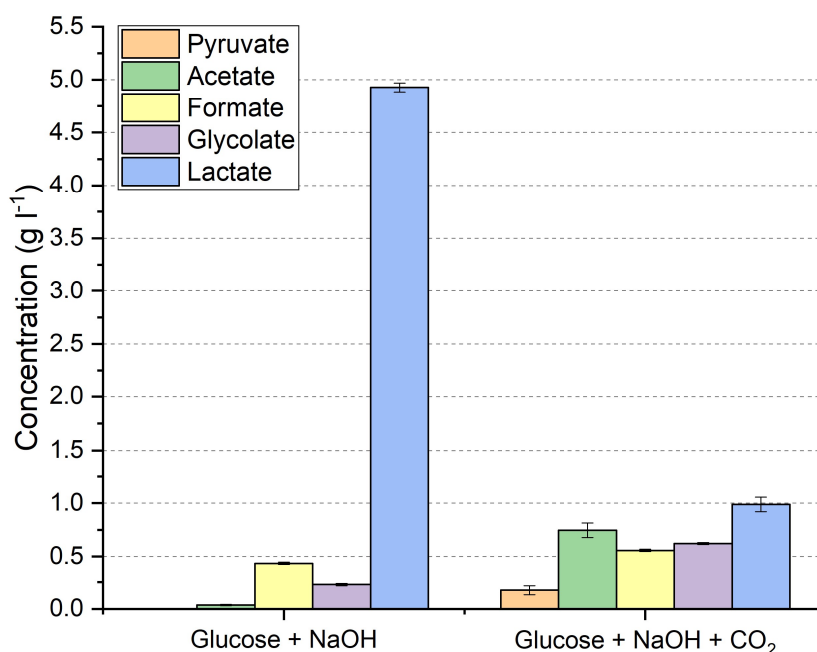
Figure 8-4 Products of hydrothermal reaction of glucose in NaOH solution in the absence and presence of CO$_2$ gas. Reaction conditions: 0.05 M glucose, 30 barg CO$_2$ (where used), 250 °C, 2 h, 50 ml 1 M NaOH solution

Particularly of interest was the impact of CO_2 on formic acid concentration. In the absence of CO_2, glucose in 1 M NaOH yields 0.436 g l^{-1} NaCOOH. With the addition of CO_2, NaCOOH increases to 0.557 g l^{-1}. This increase is proposedly caused by reduction of added CO_2, thereby demonstrating the direction conversion of CO_2 to value-added product. It is proposed that CO_2 reduction occurs *via* the formation of HCO_3^- around pH 7-8, followed by reduction by glucose and intermediate hydroxyl groups (Shen, Zhang and Jin, 2011; Chaix, Guillaume and Guillard, 2014). However, it has also been proposed that CO_2 may be reduced by lactic acid to produce pyruvic and formic acids (Figure 8-5). To validate this, a reaction containing glucose and CO_2 in 1 M NaOH was spiked with lactic acid. While no significant impact on other organic acids was observed, pyruvate and formate increased from 0.175 and 0.557 g l^{-1} to 0.254 and 0.598 g l^{-1}, respectively. Thus, although marginal, CO_2 reduction is proposed to also occur by intermediate lactic acid.
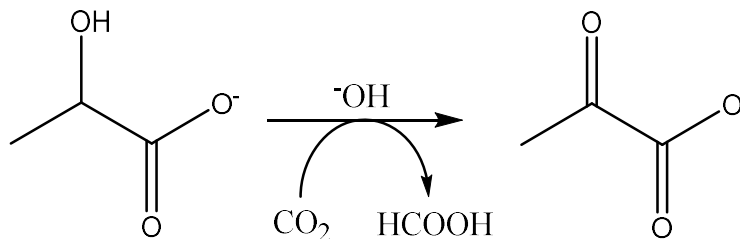
Figure 8-5 Mechanism of CO₂ reduction by lactate to form formate and pyruvate. Adapted from Shen, Zhang and Jin, 2012

Overall, formate formation from CO_2 gas in alkaline medium, 0.557 g l^{-1}, was comparable to $NaHCO_3$, 0.502 g l^{-1}. However, previous ^{13}C-labelled quantitative NMR of $NaH^{13}CO_3$ indicated that only 4.3 % of formate was derived from bicarbonate reduction. Although labelled CO_2 gas could not be employed in the present study due to cost barriers, it is predicted that the yield from CO_2 reduction remains comparably low with CO_2 gas. To enhance conversion, commercial heterogeneous catalysts were explored.

8.3.5 Catalytic testing

Two commercial catalysts were chosen for initial experiments – nickel on silica-alumina (Ni/SiAl), and copper-based methanol synthesis catalyst (CZA). Commercial catalysts are well-characterised and their use allows screening of catalysts for activity without the need for synthesis and advanced characterisation. As alumina was shown to be unstable in hydrothermal media (Section 7.3.4), an additional copper-based catalyst supported on zirconia was synthesised to improve support stability.

Organic acids formed in the presence of heterogeneous catalysts are shown in Figure 8-6. Similarly to results obtained with $NaHCO_3$, Ni/SiAl caused a decrease in all organic acids except acetate and, marginally, oxalate. As proposed in the $NaHCO_3$ study (Section 7.3.2), Ni/SiAl likely promotes gasification of glucose and degradation of HCOOH to CO_2 and H_2. Due to the initially loaded CO_2 constituting almost the entire gas phase, this hypothesis could not be analytically validated. However, in the context of increasing NaCOOH concentration, Ni/SiAl was not an effective catalyst.
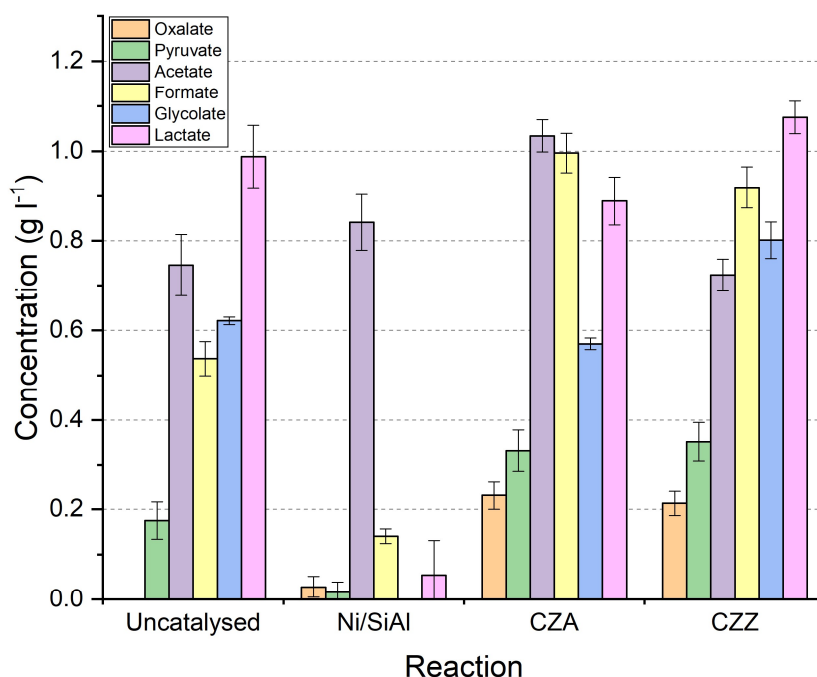
Figure 8-6 Products of hydrothermal catalytic reaction of CO_2 and glucose in NaOH solution. Reaction conditions: 0.05 M glucose, 30 barg CO_2, 1.5 g catalyst (where used), 250 °C, 2 h, 50 ml 1 M NaOH solution

On the contrary, CZA ($CuO/ZnO/Al_2O_3$) was active in promoting formate yield, increasing NaCOOH from 0.557 to 0.996 g l^{-1}. With CZA, a decrease in lactate was accompanied by an increase in oxalate, acetate and pyruvate. Based on the mechanism proposed in Section 5.2.4, this may be due to the catalyst promoting alternative routes of pyruvaldehyde conversion to acetate and pyruvate instead of lactate. Oxalate may be formed from coupling of formate ions in the oxygen-free medium, although concentrations of this species remain low. It must be noted that CZA pellets underwent a visual change post-reaction (Figure 8-7). The pellet surface appeared to be covered in metallic copper, indicating that CuO underwent reduction and likely significant sintering during the reaction. Further characterisation of CZA and other catalysts is discussed in Section 8.3.5.
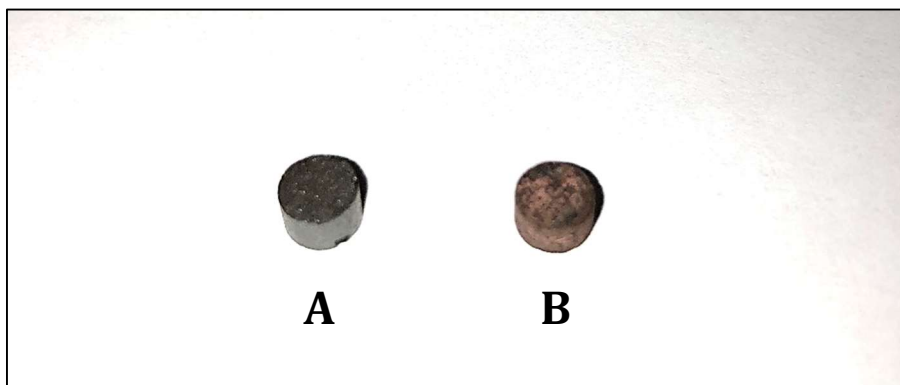
Figure 8-7 Comparison of (A) fresh CZA and (B) spent CZA. Reaction conditions: 0.05 M glucose, 30 barg CO$_2$, 1.5 g CZA pellets, 250 °C, 2 h, 50 ml 1 M NaOH solution

In contrast, CZZ showed comparable yields of oxalate and pyruvate to CZA, but also promoted lactate formation and acetate decline. This may indicate that alumina promotes acetate formation, while zirconia promotes lactate under investigated conditions. However, given CZA contains small quantities of MgO while lab-synthesised CZZ did not, this may also be attributed to this species. Further reactions with individual components of catalysts may be advantageous for assessing their activity. Furthermore, CZZ increased HCOOH yield marginally less that CZA, from 0.557 to 0.920 g l^{-1}, potentially due to differing quantities of active phase between these materials. Overall, it was found that Cu-based catalysts are active in enhancing formate yield from hydrothermal conversion of gaseous CO$_2$ and glucose in NaOH solution. Characterisation of catalysts was undertaken to observe any changes these materials undergo during reaction.

8.3.6 Catalyst characterisation

8.3.6.1 *Ni/SiAl Characterisation*

XRD of fresh and spent Ni/SiAl demonstrated that nickel undergoes changes in oxidation state during reaction (Figure 8-8). Fresh catalyst consisted of NiO and metallic Ni on amorphous SiO$_2$/Al$_2$O$_3$ (Jung and Choi, 2014). After reaction, the diffraction peaks attributed to metallic nickel increase in relative intensity, indicating that NiO undergoes reduction *in situ*. The increase in Ni peaks may also be partially attributed to Ni sintering, resulting in larger crystallite size.
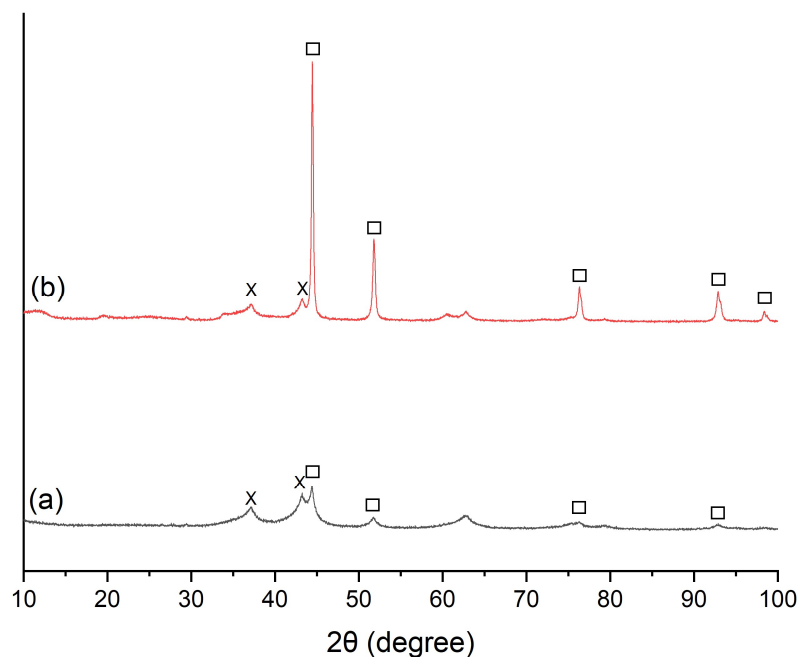
Figure 8-8 Ni/SiAl fresh (a) and spent (b) □ – Ni, x – NiO. Reaction conditions: 0.05 M glucose, 30 barg CO$_2$, 1.5 g Ni/SiAl, 250 °C, 2 h, 50 ml 1 M NaOH solution

The average crystallite size was estimated using the Scherrer Equation. In the case of the fresh catalyst, the Ni diffraction peaks were too low to accurately fit the peaks and obtain the FWHM value. However, this indicates likely small particle size and high dispersion of the nickel crystallites. The average size of the Ni crystallites in the spent sample was calculated as 32.2 ± 4.0 nm.

No discernible differences in particle morphology were observed by SEM imaging (Figure 8-9). EDS of Ni/SiAl was carried out to determine if the catalyst undergoes elemental changes (Table 8-3). EDS shows no significant changes in surface composition after reaction. Comparison of multiple surface sites found a standard deviation of 0.4 mass %.
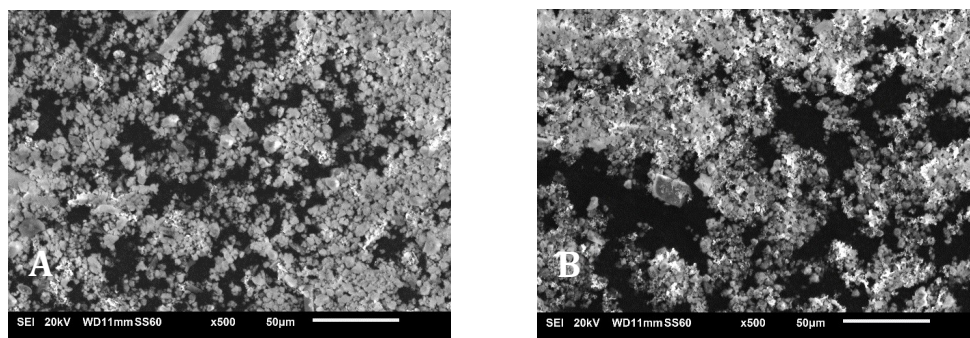
Figure 8-9 SEM of A) fresh and B) spent Ni/SiAl. Reaction conditions: 0.05 M glucose, 30 barg CO_2, 1.5 g Ni/SiAl, 250 °C, 2 h, 50 ml 1 M NaOH solution.

Table 8-3 EDS of fresh and spent Ni/SiAl. Reaction conditions: 0.05 M glucose, 30 barg CO_2, 1.5 g Ni/SiAl, 250 °C, 2 h, 50 ml 1 M NaOH solution

Ni/SiAl	Constituent Composition (%)		
	NiO	**Al_2O_3**	**SiO_2**
Fresh	77.5	2.0	20.5
Spent	76.4	2.1	21.6

In comparison to reactions with $NaHCO_3$, Ni/SiAl underwent oxidation state changes in reactions with CO_2 gas and NaOH. As no gaseous H_2 was detected in hydrothermal reaction of solely glucose in 1 M NaOH, the increase in metallic Ni on the catalyst surface may be caused by reduction of NiO to Ni by glucose. Complexation of hydroxide functional groups by Ni has been hypothesised to form a nickel-glucose complex, reducing NiO in the process and forming organic acids (Yao *et al.*, 2012). Notably, this process required highly alkaline conditions (5 M NaOH), which may explain why NiO in Ni/SiAl did not undergo reduction in reactions with $NaHCO_3$.

8.3.6.2 CZA Characterisation

In this work CZA catalyst was used as a pellet. XRD and SEM/EDS was carried out solely on the pellet surface in present work, while for BET measurements and ICP-OES analysis pellets were crushed. Thus, the cross-sectional composition of the catalyst may be different to the surface. Further determination of the pellet composition and localisation of Cu may be carried out in future by cross-sectional SEM/EDS.

Similarly to Ni/SiAl, XRD of fresh and spent CZA pellets showed that CuO undergoes reduction to metallic Cu (Ahouari *et al.*, 2013) (Figure 8-10). Peaks corresponding to CuO were assigned in fresh CZA and were absent in spent catalyst. The low intensity of CuO peaks indicates small crystallite size and high dispersion in fresh CZA. In contrast, metallic copper peaks became pronounced in spent catalyst, and ZnO assumed a more crystalline state. In the spent catalyst, the average crystallite size of metallic copper was calculated as 38.8 ± 9.7 nm. Although no evidence of alumina conversion to AlO(OH) was experimentally detected, concentrations of alumina in both Ni/SiAl and CZA were below 10 % of the catalyst mass and may be obscured by other morphological changes in the catalyst.
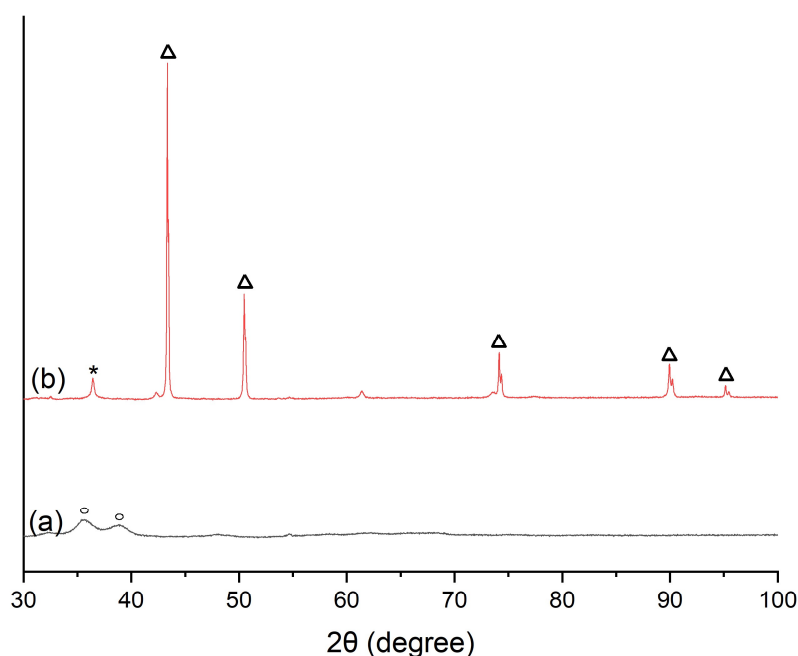
Figure 8-10 XRD of (a) fresh and (b) spent CZA catalyst. $\triangle$ - metallic Cu, $\circ$ – CuO, * - ZnO. Reaction conditions: 0.05 M glucose, 30 barg CO_2, 1.5 g CZA, 250 °C, 2 h, 50 ml 1 M NaOH solution

Conversion of CuO to Cu indicates that reduction of CuO occurs during hydrothermal reaction. Similarly to the nickel catalyst, this is proposedly due to reduction by glucose as evidenced by the lack of gaseous H_2 in control reactions of glucose in NaOH. *In situ* reduction of CuO to metallic copper by cellulose has been reported to occur firstly by hydrolysis of cellulose to glucose with 0.5 M NaOH, then by coordination of glucose to divalent copper. Reduction of Cu(II) to Cu then occurs in tandem with glyceraldehyde production.

SEM of CZA showed significant changes in catalyst surface morphology (Figure 8-11). The fresh catalyst showed large particles of a varying size distribution up to 30 μm (Figure 8-11, C). Post-reaction, particles decreased in size and appeared to agglomerate (Figure 8-11, D).
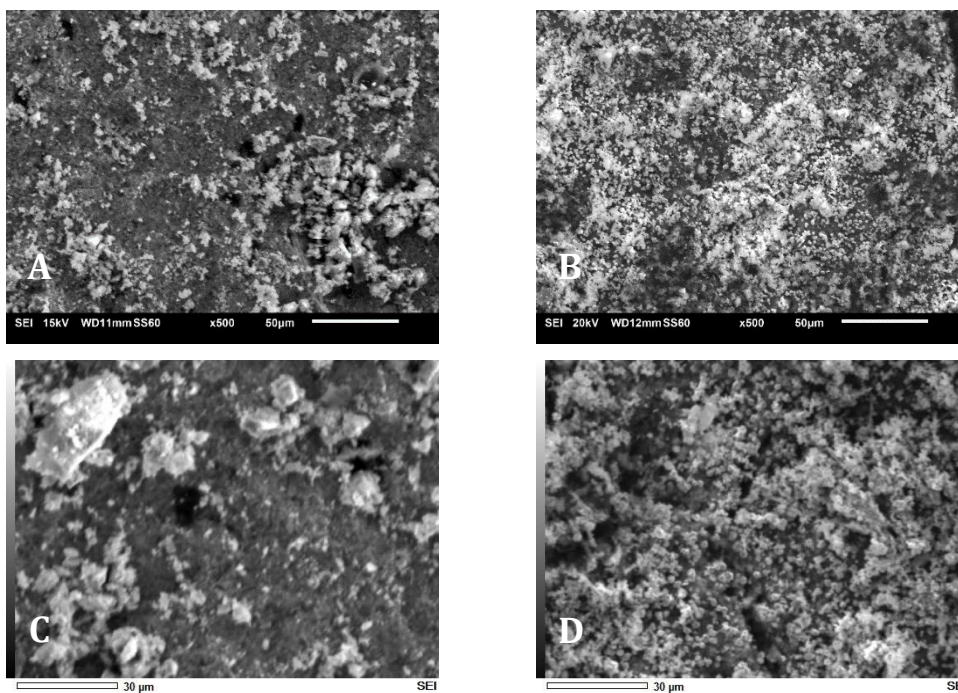
Figure 8-11 SEM of CZA catalyst. A) Fresh CZA x500 magnification, B) Spent CZA x500 magnification, C) Fresh CZA x1000 magnification and D) Spent CZA x1000 magnification

EDS of the fresh and spent pellets was carried out to determine the elemental composition of the pellet surface (Table 8-4). Surface Cu was measured as metallic Cu based on the orange coating of the spent Cu catalyst. Elemental mapping of the fresh CZA showed Cu and Zn distributed homogeneously on the surface, while Al showed some clustering (Figure 8-12).
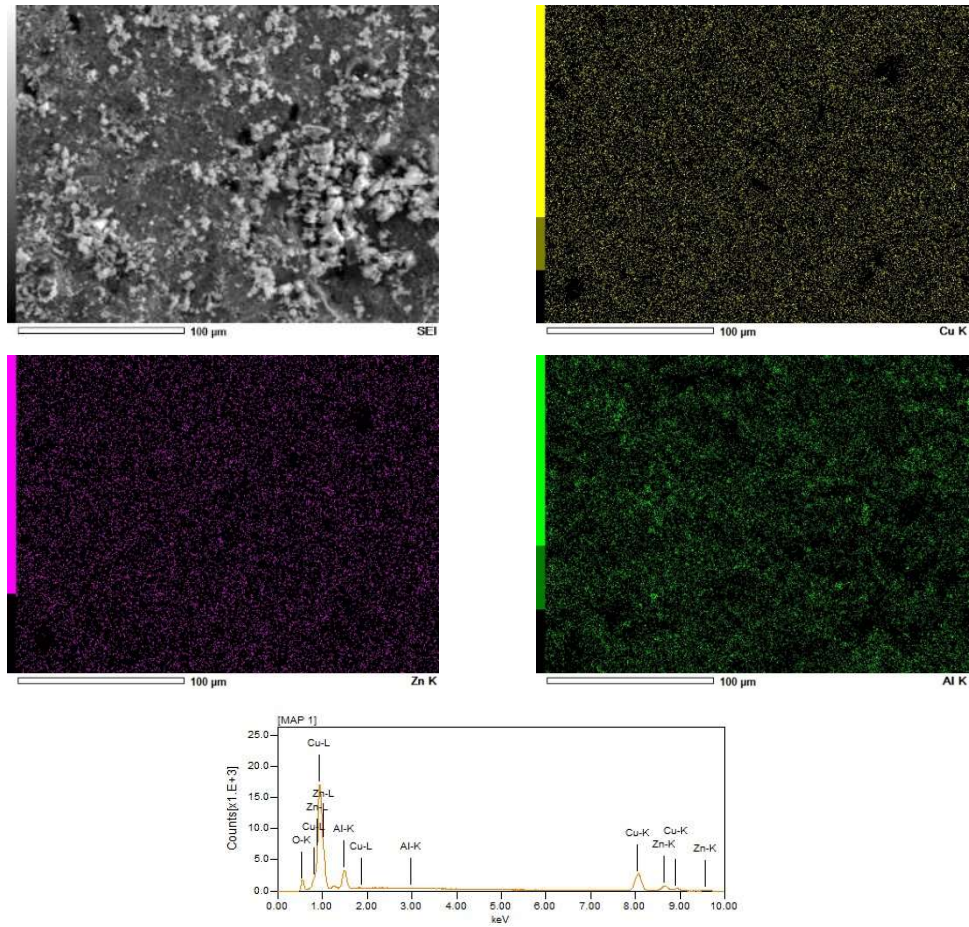
Figure 8-12 Elemental mapping of the fresh CZA pellet surface at x500 magnification

On the other hand, post-reaction CZA showed signs of particle agglomeration and no Zn and Al was detected due to Cu covering the surface (Figure 8-12). This is consistent with visual observation of the pellets, which appeared reddish-brown in colour.
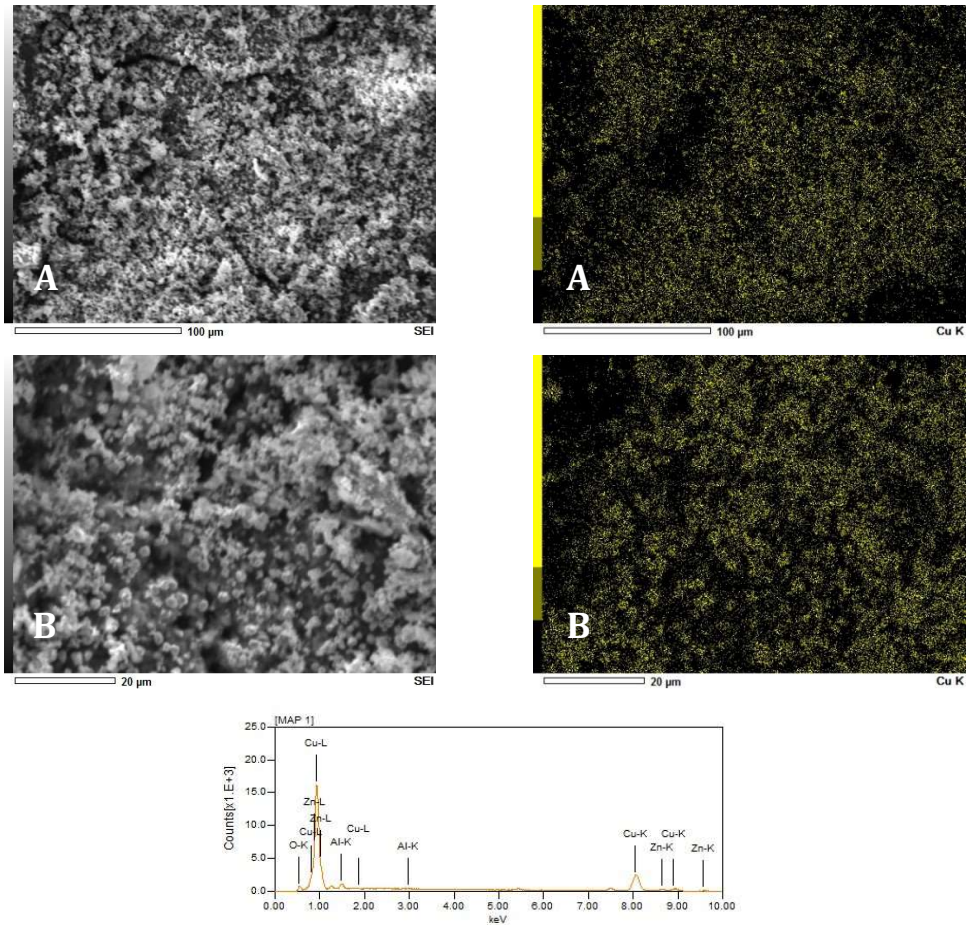
Figure 8-13   Elemental mapping of copper on spent CZA pellet surface at A) x500 magnification and B) x1500 magnification

Changes in surface composition were accompanied by a decrease in BET surface area (Table 8-4), suggesting clogging and collapse of catalyst pores. EDS of fresh pellet surfaces 63.5% CuO, increasing to 83.2 % metallic Cu in spent pellet. It is proposed that after reduction of CuO to metallic Cu, particles sinter to form a copper coating on the pellet surface which may obscure other components of the spent CZA. Average composition error was calculated at 0.6 %. BET Isotherms of fresh and spent CZA are available in Appendix H.1.

Table 8-4 Surface area and surface composition (mass %) of fresh and spent CZA catalyst (* -metallic Cu). Reaction conditions: 0.05 M glucose, 30 barg CO_2, 1.5 g CZA, 250 °C, 2 h, 50 ml 1 M NaOH solution

CZA	BET surface area ($m^2 g^{-1}$)	Composition (mass %)		
		CuO	ZnO	Al_2O_3
Fresh	92.70 ± 0.23	63.5	25	10
Spent	25.52 ± 0.04	83.2*	7.2	9.6

Both CuO and ZnO may react with concentrated alkali to form dissolved salts (Equations 8-6 and 8-7), a process that is accelerated at higher temperatures (McDowell and Johnston, 1936; Dirkse, 1986; Navarro *et al.*, 2014). CZA was submerged in 1 M NaOH solution and the time required to dissolve CO_2 into this solution to reach neutral pH was unknown. Thus, the copper and zinc leaching into solution was investigated by conducting ICP-OES analysis on acid-digested post-reaction CZA. Fresh catalyst consisted of 65 % CuO and 25 % ZnO, equivalent to approximately 52% metallic Cu and 20 % Zn. Post-reaction, digested CZA showed 3577 mg Cu and 1274 mg Zn per kg of sample, equivalent to approximately 0.4 % Cu and 0.1 % Zn. Thus, dramatic loss of Cu and Zn occurs during hydrothermal reaction, proposedly due to leaching of active phase into alkaline solution.

Equation 8-6 Dissolution of CuO in NaOH

$$2NaOH + CuO + H_2O \rightarrow Na_2[Cu(OH)_4]$$
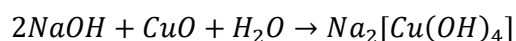
Equation 8-7 Dissolution of ZnO in NaOH

$$2NaOH + ZnO + H_2O \rightarrow Na_2[Zn(OH)_4]$$
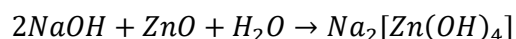
Evidence from characterisation indicates that the commercial Cu-based catalyst was highly unstable during hydrothermal reaction due to sintering and leaching. Cupric oxide underwent leaching into solution, reduction to Cu, and agglomeration on the pellet surface. These processes may occur simultaneously throughout the reaction as both CuO and metallic copper leach into alkaline solution (Mohanty *et al.*, 2018). Metallic copper coats the pellet surface, thereby preventing diffraction patterns for Zn to be obtained, however ICP-OES confirms most ZnO is also lost to solution. An alternative Cu-based catalyst supported on ZrO_2 was synthesised to assess if higher stability can be achieved with a different support.

8.3.6.3 CZZ Characterisation

XRD patterns for both fresh and spent CZZ are shown in Figure 8-14. Fresh CZZ exhibits peaks for CuO, ZnO and ZrO$_2$, while in spent CZZ the majority of distinct CuO and ZnO diffraction peaks disappear (Borovinskaya *et al.*, 2019). Notably, in contrast to CZA, no peaks corresponding to metallic Cu or Zn are present in the diffraction of spent CZZ.
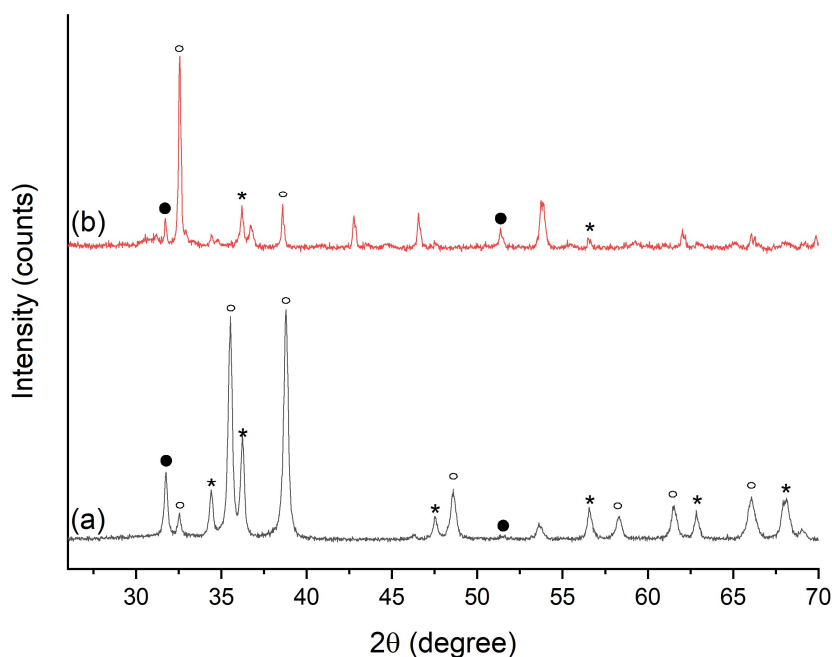
Figure 8-14 XRD of fresh (a) and spent (b) CuO/ZnO/ZrO$_2$ catalyst. Peak positions denote species: ● - ZrO$_2$, ○ - CuO, * - ZnO. Reaction conditions: 0.05 M glucose, 30 barg CO$_2$, 1.5 g CZZ, 250 °C, 2 h, 50 ml 1 M NaOH solution

Similarly to CZA catalyst, CuO crystallite particles underwent sintering during reaction. Average CuO crystallite size in fresh catalyst was calculated as 29.2 ± 2.0 nm, increasing to 38.8 ± 9.7 nm in spent catalyst. A table of calculated CuO crystallite sizes in fresh CZZ based on the Scherrer Equation can be located in Appendix G. It must be noted that in the freshly prepared catalyst, the accuracy of the Scherrer calculations is higher than in the spent catalyst. This is likely because catalyst sintering results in the formation of particles with varying sizes in the spent catalyst. BET surface area measurement showed a decrease from 19.88 ± 0.06 m^2 g^{-1} in fresh catalyst to 7.77 ± 0.03 m^2 g^{-1} in spent CZZ. Furthermore, similar to CZA, elemental composition of CZZ showed 73.7 ± 0.3% Cu, while spent catalyst contained 2.0 ± 0.3% Cu. Adsorption isotherms of fresh and spent CZZ are available in Appendix H.2.

The absence of diffraction peaks corresponding to metallic species and low Cu percentage detected by EDS indicated that CuO and ZnO were leaching to solution. ICP-OES analysis of acid-digested post-reaction CZZ found that the residual concentration of Cu was below the quantifiable range (<1.2 mg kg^{-1}), while 1421 mg kg^{-1} (0.14%) Zn remained. It must be noted that the presence of ZrO_2 in the sample leads to incomplete sample digestion in conventional acids, and therefore some Cu and Zn particles may have been retained on ZrO_2. However, it is assumed that this would have marginal effects on concentrations. Overall, CZZ followed the same trends in these measurements as CZA – a decrease in surface area and copper content of the catalyst, indicating instability. This instability is proposedly caused by submergence of the catalyst in concentrated NaOH solution resulting in the loss of catalyst active phase. Thus, modifying the catalyst support is not effective in improving stability in this case.

Comparison of SEM images of fresh and spent CZZ catalyst primarily showed that agglomeration of particles occurs after reaction (Figure 8-15). Particles appeared of more defined shape in spent CZZ, although this may be caused by submergence of the powder in NaOH solution which removed smaller particles from the crystal surfaces, making them appear clearer in images. Some particles in spent CZZ exhibited a rod-like or hexagonal base (Figure 15, D), which exhibit the irregular shape of ZnO crystals (Tymoszuk and Wojnarowicz, 2020).
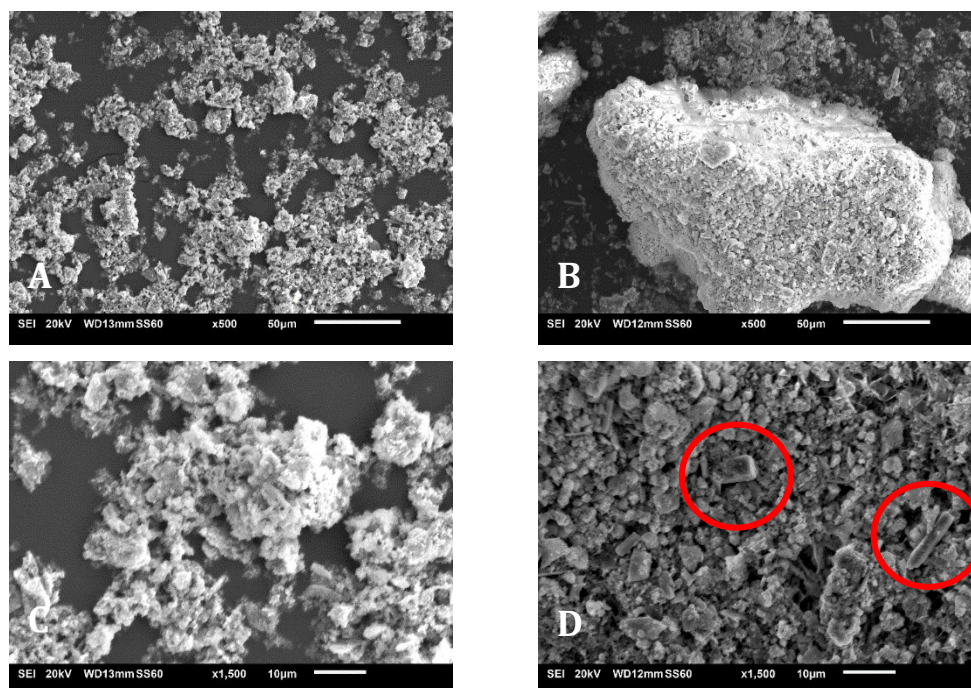
Figure 8-15 SEM of fresh and spent CZZ catalyst. A) fresh CZZ x500, B) spent CZZ x500, C) fresh CZZ x 1500, D) spent CZZ x1500

Overall, characterisation of CZZ found that, in contrast with CZA, CuO does not undergo reduction during hydrothermal reaction. This may be due to the physical form of the catalyst. It is proposed that the powdered CZZ catalyst, which consists of particles <50 μm, initially has more contact with NaOH solution than commercial CZA pellets, resulting in loss of both CuO and Cu to solution. The concentration of NaCOOH with both CZA and CZZ remained comparable at 0.996 and 0.920 g l^{-1}, respectively. Mass transport of NaOH solution into the pores of the pellet CZA catalyst may result in marginally higher stability of the CuO phase in CZA compared to powdered CZZ, resulting in marginally higher HCOOH concentrations.

At this stage it is difficult to determine the species acting as a catalyst in formate production. Metallic copper was inactive as a catalyst in $NaHCO_3$ and glucose reactions, and is therefore unlikely the sole catalytic species in the present system. However, in combination with ZnO it is possible that bicarbonate reduction occurs on the solid catalyst surface prior to its degradation. Numerous reports have used Cu alongside Zn for hydrothermal HCO_3^- reduction (Huo *et al.*, 2012; L. Y. Wang *et al.*, 2014), Furthermore, synergy between these species provides more CO_2 and H_2 adsorption sites as reported in the methanol production literature (Karelovic *et al.*, 2012; Huang *et al.*, 2015). Reduction is proposed to involve firstly adsorption of

185

CO_2/HCO_3^- on the ZnO surface and H_2 on the Cu surface, followed by hydrogenation of adsorbed CO_2 (Huo *et al.*, 2012). Alternatively, dissolved Cu hydroxide may be the active species in the reaction. Wang and co-workers have previously proposed that Cu can complex glucose in NaOH solution, leading to the formation of lactic and pyruvic acid (Wang *et al.*, 2013). To determine if this is the active species, a reaction in an alkaline aqueous medium containing copper ions may be carried out. Further investigation into the mechanism of copper-based catalysts in formate production is therefore necessary to determine the action of these catalysts and establish methods of improving their stability.

Overall, investigations into commercial catalysts in gaseous CO_2 and glucose conversion to HCOOH in alkaline media identified Cu-based catalysts as active but unstable in hydrothermal media. A high extent of copper sintering was evidenced by increased crystallite size, and decrease in surface area further demonstrate the instability of the catalyst. Most importantly, the catalyst active phase is lost by almost complete CuO and ZnO leaching to the NaOH solution, likely forming cuprate and zincate salts. To establish the catalyst components active in increasing HCOOH concentration, investigation of individual constituents would be valuable.

8.4 CONCLUSION AND FUTURE WORK

In this work, bicarbonates, carbonates and CO_2 gas were compared as precursors in hydrothermal reduction with glucose. It was found that formate yield varies greatly between K^+ and Na^+ bicarbonate, decreasing with the former proposedly due to difference in carboxylate affinity or dissolution into hydrothermal media. In reactions with carbonates, calcium carbonate was found to act as an alkali catalyst in liquefaction and no HCOOH was formed, potentially due to calcium bicarbonate not forming *in situ.* However, reactions in water-soluble Na_2CO_3 formed an array of different organic acids, including 0.408 g l^{-1} HCOO$^-$. The inclusion of CO_2 gas decreased reaction pH and increased formate concentration to 0.509 g l^{-1}, achieving comparable yields to NaHCO$_3$ (0.502 g l^{-1}). This study demonstrates the potential of using two different CO_2 sources in conjunction to obtain a desirable reduction product.

Subsequently, CO_2 in NaOH solution was studied in place of solid reagents. Studies on the impact of NaOH concentration were carried out, and 1 M NaOH solution was established as the concentration at which formate concentration was maximised. In comparison to control reactions of solely glucose in 1 M NaOH, the addition of CO_2

gas increased formate yield from 0.436 g l^{-1} to 0.557 g l^{-1}, potentially obtained by the reduction of CO_2. Commercial catalysts Ni/SiAl and CZA, as well as lab-synthesised CZZ were explored in an effort to increase $HCOO^-$ concentration, and Cu-based catalysts were found to be active. A maximum of 0.996 g l^{-1} $HCOO^-$ was achieved with CZA, although characterisation found that the catalysts is highly unstable in the reaction. Sintering of the copper was accompanied by a high loss of the active phase through leaching into the alkaline medium.

Several key aspects of CO_2/NaOH reactions with glucose are of interest for future studies. Establishing the proportion of formate that can be attributed to CO_2 gas reduction may be carried out by using ^{13}C-labelled glucose or carbon dioxide. This would be valuable both in uncatalyzed and CZA-catalysed reactions to assess the impact of CZA on the reagents. Furthermore, examining the activity of individual components of copper-based catalysts, as well as copper solutions, would provide insight into the active constituent in formate production. Identifying the mechanism of these catalysts would provide the basis of designing new, hydrothermally stable and active catalysts for CO_2 reduction in alkaline media. Finally, in a continuous system there may be sufficient time to solubilise CO_2 in NaOH prior to the solution reaching the catalyst-containing reactor, protecting it from a strongly alkaline environment. Therefore, exploring other reactor set-ups in catalyst stability studies may be another area of interest.

9   CHAPTER 9: CONCLUSIONS & FUTURE WORK

Decreased reliance on fossil fuels in the production of platform and value-added products can be achieved by developing sustainable technologies that utilise renewable energy and abundant materials as feedstock. The use of carbon dioxide as a feedstock is of increasing interest due to its earth abundance, non-toxicity and low cost (Arakawa *et al.*, 2001). Numerous methods, including photochemical and electrochemical, and hydrogenation, were explored in Chapter 2. However, these are generally plagued by low conversion efficiency, requirement of noble metal catalysts, or the use of hazardous H_2 as a co-reactant. On the contrary, hydrothermal conversion of CO_2 uses sub-critical water as the reaction medium. Furthermore, an earth abundant and economic H_2 source, such as biomass, can be used as a co-reactant to reduce CO_2.

Therefore, the primary aim of this work was to investigate the products, extent of CO_2 reduction, and catalytic activity in hydrothermal carbon dioxide conversion with biomass as a reductant. This was undertaken by developing analytical methods, optimising reaction parameters, investigating the impact of heterogeneous catalysts, and varying CO_2 precursors. This chapter includes the conclusions drawn from the experimental results and proposed further research directions for future work.

9.1   CONCLUSIONS

Hydrothermal reduction of CO_2 with biomass was initially studied using $NaHCO_3$ as a CO_2 precursor with glucose as a model compound for biomass. Experiments were conducted in a batch pressure vessel, where aqueous, gaseous and solvent-extracted products of the reaction were established. The impact of conditions, including reaction temperature and time, reagent concentration and water filling volume was established to determine the conditions at which CO_2 reduction to $HCOO^-$ may be maximised. Bulk metals were explored as heterogeneous catalysts to enhance the conversion of CO_2 to formate under optimised conditions (T = 250 °C, 2 hr, 0.50 M $NaHCO_3$, 50 ml H_2O), where Ni powder was found to be highly active. Supported Ni catalysts were then synthesised, tested, and characterised to assess their stability and activity in this reaction. Finally, several alternative CO_2 precursors – $KHCO_3$, Na_2CO_3, $CaCO_3$, CO_2 – were compared, and commercial catalysts were

assessed in a CO_2/NaOH system. Based on the results of these experiments, a number of key conclusions were drawn.

9.1.1 Analytical Method Development

Initially, the development of analytical methods was crucial to determine the products of hydrothermal conversion of $NaHCO_3$ and glucose. Numerous products have been reported in CO_2 reduction in previous studies, including CH_4, CH_3OH, HCOOH, CH_3COOH, among others. Therefore, using the correct methods to monitor different phases was key.

It was established in the Literature Review (Chapter 2) that C_1 molecules are the most likely products of CO_2 reduction. Aqueous phase analysis by GC/MS was not successful due to the formation of non-volatile, ionised products in the mildly alkaline reaction medium. It was found that HPLC of aqueous products was the most effective method of organic acid analysis. Coupling of aqueous analysis with GC/MS analysis of solvent-extracted bio-oil illustrated the complexity and number of species formed alongside organic acids, which included aromatics and cyclic ketones. Based on available literature, bio-oil products were determined to be formed from hydrothermal liquefaction of glucose. Further addition of gas phase analysis allowed compositional analysis of gaseous products, which included CO_2, H_2 and in some reactions CH_4.

Analysis of aqueous phase analysis found that formic acid, HCOOH, was the only C_1 product detected and was therefore the focus of optimisation reactions. Chapter 4 therefore formed the analytical foundation for the remaining work and provided methods for product quantification and mechanistic studies.

9.1.2 Hydrothermal Conversion of $NaHCO_3$ and Glucose to Formate

The impact of varying reaction conditions such as reaction temperature, time and reactor filling were explored to determine the conditions at which HCOOH concentration was maximised. A maximum of 0.502 g l^{-1} formate was achieved after 2 hours at 250 °C with 50 ml solution containing 0.50 M $NaHCO_3$ and 0.05 M glucose. The concentration of HCOO$^-$ declined steadily at the maximum temperature of 300 °C with increasing temperature. This was proposed to be caused by degradation of the product to CO_2 and H_2 with this hypothesis subsequently validated by gas analysis. Based on mechanistic and NMR studies, it was established that at conditions where formate concentration is maximised, over 95% is obtained from glucose liquefaction

rather than CO_2 reduction. The presence of $NaHCO_3$ creates an alkaline environment where glucose degrades through a series of base-catalysed reactions, leading to a pyruvaldehyde intermediate prior to the formation of organic acids. The complexity of reactions occurring under hydrothermal conditions was thus highlighted. This chapter formed the basis of screening heterogeneous catalyst studies with bulk metals to enhance the production of formate derived from bicarbonate reduction.

9.1.3   Bulk Metals as Heterogeneous Catalysts

Bulk copper, cobalt and nickel were investigated as heterogeneous catalysts to increase bicarbonate reduction to formate. These metals were chosen as they were previously shown to resist undergoing oxidative changes during the reaction, acting as recyclable catalysts. In presence of glucose as a H-source, no additional reducing metals are necessary.

Copper and cobalt did not exhibit catalytic activity in this reaction under the investigated conditions. However, nickel was discovered to be highly active, increasing formate concentration from 0.502 to 1.240 g l^{-1} and simultaneously increasing the concentrations of some other organic acids. ^{13}C-QNMR and ^{1}H-NMR determined that in the presence of Ni, the percentage of $HCOO^-$ derived from HCO_3^- increased from 4.3 to 26.6% of total HCOOH. Simultaneously, formic acid produced from glucose nearly doubled from 0.480 to 0.910 g l^{-1}. Simultaneously gaseous H_2 composition in reactions with Ni increased from 2 to 23.6 %.

Characterisation of the nickel powder by XRD, FTIR and SEM, as well as liquid analysis by ICP-OES, demonstrated that bulk nickel powder undergoes no changes in functionality, morphology, oxidation state, and minimal leaching of 0.0011%. It was proposed that Ni activity involves firstly dissociative H_2 adsorption, followed by hydride reduction of adsorbed HCO_3^- to $HCOO^-$. It is also likely involved in the degradation of formic acid to CO_2 and H_2. It was concluded that that bulk Ni is active and stable under investigated conditions in the presence of glucose in place of metal reductants. Nickel crucially increased the concentration of HCOOH from both bicarbonate and glucose, although it must be noted that numerous other by-products remain in solution. This chapter formed the foundation of further studies of supported Ni catalysts in the following chapter.

9.1.4 Investigation into Supported Nickel Catalysts

In this chapter supported nickel catalysts were synthesised, tested and characterised. Nickel supported on silica, alumina, rice husk-derived silica, zirconia, activated carbon were explored, as well as commercial nickel on silica-alumina. The concentration of formate decreased with all supported catalysts, while analysis showed Ni/SiAl and Ni/RH-SiO$_2$ catalysts strongly promoted H$_2$ formation. The loading of Ni on the catalysts was not found to be chiefly responsible for the decrease in product, and the impact of Ni particle size and oxidation state was instead considered. Raney-Ni studies showed that surface area and H$_2$ generation ability of the nickel strongly impact reaction products, with Raney-Ni producing primarily H$_2$ and CH$_4$. It is proposed that high concentrations of H$_2$ facilitate bicarbonate reduction to formate, which is then decomposed to CO$_2$ and H$_2$ over high surface area Raney-Ni.

Characterisation of catalysts showed that Ni/SiAl and Ni/RH-SiO$_2$ contained metallic Ni phases, while other catalysts contained NiO. Based on evidence reported in literature, it was concluded that NiO cannot be *in situ* reduced to metallic Ni under investigated conditions. Furthermore, it was proposed that the oxidation state and crystallite size of the catalyst active phase strongly impacts the H$_2$ adsorption and product yields, although further studies in this area are required. The control of particle size and oxidation state during catalyst synthesis was thus found to be critical in obtaining desired products. Furthermore, it was discovered that catalyst stability is a major challenge in hydrothermal reactions, with alumina undergoing degradation.

9.1.5 Alternative Sources of Carbon Dioxide

Finally, bicarbonates, carbonates and CO$_2$ gas were compared as precursors for hydrothermal formate production in the presence of glucose reductant. Notably, the formate yield was found to differ depending on the cation, Na$^+$ or K$^+$, in bicarbonate reactions. It is difficult to determine the causes of this phenomena but differing carboxylate affinity or dissolution in sub-critical media are potential sources. A second key takeaway was the comparable yield achieved with Na$_2$CO$_3$ in conjunction with CO$_2$ gas when compared with NaHCO$_3$ reactions. Formate concentration of 0.509 g l^{-1} was achieved with the mixed Na$_2$CO$_3$/CO$_2$ system compared with 0.502 g l^{-1} with NaHCO$_3$. This is significant as carbonates have been described as poorer precursors in hydrothermal reduction, and demonstrated the potential of

using additional CO_2 gas to lower reaction pH to favour formation of the more desirable HCO_3^- species in solution.

CO_2 gas reactions in NaOH solution also showed promising results. The addition of CO_2 gas increased formate yield to 0.557 g l^{-1} as compared to 0.436 g l^{-1} in a control reaction using solely glucose in 1 M NaOH. This additional formate was potentially obtained by the reduction of CO_2. Studies of catalysts in this system to further increase conversion to HCOOH found that Cu-bearing catalysts are highly active. A maximum of 0.996 g l^{-1} $HCOO^-$ was achieved with $CuO/ZnO/Al_2O_3$ pellets, although characterisation found that the catalyst is highly unstable in the reaction. Sintering of the copper was accompanied by a high loss of the active phase through leaching into the alkaline medium, as well as decrease in surface area. Altering the alumina support to zirconia did not improve the catalyst stability as loss of the active phase was proposed to occur under highly alkaline conditions.

9.1.6 Overall Conclusions

The most significant finding to emerge from this work was the demonstrated activity of nickel powder in reducing bicarbonate to value-added formic acid in the presence of glucose as a reductant under hydrothermal conditions. The investigations with bulk nickel powder indicated that this metal promotes both the reduction of CO_2, and simultaneously enhances the conversion of glucose to formate. However, the particle size and oxidation state of dispersed nickel was found to strongly impact the product profile. Thus, nickel-catalysed CO_2 reduction is a promising area for further exploration.

Furthermore, it was shown in this work that other CO_2-precursors may be combined to achieve similar results to those with $NaHCO_3$, a product of CO_2 capture with sodium carbonate. This allows to use carbonates and CO_2 gas in place of bicarbonate to achieve similar concentrations of the product. Although this work is preliminary, a similar system may be applied to other hydrothermal systems, for example with metal reductants and catalysts or more complex biomass feedstocks. Heterogeneous catalysts were shown to enhance the yield of formate in reactions with other CO_2 sources, although further work must be undertaken to improve catalyst stability.

9.2 SUGGESTIONS FOR FUTURE WORK

In this work, several novel findings were summarised in Section 9.1. However, there are many potential avenues for further research and improvements that can be incorporated. Recommendations for future investigations are described in the following sections, divided into analytical/characterisation improvements (Section 9.2.1) and future research directions (Section 9.2.2).

9.2.1 Analysis and Characterisation Techniques

Analytical method development was a key focus in the present work (Chapter 4). However, the final methods used were best available with time considerations, and further improvements in analysis can be carried out.

Aqueous phase analysis by HPLC may be improved by using alternative columns adapted for carbohydrate analysis. Broadening in HPLC chromatograms was attributed to the presence of sugar derivatives such as oligosaccharides. Therefore, a column such as Hi-Plex (Agilent, USA), which is specialised to organic acids, alcohols and carbohydrates, could be used. In this way, errors caused by peak deconvolution would be minimised.

Gas analysis in the present work was carried out compositionally by manually sampling gas bags. This technique introduces uncertainty due to the presence of ambient air in the sampling syringe and tubing. Therefore, online gas chromatography would improve quantitative gas analysis. Furthermore, solely permanent gases were analysed in this work. Analysis of other species that may be present, including hydrocarbons and volatile organics, could be achieved by adding a second, capillary column in tandem with the packed column used in this work.

Finally, a more sensitive method of determining gas composition may be used to monitor and compare H_2 concentrations in CO_2 reactions. For example, GC coupled with a flame-ionisation detector GC/FID can be up to 66 times more sensitive than GC/TCD in detecting certain species (Budiman, Nuryatini and Zuas, 2015). Coupling of packed and capillary columns with MS detection would allow for quantitative analysis of unknown substances, if present.

Catalyst characterisation could be improved by utilising additional steps and techniques. Primarily, changes in catalyst morphology occurring after reaction may be minimised by storing samples under vacuum prior to characterisation.

Furthermore, SEM used in the present work was unable to carry out high magnification to the nanometre scale. Therefore, higher magnification SEM, or transmission electron microscopy (TEM) may be utilised to determine the dispersion of the active phase on the support and the average particle size. This would be valuable when assessing the importance of Ni particle sizes in promoting different reactions in reactions with supported Ni catalysts. Future studies on Ni catalysts in hydrothermal bicarbonate reduction would also benefit from temperature-programmed reduction (TPR) of catalysts to determine the reduction temperature of NiO. Finally, compositional analysis of solid catalysts to determine accurately active phase loading may be achieved by probe molecule chemisorption or ICP analysis of synthesised catalysts.

9.2.2 Future Research Directions

In the present work, formic acid was the focus of hydrothermal CO_2 reduction as the main detected product of this reaction. However, there is an opportunity to amend the reaction to produce other value-added products, *e.g.* methanol. It has previously been reported that methanol formation is favoured by low pH (Huo *et al.*, 2012) This presents an opportunity to alter medium pH conditions and its impact on reduction products. Gaseous carbon dioxide may be particularly of interest for this application due to the formation of carbonic acid.

Glucose was used as a model compound for biomass in the present work. This presents an opportunity for investigating other biomass compounds in its place, such as polyols or raw biomasses. Due to the complex nature of this reaction, simple compounds may simplify analysis. For the technology to be industrially relevant, existing waste streams containing biomass must be prioritised in further studies on biomass reductants. For example, sugarcane bagasse or olive pits are major wastes produced in the sugar and olive oil industries, respectively, and are therefore good candidates for raw biomass studies. Liquid waste streams containing high quantities of sugars and carbohydrates, such as in baked goods manufacture, are also promising (Zhang *et al.*, 2013).

A key area of further research is into the activity of nickel and nickel-bearing materials. As discussed in Chapter 5, nickel present in the reactor vessel alloy may influence the degradation of HCOOH at higher temperatures (section 5.2.3). Overall, investigation of supported and commercial Ni catalysts yielded several interesting

results. Primarily, it was established that the oxidation state and crystallite size of the catalyst active phase must be further investigated with experimentation. It is proposed that the Ni oxidation state of the fresh catalyst has a strong impact on the overall reaction as it impacts H_2 adsorption. Thus, testing of NiO powder would be valuable to assess the activity of the oxide and determine if this species can be reduced *in situ* in the system even in bulk form.

The development of hydrothermally-stable catalysts is a significant challenge in the use of heterogeneous catalysts. Therefore, design and testing of stable catalysts is a key avenue for further investigations. Catalyst characterisation of supported nickel catalysts found that zirconia exhibited the highest stability of all supports and is a promising material for further studies. Reducing the NiO/ZrO_2 pre-reaction and monitoring formate and H_2 could confirm the activity of supported metallic Ni in formate formation and degradation, as well as the role of crystallite size in reaction rates.

Further investigation into the action of Raney-nickel in aqueous phase reforming (APR) of glucose and other sugar solutions would be valuable. Raney-Ni exhibited high activity in converting glucose solution to gases in the presence of CO_2 gas. Thus, further investigation into Raney-Ni as an APR catalyst with CO_2 precursors as co-catalysts is a promising research route. The production of H_2 and alkanes from liquid solution may be particularly applicable to fields such as juice and concentrate manufacturing, where waste streams contain high concentrations of sugars and sweeteners.

Several key aspects of CO_2/NaOH reactions with glucose are also of interest for future studies. Establishing the proportion of formate that can be attributed to CO_2 gas reduction may be carried out by using ^{13}C-labelled glucose or carbon dioxide. This would be valuable both in uncatalyzed and CZA-catalysed reactions to assess the impact of CZA on the reagents. Furthermore, examining the activity of individual components of copper-based catalysts, as well as copper solutions, would provide insight into the active constituent in formate production. Identifying structure-performance relationships for these catalysts would provide the basis of designing new, hydrothermally stable and active catalysts for CO_2 reduction in alkaline media. It must be noted that no optimisation of the nickel or copper catalysts, such as metal

loading or quantity added, was carried out in the present work and may have drastic effects. Thus, catalyst optimisation is a key focus of future work.

Finally, in a continuous system there may be sufficient time to solubilise CO_2 in NaOH prior to the solution reaching the catalyst-containing reactor, protecting it from a strongly alkaline environment. Continuous mode of operation involves continuous addition of feedstock and effluent removal and has the advantage of higher productivity and ease of operation. Furthermore, large-scale operation of batch processes have higher associated operating costs (Jana, 2018). Therefore, exploring other reactor set-ups in catalyst stability studies may be another area of interest.

9.3 SUMMARY

In this work, hydrothermal reduction of carbon dioxide was investigated with glucose reductant and heterogeneous catalysts. Analytical methods were developed to analyse aqueous, organic and gaseous composition of products. Formic acid concentration from $NaHCO_3$ was maximised by optimising reaction parameters in uncatalyzed reactions, follow by exploration of bulk metal catalysts. Nickel was found to be highly active in the reaction, although in supported Ni catalysts promotion of product degradation indicates that further research is required in this sphere. Studies of different carbon dioxide precursors showed that comparable concentrations of HCOOH could be obtained with carbonates coupled with CO_2 gas compared to sodium bicarbonate, expanding the applications of hydrothermal technology. Coupled with renewable energy, hydrothermal technology remains a promising avenue for waste valorisation.

REFERENCES

Abbas, Z., Mezher, T. and Abu-Zahra, M. R. M. (2013) 'CO2 purification. Part I: Purification requirement review and the selection of impurities deep removal technologies', *International Journal of Greenhouse Gas Control*. Elsevier, 16, pp. 324–334. doi: 10.1016/j.ijggc.2013.01.053.

Abelló, S. and Montané, D. (2011) 'Exploring iron-based multifunctional catalysts for fischer-tropsch synthesis: A review', *ChemSusChem*. Wiley-VCH Verlag, pp. 1538–1556. doi: 10.1002/cssc.201100189.

Ahmed, O. H., Altarawneh, M., Jiang, Z. T., Al-Harahsheh, M. and Dlugogorski, B. Z. (2017) 'Reactions of products from thermal degradation of PVC with nanoclusters of A-Fe2O3 (hematite)', *Chemical Engineering Journal*. Elsevier B.V., 323, pp. 396–405. doi: 10.1016/j.cej.2017.04.047.

Ahouari, H., Soualah, A., Le Valant, A., Pinard, L., Magnoux, P. and Pouilloux, Y. (2013) 'Methanol synthesis from CO2 hydrogenation over copper based catalysts', *Reaction Kinetics, Mechanisms and Catalysis*, 110(1), pp. 131–145. doi: 10.1007/s11144-013-0587-9.

Alper, E. and Orhan, O. Y. (2017) 'CO2 utilization: Developments in conversion processes', *Petroleum*. KeAi Communications Co., 3(1), pp. 109–126. doi: 10.1016/j.petlm.2016.11.003.

Álvarez-Falcón, L., Viñes, F., Notario-Estévez, A. and Illas, F. (2016) 'On the hydrogen adsorption and dissociation on Cu surfaces and nanorows', *Surface Science*. North-Holland, 646, pp. 221–229. doi: 10.1016/j.susc.2015.08.005.

Álvarez, A., Bansode, A., Urakawa, A., Bavykina, A. V, Wezendonk, T. A., Makkee, M., Gascon, J. and Kapteijn, F. (2017) 'Challenges in the Greener Production of Formates/Formic Acid, Methanol, and DME by Heterogeneously Catalyzed CO2 Hydrogenation Processes', *Chemical Reviews*, 117(14), pp. 9804–9838. doi: 10.1021/acs.chemrev.6b00816.

Álvarez, A., Borges, M., Corral-Pérez, J. J., Olcina, J. G., Hu, L., Cornu, D., Huang, R., Stoian, D. and Urakawa, A. (2017) 'CO2 Activation over Catalytic Surfaces', *ChemPhysChem*, 18(22), pp. 3135–3141. doi: 10.1002/cphc.201700782.

References

Andérez-Fernández, M., Pérez, E., Martín, A. and Bermejo, M. D. (2017) 'Hydrothermal CO2 reduction using biomass derivatives as reductants', *Journal of Supercritical Fluids*. Elsevier, 133(2018), pp. 658–664. doi: 10.1016/j.supflu.2017.10.010.

Anderez, M., Perez, E., Martin, A., McGregor, J. and Bermejo, M. D. (2019) 'Synergistic hydrothermal CO2 conversion and biomass liquefaction', *Nature*.

Arakawa, H., Aresta, M., Armor, J. N., Barteau, M. A., Beckman, E. J., Bell, A. T., Bercaw, J. E., Creutz, C., Dinjus, E., Dixon, D. A., Domen, K., DuBois, D. L., Eckert, J., Fujita, E., Gibson, D. H., Goddard, W. A., Goodman, D. W., Keller, J., Kubas, G. J., Kung, H. H., Lyons, J. E., Manzer, L. E., Marks, T. J., Morokuma, K., Nicholas, K. M., Periana, R., Que, L., Rostrup-Nielson, J., Sachtler, W. M. H., Schmidt, L. D., Sen, A., Somorjai, G. A., Stair, P. C., Ray Stults, B. and Tumas, W. (2001) 'Catalysis research of relevance to carbon management: Progress, challenges, and opportunities', *Chemical Reviews*, 101(4), pp. 953–996. doi: 10.1021/cr000018s.

ASTM (2001) *Standard Test Method for Ash in Wood D1102 - 84*. West Conshohocken. doi: 10.1520/mnl10913m.

ASTM (2011) 'Standard Test Method for Volatile Matter in the Analysis of Particulate Wood Fuels E872 - 82', *ASTM International*, 82(Reapproved 2006), pp. 14–16. doi: 10.1520/E0872-82R06.2.

Atia, A. and Mohammedi, K. (2018) 'A Review on the Application of Enhanced Oil/Gas Recovery through CO2 Sequestration', in *Carbon Dioxide Chemistry, Capture and Oil Recovery*. InTechOpen, pp. 241–253. doi: 10.5772/intechopen.79278.

Azadi, P., Khodadadi, A. A., Mortazavi, Y. and Farnood, R. (2009) 'Hydrothermal gasification of glucose using Raney nickel and homogeneous organometallic catalysts', *Fuel Processing Technology*. Elsevier, 90(1), pp. 145–151. doi: 10.1016/j.fuproc.2008.08.009.

Behrendt, F., Neubauer, Y., Oevermann, M., Wilmes, B. and Zobel, N. (2008) 'Direct liquefaction of biomass', *Chemical Engineering and Technology*, 31(5), pp. 667–677. doi: 10.1002/ceat.200800077.

Benton, A. F. and Emmett, P. H. (1924) 'The reduction of nickelous and ferric oxides by hydrogen', *Journal of the American Chemical Society*. American Chemical Society, 46(12), pp. 2728–2737. doi: 10.1021/ja01677a018.

References

Berndt, M. E., Allen, D. E. and Seyfried, W. E. (1996) 'Reduction of CO2 during serpentinization of olivine at 300C and 500 bar', *Geology*, 24(4), pp. 351–354. doi: 10.1130/0091-7613(1996)024.

Bhattacharya, P., Steele, P. H., Hassan, E. B. M., Mitchell, B., Ingram, L. and Pittman, C. U. (2009) 'Wood/plastic copyrolysis in an auger reactor: Chemical and physical analysis of the products', *Fuel*. Elsevier Ltd, 88(7), pp. 1251–1260. doi: 10.1016/j.fuel.2009.01.009.

Bhaumik, P. and Dhepe, P. L. (2016) 'Conversion of biomass into sugars', in Murzin, D. and Simakova, O. (eds) *Biomass Sugars for Non-Fuel Applications*. Cambridge: RSC Green Chemistry, pp. 1–53. doi: 10.1039/9781782622079-00001.

Bidlingmeyer, B. A. (1992) *Practical HPLC Methodology and Applications*. New York: John Wiley & Sons, Inc.

Blumberg, L. M. (2012) 'Theory of Gas Chromatography', in Poole, C. (ed.) *Gas Chromatography*. Amsterdam: Elsevier, pp. 19–78.

Blunt, M., Fayers, F. J. and Orr, F. M. (1993) 'Carbon dioxide in enhanced oil recovery', *Energy Conversion and Management*, 34(9–11), pp. 1197–1204. doi: 10.1016/0196-8904(93)90069-M.

Bonaventura, D., Chacartegui, R., Valverde, J. M., Becerra, J. A. and Verda, V. (2017) 'Carbon capture and utilization for sodium bicarbonate production assisted by solar thermal power', *Energy Conversion and Management*, 149, pp. 860–874. doi: 10.1016/j.enconman.2017.03.042.

Borovinskaya, E. S., Trebbin, S., Alscher, F. and Breitkopf, C. (2019) 'Synthesis, modification, and characterization of CuO/ZnO/ZrO2 mixed metal oxide catalysts for CO2/H2 conversion', *Catalysts*. MDPI AG, 9(12), p. 1037. doi: 10.3390/catal9121037.

Budiman, H., Nuryatini and Zuas, O. (2015) 'Comparison between GC-TCD and GC-FID for the determination of propane in gas mixture', *Procedia Chemistry*. Elsevier, 16, pp. 465–472. doi: 10.1016/J.PROCHE.2015.12.080.

Bursová, M., Hložek, T. and Čabala, R. (2015) 'Simultaneous determination of methanol, ethanol and formic acid in serum and urine by headspace GC-FID', *Journal of Analytical Toxicology*. Narnia, 39(9), pp. 741–745. doi: 10.1093/jat/bkv075.

References

Butler, J. N. (1991) *Carbon Dioxide Equilibria and their Applications*. 2nd edn. Chelsea: Lewis Publishers, Inc. doi: 10.1201/9781315138770.

Cai, J., Han, Y., Chen, S., Crumlin, E. J., Yang, B., Li, Y. and Liu, Z. (2019) 'CO2 Activation on Ni(111) and Ni(100) Surfaces in the Presence of H2O: An Ambient-Pressure X-ray Photoelectron Spectroscopy Study', *Journal of Physical Chemistry C*, 123(19), pp. 12176–12182. doi: 10.1021/acs.jpcc.8b11698.

Calvo, L. and Vallejo, D. (2002) 'Formation of organic acids during the hydrolysis and oxidation of several wastes in sub- and supercritical water', *Industrial and Engineering Chemistry Research*, 41(25), pp. 6503–6509. doi: 10.1021/ie020441m.

Cantero, D. A., Álvarez, A., Bermejo, M. D. and Cocero, M. J. (2015) 'Transformation of glucose into added value compounds in a hydrothermal reaction media', *Journal of Supercritical Fluids*. Elsevier, 98, pp. 204–210. doi: 10.1016/j.supflu.2014.12.015.

Centi, G., Quadrelli, E. A. and Perathoner, S. (2013) 'Catalysis for CO2 conversion: A key technology for rapid introduction of renewable energy in the value chain of chemical industries', *Energy and Environmental Science*, 6(6), pp. 1711–1731. doi: 10.1039/c3ee00056g.

Chaix, E., Guillaume, C. and Guillard, V. (2014) 'Oxygen and Carbon Dioxide Solubility and Diffusivity in Solid Food Matrices: A Review of Past and Current Knowledge', *Comprehensive Reviews in Food Science and Food Safety*. Blackwell Publishing Inc., 13(3), pp. 261–286. doi: 10.1111/1541-4337.12058.

Chang, C. J., Chiu, K. L., Chen, Y. L. and Chang, C. Y. (2000) 'Separation of catechins from green tea using carbon dioxide extraction', *Food Chemistry*, 68(1), pp. 109–113. doi: 10.1016/S0308-8146(99)00176-4.

Che Man, Y. B., Syahariza, Z. A. and Rohman, A. (2010) 'Fourier Transform Infrared (FTIR) Spectroscopy: Development, Techniques, and Application in the Analyses of Fats and Oils', in Rees, O. J. (ed.) *Fourier Transform Infrared Spectroscopy: Developments, Techniques and Applications*. New York: Nova Science Publishers, Incorporated, pp. 1–26.

Chen, Q. and Qian, Y. (2001) 'Carbon dioxide thermal system: An effective method for the reduction of carbon dioxide', *Chemical Communications*, (15), pp. 1402–1403. doi: 10.1039/b100183n.

References

Chen, Q. W. and Bahnemann, D. W. (2000) 'Reduction of carbon dioxide by magnetite: Implications for the primordial synthesis of organic molecules', *Journal of the American Chemical Society*, 122(5), pp. 970–971. doi: 10.1021/ja991278y.

Chen, X., Liu, Y. and Wu, J. (2020) 'Sustainable production of formic acid from biomass and carbon dioxide', *Molecular Catalysis*. Elsevier B.V., 483. doi: 10.1016/j.mcat.2019.110716.

Chen, X. Y., Sue Huh, H. and Lee, S. W. (2007) 'Hydrothermal synthesis of boehmite (γ-AlOOH) nanoplatelets and nanowires: pH-controlled morphologies', *Nanotechnology*. IOP Publishing, 18(28), p. 285608. doi: 10.1088/0957-4484/18/28/285608.

Cheng, F., Dupont, V. and Twigg, M. V. (2016) 'Temperature-programmed reduction of nickel steam reforming catalyst with glucose', *Applied Catalysis A: General*. Elsevier, 527, pp. 1–8. doi: 10.1016/J.APCATA.2016.08.013.

Chesny, H. H. (1932) 'Process of precipitating sodium bicarbonate from solutions in form of coarse crystals'. USA: United States. Available at: https://patents.google.com/patent/US1865832A/en.

Chetty, R., Varjani, S., Keerthiga, G., Srinath, S. and Rajmohan, K. S. (2019) 'Electrochemical Reduction of Carbon Dioxide into Useful Low-Carbon Fuels', in Winter, F., Agarwal, R. A., Hrdlicka, J., and Varjani, S. (eds) *CO2 Separation, Purification and Conversion to Chemicals and Fuels*. Singapore: Springer Nature, pp. 119–152. Available at: http://www.springer.com/series/15901.

Conner, W. C. and Falconer, J. L. (1995) 'Spillover in Heterogeneous Catalysis', *Chemical Reviews*. American Chemical Society, 95(3), pp. 759–788. doi: 10.1021/cr00035a014.

Corma Canos, A., Iborra, S. and Velty, A. (2007) 'Chemical routes for the transformation of biomass into chemicals', *Chemical Reviews*, 107(6), pp. 2411–2502. doi: 10.1021/cr050989d.

Cowan, B. (1997) 'Introduction', in *Nuclear Magnetic Resonance and Relaxation*. Cambridge: Cambridge University Press, pp. 1–19. doi: 10.1017/CBO9780511524226.002.

Crane, K. and Normark, W. R. (1977) 'Hydrothermal activity and crestal structure of the East Pacific Rise at 21°N', *Journal of Geophysical Research*. American Geophysical

References

Union (AGU), 82(33), pp. 5336–5348. doi: 10.1029/jb082i033p05336.

Cuéllar-Franca, R. M. and Azapagic, A. (2015) 'Carbon capture, storage and utilisation technologies: A critical analysis and comparison of their life cycle environmental impacts', *Journal of CO2 Utilization*. Elsevier Ltd, pp. 82–102. doi: 10.1016/j.jcou.2014.12.001.

Cui, S. T. and Harris, J. G. (1994) 'Ion association and liquid structure in supercritical water solutions of sodium chloride: a microscopic view from molecular dynamics simulations', *Chemical Engineering Science*. Pergamon, 49(17), pp. 2749–2763. doi: 10.1016/0009-2509(94)E0095-8.

Cummins, P. M., Rochfort, K. D. and O'Connor, B. F. (2017) 'Ion-exchange chromatography: Basic principles and application', in *Methods in Molecular Biology*. Humana Press, New York, NY, pp. 209–223. doi: 10.1007/978-1-4939-6412-3_11.

Damodaran, K. V., Nagarajan, V. S. and Rao, K. J. (1990) 'A molecular dynamics study of ZrO2 SiO2 system', *Journal of Non-Crystalline Solids*, 124(2–3), pp. 233–241. doi: 10.1016/0022-3093(90)90268-Q.

Dar, F. A., Sofi, A. H. and Shah, M. A. (2015) 'Boehmite (AlOOH) nanostrips and their growth mechanism', *International Nano Letters*, 5(2), pp. 67–70. doi: 10.1007/s40089-015-0138-7.

Davies, G., Driver, J., Ward, A., Negahdar, L. and Mcgregor, J. (2021) 'Operando studies of aerosol-assisted sol-gel catalyst synthesis via combined optical trapping and raman spectroscopy', *Journal of Physical Chemistry C*. American Chemical Society, 125(41), pp. 22591–22602. doi: 10.1021/acs.jpcc.1c07517.

DBEIS (2020) *2018 UK Greenhouse Gas Emissions, Final figures*, *National Statistics*. Available at: https://www.ipcc-nggip.iges.or.jp/public/2006gl/index.html (Accessed: 15 April 2020).

Deutschmann, O., Knözinger, H., Kochloefl, K. and Turek, T. (2011) 'Heterogeneous Catalysis and Solid Catalysts, 2. Development and Types of Solid Catalysts', in *Ullmann's Encyclopedia of Industrial Chemistry*, pp. 223–269. doi: 10.1002/14356007.o05.

Dirkse, T. P. (1986) 'Zinc Oxide and Hydroxide', in *Copper, Silver, Gold & Zinc, Cadmium, Mercury Oxides & Hydroxides*. NIST, pp. 156–269. doi: 10.1016/b978-0-08-

References

032497-5.50013-5.

Driggers, R. G., Friedman, M. H. and Nichols, J. (2012) *Introduction to Infrared and Electro-optical Systems*. Artech House. Available at: http://cds.cern.ch/record/1616763 (Accessed: 18 February 2022).

Ehlers, D., Czech, E., Quirin, K. W. and Weber, R. (2006) 'Distribution of aflatoxins between extract and extraction residue of paprika using supercritical carbon dioxide', *Phytochemical Analysis*. John Wiley & Sons, Ltd, 17(2), pp. 114–120. doi: 10.1002/pca.894.

Ekman, R., Silberring, J., Westman-Brinkmalm, A. M. and Kraj, A. (eds) (2009) *Mass Spectrometry: Instrumentation, Interpretation and Application*. Hoboken: John Wiley & Sons, Inc.

El-Kemary, M., Nagy, N. and El-Mehasseb, I. (2013) 'Nickel oxide nanoparticles: Synthesis and spectral studies of interactions with glucose', *Materials Science in Semiconductor Processing*. Pergamon, 16(6), pp. 1747–1752. doi: 10.1016/j.mssp.2013.05.018.

Elliott, D. C., Sealock, L. J. and Baker, E. (1994) 'Chemical Processing in High-Pressure Aqueous Environments. 3. Batch Reactor Process Development Experiments for Organics Destruction', *Industrial and Engineering Chemistry Research*, 33(3), pp. 558–565. doi: 10.1021/ie00027a012.

EPA (2019) *Inventory of U.S. Greenhouse Gas Emissions and Sinks*.

Farlow, M. W. and Adkins, H. (1935) 'The Hydrogenation of Carbon Dioxide and a Correction of the Reported Synthesis of Urethans', *J. Am. Chem. Soc.*, 57(11), pp. 2222–2223. doi: 10.1021/ja01314a054.

Feliczak-Guzik, A. (2018) 'Hierarchical zeolites: Synthesis and catalytic properties', *Microporous and Mesoporous Materials*. Elsevier Inc., 259, pp. 33–45. doi: 10.1016/j.micromeso.2017.09.030.

Feng, B., An, H. and Tan, E. (2007) 'Screening of CO_2 adsorbing materials for zero emission power generation systems', *Energy and Fuels*, 21(2), pp. 426–434. doi: 10.1021/ef0604036.

Fidalgo, B., Zubizarreta, L., Bermúdez, J. M., Arenillas, A. and Menéndez, J. A. (2010)

References

'Synthesis of carbon-supported nickel catalysts for the dry reforming of CH4', *Fuel Processing Technology*, 91(7), pp. 765–769. doi: 10.1016/j.fuproc.2010.02.011.

Fisher, I. A. and Bell, A. T. (1997) 'In-situ infrared study of methanol synthesis from H2/CO2 over Cu/SiO2 and Cu/ZrO2/SiO2', *Journal of Catalysis*, 172(1), pp. 222–237. doi: 10.1006/jcat.1997.1870.

Galkin, S. V. and Demina, L. (2016) *Trace metal biogeochemistry and ccology of deep-sea hydrothermal vent systems*, *Handbook of Environmental Chemistry*. Edited by L. Demina and S. V. Galkin. Switzerland: Springer International Publishing. doi: 10.1007/698_2016_3.

Gangwal, S., Meng, J., McCabe, K., Larson, E. and Mastro, K. (2016) *Mild Biomass Liquefaction Process for Economic Production of Stabilized Refinery-Ready Bio-oil*. Golden, CO (United States). doi: 10.2172/1337870.

Gao, P., Li, G., Yang, F., Lv, X. N., Fan, H., Meng, L. and Yu, X. Q. (2013) 'Preparation of lactic acid, formic acid and acetic acid from cotton cellulose by the alkaline pre-treatment and hydrothermal degradation', *Industrial Crops and Products.* Elsevier, 48, pp. 61–67. doi: 10.1016/j.indcrop.2013.04.002.

George, R. M. (1993) 'Freezing proceseses used in the food industry', *Trends in Food Science and Technology*, 4(5), pp. 134–138. doi: 10.1016/0924-2244(93)90032-6.

Gjernes, E., Helgesen, L. I. and Maree, Y. (2013) 'Health and environmental impact of amine based post combustion CO 2 capture', in *Energy Procedia*, pp. 735–742. doi: 10.1016/j.egypro.2013.05.162.

Godart, P., Fischman, J., Seto, K. and Hart, D. (2019) 'Hydrogen production from aluminum-water reactions subject to varied pressures and temperatures', *International Journal of Hydrogen Energy*. Pergamon, 44(23), pp. 11448–11458. doi: 10.1016/j.ijhydene.2019.03.140.

Goeppert, A., Czaun, M., Jones, J. P., Surya Prakash, G. K. and Olah, G. A. (2014) 'Recycling of carbon dioxide to methanol and derived products-closing the loop', *Chemical Society Reviews*, pp. 7995–8048. doi: 10.1039/c4cs00122b.

Gomez, L. Q., Shehab, A. K., Al-Shathr, A., Ingram, W., Konstantinova, M., Cumming, D. and McGregor, J. (2020) 'H2-free Synthesis of Aromatic, Cyclic and Linear Oxygenates from CO2', *ChemSusChem*. Wiley-VCH Verlag, 13(3), pp. 647–658. doi:

References

10.1002/cssc.201902340.

Griffin, P. W., Hammond, G. P. and Norman, J. B. (2018) 'Industrial energy use and carbon emissions reduction in the chemicals sector: A UK perspective', *Applied Energy*, 227, pp. 587–602. doi: 10.1016/j.apenergy.2017.08.010.

Gross, J. H. (2017) 'Introduction', in *Mass Spectrometry*. Third Ed. Springer International Publishing, pp. 1–28. doi: 10.1007/978-3-319-54398-7.

Gui, X., Tang, Z. and Fei, W. (2011) 'Solubility of CO2 in alcohols, glycols, ethers, and ketones at high pressures from (288.15 to 318.15) K', *Journal of Chemical and Engineering Data*, 56(5), pp. 2420–2429. doi: 10.1021/je101344v.

Günther, H. (2013) 'The Physical Basis of the Nuclear Magnetic Resonance Experiment', in *NMR Spectroscopy. Basic Principles, Concepts and Applications in Chemistry*. Wiley-VCH, pp. 13–28. Available at: https://www.wiley.com/en-gb/NMR+Spectroscopy%3A+Basic+Principles%2C+Concepts+and+Applications+in+Chemistry%2C+3rd+Edition-p-9783527330003 (Accessed: 18 February 2022).

Hahn, M. W., Copeland, J. R., Vanpelt, A. H. and Sievers, C. (2013) 'Stability of amorphous silica-alumina in hot liquid water', *ChemSusChem*. John Wiley & Sons, Ltd, 6(12), pp. 2304–2315. doi: 10.1002/cssc.201300532.

Hakim, A., Marliza, T. S., Abu Tahari, N. M., Wan Isahak, R. W. N., Yusop, R. M., Mohamed Hisham, W. M. and Yarmo, A. M. (2016) 'Studies on CO2Adsorption and Desorption Properties from Various Types of Iron Oxides (FeO, Fe2O3, and Fe3O4)', *Industrial and Engineering Chemistry Research*, 55(29), pp. 7888–7897. doi: 10.1021/acs.iecr.5b04091.

Han, S. J., Yoo, M., Kim, D. W. and Wee, J. H. (2011) 'Carbon dioxide capture using calcium hydroxide aqueous solution as the absorbent', *Energy and Fuels*, 25(8), pp. 3825–3834. doi: 10.1021/ef200415p.

Hardy, L. I. and Gillham, R. W. (2002) 'Formation of Hydrocarbons from the Reduction of Aqueous CO 2 by Zero-Valent Iron', *Environmental Science & Technology*, 30(1), pp. 57–65. doi: 10.1021/es950054m.

Harwood, L. M. and Claridge, T. D. W. (1997) 'Nuclear magnetic resonance spectroscopy: the basics', in *Introduction to Organic Spectroscopy*. Oxford: Oxford University Press, pp. 33–54.

References

Hayashi, H., Taniuchi, J., Furuyashiki, N., Sugiyama, S., Hirano, S., Shigemoto, N. and Nonaka, T. (1998) 'Efficient Recovery of Carbon Dioxide from Flue Gases of Coal-Fired Power Plants by Cyclic Fixed-Bed Operations over K2CO3-on-Carbon', *Industrial and Engineering Chemistry Research*, 37(1), pp. 185–191. doi: 10.1021/ie9704455.

He, C., Tian, G., Liu, Z. and Feng, S. (2010) 'A mild hydrothermal route to fix carbon dioxide to simple carboxylic acids', *Organic Letters*. Cambridge University Press, 12(4), pp. 649–651. doi: 10.1021/ol9025414.

He, R., Hu, B., Zhong, H., Jin, F., Fan, J., Hu, Y. H. and Jing, Z. (2019) 'Reduction of CO2 with H2S in a simulated deep-sea hydrothermal vent system', *Chemical Communications*. The Royal Society of Chemistry, 55(8), pp. 1056–1059. doi: 10.1039/c8cc08075e.

Hicks, J. C., Drese, J. H., Fauth, D. J., Gray, M. L., Qi, G. and Jones, C. W. (2008) 'Designing adsorbents for CO2 capture from flue gas-hyperbranched aminosilicas capable of capturing CO2 reversibly', *Journal of the American Chemical Society*, 130(10), pp. 2902–2903. doi: 10.1021/ja077795v.

Horita, J. and Berndt, M. E. (1999) 'Abiogenic methane formation and isotopic fractionation under hydrothermal conditions', *Science*. American Association for the Advancement of Science, 285(5430), pp. 1055–1057. doi: 10.1126/science.285.5430.1055.

Hotchkiss, J. H., Werner, B. G. and Lee, E. Y. C. (2006) 'Addition of Carbon Dioxide to Dairy Products to Improve Quality: A Comprehensive Review', *Comprehensive Reviews in Food Science and Food Safety*. John Wiley & Sons, Ltd, 5(4), pp. 158–168. doi: 10.1111/j.1541-4337.2006.00008.x.

Huang, C., Chen, S., Fei, X., Liu, D. and Zhang, Y. (2015) 'Catalytic Hydrogenation of CO2 to Methanol: Study of Synergistic Effect on Adsorption Properties of CO2 and H2 in CuO/ZnO/ZrO2 System', *Catalysts*, 5(4), pp. 1846–1861. doi: 10.3390/catal5041846.

Hunt, A. J., Sin, E. H. K., Marriott, R. and Clark, J. H. (2010) 'Generation, capture, and utilization of industrial carbon dioxide', *ChemSusChem*. Wiley-VCH Verlag, 3(3), pp. 306–322. doi: 10.1002/cssc.200900169.

Hunter, S. E. and Savage, P. E. (2003) 'Acid-catalyzed reactions in carbon dioxide-enriched high-temperature liquid water', *Industrial and Engineering Chemistry*

References

Research, 42(2), pp. 290–294. doi: 10.1021/ie020565z.

Hunter, S. E. and Savage, P. E. (2008) 'Quantifying rate enhancements for acid catalysis in CO2-enriched high-temperature water', *AIChE Journal*, 54(2), pp. 516–528. doi: 10.1002/aic.11392.

Huo, Z., Hu, M., Zeng, X., Yun, J. and Jin, F. (2012) 'Catalytic reduction of carbon dioxide into methanol over copper under hydrothermal conditions', in *Catalysis Today*, pp. 25–29. doi: 10.1016/j.cattod.2012.06.013.

IEA (2011) *Carbon Capture and Storage in Industrial Applications*, *Technology Roadmap*. doi: 10.1007/1-4020-0612-8_961.

IEA (2019a) *Putting CO2 to Use: Creating value from emissions*. Available at: https://www.iea.org/topics/carbon-capture-and-storage/policiesandinvestment/ (Accessed: 21 April 2020).

IEA (2019b) *The Future of Hydrogen*. Paris. Available at: https://www.iea.org/reports/the-future-of-hydrogen.

Inoue, T., Fujishima, A., Konishi, S. and Honda, K. (1979) 'Photoelectrocatalytic reduction of carbon dioxide in aqueous suspensions of semiconductor powders', *Nature*, 277, pp. 637–638.

Isahak, W. N. R. W., Hisham, M. W., Yarmo, M. A. and Yun Hin, T. Y. (2012) 'A review on bio-oil production from biomass by using pyrolysis method', *Renewable and Sustainable Energy Reviews*, 16(8), pp. 5910–5923. doi: 10.1016/j.rser.2012.05.039.

Jana, A. K. (2018) 'Continuous Stirred Tank Reactor', in *Chemical Process Modelling and Computer Simulation*. Delhi: PHI Learning Pvt. Ltd., pp. 75–104.

Jenkins, R. and Snyder, R. L. (1996) *Introduction to X-ray Powder Diffractometry*, *Introduction to X-ray Powder Diffractometry*. Hoboken, NJ, USA: John Wiley & Sons, Inc. doi: 10.1002/9781118520994.

Jessop, P. G. and Subramaniam, B. (2007) 'Gas-expanded liquids', *Chemical Reviews*, 107(6), pp. 2666–2694. doi: 10.1021/cr040199o.

Ji, F., Zhou, H. and Yang, Q. (2008) 'The abiotic formation of hydrocarbons from dissolved CO2 under hydrothermal conditions with cobalt-bearing magnetite', *Origins of Life and Evolution of Biospheres*, 38(2), pp. 117–125. doi: 10.1007/s11084-008-

References

9124-7.

Jiménez-González, C., Constable, D. J. C. and Ponder, C. S. (2012) 'Evaluating the "greenness" of chemical processes and products in the pharmaceutical industry - A green metrics primer', *Chemical Society Reviews*, 41(4), pp. 1485–1498. doi: 10.1039/c1cs15215g.

Jin, F., Gao, Y., Jin, Y., Zhang, Y., Cao, J., Wei, Z. and Smith, R. L. (2011) 'High-yield reduction of carbon dioxide into formic acid by zero-valent metal/metal oxide redox cycles', *Energy and Environmental Science*, 4(3), pp. 881–884. doi: 10.1039/c0ee00661k.

Jin, F., Yun, J., Li, G., Kishita, A., Tohji, K. and Enomoto, H. (2008) 'Hydrothermal conversion of carbohydrate biomass into formic acid at mild temperatures', *Green Chemistry*, 10(6), pp. 612–615. doi: 10.1039/b802076k.

Jin, F., Zeng, X., Liu, J., Jin, Y., Wang, L., Zhong, H., Yao, G. and Huo, Z. (2014) 'Highly efficient and autocatalytic H 2 O dissociation for CO 2 reduction into formic acid with zinc', *Scientific Reports*, 4. doi: 10.1038/srep04503.

Jindal, M. K. and Jha, M. K. (2016) 'Catalytic Hydrothermal Liquefaction of Waste Furniture Sawdust to Bio-oil', *Indian Chemical Engineer*. Taylor and Francis Ltd., 58(2), pp. 157–171. doi: 10.1080/00194506.2015.1006145.

Jing, S., Cao, X., Zhong, L., Peng, X., Sun, R. and Liu, J. (2018) 'Effectively enhancing conversion of cellulose to HMF by combining in-situ carbonic acid from CO2 and metal oxides', *Industrial Crops and Products*. Elsevier B.V., 126, pp. 151–157. doi: 10.1016/j.indcrop.2018.10.028.

Joni, I. M., Nulhakim, L., Vanitha, M. and Panatarani, C. (2018) 'Characteristics of crystalline silica (SiO2) particles prepared by simple solution method using sodium silicate (Na2SiO3) precursor', in *Journal of Physics: Conference Series*. doi: 10.1088/1742-6596/1080/1/012006.

Jović, V. D., Maksimović, V., Pavlović, M. G. and Popov, K. I. (2006) 'Morphology, internal structure and growth mechanism of electrodeposited Ni and Co powders', *Journal of Solid State Electrochemistry*, 10(6), pp. 373–379. doi: 10.1007/s10008-005-0687-1.

Jung, H. J. and Choi, M. Y. (2014) 'Specific solvent produces specific phase Ni

References

nanoparticles: A pulsed laser ablation in solvents', *Journal of Physical Chemistry C*. American Chemical Society, 118(26), pp. 14647–14654. doi: 10.1021/jp503009a.

Kabra, S. K., Turpeinen, E., Huuhtanen, M., Keiski, R. L. and Yadav, G. D. (2016) 'Direct synthesis of formic acid from carbon dioxide and hydrogen: A thermodynamic and experimental study using poly-urea encapsulated catalysts', *Chemical Engineering Journal*, 285, pp. 625–634. doi: 10.1016/j.cej.2015.09.101.

Kalnay, E. and Cai, M. (2003) 'Impact of urbanization and land-use change on climate', *Nature*. Nature Publishing Group, 423(6939), pp. 528–531. doi: 10.1038/nature01675.

Karagül-Yüceer, Y., Coggins, P. C., Wilson, J. C. and White, C. H. (1999) 'Carbonated Yogurt - Sensory Properties and Consumer Acceptance', *Journal of Dairy Science*, 82(7), pp. 1394–1398. doi: 10.3168/jds.S0022-0302(99)75365-8.

Karatzas, X., Jansson, K., González, A., Dawody, J. and Pettersson, L. J. (2011) 'Autothermal reforming of low-sulfur diesel over bimetallic RhPt supported on Al2O3, CeO2-ZrO2, SiO2 and TiO2', *Applied Catalysis B: Environmental*. Elsevier, 106(3–4), pp. 476–487. doi: 10.1016/j.apcatb.2011.06.006.

Karelovic, A., Bargibant, A., Fernandez Rojas, C. and Ruiz, P. (2012) 'Effect of the structural and morphological properties of Cu/ZnO catalysts prepared by citrate method on their activity toward methanol synthesis from CO2 and H2 under mild reaction conditions', *Catalysis Today*. Elsevier Science Publishers, 197(2012), pp. 109–118. doi: 10.1016/j.cattod.2012.07.029.

Katryniok, B., Paul, S. and Dumeignil, F. (2013) 'Recent developments in the field of catalytic dehydration of glycerol to acrolein', *ACS Catalysis*. American Chemical Society, 3(8), pp. 1819–1834. doi: 10.1021/cs400354p.

Kishita, A., Sugai, Y., Koizumi, S., Jin, F., Enomoto, H. and Moriya, T. (2005) *Hydrothermal Cracking of Polyethylene, Polypropylene, and/or Polystyrene Mixtures under Supercritical Water Condition*, *J. Jpn. Pet. Inst.* doi: 10.4144/rpsj.52.14.

Kishita, A., Takahashi, S., Kamimura, H., Miki, M., Moriya, T. and Enomoto, H. (2003) 'Upgrading of Bitumen by Hydrothermal Visbreaking in Supercritical Water with Alkali', *J. Jpn. Pet. Inst.*, 46(4), pp. 215–221.

Klee, M. S. (2012) 'Detectors', in Poole, C. (ed.) *Gas Chromatography*. Amsterdam:

References

Elsevier B.V., pp. 301–342.

Koven, A. B., Tong, S. S., Farnood, R. R. and Jia, C. Q. (2017) 'Alkali-thermal gasification and hydrogen generation potential of biomass', *Frontiers of Chemical Science and Engineering*. Higher Education Press, 11(3), pp. 369–378. doi: 10.1007/s11705-017-1662-y.

Kregiel, D. (2015) 'Health safety of soft drinks: Contents, containers, and microorganisms', *BioMed Research International*, 2015. doi: 10.1155/2015/128697.

Kresse, G. (2000) 'Dissociation and sticking of H2 on the Ni(111), (100), and (110) substrate', *Physical Review B - Condensed Matter and Materials Physics*. American Physical Society, 62(12), pp. 8295–8305. doi: 10.1103/PhysRevB.62.8295.

Kruse, A. (2009) 'Hydrothermal biomass gasification', *Journal of Supercritical Fluids*, 47(3), pp. 391–399. doi: 10.1016/j.supflu.2008.10.009.

Kruse, A. and Dinjus, E. (2007) 'Hot compressed water as reaction medium and reactant. Properties and synthesis reactions', *Journal of Supercritical Fluids*, 39(3), pp. 362–380. doi: 10.1016/j.supflu.2006.03.016.

Kuhlmann, B., Arnett, E. M. and Siskin, M. (1994) 'Classical Organic Reactions in Pure Superheated Water', *Journal of Organic Chemistry*, 59(11), pp. 3098–3101. doi: 10.1021/jo00090a030.

Van Der Laan, G. P. and Beenackers, A. A. C. M. (1999) 'Catalysis Reviews Science and Engineering Kinetics and Selectivity of the Fischer-Tropsch Synthesis: A Literature Review Kinetics and Selectivity of the Fischer-Tropsch Synthesis: A Literature Review', *CATAL. REV.-SCI. ENG*, 41(4), pp. 255–318. doi: 10.1081/CR-100101170.

Lange, J. P. (2001) 'Methanol synthesis: A short review of technology improvements', *Catalysis Today*, 64(1–2), pp. 3–8. doi: 10.1016/S0920-5861(00)00503-4.

Laurenczy, G., Joo, F. and Nadasdi, L. (2000) 'Formation and characterization of water-soluble hydrido-ruthenium(II) complexes of 1,3,5-triaza-7-phosphaadamantane and their catalytic activity in hydrogenation of CO2 and HCO3- in aqueous solution', *Inorganic Chemistry*. American Chemical Society, 39(22), pp. 5083–5088. doi: 10.1021/ic000200b.

Lazar, M., Varghese, S. and Nair, S. (2012) 'Photocatalytic Water Treatment by

References

Titanium Dioxide: Recent Updates', *Catalysts*, 2(4), pp. 572–601. doi: 10.3390/catal2040572.

Lazzarini, A., Piovano, A., Pellegrini, R., Agostini, G., Rudić, S., Lamberti, C. and Groppo, E. (2016) 'Graphitization of Activated Carbons: A Molecular-level Investigation by INS, DRIFT, XRD and Raman Techniques', in *Physics Procedia*. Elsevier, pp. 20–26. doi: 10.1016/j.phpro.2016.11.076.

Le, Y., Zhong, H., Yang, Y., He, R., Yao, G. and Jin, F. (2017) 'Mechanism study of reduction of CO 2 into formic acid by in-situ hydrogen produced from water splitting with Zn: Zn/ZnO interface autocatalytic role', *Journal of Energy Chemistry*, 26(5), pp. 936–941. doi: 10.1016/j.jechem.2017.03.013.

Leeke, G., Gaspar, F. and Santos, R. (2002) 'Influence of water on the extraction of essential oils from a model herb using supercritical carbon dioxide', *Industrial and Engineering Chemistry Research*, 41(8), pp. 2033–2039. doi: 10.1021/ie010845z.

Lermontov, S. A., Shkavrov, S. V. and Kuryleva, N. V. (2003) 'Uncatalyzed Meerwein-Ponndorf-Verley reduction of trifluoromethyl carbonyl compounds by high-temperature secondary alcohols', *Journal of Fluorine Chemistry*, 121(2), pp. 223–225. doi: 10.1016/S0022-1139(03)00036-8.

Leung, D. Y. C., Caramanna, G. and Maroto-Valer, M. M. (2014) 'An overview of current status of carbon dioxide capture and storage technologies', *Renewable and Sustainable Energy Reviews*. Elsevier, 39, pp. 426–443. doi: 10.1016/j.rser.2014.07.093.

Li, C. and Chen, Y. W. (1995) 'Temperature-programmed-reduction studies of nickel oxide/alumina catalysts: effects of the preparation method', *Thermochimica Acta*. Elsevier, 256(2), pp. 457–465. doi: 10.1016/0040-6031(94)02177-P.

Li, H., Fang, Z., Smith, R. L. and Yang, S. (2016) 'Efficient valorization of biomass to biofuels with bifunctional solid catalytic materials', *Progress in Energy and Combustion Science*. Elsevier Ltd, pp. 98–194. doi: 10.1016/j.pecs.2016.04.004.

Li, L., Zhang, X., Luan, Z., Du, Z., Xi, S., Wang, B., Cao, L., Lian, C. and Yan, J. (2018) 'In Situ Quantitative Raman Detection of Dissolved Carbon Dioxide and Sulfate in Deep-Sea High-Temperature Hydrothermal Vent Fluids', *Geochemistry, Geophysics, Geosystems*. John Wiley & Sons, Ltd, 19(6), pp. 1809–1823. doi: 10.1029/2018GC007445.

References

Lim, L. T., Auras, R. and Rubino, M. (2008) 'Processing technologies for poly(lactic acid)', *Progress in Polymer Science (Oxford)*, pp. 820–852. doi: 10.1016/j.progpolymsci.2008.05.004.

Lindsay, S. (1992) *High performance liquid chromatography*. 2nd edn, *ACOL*. 2nd edn. Edited by J. Barnes. Chichester: John Wiley & Sons, Inc. doi: 10.12968/hmed.2014.75.Sup2.C18.

Lindsey, A. S. and Jeskey, H. (1957) 'The Kolbe-Schmitt Reaction', *Chem. Rev.*, 57(4), pp. 583–620. doi: 10.1021/cr50016a001.

Lingampalli, S. R., Ayyub, M. M. and Rao, C. N. R. (2017) 'Recent Progress in the Photocatalytic Reduction of Carbon Dioxide', *ACS Omega*, 2(6), pp. 2740–2748. doi: 10.1017/CBO9781107415324.004.

Liu, C., Shih, K., Gao, Y., Li, F. and Wei, L. (2012) 'Dechlorinating transformation of propachlor through nucleophilic substitution by dithionite on the surface of alumina', *Journal of Soils and Sediments*, 12(5), pp. 724–733. doi: 10.1007/s11368-012-0506-0.

Liu, Q., Cao, X., Wang, T., Wang, C., Zhang, Q. and Ma, L. (2015) 'Synthesis of shape-controllable cobalt nanoparticles and their shape-dependent performance in glycerol hydrogenolysis', *RSC Advances*. Royal Society of Chemistry, 5(7), pp. 4861–4871. doi: 10.1039/c4ra13395a.

Liu, Q., Yang, X., Li, L., Miao, S., Li, Yong, Li, Yanqin, Wang, X., Huang, Y. and Zhang, T. (2017) 'Direct catalytic hydrogenation of CO2 to formate over a Schiff-base-mediated gold nanocatalyst', *Nature Communications*, 8(1). doi: 10.1038/s41467-017-01673-3.

Liu, Z., Tian, G., Zhu, S., He, C., Yue, H. and Feng, S. (2013) 'Ready hydrothermal reactions from carbon dioxide to methane', *ACS Sustainable Chemistry and Engineering*, 1(3), pp. 313–315. doi: 10.1021/sc3001146.

Lu, L., Zhong, H., Wang, T., Wu, J., Jin, F. and Yoshioka, T. (2020) 'A new strategy for CO2 utilization with waste plastics: Conversion of hydrogen carbonate into formate using polyvinyl chloride in water', *Green Chemistry*, 22(2), pp. 352–358. doi: 10.1039/c9gc02484k.

Lu, Q. and Jiao, F. (2016) 'Electrochemical CO2 reduction: Electrocatalyst, reaction mechanism, and process engineering', *Nano Energy*, 29, pp. 439–456. doi: 10.1016/j.nanoen.2016.04.009.

References

Lundsted, L. G. (1949) 'The Hydrogenation of Sodium Bicarbonate to Sodium Formate', *Journal of the American Chemical Society*, 71(1), pp. 323–324. doi: 10.1021/ja01169a090.

Lyu, L., Jin, F., Zhong, H., Chen, H. and Yao, G. (2015) 'A novel approach to reduction of CO_2 into methanol by water splitting with aluminum over a copper catalyst', *RSC Advances*, 5(40), pp. 31450–31453. doi: 10.1039/c5ra02872h.

Lyu, L., Zeng, X., Yun, J., Wei, F. and Jin, F. (2014) 'No catalyst addition and highly efficient dissociation of H_2O for the reduction of CO_2 to formic acid with Mn', *Environmental Science and Technology*, 48(10), pp. 6003–6009. doi: 10.1021/es405210d.

Lyu, S., Wang, L., Zhang, J., Liu, C., Sun, J., Peng, B., Wang, Y., Rappé, K. G., Zhang, Y., Li, J. and Nie, L. (2018) 'Role of Active Phase in Fischer-Tropsch Synthesis: Experimental Evidence of CO Activation over Single-Phase Cobalt Catalysts', *ACS Catalysis*. American Chemical Society, 8(9), pp. 7787–7798. doi: 10.1021/acscatal.8b00834.

Majedi, A., Davar, F. and Abbasi, A. (2014) 'Sucrose-mediated sol–gel synthesis of nanosized pure and S-doped zirconia and its catalytic activity for the synthesis of acetyl salicylic acid', *Journal of Industrial and Engineering Chemistry*. Elsevier, 20(6), pp. 4215–4223. doi: 10.1016/J.JIEC.2014.01.023.

Martínez, J., Hernández, E., Alfaro, S., Medina, R. L., Aguilar, G. V., Albiter, E. and Valenzuela, M. A. (2019) 'High selectivity and stability of nickel catalysts for CO_2 Methanation: Support effects', *Catalysts*. MDPI AG, 9(1), p. 24. doi: 10.3390/catal9010024.

Matsumoto, T., Kubota, J., Kondo, J. N., Hirose, C. and Domen, K. (1999) 'Adsorption structures of carbon dioxide on NiO(111) and hydroxylated NiO(111) studied by infrared reflection adsorption spectroscopy', *Langmuir*. American Chemical Society, 15(6), pp. 2158–2161. doi: 10.1021/la9810298.

Matsuno, K. (2016) 'Hydrothermal Reaction', in *Encyclopedia of Astrobiology*. Berlin, Heidelberg: Springer Berlin Heidelberg, pp. 1160–1162. doi: 10.1007/978-3-662-44185-5_760.

McCollom, T. M. and Seewald, J. S. (2001) 'A reassessment of the potential for reduction of dissolved CO_2 to hydrocarbons during serpentinization of olivine',

References

Geochimica et Cosmochimica Acta, 65(21), pp. 3769–3778. doi: 10.1016/S0016-7037(01)00655-X.

McDowell, L. A. and Johnston, H. L. (1936) 'The Solubility of Cupric Oxide in Alkali and the Second Dissociation Constant of Cupric Acid. The Analysis of Very Small Amounts of Copper', *Journal of the American Chemical Society*. American Chemical Society, 58(10), pp. 2009–2014. doi: 10.1021/ja01301a054.

McMaster, M. C. and McMaster, C. (1998) *GC/MS : a practical user's guide*. New York: Wiley. Available at: https://books.google.com/books/about/GC_MS.html?id=a2FsQgAACAAJ

Meisel, T., Halmos, Z., Seybold, K. and Pungor, E. (1975) 'The thermal decomposition of alkali metal formates', *Journal of Thermal Analysis*, 7, pp. 73–80.

Merabti, R., Bachari, K., Halliche, D., Rassoul, Z. and Saadi, A. (2010) 'Synthesis and characterization of activated carbon-supported copper or nickel and their catalytic behavior towards benzaldehyde hydrogenation', *Reaction Kinetics, Mechanisms and Catalysis*. Springer, 101(1), pp. 195–208. doi: 10.1007/s11144-010-0215-x.

Metz, B., Davidson, O., De Coninck, H., Loos, M. and Meyer, L. (2005) *Carbon dioxide capture and storage*, *IPCC Special Report*. doi: 10.1557/mrs2008.63.

Michiels, K., Peeraer, B., Van Dun, W., Spooren, J. and Meynen, V. (2015) 'Hydrothermal conversion of carbon dioxide into formate with the aid of zerovalent iron: The potential of a two-step approach', *Faraday Discussions*. Royal Society of Chemistry, 183, pp. 177–195. doi: 10.1039/c5fd00104h.

Milanović, M., Obrenović, Z., Stijepović, I. and Nikolić, L. M. (2018) 'Nanocrystalline boehmite obtained at room temperature', *Ceramics International*. Elsevier Ltd, 44(11), pp. 12917–12920. doi: 10.1016/j.ceramint.2018.04.103.

Miller, M. B., Chen, D. L., Luebke, D. R., Johnson, J. K. and Enick, R. M. (2011) 'Critical assessment of CO2 solubility in volatile solvents at 298.15 K', *Journal of Chemical and Engineering Data*, 56(4), pp. 1565–1572. doi: 10.1021/je101161d.

Minowa, T. and Inoue, S. (1999) 'Hydrogen production from biomass by catalytic gasification in hot compressed water', *Renewable Energy*, 16(1–4), pp. 1114–1117. doi: 10.1016/s0960-1481(98)00436-4.

References

Mironenko, R. M., Belskaya, O. B., Talsi, V. P., Gulyaeva, T. I., Kazakov, M. O., Nizovskii, A. I., Kalinkin, A. V., Bukhtiyarov, V. I., Lavrenov, A. V. and Likholobov, V. A. (2014) 'Effect of γ-Al2O3 hydrothermal treatment on the formation and properties of platinum sites in Pt/γ-Al2O 3 catalysts', *Applied Catalysis A: General*. Elsevier, 469, pp. 472–482. doi: 10.1016/j.apcata.2013.10.027.

Miyazawa, T. and Funazukuri, T. (2005) 'Polysaccharide hydrolysis accelerated by adding carbon dioxide under hydrothermal conditions', *Biotechnology Progress*, 21(6), pp. 1782–1785. doi: 10.1021/bp050214q.

Mohanty, U. S., Rintala, L., Halli, P., Taskinen, P. and Lundström, M. (2018) 'Hydrometallurgical approach for leaching of metals from copper rich side stream originating from base metal production', *Metals*, 8(1). doi: 10.3390/met8010040.

Moldoveanu, S. C. and David, V. (2013) 'Basic Information about HPLC', in *Essentials in Modern HPLC Separations*. Waltham , MA: Elsevier, pp. 1–51. doi: 10.1016/b978-0-12-385013-3.00001-x.

Moldoveanu, S. and David, V. (2013) *Essentials in Modern HPLC Separations*. Amsterdam: Elsevier.

Möller, M., Nilges, P., Harnisch, F. and Schröder, U. (2011) 'Subcritical Water as Reaction Environment: Fundamentals of Hydrothermal Biomass Transformation', *ChemSusChem*, 4(5), pp. 566–579. doi: 10.1002/cssc.201000341.

Moret, S., Dyson, P. J. and Laurenczy, G. (2014) 'Direct synthesis of formic acid from carbon dioxide by hydrogenation in acidic media', *Nature Communications*. Nature Publishing Group, 5(1), p. 4017. doi: 10.1038/ncomms5017.

Morgan, N. Y. and Smith, P. D. (2010) 'HPLC Detectors', in Corradini, D. and Philips, T. M. (eds) *Handbook of HPLC*. 2nd Ed. Boca Raton: Taylor & Francis Group, pp. 207–228.

Morrison, A. R. T., van Beusekom, V., Ramdin, M., van den Broeke, L. J. P., Vlugt, T. J. H. and de Jong, W. (2019) 'Modeling the Electrochemical Conversion of Carbon Dioxide to Formic Acid or Formate at Elevated Pressures', *Journal of The Electrochemical Society*, 166(4), pp. E77–E86. doi: 10.1149/2.0121904jes.

Mortensen, P. M., Gardini, D., De Carvalho, H. W. P., Damsgaard, C. D., Grunwaldt, J. D., Jensen, P. A., Wagner, J. B. and Jensen, A. D. (2014) 'Stability and resistance of nickel catalysts for hydrodeoxygenation: Carbon deposition and effects of sulfur, potassium,

References

and chlorine in the feed', *Catalysis Science and Technology*. Royal Society of Chemistry, 4(10), pp. 3672–3686. doi: 10.1039/c4cy00522h.

Murphy, P. J. and Meyer, G. (1998) 'A gold-copper association in ultramafic-hosted hydrothermal sulfides from the Mid-Atlantic Ridge', *Economic Geology*. GeoScienceWorld, 93(7), pp. 1076–1083. doi: 10.2113/gsecongeo.93.7.1076.

Nahar, S., Zain, M. F. M., Kadhum, A. A. H., Hasan, H. A. and Hasan, M. R. (2017) 'Advances in photocatalytic CO2 reduction with water: A review', *Materials*, 10(6). doi: 10.3390/ma10060629.

Natarajan, E., Nordin, A. and Rao, A. N. (1998) 'Overview of combustion and gasification of rice husk in fluidized bed reactors', *Biomass and Bioenergy*, 14(5–6), pp. 533–546. doi: 10.1016/S0961-9534(97)10060-5.

Navarro, M., May, P. M., Hefter, G. and Königsberger, E. (2014) 'Solubility of CuO(s) in highly alkaline solutions', *Hydrometallurgy*. Elsevier, 147–148, pp. 68–72. doi: 10.1016/j.hydromet.2014.04.018.

Naydowski, C. (2001) 'Calcium Carbonate and Its Industrial Application', in Tegethoff, F. W. (ed.) *Calcium Carbonate: From the Cretaceous Period into the 21st Century*. Basel: Springer, pp. 199–274. doi: 10.2165/00128415-201113760-00029.

Neiva, E. G. C., Oliveira, M. M., Marcolino, L. H. and Zarbin, A. J. G. (2016) 'Nickel nanoparticles with hcp structure: Preparation, deposition as thin films and application as electrochemical sensor', *Journal of Colloid and Interface Science*. Academic Press, 468, pp. 34–41. doi: 10.1016/j.jcis.2016.01.036.

Nelson, T. O., Coleman, L. J. I., Green, D. A. and Gupta, R. P. (2009) 'The dry carbonate process: Carbon dioxide recovery from power plant flue gas', in *Energy Procedia*, pp. 1305–1311. doi: 10.1016/j.egypro.2009.01.171.

Ni, Z., Zhong, H., Yang, Y., Yao, G., Jin, B. and Jin, F. (2019) 'One-Step Conversion of NaHCO3 into Formate and Simultaneous Synthesis of AlO(OH) from Waste Al-Can in Water', *ACS Sustainable Chemistry and Engineering*, 7(6), pp. 5827–5834. doi: 10.1021/acssuschemeng.8b05681.

Nielsen, M., Hafreager, A., Brogaard, R. Y., De Wispelaere, K., Falsig, H., Beato, P., Van Speybroeck, V. and Svelle, S. (2019) 'Collective action of water molecules in zeolite dealumination', *Catalysis Science and Technology*, 9(14), pp. 3721–3725. doi:

References

10.1039/c9cy00624a.

Nielsen, R. H. and Wilfing, G. (2010) 'Zirconium and Zirconium Compounds', in *Ullmann's Encyclopedia of Industrial Chemistry*. Weinheim, Germany: Wiley-VCH Verlag GmbH & Co. KGaA, pp. 753–778. doi: 10.1002/14356007.a28_543.pub2.

Nölte, J. (2021) *ICP Emission Spectrometry : A Practical Guide*. 2nd edn. Weinheim, Germany: Wiley-VCH Verlag. Available at: https://www.wiley.com/en-gb/ICP+Emission+Spectrometry%3A+A+Practical+Guide%2C+2nd+Edition-p-9783527346578 (Accessed: 16 February 2022).

North, M. (2015) 'What is CO2? Thermodynamics, Basic Reactions and Physical Chemistry', in *Carbon Dioxide Utilisation: Closing the Carbon Cycle: First Edition*. Elsevier Inc., pp. 3–17. doi: 10.1016/B978-0-444-62746-9.00001-3.

Ogi, T., Yokoyama, S.-Y. and Koguchi, K. (1985) 'Direct liquefaction of wood by alkali and alkaline earth salt in an aqueous phase', *Chemistry Letters*, 14(8), pp. 1199–1202. doi: 10.1246/cl.1985.1199.

Ogwang, G., Olupot, P. W., Kasedde, H., Menya, E., Storz, H. and Kiros, Y. (2021) 'Experimental evaluation of rice husk ash for applications in geopolymer mortars', *Journal of Bioresources and Bioproducts*. Elsevier, 6(2), pp. 160–167. doi: 10.1016/j.jobab.2021.02.008.

Olajire, A. A. (2013) 'Valorization of greenhouse carbon dioxide emissions into value-added products by catalytic processes', *Journal of CO2 Utilization*. Elsevier, pp. 74–92. doi: 10.1016/j.jcou.2013.10.004.

Omran, A., Menor-Salvan, C., Springsteen, G. and Pasek, M. (2020) 'The Messy Alkaline Formose Reaction and Its Link to Metabolism', *Life 2020, Vol. 10, Page 125*. Multidisciplinary Digital Publishing Institute, 10(8), p. 125. doi: 10.3390/LIFE10080125.

Paraskevaidi, M., Martin-Hirsch, P. L. and Martin, F. L. (2018) 'ATR-FTIR spectroscopy tools for medical 4 diagnosis and disease investigation', in *Nanotechnology Characterization Tools for Biosensing and Medical Diagnosis*. Springer Berlin Heidelberg, pp. 163–211. doi: 10.1007/978-3-662-56333-5_4.

Pastorczak, M., Van Der Post, S. T. and Bakker, H. J. (2013) 'Cooperative hydration of carboxylate groups with alkali cations', *Physical Chemistry Chemical Physics*. Royal

References

Society of Chemistry, 15(41), pp. 17767–17770. doi: 10.1039/c3cp52419a.

Patel, C. K., Sarma, P. J. and De, M. (2015) 'Comparative parametric study on development of porous structure of aluminium oxide in presence of anionic and cationic surfactants', *Ceramics International*. Elsevier, 41(3), pp. 3578–3588. doi: 10.1016/j.ceramint.2014.10.186.

Patel, H. A., Byun, J. and Yavuz, C. T. (2017) 'Carbon Dioxide Capture Adsorbents: Chemistry and Methods', *ChemSusChem*, 10(7), pp. 1303–1317. doi: 10.1002/cssc.201601545.

Pegov, S. A. (2008) 'Methane in the Atmosphere', in *Encyclopedia of Ecology, Five-Volume Set*. Elsevier Inc., pp. 2325–2328. doi: 10.1016/B978-008045405-4.00744-8.

Pereira, M., Beck, P. H., Muller, D. G., Moreira, J. B., da Silva, J. S. and Durigon, A. M. M. (2016) 'Extraction of Organosolv Lignin from Rice Husk under Reflux Conditions', *Biological and Chemical Research*, (March 2018), pp. 87–98. Available at: www.ss-pub.org/wp-content/uploads/2017/04/BCR2017010301.pdf (Accessed: 24 January 2022).

Poerschmann, J., Weiner, B., Koehler, R. and Kopinke, F. D. (2017) 'Hydrothermal Carbonization of Glucose, Fructose, and Xylose - Identification of Organic Products with Medium Molecular Masses', *ACS Sustainable Chemistry and Engineering*, 5(8), pp. 6420–6428. doi: 10.1021/acssuschemeng.7b00276.

Puchajda, B., Oleszkiewicz, J., Sparling, R. and Reimers, R. (2006) 'Low-Temperature Inactivation of Fecal Coliforms in Sludge Digestion', *Water Environment Research*. Wiley, 78(7), pp. 680–685. doi: 10.2175/106143006x101638.

Qin, Z., Zhou, Y., Jiang, Y., Liu, Z. and Ji, H. (2017) 'Recent Advances in Heterogeneous Catalytic Hydrogenation of CO2 to Methane', in *New Advances in Hydrogenation Processes - Fundamentals and Applications*. InTech. doi: 10.5772/65407.

Le Quéré, C., Peters, G. P., Andres, R. J., Andrew, R. M., Boden, T. A., Ciais, P., Friedlingstein, P., Houghton, R. A., Marland, G., Moriarty, R., Sitch, S., Tans, P., Arneth, A., Arvanitis, A., Bakker, D. C. E., Bopp, L., Canadell, J. G., Chini, L. P., Doney, S. C., Harper, A., Harris, I., House, J. I., Jain, A. K., Jones, S. D., Kato, E., Keeling, R. F., Klein Goldewijk, K., Körtzinger, A., Koven, C., Lefèvre, N., Maignan, F., Omar, A., Ono, T., Park, G. H., Pfeil, B., Poulter, B., Raupach, M. R., Regnier, P., Rödenbeck, C., Saito, S., Schwinger, J.,

References

Segschneider, J., Stocker, B. D., Takahashi, T., Tilbrook, B., Van Heuven, S., Viovy, N., Wanninkhof, R., Wiltshire, A. and Zaehle, S. (2014) 'Global carbon budget 2013', *Earth System Science Data*, 6(1), pp. 235–263. doi: 10.5194/essd-6-235-2014.

Rackley, S. A. (2017) 'Carbon capture from power generation', in *Carbon Capture and Storage*. 2nd edn. Oxford, UK: Butterworth-Heinemann, pp. 75–101. doi: 10.1016/b978-0-12-812041-5.00004-0.

Ramalla, I., Gupta, R. K. and Bansal, K. (2015) 'Effect on superhydrophobic surfaces on electrical porcelain insulator, improved technique at polluted areas for longer life and reliability', *International Journal of Engineering & Technology*. Science Publishing Corporation, 4(4), p. 509. doi: 10.14419/ijet.v4i4.5405.

Raval, N., Maheshwari, R., Kalyane, D., Youngren-Ortiz, S. R., Chougule, M. B. and Tekade, R. K. (2018) 'Importance of physicochemical characterization of nanoparticles in pharmaceutical product development', in *Basic Fundamentals of Drug Delivery*. Elsevier, pp. 369–400. doi: 10.1016/B978-0-12-817909-3.00010-8.

Ravindra, M. R., Rao, K. J., Nath, B. S. and Ram, C. (2014) 'Carbonated fermented dairy drink – effect on quality and shelf life', *Journal of Food Science and Technology*, 51(11), pp. 3397–3403. doi: 10.1007/s13197-012-0854-1.

Reimer, L. (1998) 'Introduction', in *Scanning Electron Microscopy*. Berlin Heidelberg: Springer, pp. 1–12. doi: 10.1007/978-3-540-38967-5_1.

Reuhs, B. L. (2017) 'High-Performance Liquid Chromatography', in Nielsen, S. (ed.) *Food Analysis. Food Science Text Series*. Springer, Cham, pp. 213–226. doi: 10.1007/978-3-319-45776-5.

Richardson, J. T., Scates, R. and Twigg, M. V. (2003) 'X-ray diffraction study of nickel oxide reduction by hydrogen', *Applied Catalysis A: General*. Elsevier, 246(1), pp. 137–150. doi: 10.1016/S0926-860X(02)00669-5.

Riemenschneider, W. and Tanifuji, M. (2012) 'Oxalic acid', in *Ullmann's Encyclopedia of Industrial Chemistry*. Weinheim: Wiley-VCH Verlag GmbH & Co. KGaA, pp. 529–541.

Riza, F. V. and Rahman, I. A. (2015) *The properties of compressed earth-based (CEB) masonry blocks*, *Eco-efficient Masonry Bricks and Blocks: Design, Properties and Durability*. Elsevier Ltd. doi: 10.1016/B978-1-78242-305-8.00017-6.

References

Rodella, C. B., Kellermann, G., Francisco, M. S. P., Jordão, M. H. and Zanchet, D. (2008) 'Textural and structural analyses of industrial raney nickel catalyst', *Industrial and Engineering Chemistry Research*. American Chemical Society, 47(22), pp. 8612–8618. doi: 10.1021/ie800543t.

Roldan, A., Hollingsworth, N., Roffey, A., Islam, H. U., Goodall, J. B. M., Catlow, C. R. A., Darr, J. A., Bras, W., Sankar, G., Holt, K. B., Hogarth, G. and De Leeuw, N. H. (2015) 'Bio-inspired CO2conversion by iron sulfide catalysts under sustainable conditions', *Chemical Communications*, 51(35), pp. 7501–7504. doi: 10.1039/c5cc02078f.

Roman-Gonzalez, D., Moro, A., Burgoa, F., Pérez, E., Nieto-Márquez, A., Martín, Á. and Bermejo, M. D. (2018) '2Hydrothermal CO2 conversion using zinc as reductant: Batch reaction, modeling and parametric analysisof the process', *Journal of Supercritical Fluids*. Elsevier B.V., 140, pp. 320–328. doi: 10.1016/j.supflu.2018.07.003.

Román-Leshkov, Y., Moliner, M., Labinger, J. A. and Davis, M. E. (2010) 'Mechanism of glucose isomerization using a solid lewis acid catalyst in water', *Angewandte Chemie - International Edition*. John Wiley & Sons, Ltd, 49(47), pp. 8954–8957. doi: 10.1002/anie.201004689.

Rönsch, S., Schneider, J., Matthischke, S., Schlüter, M., Götz, M., Lefebvre, J., Prabhakaran, P. and Bajohr, S. (2016) 'Review on methanation - From fundamentals to current projects', *Fuel*. doi: 10.1016/j.fuel.2015.10.111.

Rouquerol, F., Rouquerol, J. (Jean) and Sing, K. S. W. (1999) 'Assessment of Surface Area', in *Adsorption by Powders and Porous Solids*. Academic Press, p. 467. doi: 10.1016/b978-0-12-598920-6.x5000-3.

Russell, J. A., Miller, R. K. and Molton, P. M. (1983) 'Formation of aromatic compounds from condensation reactions of cellulose degradation products', *Biomass*, 3(1), pp. 43–57. doi: 10.1016/0144-4565(83)90007-0.

S. Elshazly, E. and A. A. Abdelal, O. (2013) 'Nickel Stabilized Zirconia for SOFCs: Synthesis and Characterization', *International Journal of Metallurgical Engineering*. Scientific & Academic Publishing, 1(6), pp. 130–134. doi: 10.5923/j.ijmee.20120106.07.

Samanta, A., Zhao, A., Shimizu, G. K. H., Sarkar, P. and Gupta, R. (2012) 'Post-combustion CO 2 capture using solid sorbents: A review', *Industrial and Engineering*

Chemistry Research, 51(4), pp. 1438–1463. doi: 10.1021/ie200686q.

Sanz-Pérez, E. S., Murdock, C. R., Didas, S. A. and Jones, C. W. (2016) 'Direct Capture of CO2 from Ambient Air', *Chemical Reviews*, 116(19), pp. 11840–11876. doi: 10.1021/acs.chemrev.6b00173.

Sato, A. G., Volanti, D. P., Meira, D. M., Damyanova, S., Longo, E. and Bueno, J. M. C. (2013) 'Effect of the ZrO2 phase on the structure and behavior of supported Cu catalysts for ethanol conversion', *Journal of Catalysis*. Elsevier Inc., 307, pp. 1–17. doi: 10.1016/j.jcat.2013.06.022.

Schatten, H. (2010) 'The role of scanning electron microscopy in cell and molecular biology: SEM basics, past accomplishments, and new frontiers', in Schatten, H. (ed.) *Scanning Electron Microscopy for the Life Sciences*. Cambridge University Press, pp. 1–15. doi: 10.1017/CBO9781139018173.002.

Shen, Z., Gu, M., Zhang, M., Sang, W., Zhou, X., Zhang, Y. and Jin, F. (2014) 'The mechanism for production of abiogenic formate from CO2 and lactate from glycerine: Uncatalyzed transfer hydrogenation of CO2 with glycerine under alkaline hydrothermal conditions', *RSC Advances*, 4(29), pp. 15256–15263. doi: 10.1039/c4ra00777h.

Shen, Z., Zhang, Y. and Jin, F. (2011) 'From NaHCO3 into formate and from isopropanol into acetone: Hydrogen-transfer reduction of NaHCO3 with isopropanol in high-temperature water', *Green Chemistry*, 13(4), pp. 820–823. doi: 10.1039/c0gc00627k.

Shen, Z., Zhang, Y. and Jin, F. (2012) 'The alcohol-mediated reduction of CO2 and NaHCO3 into formate: a hydrogen transfer reduction of NaHCO3 with glycerine under alkaline hydrothermal conditions', *RSC Adv.*, 2(3), pp. 797–801. doi: 10.1039/C1RA00886B.

Shenoy, U. S. and Shetty, A. N. (2014) 'Simple glucose reduction route for one-step synthesis of copper nanofluids', *Applied Nanoscience (Switzerland)*. Springer Nature, 4(1), pp. 47–54. doi: 10.1007/s13204-012-0169-6.

Da Silva, C. N., Júnior, J. M. S., Veiga, A. G., Muchave, G. J., Aranda, D. A. G., Afonso, J. C. and Ribeiro, E. S. (2019) 'Characterization of silicon-aluminum-zirconium oxide obtained by the sol-gel process', *Quimica Nova*, 42(5), pp. 513–521. doi: 10.21577/0100-4042.20170364.

References

Sing, K. (2001) 'The use of nitrogen adsorption for the characterisation of porous materials', *Colloids and Surfaces A: Physicochemical and Engineering Aspects*, 187–188, pp. 3–9. doi: 10.1016/S0927-7757(01)00612-4.

Sithersingh, M. J. and Snow, N. H. (2012) 'Headspace-Gas Chromatography', in Poole, C. (ed.) *Gas Chromatography*. Amsterdam: Elsevier, pp. 221–233. doi: 10.1016/B978-0-12-385540-4.00030-4.

Skorek, A. and Włodarczyk, R. (2018) 'The use of methane in practical solutions of environmental engineering', *Journal of Ecological Engineering*. Polish Society of Ecological Engineering (PTIE), 19(2), pp. 172–178. doi: 10.12911/22998993/82427.

Sluiter, A., Hames, B., Hyman, D., Payne, C., Ruiz, R., Scarlata, C., Sluiter, J., Templeton, D. and Wolfe, J. (2008) 'Determination of Total Solids in Biomass and Total Dissolved Solids in Liquid Process Samples Laboratory Analytical Procedure (LAP) Issue Date: 3/31/2008'. Available at: www.nrel.gov (Accessed: 11 November 2019).

Smith, B. (2018) *Infrared Spectral Interpretation*, *Infrared Spectral Interpretation*. CRC Press. doi: 10.1201/9780203750841.

Sominsky, L., Rozental, E., Gottlieb, H., Gedanken, A. and Hoz, S. (2004) 'Uncatalyzed Meerwein-Ponndorf-Oppenauer-Verley Reduction of Aldehydes and Ketones under Supercritical Conditions', *Journal of Organic Chemistry*, 69(5), pp. 1492–1496. doi: 10.1021/jo035251f.

Song, C. (2006) 'Global challenges and strategies for control, conversion and utilization of CO2 for sustainable development involving energy, catalysis, adsorption and chemical processing', *Catalysis Today*, 115(1–4), pp. 2–32. doi: 10.1016/j.cattod.2006.02.029.

Sparkman, O. D., Penton, Z. and Kitson, F. G. (2011) *Gas Chromatography and Mass Spectrometry: A Practical Guide*, *Gas Chromatography and Mass Spectrometry: A Practical Guide*. doi: 10.1016/C2009-0-17039-3.

Srokol, Z., Bouche, A. G., Van Estrik, A., Strik, R. C. J., Maschmeyer, T. and Peters, J. A. (2004) 'Hydrothermal upgrading of biomass to biofuel; studies on some monosaccharide model compounds', *Carbohydrate Research*. Elsevier, 339(10), pp. 1717–1726. doi: 10.1016/j.carres.2004.04.018.

Stauffer, E., Dolan, J. A. and Newman, R. (2008) 'Gas Chromatography and Gas

References

Chromatography—Mass Spectrometry', in *Fire Debris Analysis*. Elsevier, pp. 235–293. doi: 10.1016/b978-012663971-1.50012-9.

Styring, P., Jansen, D., de Coninck, H., Reith, H. and Armstrong, K. (2011) *Carbon Capture and Utilisation in the green economy*, *Centre for Low Carbon Futures 2011 and CO2Chem Publishing 2012*.

Su, J., Lu, M. and Lin, H. (2015) 'High yield production of formate by hydrogenating CO_2 derived ammonium carbamate/carbonate at room temperature', *Green Chemistry*. The Royal Society of Chemistry, 17(5), pp. 2769–2773. doi: 10.1039/c5gc00397k.

Su, J., Yang, L., Lu, M. and Lin, H. (2015) 'Highly efficient hydrogen storage system based on ammonium bicarbonate/formate redox equilibrium over palladium nanocatalysts', *ChemSusChem*. Wiley-VCH Verlag, 8(5), pp. 813–816. doi: 10.1002/cssc.201403251.

Su, J., Yang, L., Yang, X., Lu, M., Luo, B. and Lin, H. (2015) 'Simultaneously converting carbonate/bicarbonate and biomass to value-added carboxylic acid salts by aqueous-phase hydrogen transfer', *ACS Sustainable Chemistry and Engineering*, 3(1), pp. 195–203. doi: 10.1021/sc5007158.

Su, T. M., Qin, Z. Z., Ji, H. B., Jiang, Y. X. and Huang, G. (2016) 'Recent advances in the photocatalytic reduction of carbon dioxide', *Environmental Chemistry Letters*. Springer Verlag, 14(1), pp. 99–112. doi: 10.1007/s10311-015-0528-0.

Suh, Y. W., Moon, S. H. and Rhee, H. K. (2000) 'Active sites in Cu/ZnO/ZrO2 catalysts for methanol synthesis from CO/H2', *Catalysis Today*. Elsevier, 63(2–4), pp. 447–452. doi: 10.1016/S0920-5861(00)00490-9.

Sun, Z., Ma, T., Tao, H., Fan, Q. and Han, B. (2017) 'Fundamentals and Challenges of Electrochemical CO_2 Reduction Using Two-Dimensional Materials', *Chem*, 3(4), pp. 560–587. doi: 10.1016/j.chempr.2017.09.009.

Takahashi, H., Liu, L. H., Yashiro, Y., Ioku, K., Bignall, G., Yamasaki, N. and Kori, T. (2006) 'CO_2 reduction using hydrothermal method for the selective formation of organic compounds', *Journal of Materials Science*, 41(5), pp. 1585–1589. doi: 10.1007/s10853-006-4649-5.

Takenouchi, S. and Kennedy, G. C. (1964) 'The binary system H2O-CO2 at high

References

temperatures and pressures', *American Journal of Science*, 262(9), pp. 1055–1074. doi: 10.2475/ajs.262.9.1055.

Tanabe, K. (1985) 'Surface and catalytic properties of ZrO2', *Materials Chemistry and Physics*. Elsevier, 13(3–4), pp. 347–364. doi: 10.1016/0254-0584(85)90064-1.

Taniwaki, M. H., Hocking, A. D., Pitt, J. I. and Fleet, G. H. (2009) 'Growth and mycotoxin production by food spoilage fungi under high carbon dioxide and low oxygen atmospheres', *International Journal of Food Microbiology*, 132(2–3), pp. 100–108. doi: 10.1016/j.ijfoodmicro.2009.04.005.

Taouatas, N., Drugan, M. M., Heck, A. J. R. and Mohammed, S. (2008) 'Straightforward ladder sequencing of peptides using a Lys-N metalloendopeptidase', *Nature Methods*, 5(5), pp. 405–407. doi: 10.1038/nmeth.1204.

Thabet, A., Basheer, C., Maung, T. H., Al-Muallem, H. A. and Kalanthoden, A. N. (2015) 'Rice Husk Supported Catalysts for Degradation of Chlorobenzenes in Capillary Microreactor', *Journal of Nanomaterials*, 2015. doi: 10.1155/2015/912036.

Theo, W. L., Lim, J. S., Hashim, H., Mustaffa, A. A. and Ho, W. S. (2016) 'Review of pre-combustion capture and ionic liquid in carbon capture and storage', *Applied Energy*. Elsevier Ltd, 183, pp. 1633–1663. doi: 10.1016/j.apenergy.2016.09.103.

Tivey, M. (2007) 'Generation of Seafloor Hydrothermal Vent Fluids and Associated Mineral Deposits', *Oceanography*, 20(1), pp. 50–65. doi: 10.5670/oceanog.2007.80.

Toews, K. L., Shroll, R. M., Wai, C. M. and Smart, N. G. (1995) 'pH-Defining Equilibrium Between Water and Supercritical CO2. Influence on SFE of Organics and Metal Chelates', *Analytical Chemistry*, 67(22), pp. 4040–4043. doi: 10.1021/ac00118a002.

Toor, S. S., Rosendahl, L. and Rudolf, A. (2011) 'Hydrothermal liquefaction of biomass: A review of subcritical water technologies', *Energy*. Pergamon, pp. 2328–2342. doi: 10.1016/j.energy.2011.03.013.

Trojer, L., Greiderer, A., Bisjak, C., Wieder, W., Heigl, N., Huck, C. and Bonn, G. (2010) 'Monolithic Stationary Phases in HPLC', in Corradini, D. and Philips, T. M. (eds) *Handbook of HPLC*. Boca Raton: Taylor & Francis Group, pp. 3–45. doi: 10.1201/ebk1574445541-c1.

Tymoszuk, A. and Wojnarowicz, J. (2020) 'Zinc oxide and zinc oxide nanoparticles

References

impact on in vitro germination and seedling growth in allium cepa L.', *Materials*. Multidisciplinary Digital Publishing Institute, 13(12), pp. 1–16. doi: 10.3390/ma13122784.

Vansant, E. F., Vrancken, K. C. and Van Der Voort, P. (1995) *Characterization and Chemical Modification of the Silica Surface*, *Studies in Surface Science and Catalysis*. Elsevier Science Ltd. Available at: https://www.elsevier.com/books/characterization-and-chemical-modification-of-the-silica-surface/vansant/978-0-444-81928-4 (Accessed: 17 February 2022).

Vansant, J. (2003) 'Carbon Dioxide Emission and Merchant Market in tbe European Union', in Aresta, M. (ed.) *Carbon Dioxide Recovery and Utilization*. 1st edn. Dordrecht: Springer Netherlands, pp. 3–49. doi: 10.1007/9789401702454.

Viinikainen, T., Rönkkönen, H., Bradshaw, H., Stephenson, H., Airaksinen, S., Reinikainen, M., Simell, P. and Krause, O. (2009) 'Acidic and basic surface sites of zirconia-based biomass gasification gas clean-up catalysts', *Applied Catalysis A: General*, 362(1–2), pp. 169–177. doi: 10.1016/j.apcata.2009.04.037.

Vitha, M. F. (2016) 'Gas Chromatography', in *Chromatography : Principles and Instrumentation*. Hoboken, NJ, USA: John Wiley & Sons, Inc., pp. 61–80.

Wang, F., Wang, Y., Jin, F., Yao, G., Huo, Z., Zeng, X. and Jing, Z. (2014) 'One-pot hydrothermal conversion of cellulose into organic acids with cuo as an oxidant', *Industrial and Engineering Chemistry Research*. American Chemical Society, 53(19), pp. 7939–7946. doi: 10.1021/ie404311d.

Wang, L. Y., Yao, G. D., Jing, Z. Z. and Jin, F. M. (2014) 'Hydrothermal Conversion of CO2 into Formic Acid with Zinc and Copper Powders under Low Temperature', *Advanced Materials Research*, 1073–1076, pp. 39–42. doi: 10.4028/www.scientific.net/AMR.1073-1076.39.

Wang, X., Yang, Y., Zhong, H., He, R., Cheng, J. and Jin, F. (2019) 'In situ formed Raney-Ni/Fe3O4 catalyzed reduction of NaHCO3 into acetate with Fe as reductant in water', *Catalysis Today*. doi: 10.1016/j.cattod.2019.06.030.

Wang, Y., Jin, F., Sasaki, M., Wahyudiono, Wang, F., Jing, Z. and Goto, M. (2013) 'Selective conversion of glucose into lactic acid and acetic acid with copper oxide under hydrothermal conditions', *AIChE Journal*, 59(6), pp. 2096–2104. doi:

References

10.1002/aic.13960.

Wang, Y., Wang, F., Li, C. and Jin, F. (2016) 'Kinetics and mechanism of reduction of CO2 by glycerol under alkaline hydrothermal conditions', *International Journal of Hydrogen Energy*. Elsevier Ltd, 41(21), pp. 9128–9134. doi: 10.1016/j.ijhydene.2016.02.009.

Wang, Z. (2010) 'Lobry de Bruyn-Alberda van Ekenstein Transformation', in Wang, Z. (ed.) *Comprehensive Organic Name Reactions and Reagents*. John Wiley & Sons, Inc., pp. 1763–1766. doi: 10.1002/9780470638859.conrr396.

Wang, Z., Wu, W., Bian, X. and Wu, Y. (2016) 'Synthesis and characterization of amorphous Al2O3 and γ-Al2O3 by spray pyrolysis', *Green Processing and Synthesis*. Walter de Gruyter GmbH, 5(3), pp. 305–310. doi: 10.1515/gps-2015-0128.

Wei, J., Ge, Q., Yao, R., Wen, Z., Fang, C., Guo, L., Xu, H. and Sun, J. (2017) 'Directly converting CO2 into a gasoline fuel', *Nature Communications*. Nature Publishing Group, 8(May), pp. 1–8. doi: 10.1038/ncomms15174.

Wellendorff, J., Silbaugh, T. L., Garcia-Pintos, D., Nørskov, J. K., Bligaard, T., Studt, F. and Campbell, C. T. (2015) 'A benchmark database for adsorption bond energies to transition metal surfaces and comparison to selected DFT functionals', *Surface Science*. North-Holland, 640, pp. 36–44. doi: 10.1016/j.susc.2015.03.023.

Wu, B., Gao, Y., Jin, F., Cao, J., Du, Y. and Zhang, Y. (2009) 'Catalytic conversion of NaHCO3 into formic acid in mild hydrothermal conditions for CO2 utilization', *Catalysis Today*, 148(3–4), pp. 405–410. doi: 10.1016/j.cattod.2009.08.012.

Wu, J., Wang, S. and Zheng, H. (2016) 'The influence of ionic strength on carbonate-based spectroscopic barometry for aqueous fluids: an in-situ Raman study on Na2CO3-NaCl solutions', *Scientific Reports*. Nature Publishing Group, 6(1), pp. 1–9. doi: 10.1038/srep39088.

Wu, X., Liang, J., Wu, Y., Hu, H., Huang, S. and Wu, K. (2017) 'Co-liquefaction of microalgae and polypropylene in sub-/super-critical water', *RSC Advances*, 7(23), pp. 13768–13776. doi: 10.1039/c7ra01030c.

Yahia, E. M. (2009) *Modified and Controlled Atmospheres for the Storage, Transportation, and Packaging of Horticultural Commodities*. Boca Raton, USA: CRC Press.

References

Yan, W. H., Duan, P. G., Wang, F. and Xu, Y. P. (2016) 'Composition of the bio-oil from the hydrothermal liquefaction of duckweed and the influence of the extraction solvents', *Fuel*. Elsevier Ltd, 185, pp. 229–235. doi: 10.1016/j.fuel.2016.07.117.

Yan, X., Jin, F., Tohji, K., Moriya, T. and Enomoto, H. (2007) 'Production of lactic acid from glucose by alkaline hydrothermal reaction', *Journal of Materials Science*, 42(24), pp. 9995–9999. doi: 10.1007/s10853-007-2012-0.

Yang, H., Zhang, C., Gao, P., Wang, H., Li, X., Zhong, L., Wei, W. and Sun, Y. (2017) 'A review of the catalytic hydrogenation of carbon dioxide into value-added hydrocarbons', *Catalysis Science and Technology*. Royal Society of Chemistry, 7(20), pp. 4580–4598. doi: 10.1039/c7cy01403a.

Yang, Y., Zhong, H., He, R., Wang, X., Cheng, J., Yao, G. and Jin, F. (2019) 'Synergetic conversion of microalgae and CO2 into value-added chemicals under hydrothermal conditions', *Green Chemistry*. The Royal Society of Chemistry, 21(6), pp. 1247–1252. doi: 10.1039/c8gc03645d.

Yang, Y., Zhong, H., Yao, G., He, R., Jin, B. and Jin, F. (2018) 'Hydrothermal reduction of NaHCO3 into formate with hexanehexol', *Catalysis Today*, 318, pp. 10–14. doi: 10.1016/j.cattod.2017.09.005.

Yao, G., Duo, J., Jin, B., Zhong, H., Lyu, L., Ma, Z. and Jin, F. (2017) 'Highly-efficient and autocatalytic reduction of NaHCO3 into formate by in situ hydrogen from water splitting with metal/metal oxide redox cycle', *Journal of Energy Chemistry*, 26(5), pp. 881–890. doi: 10.1016/j.jechem.2017.08.011.

Yao, G., Zeng, X., Jin, Y., Zhong, H., Duo, J. and Jin, F. (2015) 'Hydrogen production by water splitting with Al and in-situ reduction of CO2 into formic acid', in *International Journal of Hydrogen Energy*, pp. 14284–14289. doi: 10.1016/j.ijhydene.2015.04.073.

Yao, G., Zeng, X., Li, Q., Wang, Y., Jing, Z. and Jin, F. (2012) 'Direct and highly efficient reduction of NiO into Ni with cellulose under hydrothermal conditions', *Industrial and Engineering Chemistry Research*. American Chemical Society, 51(23), pp. 7853–7858. doi: 10.1021/ie300474h.

Yoo, M., Han, S. J. and Wee, J. H. (2013) 'Carbon dioxide capture capacity of sodium hydroxide aqueous solution', *Journal of Environmental Management*, 114, pp. 512–519. doi: 10.1016/j.jenvman.2012.10.061.

References

Yu, J. and Savage, P. E. (1998) 'Decomposition of Formic Acid under Hydrothermal Conditions', *Industrial and Engineering Chemistry Research*. American Chemical Society, 37(1), pp. 2–10. doi: 10.1021/ie970182e.

Yu, J., Sun, L., Ma, C., Qiao, Y. and Yao, H. (2016) 'Thermal degradation of PVC: A review', *Waste Management*. Elsevier Ltd, 48, pp. 300–314. doi: 10.1016/j.wasman.2015.11.041.

Yu, K. M. K., Curcic, I., Gabriel, J. and Tsang, S. C. E. (2008) 'Recent advances in CO2 capture and utilization.', *ChemSusChem*, pp. 893–899. doi: 10.1002/cssc.200800169.

Yun Yang, B. and Montgomery, R. (1996) 'Alkaline degradation of glucose: Effect of initial concentration of reactants', *Carbohydrate Research*, 280(1), pp. 27–45. doi: 10.1016/0008-6215(95)00294-4.

Zeković, Z., Pfaf-Šovljanski, I. and Grujić, O. (2007) 'Supercritical fluid extraction of hops', *Journal of the Serbian Chemical Society*, 72(1), pp. 81–87. doi: 10.2298/JSC0701081Z.

Zeng, X., Jin, F., Huo, Z., Mogi, T., Kishita, A. and Enomoto, H. (2011) 'Reduction of carbon dioxide in hydrothermal cracking of polymer wastes', *Energy and Fuels*, 25(6), pp. 2749–2752. doi: 10.1021/ef200440k.

Zhang, A. Y. Z., Sun, Z., Leung, C. C. J., Han, W., Lau, K. Y., Li, M. and Lin, C. S. K. (2013) 'Valorisation of bakery waste for succinic acid production', *Green Chemistry*, 15(3), pp. 690–695. doi: 10.1039/c2gc36518a.

Zhang, F., Guo, L., Xu, S. and Zhang, R. (2015) 'Preparation of Nickel-Aluminum-Containing Layered Double Hydroxide Films by Secondary (Seeded) Growth Method and Their Electrochemical Properties', *Langmuir*. American Chemical Society, 31(24), pp. 6704–6712. doi: 10.1021/acs.langmuir.5b00619.

Zhang, L., Lin, J. and Chen, Y. (1992) 'Studies of surface NiO species in NiO/SiO2 catalysts using temperature-programmed reduction and X-ray diffraction', *Journal of the Chemical Society, Faraday Transactions*, 88(14), pp. 2075–2078. doi: 10.1039/FT9928802075.

Zhang, X., Singh, B., He, X., Gundersen, T., Deng, L. and Zhang, S. (2014) 'Post-combustion carbon capture technologies: Energetic analysis and life cycle assessment', *International Journal of Greenhouse Gas Control*. Elsevier Ltd, 27, pp.

References

289–298. doi: 10.1016/j.ijggc.2014.06.016.

Zhong, H., Gao, Y., Yao, G., Zeng, X., Li, Q., Huo, Z. and Jin, F. (2015) 'Highly efficient water splitting and carbon dioxide reduction into formic acid with iron and copper powder', *Chemical Engineering Journal*, 280, pp. 215–221. doi: 10.1016/j.cej.2015.05.098.

Zhong, H., Jin, F., Wu, B., Chen, H., Yao, G., Jin, F., Zhou, Q. and Wu, B. (2010) 'Hydrothermal conversion of CO2 into formic acid on the catalysis of Cu', in *AIP Conference Proceedings*, pp. 213–216. doi: 10.1063/1.3529280.

Zhong, H., Wang, L., Yang, Y., He, R., Jing, Z. and Jin, F. (2019) 'Ni and Zn/ZnO Synergistically Catalyzed Reduction of Bicarbonate into Formate with Water Splitting', *ACS Applied Materials and Interfaces*, 11(45), pp. 42149–42155. doi: 10.1021/acsami.9b14039.

Zhong, H., Yao, G., Cui, X., Yan, P., Wang, X. and Jin, F. (2019) 'Selective conversion of carbon dioxide into methane with a 98% yield on an in situ formed Ni nanoparticle catalyst in water', *Chemical Engineering Journal*, 357, pp. 421–427. doi: 10.1016/j.cej.2018.09.155.

Zhu, Y., Yang, Y., Wang, X., Zhong, H. and Jin, F. (2019) 'Pd/C-catalyzed reduction of NaHCO3 into formate with 2-pyrrolidone under hydrothermal conditions', *Energy Science and Engineering*. Wiley, 7(3), pp. 881–889. doi: 10.1002/ese3.317.

APPENDICES

A. FORMIC ACID ION CHROMATOGRAPHY CALIBRATION CURVE

Liquid product analysis carried out using an Metrohm 883 Basic IC plus ion chromatographer equipped with Metrosep A Supp 4 column (250/4.0 mm) (both Metrohm, UK). An eluent of 1.7 mM $NaHCO_3$ with 1.8 mM Na_2CO_3 was used with a flow rate of 0.5 ml min^{-1} with 100 mM H_2SO_4 as regen. Solutions were prepared by degassing 1 L of deionised H_2O in a sonicator for 20 minutes, followed by addition of $NaHCO_3/Na_2CO_3$ or H_2SO_4. The column was left to equilibrate for a minimum of one hour before analysis. Standards of 100 ppm formic acid was prepared from commercially purchased chemicals followed by serial dilution to obtain eight standards (Figure 0-1).
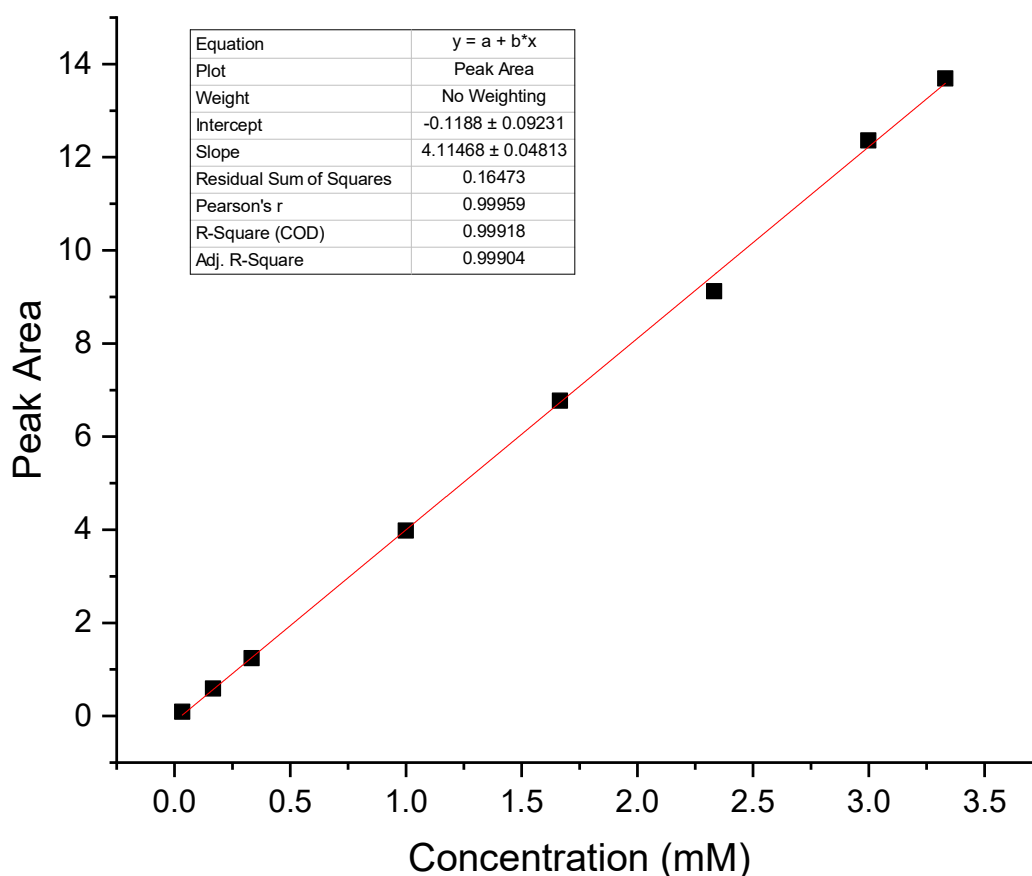

Equation	y = a + b*x
Plot	Peak Area
Weight	No Weighting
Intercept	-0.1188 ± 0.09231
Slope	4.11468 ± 0.04813
Residual Sum of Squares	0.16473
Pearson's r	0.99959
R-Square (COD)	0.99918
Adj. R-Square	0.99904

Figure 0-1 Calibration curve obtained by analysis of formic acid standards by ion chromatography. Analysis parameters: 0.5 ml min^{-1} 1.7 mM $NaHCO_3$/1.8 mM Na_2CO_3

B. HPLC STANDARDS RETENTION TIMES

A series of standards was selected from reviewing literature on similar reaction systems. The identity of standards and their retention time by refractive index detection (RID) and photo-diode array detection (PDAD) are shown in Table 0-1.

Table 0-1 HPLC Standards and associated retention time by refractive index detection (RID) and photo-diode array detection (PDAD)

Entry	Standard	Retention Time	
		RID	PDAD
1	Bicarbonate	6.8	6.52
2	Carbonate	6.75	-
3	Sulfuric acid	-	6.9
4	Oxalic acid	7.46	7.35
5	Citric acid	8.88	8.8
6	Maleic acid	9.0	8.89
7	Glucose	9.88	-
8	Pyruvic acid	10.3	10.21
9	Glyoxylic acid	10.42	10.29
10	Fructose	10.7	10.4
11	Glyceraldehyde	12.1	12.0
12	Lactic acid	13.63	13.5
13	Pyruvaldehyde	12.96	12.82
14	Glycolic acid	13.25	13.1
15	Glycolaldehyde	13.29	13.16
16	Dihydroxyacetone	14.38	14.25
17	Formaldehyde	14.4	-
18	Formic acid	14.6	14.75
19	Acetic acid	15.95	15.85
20	Levulinic acid	17	16.9
21	Ethylene glycol	17	-
22	1,2-Propanediol	17.95	-
23	Propanoic acid	-	18.4
24	Acrylic acid	18.63	18.52
25	Methanol	19.88	-
26	Ethanol	22.5	-
27	Acetone	23	22.85
28	Isovaleric acid	25.75	25.65
29	5-HMF	32.8	32.7
30	Furfural	46.6	46.5

C. HPLC CALIBRATION CURVES

A series of calibration curves were produced for quantification of organic acids in the present work. Calibration curves were produced by making up stock solutions from commercial reagents, followed by serial dilutions to obtain a minimum of three calibration points. Calibration was carried out from detection by PDAD. The resulting calibration curves are demonstrated in Appendix C.
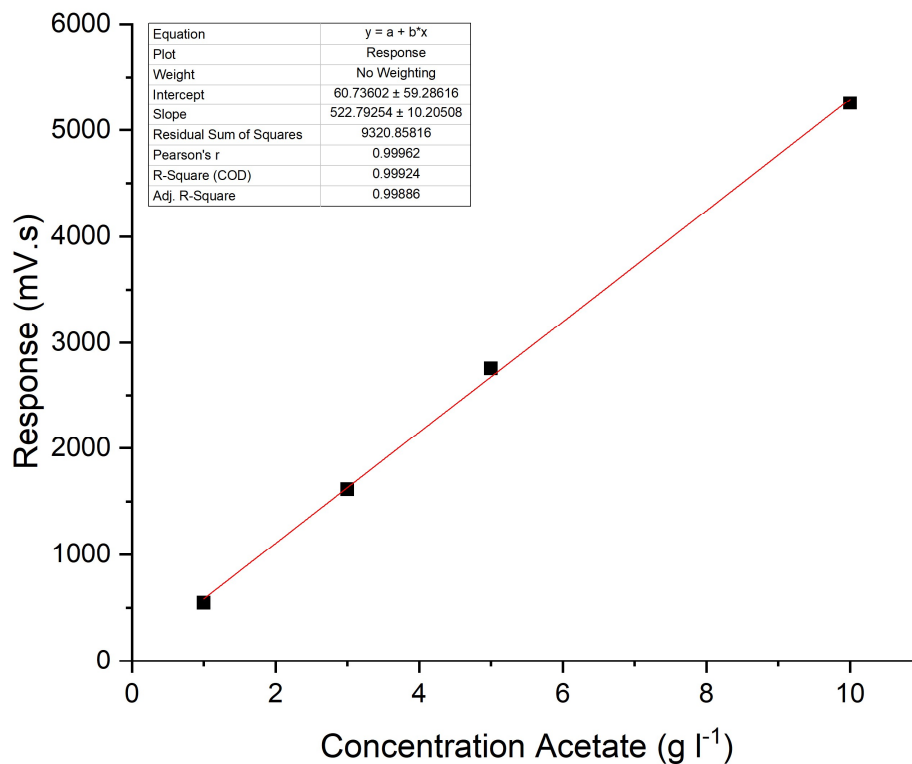

Equation	y = a + b*x
Plot	Response
Weight	No Weighting
Intercept	60.73602 ± 59.28616
Slope	522.79254 ± 10.20508
Residual Sum of Squares	9320.85816
Pearson's r	0.99962
R-Square (COD)	0.99924
Adj. R-Square	0.99886

Figure 0-2 Acetate calibration curve obtained by HPLC analysis of standards. Analysis parameters: 0.6 ml min⁻¹ 5 mM H₂SO₄, 60 °C oven, PDAD set to 30 °C and 210 nm
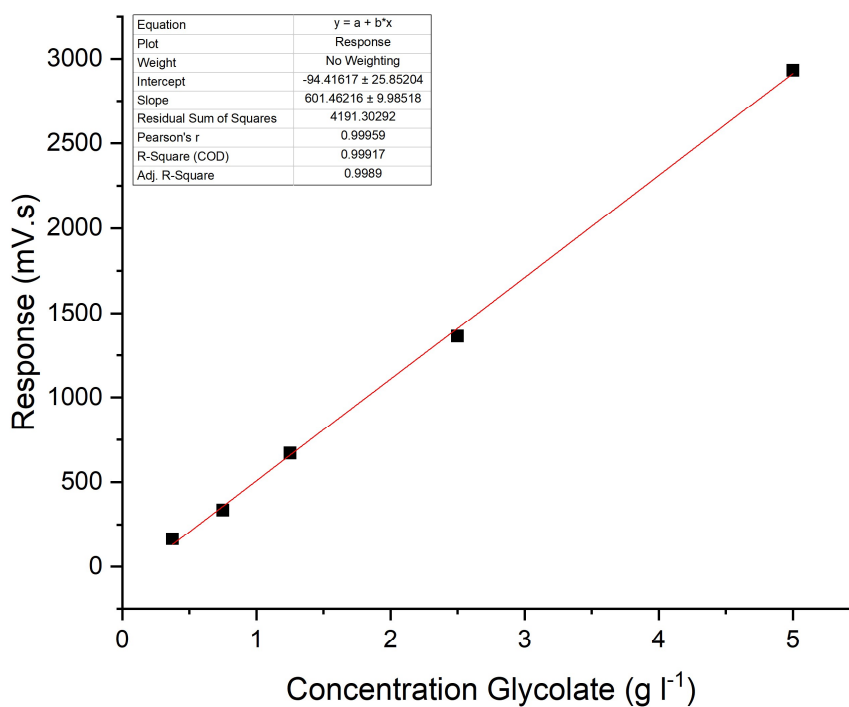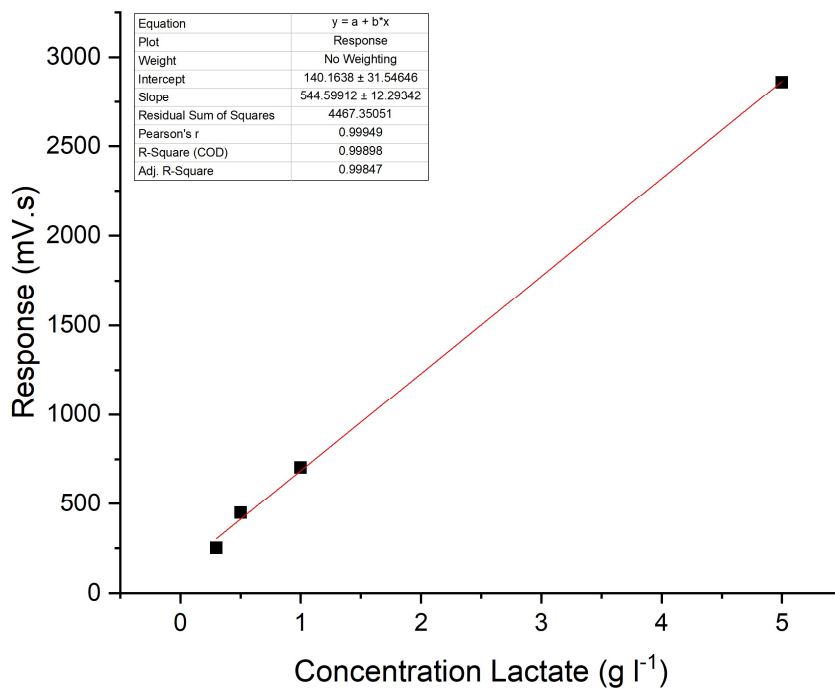
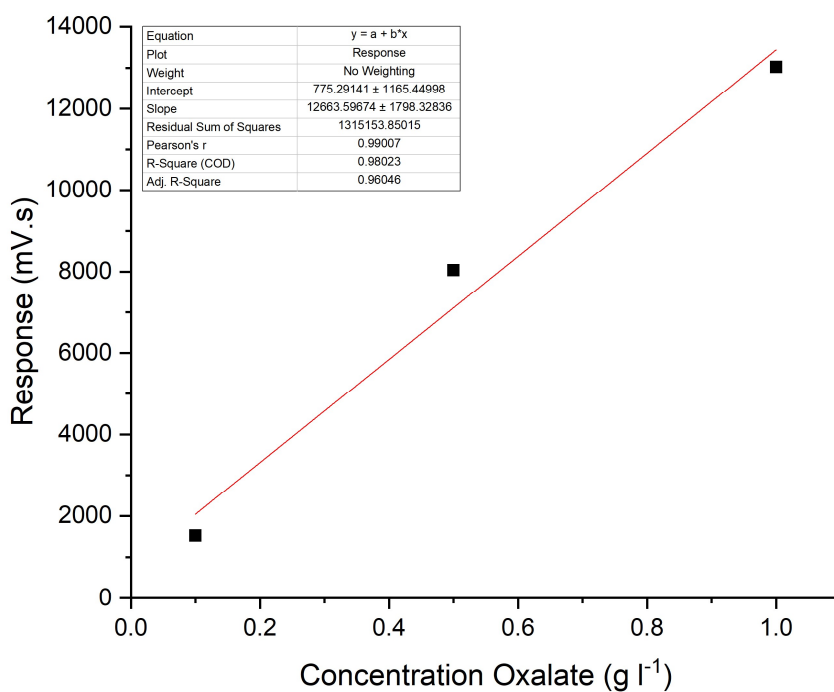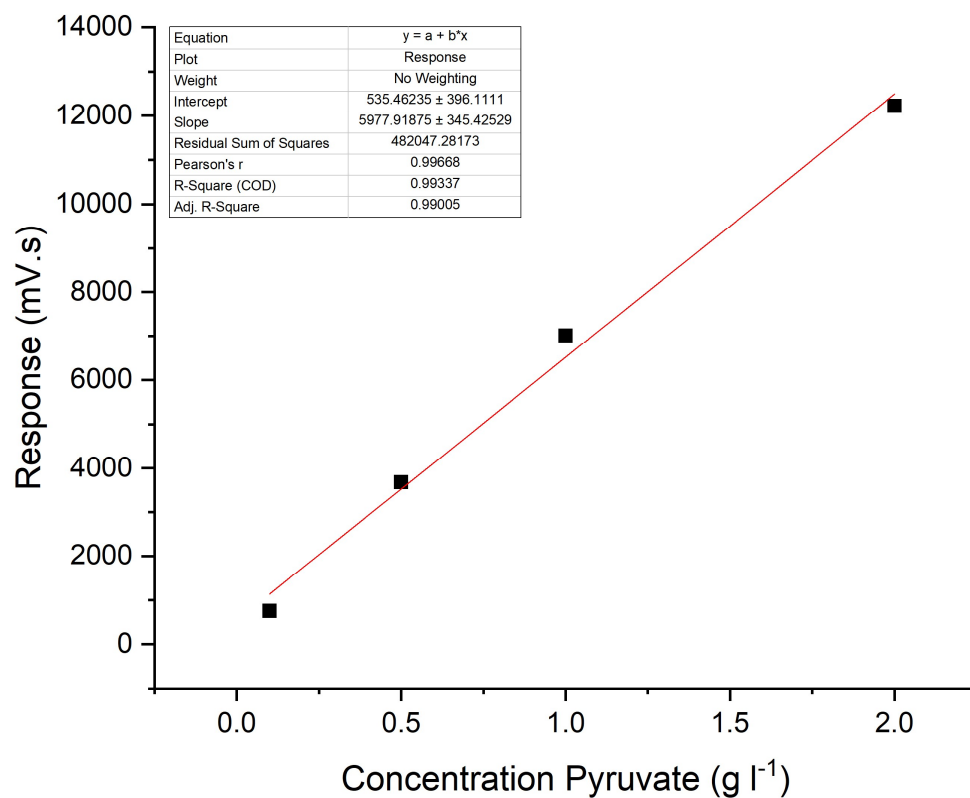| Equation	y = a + b*x
Plot	Response
Weight	No Weighting
Intercept	46.25433 ± 28.7179
Slope	873.51146 ± 4.51351
Residual Sum of Squares	30382.88144
Pearson's r	0.99991
R-Square (COD)	0.99981
Adj. R-Square	0.99979
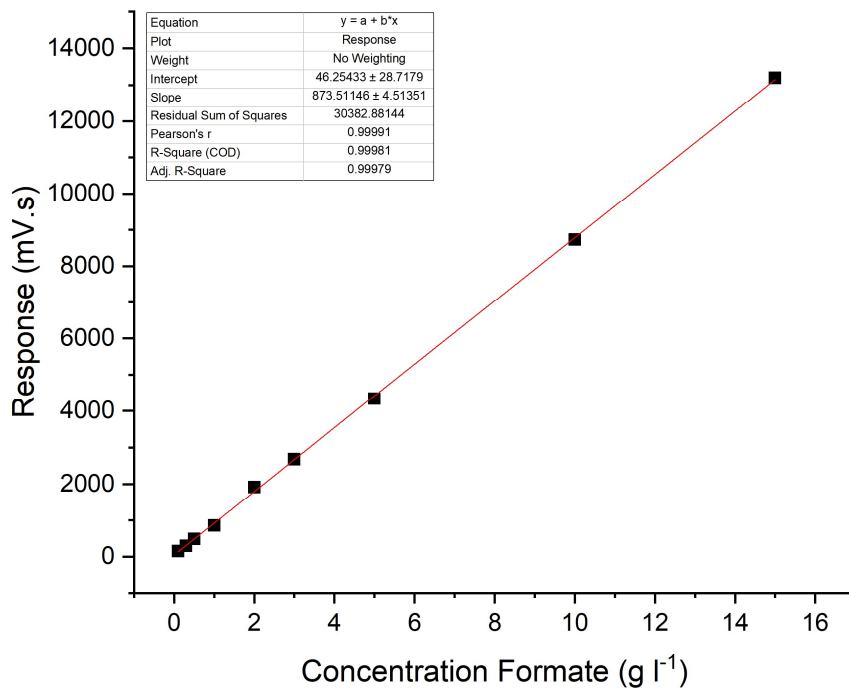
Figure 0-3 Formate calibration curve obtained by HPLC analysis of standards. Analysis parameters: 0.6 ml min^{-1} 5 mM H$_2$SO$_4$, 60 °C oven, PDAD set to 30 °C and 210 nm

Equation	y = a + b*x
Plot	Response
Weight	No Weighting
Intercept	-94.41617 ± 25.85204
Slope	601.46216 ± 9.98518
Residual Sum of Squares	4191.30292
Pearson's r	0.99959
R-Square (COD)	0.99917
Adj. R-Square	0.9989

Figure 0-4 Glycolate calibration curve obtained by HPLC analysis of standards. Analysis parameters: 0.6 ml min^{-1} 5 mM H$_2$SO$_4$, 60 °C oven, PDAD set to 30 °C and 210 nm

Equation	y = a + b*x
Plot	Response
Weight	No Weighting
Intercept	140.1638 ± 31.54646
Slope	544.59912 ± 12.29342
Residual Sum of Squares	4467.35051
Pearson's r	0.99949
R-Square (COD)	0.99898
Adj. R-Square	0.99847

Figure 0-5 Lactate calibration curve obtained by HPLC analysis of standards. Analysis parameters: 0.6 ml min^{-1} 5 mM H$_2$SO$_4$, 60 °C oven, PDAD set to 30 °C and 210 nm

Equation	y = a + b*x
Plot	Response
Weight	No Weighting
Intercept	775.29141 ± 1165.44998
Slope	12663.59674 ± 1798.32836
Residual Sum of Squares	1315153.85015
Pearson's r	0.99007
R-Square (COD)	0.98023
Adj. R-Square	0.96046

Figure 0-6 Oxalate calibration curve obtained by HPLC analysis of standards. Analysis parameters: 0.6 ml min^{-1} 5 mM H$_2$SO$_4$, 60 °C oven, PDAD set to 30 °C and 210 nm

Equation	y = a + b*x
Plot	Response
Weight	No Weighting
Intercept	535.46235 ± 396.1111
Slope	5977.91875 ± 345.42529
Residual Sum of Squares	482047.28173
Pearson's r	0.99668
R-Square (COD)	0.99337
Adj. R-Square	0.99005

Figure 0-7 Pyruvate calibration curve obtained by HPLC analysis of standards. Analysis parameters: 0.6 ml min^{-1} 5 mM H$_2$SO$_4$, 60 °C oven, PDAD set to 30 °C and 210 nm

D. FTIR SPECTRA

9.3.1   D.1 FTIR of Cobalt
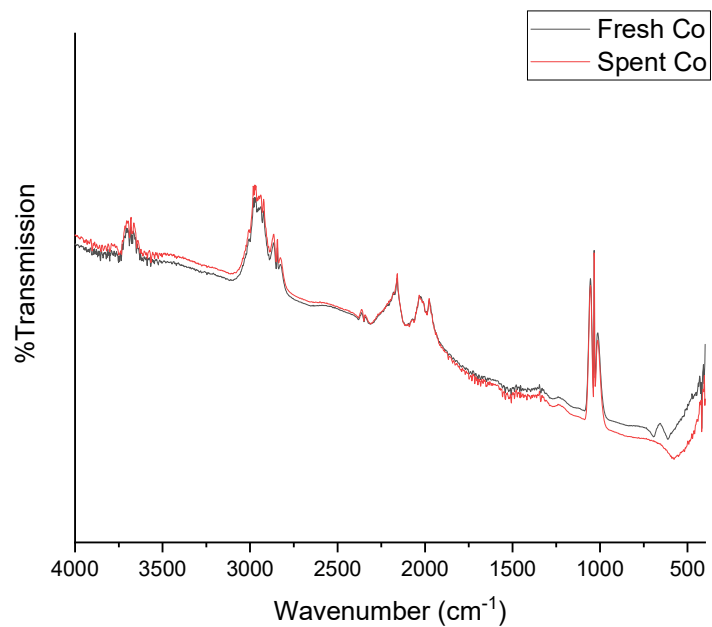
Figure 0-8 FTIR of fresh (black) and spent (red) Co powder after hydrothermal reaction (reaction conditions: 0.50 M NaHCO$_3$, 0.05 M glucose, 250 °C, 2 h, 50 ml H$_2$O). Spectra acquired in transmission mode at a resolution of 8 cm^{-1} with 32 scans over the range 400-4000 cm^{-1}

Appendices

9.3.2 D.2 FTIR of Copper
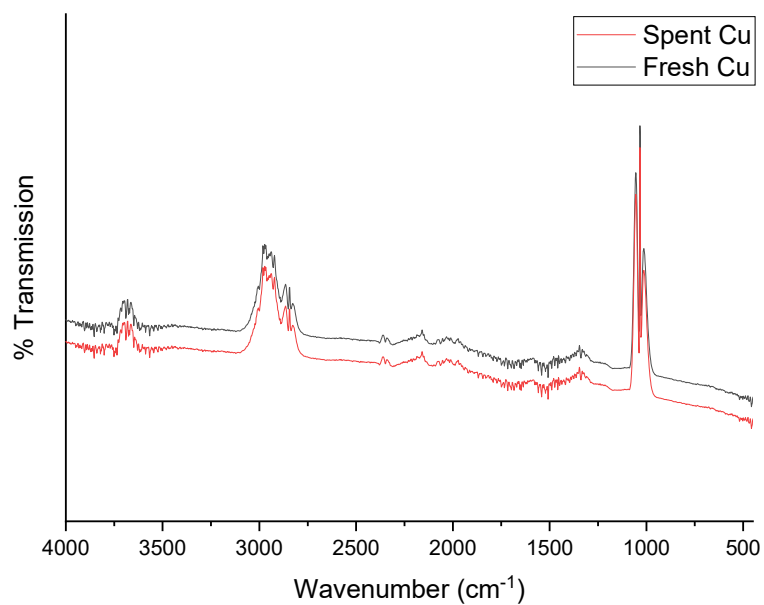
Figure 0-9 FTIR of fresh (black) and spent (red) Ni powder after hydrothermal reaction (reaction conditions: 0.50 M NaHCO₃, 0.05 M glucose, 250 °C, 2 h, 50 ml H₂O). Spectra acquired in transmission mode at a resolution of 8 cm⁻¹ with 32 scans over the range 400-4000 cm⁻¹

E. XRD REFERENCE DATA CARDS

The following Appendices E.1-E.7 depict XRD reference data cards for inorganic species as selected from the PDF-4+ 2021 database (ICDD, USA). Cards were used to reference peaks observed in diffraction patterns of analysed substances.

9.3.3   E.1 Metallic Ni – 04-004-6330

© 2022 International Centre for Diffraction Data. All rights reserved.
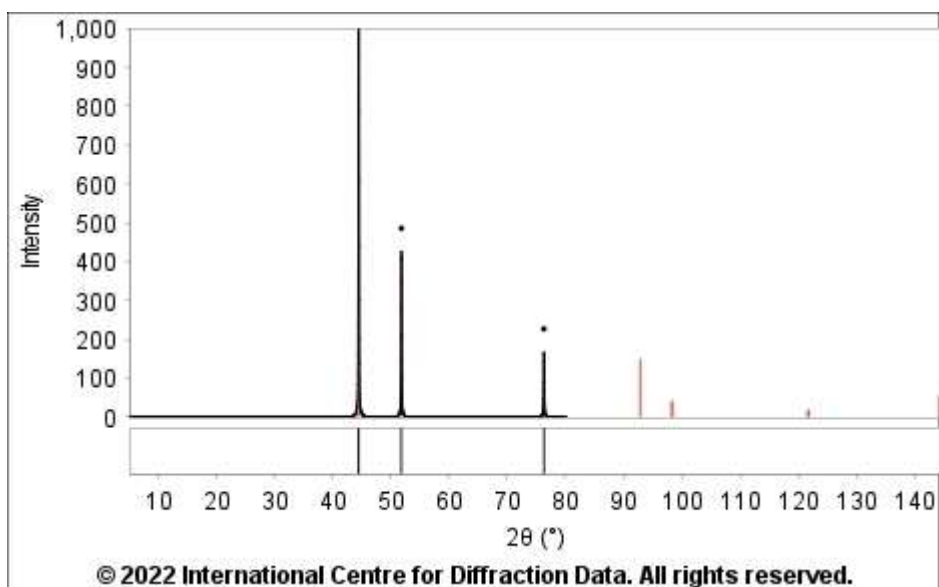
9.3.4   E.2 Nickel oxide (NiO) - 01-071-1179

© 2022 International Centre for Diffraction Data. All rights reserved.
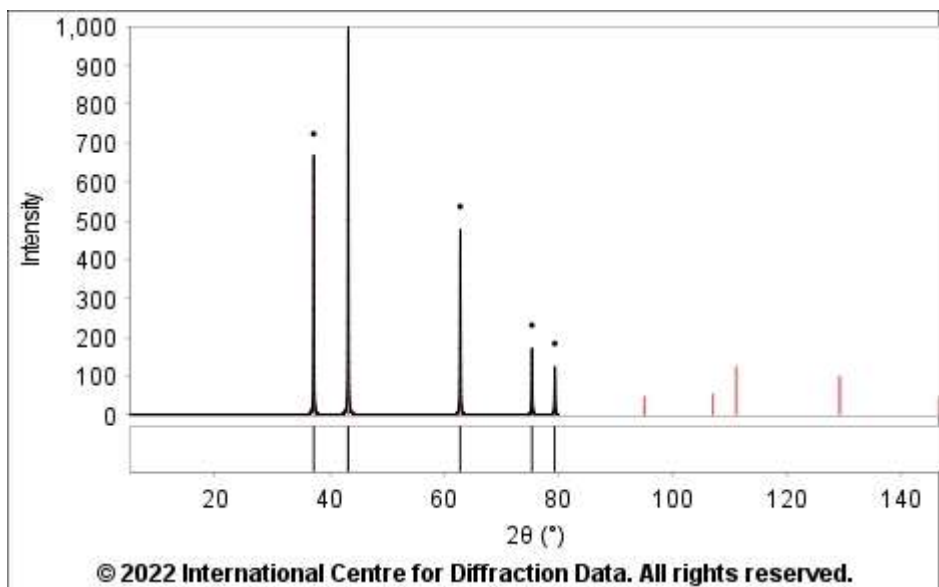
9.3.5 E.3 Aluminium oxide hydroxide [AlO(OH)] – 00-021-1307
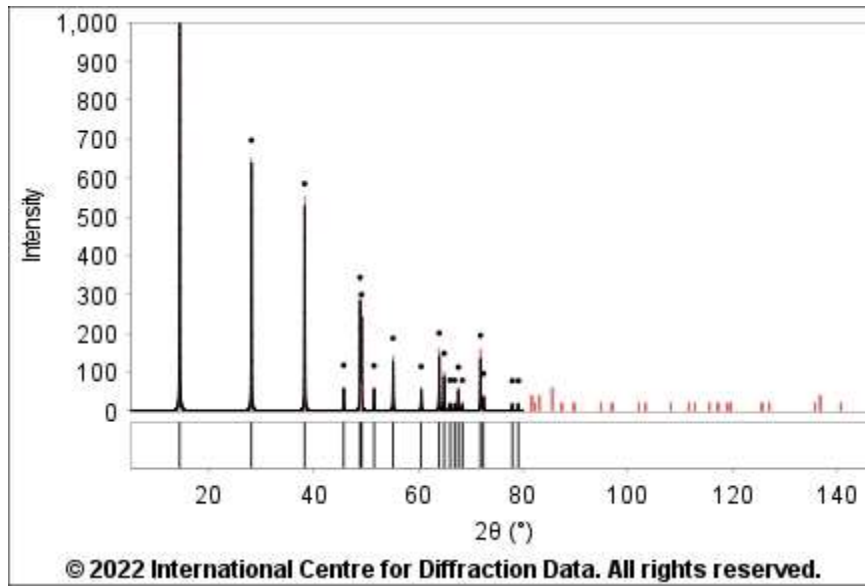
9.3.6 E.4 Silicon dioxide (SiO$_2$) crystalline – 01-071-1179
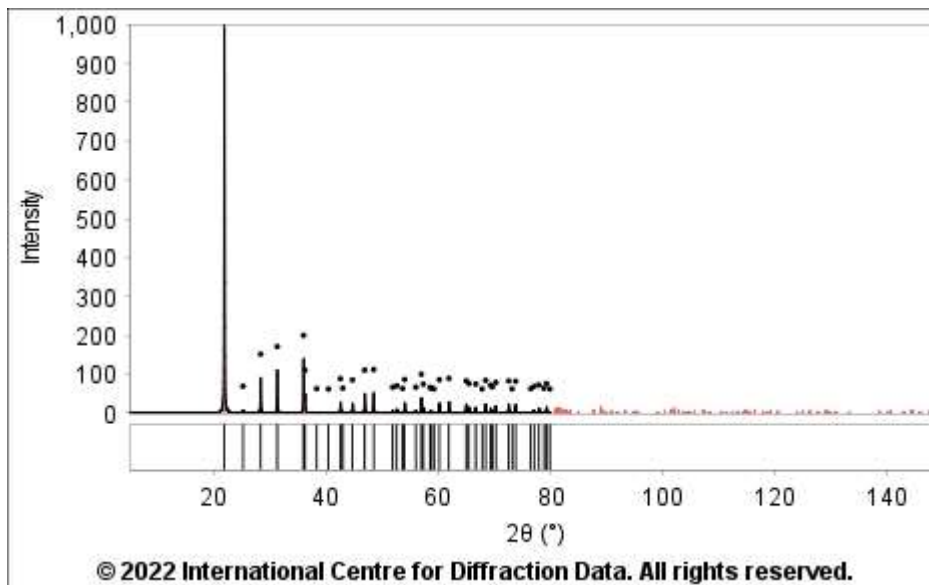
Appendices

9.3.7 E.5 Calcium silicate (Ca$_2$SiO$_4$) - 00-061-0379
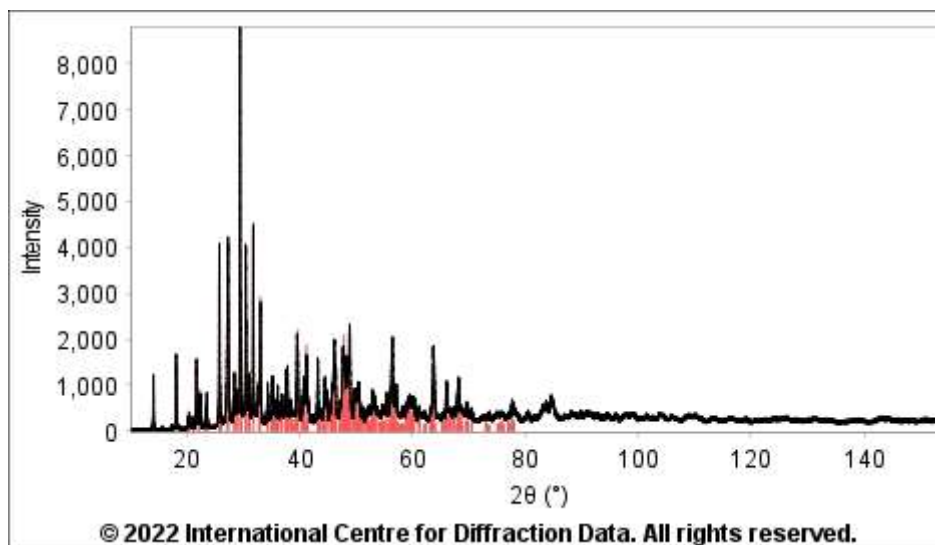
9.3.8 E.6 Lattice Na$_{15.6}$ Ca$_{3.84}$ (S$_{12}$O$_{36}$) – 01-075-1332

240
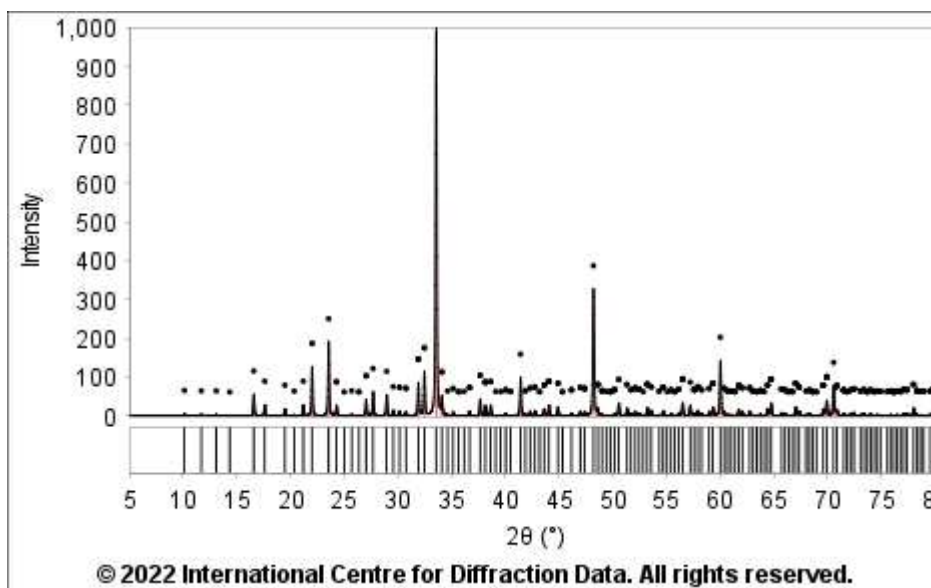
Appendices

9.3.9 E.7 Zirconium dioxide (ZrO_2) – 01-080-0966
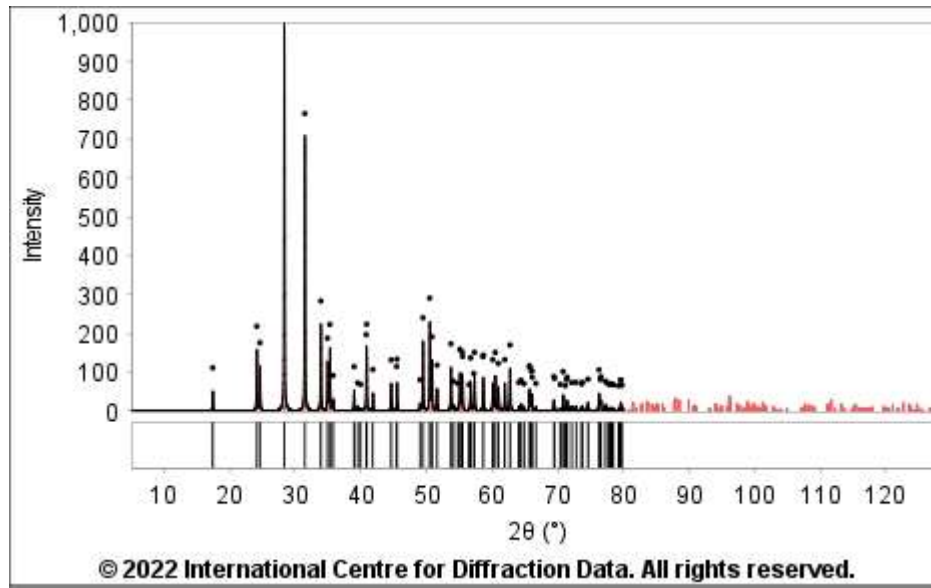
F. XRD OF 25 WT% NI/ZRO₂
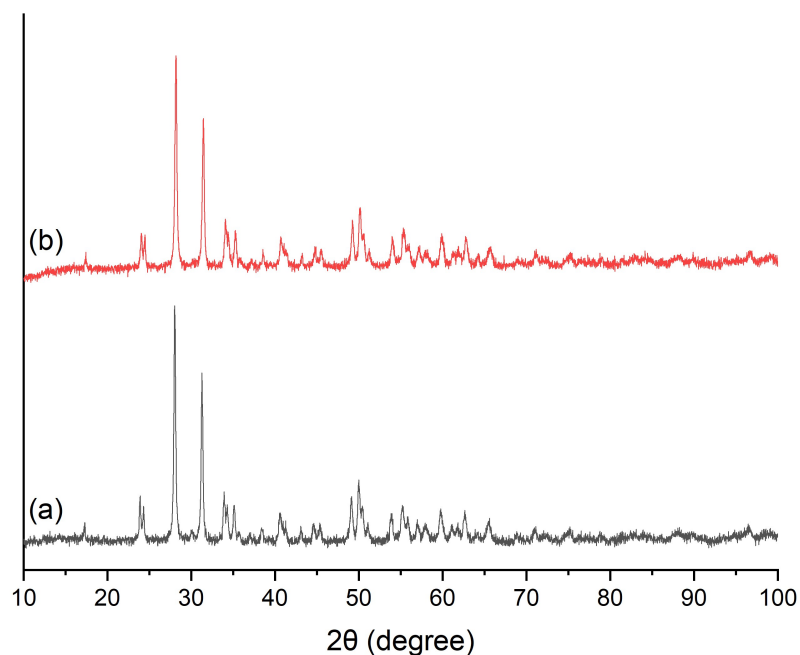
Figure 0-10 XRD of (a) fresh and (b) spent 25 wt% Ni/ZrO₂, x – NiO, ●– ZrO₂. Reaction conditions: 0.50 M NaHCO₃, 0.05 M glucose, 1 g Ni/ZrO₂, 250 °C, 2 h, 50 ml H₂O

G. SCHERRER EQUATION DATA FOR CRYSTALLITE SIZE CALCULATION

Table 0-2 CuO Peak info for Scherrer calculation of crystallite size – fresh CZZ

Peak Position (2θ)	FWHM	Crystallite size (nm)
35.52	0.30	28.4
38.79	0.27	32.4
48.59	0.33	27.4
58.30	0.32	29.8
61.54	0.34	27.9

H. NITROGEN SORPTION ISOTHERMS

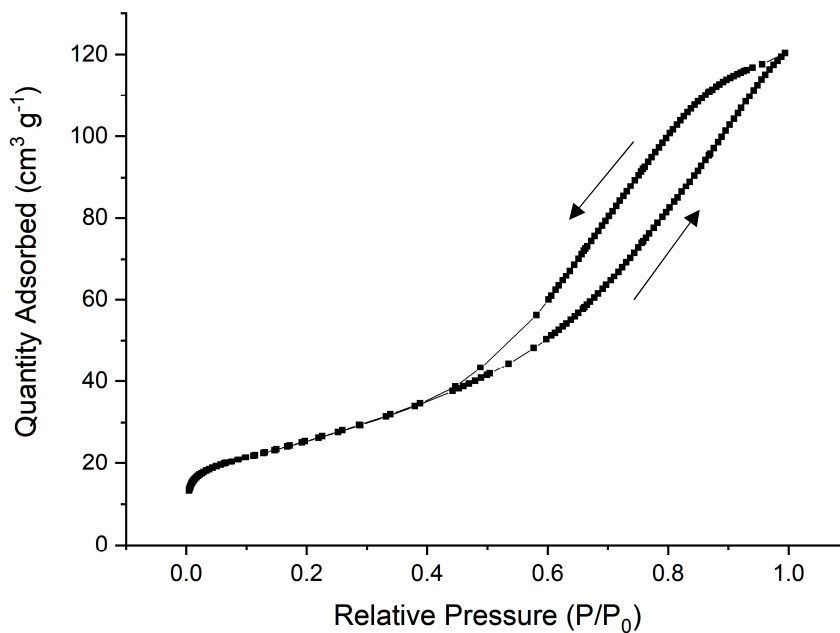### 9.3.10 H.1 Sorption Isotherm of CZA

Figure 0-11 Fresh CZA N₂ Sorption Isotherm
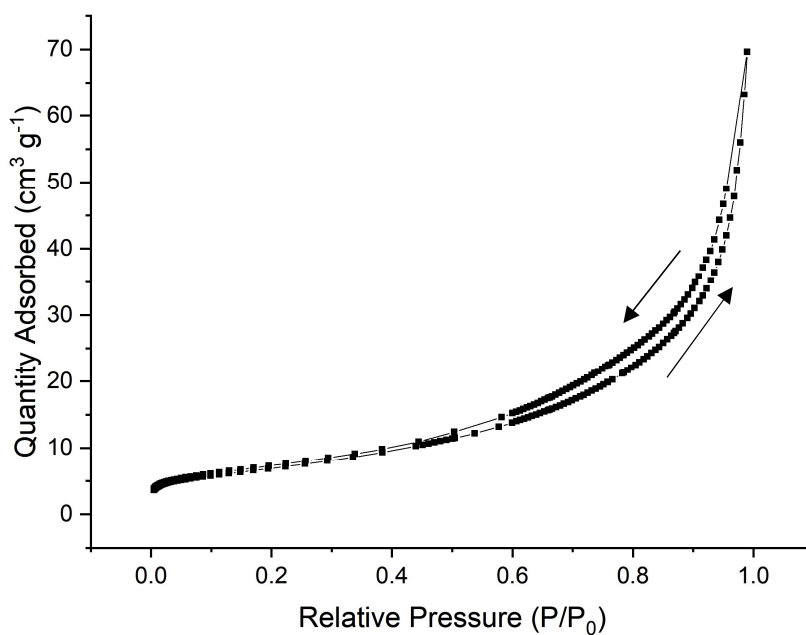

Figure 0-12 Spent CZA N₂ Sorption Isotherm
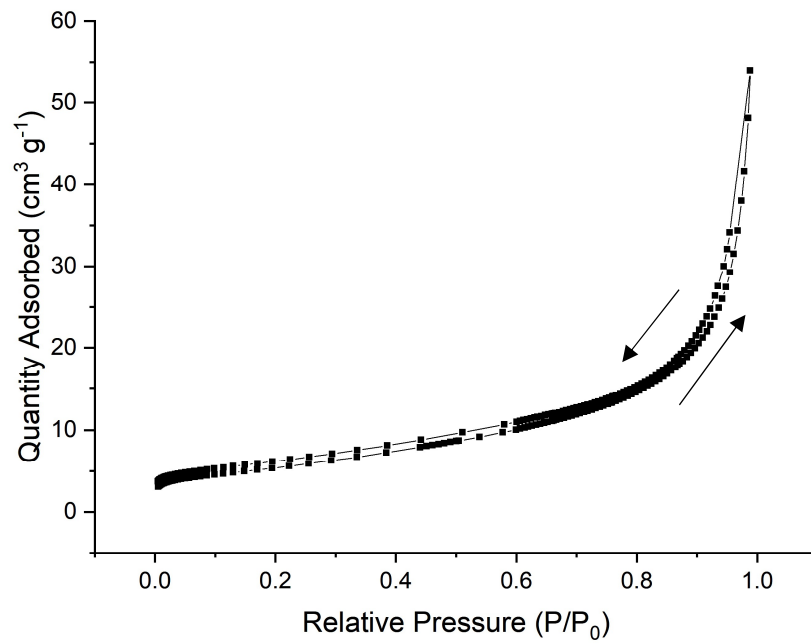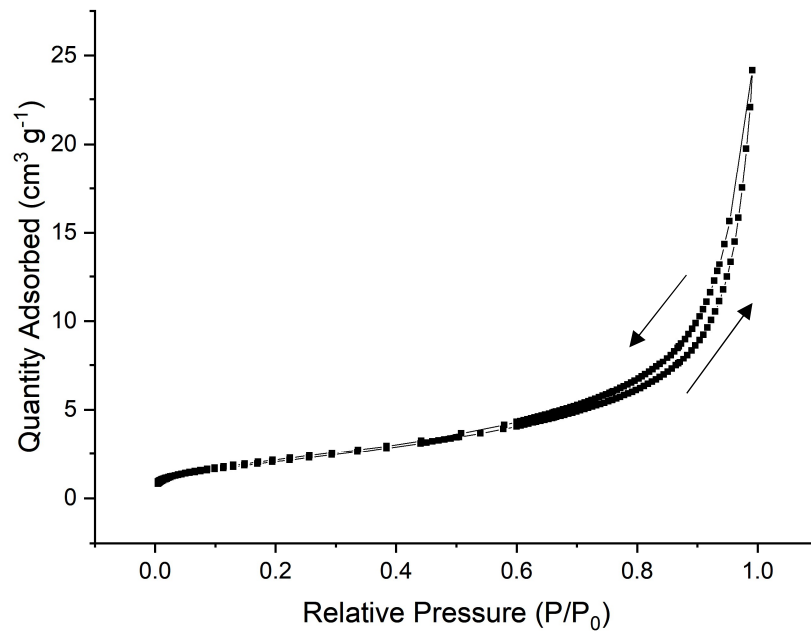
9.3.11 H.2 Sorption Isotherm of CZZ

Figure 0-13 Fresh CZZ Sorption Isotherm

Figure 0-14 Spent CZZ Sorption Isotherm